Etude de l'incorporation de Bismuth lors de l'épitaxie par jets moléculaires de matériaux antimoniures

Olivier Delorme

THÈSE POUR OBTENIR LE GRADE DE DOCTEUR DE L'UNIVERSITÉ DE MONTPELLIER

Spécialité : Électronique

École doctorale : Information, Structures, Systèmes

Unité de recherche : Institut d'Électronique et des Systèmes – UMR 5214

Etude de l'incorporation de Bismuth lors de l'épitaxie par jets moléculaires de matériaux antimoniures

Présentée par Olivier DELORME
Le 8 juillet 2019

Sous la direction de Eric TOURNIÉ
et Jean-Baptiste RODRIGUEZ

Devant le jury composé de

Chantal FONTAINE, Directeur de recherche CNRS, LAAS	Rapporteur
Ludovic DESPLANQUE, Maître de conférences, IEMN – Université de Lille	Rapporteur
Gilles PATRIARCHE, Directeur de recherche CNRS, C2N – Université Paris-Saclay	Examinateur
Hélène CARRERE, Maître de conférences, LPCNO – Université Toulouse III	Examinateur
Henri MARIETTE, Directeur de recherche CNRS, Institut Néel Grenoble	Examinateur
Eric TOURNIÉ, Professeur, IES – Université Montpellier	Directeur de thèse
Jean-Baptiste RODRIGUEZ, Chargé de recherche CNRS, IES – Université Montpellier	Co-encadrant de thèse

UNIVERSITÉ DE MONTPELLIER

THÈSE POUR OBTENIR LE GRADE DE DOCTEUR DE L'UNIVERSITÉ DE MONTPELLIER

Spécialité : Électronique

École doctorale : Information, Structures, Systèmes

Unité de recherche : Institut d'Électronique et des Systèmes – UMR 5214

Etude de l'incorporation de Bismuth lors de l'épitaxie par jets moléculaires de matériaux antimoniures

Présentée par Olivier DELORME
Le 8 juillet 2019

Sous la direction de Eric TOURNIÉ
et Jean-Baptiste RODRIGUEZ

Devant le jury composé de

Chantal FONTAINE, Directeur de recherche CNRS, LAAS	Rapporteur
Ludovic DESPLANQUE, Maître de conférences, IEMN – Université de Lille	Rapporteur
Gilles PATRIARCHE, Directeur de recherche CNRS, C2N – Université Paris-Saclay	Examinateur
Hélène CARRERE, Maître de conférences, LPCNO – Université Toulouse III	Examinateur
Henri MARIETTE, Directeur de recherche CNRS, Institut Néel Grenoble	Examinateur
Eric TOURNIÉ, Professeur, IES – Université Montpellier	Directeur de thèse
Jean-Baptiste RODRIGUEZ, Chargé de recherche CNRS, IES – Université Montpellier	Co-encadrant de thèse

UNIVERSITÉ DE MONTPELLIER

Molecular Beam Epitaxy of bismide antimonide alloys

Remerciements

Avec ce manuscrit s'achève mon aventure au sein du groupe Nanomir, après quasiment quatre ans de dur labeur. Arrivé petit stagiaire master 1, me voilà docteur ! Si on m'avait dit…

Je remercie tout d'abord la fière équipe du formidable projet BIOMAN, Eric Tournié, Jean-Baptiste Rodriguez et Laurent Cerutti (je n'oublie pas celui qui m'a fait entrer dans le groupe Nanomir après une terrible sélection) pour leur pédagogie, leur patience à toute épreuve et leur gentillesse. Disponibles à toute heure (même à 21h quand le molly tombe dans la MBE), je ne me suis jamais senti abandonné face à la MBE et à cet étrange atome qu'est le Bismuth. Si l'on ajoute à cela une bonne humeur constante, on obtient une excellente équipe d'encadrement qui a su rendre agréable cette tâche difficile qu'est la thèse. J'ai également particulièrement apprécié les moments « hors labo » avec vous, des finales de coupes du monde bien arrosées aux beach volley endiablés (et douloureux pour certains). Il ne manquerait plus qu'un humour qui tienne la route, mais on ne peut pas tout avoir. Vous m'avez fait aimer la recherche, bravo et merci.

En dehors de ce noyau dur, je remercie les différentes personnes de l'IES qui ont contribué à ce travail. Tout d'abord, Guilhem Boissier (maître yogi, détenteur du marteau d'argent) et Jean-Marc Aniel, maillons essentiels de l'équipe MBE sans qui nous serions bien désarmés face à tous les problèmes rencontrés et qui m'ont personnellement beaucoup appris ; Thierry Talercio pour son aide sur ce formidable setup de PL et ses analyses de match ; Frédéric Pichot et Jean-Marie Peiris pour le MEB et l'EDX ; Michel Ramonda pour l'expertise AFM.

Je remercie également nos collaborateurs européens pour tous les échanges enrichissants autour de nos échantillons : les TEMistes du PDI Esperanza Luna et Achim Trampert, pour m'avoir chaleureusement accueilli à Berlin et pour leur étude de ce matériau complexe à appréhender, dans des conditions bien souvent difficiles ; l'équipe de Robert Kudrawiec de l'université de Wroclaw pour leur travail de qualité.

Enfin, je tiens à remercier l'ensemble des membres du jury en commençant par Henri Mariette qui a accepté la lourde tâche d'être président ; les examinateurs Gilles Patriarche et Hélène Carrère pour leurs questions épineuses sur le TEM et la PL. Enfin, je remercie tout particulièrement les rapporteurs Chantal Fontaine et Ludovic Desplanque pour l'attention portée à mon travail.

Table of contents

Chapter 1:   Motivation and historical overview

In this first chapter, we present the antimonide compound family and their applications. Then, the interest of GaSbBi will be discussed. We will also review the state of the art of III-V-Bi alloys. Finally, the objectives of this thesis and the different chapters will be detailed.

1.1   The antimonides

The antimonides are compound semiconductors based on GaSb, InAs, AlSb and InSb III-V semiconductors, as well as their associated ternary, quaternary or quinary alloys, *e.g.* AlGa(In)AsSb or GaInAsSb. They are usually fabricated using Molecular Beam Epitaxy (MBE) on GaSb or InAs high quality substrates. The particularity of these materials lies in the large variety of alloys achievable, spanning a very wide range of band-gaps, allowing the realization of quantum-well (QW) lasers operating from the near [Cerutti-2015] to the mid-infrared [Hosoda-2010] (Fig. 1.1a). This material system is also unique in terms of band-offsets: InAs has a type-III band alignment with GaSb for example, with the maximum of the valence band of GaSb lying at a higher energy than the minimum of the conduction band of InAs (Fig. 1.1b). This semi-metallic interface is particularly interesting, since it allows fabricating superlattices having a fundamental transition energy as small as desired [Wei-2002, Rhiger-2011, Tan-2018] or very efficient carrier transfer from the valence band to the conduction band. This original feature has been successfully used to design high-performance photodetector arrays covering the whole infrared range [Razeghi and Nguyen-2014], but is also at play in topological insulator structures and Inter-band Cascade Lasers (ICLs) for example [Liu-2008, Vurgaftman-2015].

Additionally, InAs and AlSb have one of the largest conduction band offset achievable with semiconductor materials, which stemmed the development of quantum-cascade lasers (QCLs) from the mid-wavelength infrared range [Laffaille-2012] to the far infrared range [Bahriz-2015] using these two binaries.

Beyond the natural use of antimonides for infrared optoelectronic, a lot of research has also been conducted on high-speed/low-consumption electronics with these materials, because of the very large mobilities and narrow band-gaps achievable [Gardes-2014]. Finally, it was recently shown that the antimonides are serious candidates for the direct integration of III-V semiconductor on silicon [Reboul-2011, Castellano-2017, Nguyen-Van-2018, Tournie-2018].
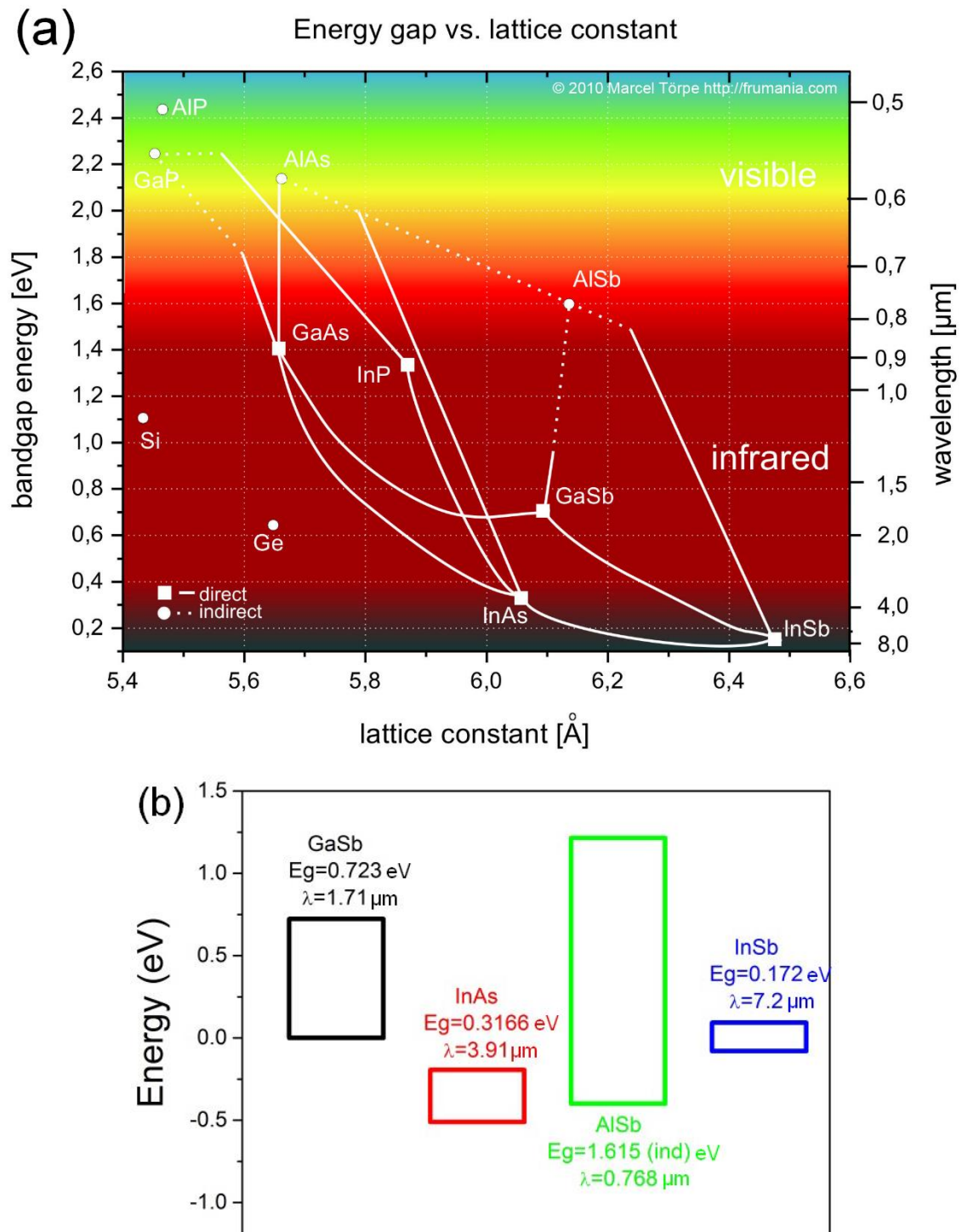
Fig. 1.1: (a) Bandgap versus lattice-constant for various semiconductor materials. Image taken from http://lab.frumania.com/wp-content/uploads/2010/06/bandgap_edit.jpg (b) The band alignment between the different antimonide materials, GaSb and InAs have a type-III alignment.

All these assets are at the origin of an intense research by a worldwide community. Optoelectronic devices made from antimonides find application in different fields, from trace-gas

detection and gas spectroscopy [Willer-2006, Scholle-2010, Tittel and Lewicki-2013, Reyes-Reyes-2014, Waclawek-2014, Bolshov-2015] to night-vision [O'Malley-2010], astronomy [Winnewisser-1994, Abedin-2004], non-invasive medical diagnosis [Scholle-2010, Godoy-2015, Gurjarpadhye-2015, Schwaighofer-2017] and strategic military applications [Tidrow and Dyer-2001, Coffey-2011, Vizbaras-2014].

1.2   Motivation for the development of GaSbBi

Incorporating Bi into antimonide alloys is extremely promising in terms of new device design possibilities. On one hand, the lattice parameter of GaBi is close to 6.3 angstrom [Janotti-2002, Tixier-2003b, Rajpalke-2014a] making it possible to grow coherently strained layers on GaSb. On the other hand, there is a large difference between the band-gaps of GaSb (0.812 eV) [Vurgaftman-2001] and GaBi (estimated between -2.91 eV and -1.45 eV) [Janotti-2002, Ferhat and Zaoui-2006, Samajdar-2014, Polak-2015] due to the semi-metallic nature of Bi. Any antimonide alloy comprising Bi would thus see its electronic properties drastically modified. Among them, GaSbBi is an alloy that has a strong potential for emission in the 2 - 5 µm range. Indeed, the heterostructure formed by GaSb and GaSbBi is expected to have a type-I band alignment (Fig. 1.2a), allowing the realization of efficient quantum wells emitting in the whole mid-wave IR domain. Advantages of such lasers compared to the state-of-the-art devices (interband cascade lasers (ICLs) or lasers with type-I quinaries QW barriers) in the mid-wave IR are listed below and illustrated on Fig. 1.2:

- Simpler design,
- GaSb QW barriers allow a better heat dissipation than the quaternary or quinary alloys,
- The hole confinement improves as the Bi content (and therefore the emission wavelength) is increased,
- The spin-orbit splitting is drastically increased by the adjunction of Bi (Fig. 1.2b) [Sweeney and Jin-2013], leading to a decrease of the Auger losses,
- The active region is aluminum-free, which is known to be beneficial for the device lifetime
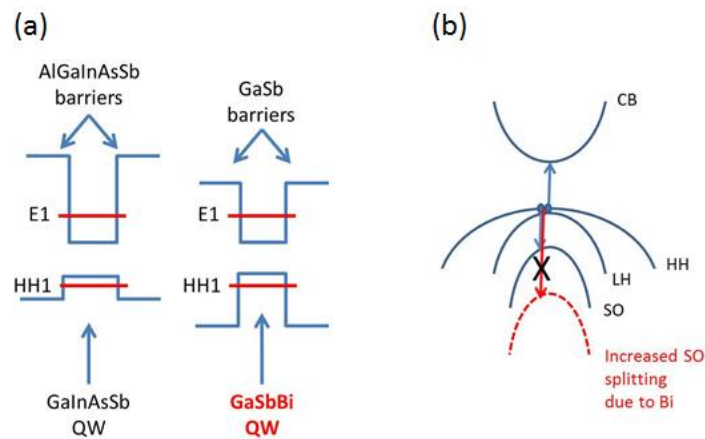
Fig. 1.2: (a) Standard type-I QW for emission beyond 3 µm are complex and so far limited to an emission wavelength ~3.5 µm. The use of GaSbBi as the QW material drastically reduce the growth complexity and allows the use of Al-free barriers. (b) The use of Bi in the QW allows reaching wavelength not achievable with common antimonides thanks to the reduction of Auger losses due to the resonance between the bandgap energy and the split-off band energy, by increasing significantly of the latter.

1.3   Historical review of III-V-Bi alloys

Bi is the heaviest group V element. Despite its negligible toxicity, Bi has long been neglected as a member of the III-V compound semiconductor family [Rao-2002]. This is firstly due to the difficulties in fabricating III-Bi binary alloys. Indeed, the structural and electronic parameters of III-Bi binaries (BBi, AlBi, GaBi and InBi) are essential to understand and predict the properties of III-V-Bi compounds (GaSbBi, GaAsBi, InAsBi ect.). However, no natural binary bismide exists on earth and the only successfully synthesized one is InBi, which demonstrated a PbO crystal structure [Binnie-1956, Keen-2014]. Epitaxy of GaBi and AlBi was also attempted, but no epitaxial growth could be achieved. Due to the lack of experimental results, the parameters of III-Bi binaries were predicted using different theoretical models. As this manuscript is focused on the growth of GaSbBi and GaInSbBi alloys, we will only detail the properties of GaBi and InBi binaries. GaBi is predicted to crystallize in Zinc-Blende structure, while PbO is estimated to be the most stable phase for InBi, agreeing with the experimental results [Ferhat and Zaoui-2006]. GaBi and InBi exhibit semi-metallic characteristics, with negative bandgaps calculated between -2.91 to -1.45 eV for GaBi and close to -1.6 eV for InBi [Janotti-2002, Ferhat and Zaoui-2006, Samajdar-2014, Polak-2015]. Additionally, these two binaries were found to have a very large spin orbit splitting energy (ΔSO) (Fig. 1.3), a critical characteristic in order to reduce the Auger recombination losses [Carrier and Wei-2004, Fluegel-2006].
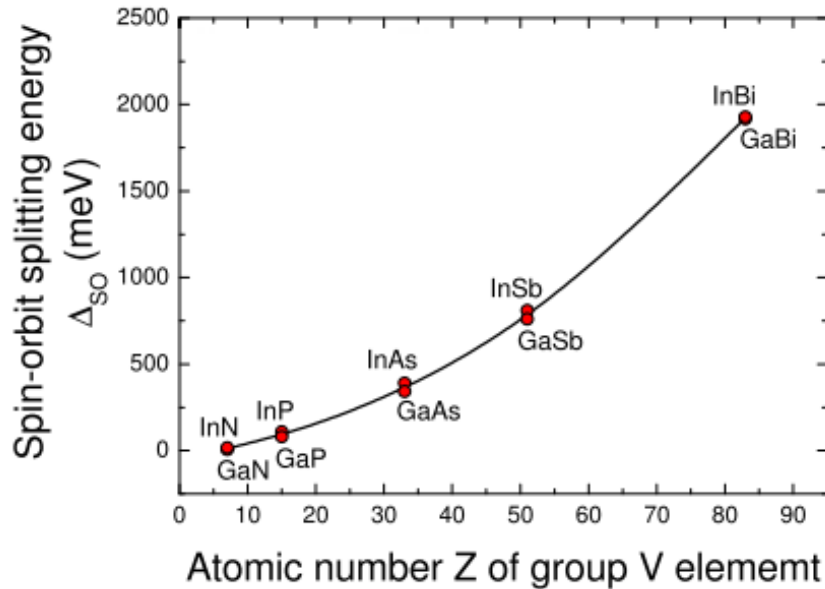
Fig. 1.3: Variation of the spin-orbit splitting energy as a function of group V atomic number for III-V binary compounds. Graph from [Sweeney and Jin-2013].

The idea of using Bi with the standard III-V semiconductors has been around since the late 1960s when Jean-Louis *et al.* reported the growth of bulk InSbBi crystals by the Czochralski method [Jean-Louis-1969, Jean-Louis and Hamon-1969, Joukoff and Jean-Louis-1972]. This work was motivated by the aforementioned semi-metallic nature of InBi, which should cause an extension of the InSb wavelength to reach the 8-14 μm IR atmospheric window. Unfortunately the solubility of Bi on the substitutional sites in InSbBi was found to be limited to 2.2% for equilibrium crystal growth techniques, because InBi has a PbO lattice whereas InSb has a cubic lattice. Nevertheless a bandgap reduction of 36 meV/%Bi was observed. Later on, non-equilibrium growth techniques such as MBE [Oe-1981, Noreika-1982] or MOCVD [Wagener-2000] enabled to obtain metastable films with higher Bi contents. But the Bi composition obtained at the time remained nevertheless rather small (∼3%) and the sample surfaces were covered with Bi droplets.

In the next twenty years, work on Bi-containing alloys was focused on the development of new IR photodetectors. The growth of InAsSbBi and InAsBi alloys were particularly investigated. Humphreys *et al.* achieved the first MOCVD growth of InAsSbBi with a maximum Bi content of 4% in 1988 [Humphreys-1988]. Ma *et al.* demonstrated the first successful growth of InAsBi with Bi content up to 2.6% and a bandgap reduction of 55 meV/%Bi was observed [Ma-1989]. Finally, the team of Razeghi from the Northwestern University reported InSbBi-based photodectors exhibiting extended cutoff wavelengths of 7.7 μm at 77 K or 10.6 μm at RT for different Bi compositions of 4 and 5 % Bi, respectively [Lee-1997, Lee-1998].

In the early 2000s, Bi was used as a surfactant to improve the quality of GaAs(N) dilute nitrides and to promote the incorporation of N into GaAs [Tixier-2003a, Young-2005]. Indeed, Bismuth is a large atom which hardly incorporates into the growing film under typical growth conditions, but rather segregates to the surface where its presence modifies the kinetics of the other impinging atoms. Such effect has been used to improve the luminescence efficiency and to smooth the surface of GaNAs layers for example [Tixier-2003a]. The successful use of Bi as a surfactant encouraged new experiments regarding its incorporation into GaAs. The growth of GaAsBi alloys with a Bi content of 2% was firstly achieved by Oe and Okamoto in 1998 [Oe and Okamoto-1998]. Thanks to drastic deviations from typical GaAs growth condition in MBE or MOCVD [Oe-2002, Tixier-2003b, Yoshimoto-2003], the maximum incorporation of Bi was increased up to 4.5% in GaAs, using both a low growth temperature (∼360°C) and a low V/III flux ratio. More recently, a careful control of the Ga/As flux ratio combined with a growth temperature lower than 300°C allowed to incorporate 22% of active Bi in the layer [Lewis-2012].

The incorporation of Bi into GaAs presents undeniable benefits. A giant bandgap reduction of 88 meV/%Bi and a strong increase of the ΔSO energy were observed (Fig. 1.4). Indeed, ΔSO becomes larger than the bandgap energy for Bi ~10%. In this case, Auger recombination involving holes in the spin-orbit and the heavy-hole band and inter-valence band absorption (IVBA) are suppressed, allowing a reduction of the Auger losses mainly responsible of the threshold current in current telecom laser devices [Phillips-1999]. Additionally, it was reported that the incorporation of Bi had a minor influence on the carrier mobility [Kini-2009, Beaton-2010], contrary to nitrides [Young-2003]. These solid arguments make GaAsBi alloys promising for the development of highly efficient telecom laser devices.
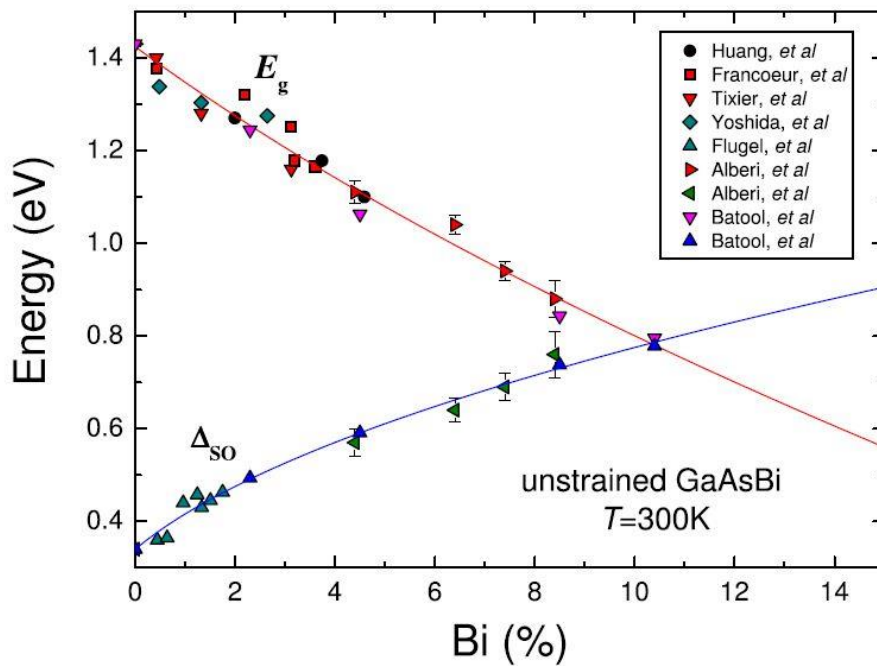
Fig. 1.4: Energy of the band gap E_g and spin-orbit splitting energy in unstrained GaAsBi as a function of Bi composition. The points are experimental data while the solid curves for E_g and ΔSO are theoretical calculations. Graph from [Sweeney and Jin-2013]

Therefore, GaAsBi-based QWs structures have been investigated. In 2008, Tominaga *et al.* reported GaAs$_{0.895}$Bi$_{0.105}$/GaAs multi quantum wells which demonstrated photoluminescence (PL) emission close to 1.3 µm at RT [Tominaga-2008]. The effect of thermal annealing on GaAsBi-based QWs was also studied by different groups. For example, Makhloufi *et al.* showed that the PL efficiency from GaAsBi QWs with 7% of Bi and emitting at 1.17 µm at 20 K was improved thanks to thermal annealing, contributing to decrease the density of localized defects due to Bi aggregates or alloy disorders [Makhloufi-2014].

In 2013, in the framework of the European project BIANCHO, the first electrically pumped laser operating at RT under pulsed excitation was demonstrated from a structure comprising $GaAs_{0.98}Bi_{0.02}$ QWs [Ludewig-2013]. Although the threshold density was high, the emission wavelength was longer than with GaAs QWs. In 2014, the University of Kyoto fabricated a laser structure by MBE with 4% Bi in the GaAs QWs [Fuyuki-2014]. Pulsed lasing emission at 1.045 µm (RT) was obtained, with reduced thermal tunability. In 2015, GaAsBi-based MQW lasers with Bi content up to 8% were grown by combining MBE and MOVPE, with a maximum lasing wavelength of 1.06 µm and a threshold current density of 12.5 kA/cm^2 at RT [Marko-2015]. Temperature- and pressure dependent measurements of stimulated and pure spontaneous emission measurements showed that this high threshold density was caused by non-radiative defect-related recombination and inhomogeneous carrier distribution. This was attributed by the authors to the inhomogeneous QW width and non-uniform Bi composition. More recently, a GaAsBi/GaAs laser diode with 5.8% Bi was realized, with emission up to 1.142 µm at RT. For the first time, continuous wave lasing was demonstrated, up to 273 K [Wu-2017]. Even if most investigations currently focus on GaAsBi, the incorporation of Bi in other III-V semiconductors has also been attempted. In 2014, a layer of $InPBi_{0.024}$ grown by gas source MBE on an InP substrate presented a band-edge absorption at 1.05 µm, representing a redshift of 120 nm with respect to InP [Gu-2014]. In addition, a photodiode made of $InAsBi_{0.02}$ grown by MBE on InAs substrate allowed to demonstrate a long cut-off wavelength of 3.95 µm combined with a lower temperature dependence of the band gap with respect to InAs photodiodes [Sandall-2014].

Regarding the work more specifically focused on the use of Bi with antimonides, a few studies were carried out in order to understand Bi incorporation in GaSb since 2012. The earliest reports on epitaxial GaSbBi alloys show Bi incorporation as low as 0.8% either by MBE or LPE (Fig. 1.5a) [Das-2012, Song-2012]. Attempts to grow GaSbBi alloys by MBE with higher Bi-content resulted in the formation of Ga-Bi droplets on the surface [Duzik and Millunchick-2014]. Varying the growth temperature and the Bi/Sb flux ratio, Rajpalke *et al.* demonstrated GaSbBi epilayers with smooth surface and high crystalline quality [Rajpalke-2013]. They also observed a reduction of the band-gap of the material corresponding to ~35 meV/%Bi (Fig. 1.5b). The PL wavelength shifted up to 3 µm for layers with 9.6% of Bi [Rajpalke-2014a]. Very preliminary studies were also published on the quaternary alloys AlGaSbBi and GaInSbBi [Kopaczek-2014a]. As expected, the incorporation of Bi resulted in a decrease of the band gap of these alloys, as well as a smaller variation of the band-gap with temperature.
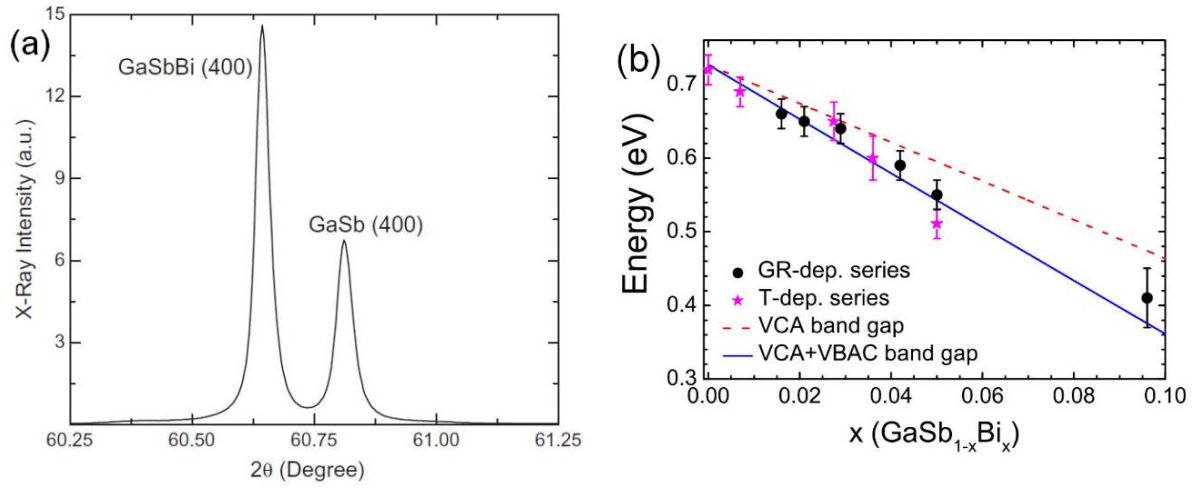
Fig. 1.5: (a) HRXRD rocking curve for LPE GaSbBi on GaSb substrate. Graph from [Das-2012]. (b) Bandgap of GaSbBi layers as a function of the Bi content. The dashed and solid line depict the variation of the bandgap calculated using virtual crystal approximation and the valence band anticrossing model, respectively. Graph from [Rajpalke-2014a].

1.4 Thesis overview

Fig. 1.6: Chronological evolution of number of publications on dilute bismide since 1997. Figure taken from [Wang-2017]

Alloying Bi with III-V alloys presents strong advantages and the interest of the scientific community keeps growing (Fig. 1.6). GaSbBi is definitely a promising alloy for the development of new optoelectronic devices in the 2 – 5 μm range. At the beginning of this thesis, the literature on GaSbBi was very limited, and only a few groups were working on the growth of this material at that time. Furthermore, despite the fact that our group had a long experience in growing antimonide semiconductors, the epitaxy of dilute bismide alloys had never been attempted at IES. Therefore, we started our work on the incorporation of Bi into antimonides from scratch. The objectives were:

- to optimize the growth conditions and find the incorporation limits into GaSb and GaInSb,
- to investigate the microstructure of III-Sb-Bi materials and heterostructures,
- to elucidate the electronic properties of III-Sb-Bi materials,
- to evaluate the potential of III-Sb-Bi alloys for mid-IR optoelectronic devices.

Chapter 2 details the MBE growth of GaSbBi and our investigations on the influence of the growth conditions on the incorporation of Bi. The careful optimization of the growth temperature and the different fluxes lead to the incorporation of 14% Bi, the highest content to date. Additionally, a new way to set the growth conditions was proposed.

Chapter 3 is closely linked to chapter 2. Using our study of the growth of GaSbBi, we have grown GaSbBi/GaSb MQW structures which were in-depth characterized in collaboration with the Paul Drüde Institute of Berlin and the Wroclaw University. Finally, the first GaSbBi-based laser device was fabricated and demonstrated continuous wave lasing at 80 K and emission close to 2.7 µm at 300 K under pulsed operation.

In the fourth chapter, we present our investigations on a more complex alloy, GaInSbBi. The interplay between In and Bi incorporation was studied in details. The first ever GaInSbBi/GaSb MQW structures were also fabricated, exhibiting PL emission around 2.6 µm at RT.

Chapter 2: Molecular Beam Epitaxy of GaSbBi epilayers

As seen in the previous chapter, the incorporation of Bi into III-V alloys is challenging and requires very specific growth conditions. In this context, the first step to achieve the epitaxy of GaSbBi is to study the influence of the different growth parameters on the incorporation of Bi into GaSb. In this second chapter, the impact of the growth temperature, of the V/III ratio and of the Bi flux was investigated. As these parameters are particularly difficult to set, a new *in-situ* method using RHEED was demonstrated to optimize the growth conditions. The optical and structural properties of the layers were characterized by several techniques. This work allowed growing GaSbBi layers with record Bi contents.

2.1 Molecular beam epitaxy

2.1.1 The molecular beam epitaxy reactor

The samples were grown by molecular beam epitaxy in a RIBER COMPACT 21 reactor equipped with 11 cells (Fig. 2.1). The element-III sources (Al, In, Ga) are double-filament cells, while Sb_2 and As_2 are provided by valved cracker-cells. The growth chamber is also equipped with different *in-situ* monitoring tools: an electron gun and a phosphorus screen used for RHEED measurements; a retractable ion beam gauge to measure the beam-equivalent-pressures (BEPs) of the flux, a mass spectrometer to analyze the different species in the chamber and an optical pyrometer to monitor the substrate temperature. Because of the extreme sensitivity of the Bi content as well as of the overall GaSbBi material quality to the Sb flux, care was taken to avoid any hysteresis effect on the Sb valve aperture by proceeding systematically in the same way, *i.e.* full opening the valve before setting the desired aperture. Using this procedure, a very good reproducibility of the Sb flux for a given valve aperture was achieved. Finally, the Bi and dopants (Be, Te, Si) sources are single-filament cells. The MBE sources allow highly stable fluxes, with BEP fluctuation as low as 1×10^{-9} Torr for Bi and 5×10^{-9} for the other elements.
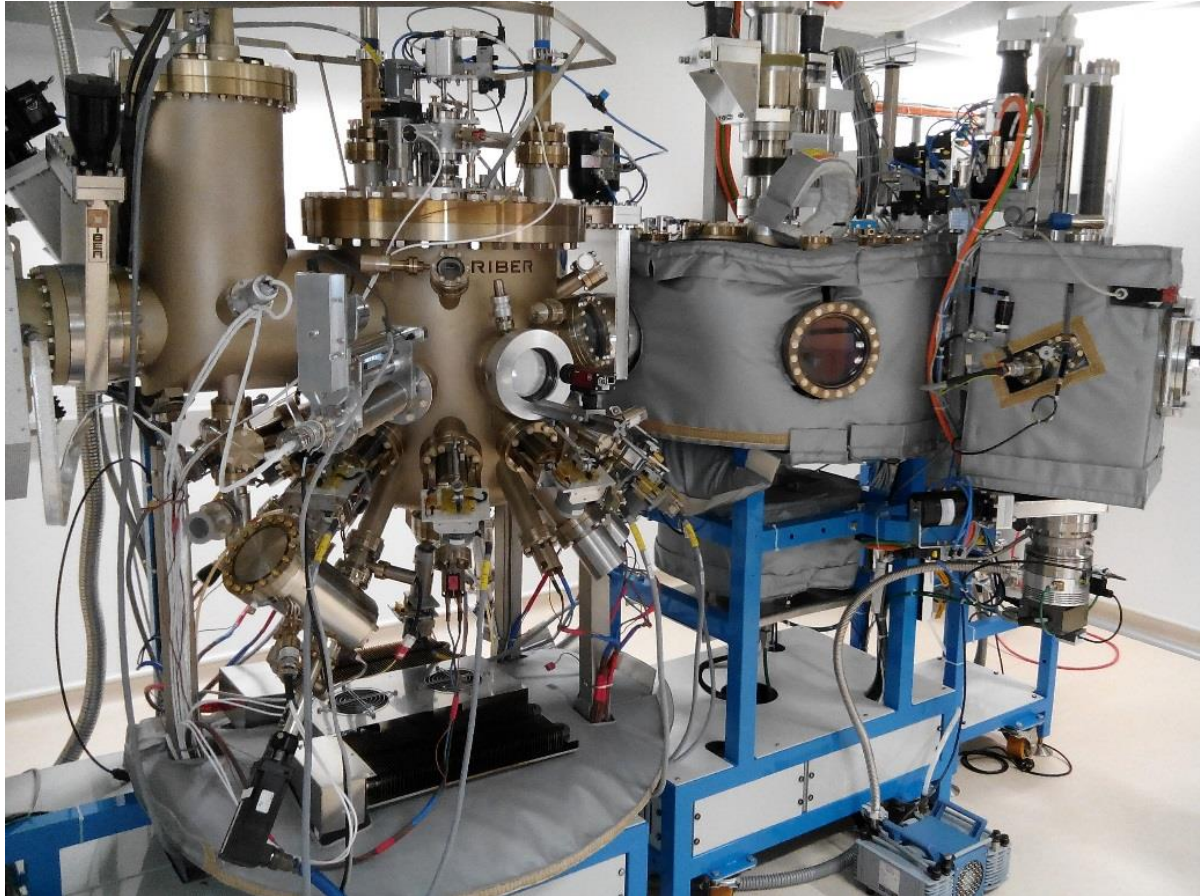
Fig. 2.1: Our MBE system, the RIBER Compact 21

2.1.2 Sample preparation and characterization

Quarters of two inch GaSb (001) n- and p-doped substrates were used in this study. They were first outgassed at 150°C by infrared lights in the load-lock chamber. After transfer in the growth chamber, the samples were heated up to 550°C under an Sb flux in order to remove the oxide from the surface. A 100 nm thick GaSb buffer layer was then grown at a rate of 0.25 ML/s at 500°C in order to smooth out the surface and burry any remaining impurities. Next, the samples were cooled down to the desired growth temperature. The Sb flux was turned off for temperatures lower than 380°C in order to avoid the deposition of an Sb layer on the surface. When the Sb flux was stopped, one monolayer (ML) of Ga was deposited to replace the Sb-rich (1 x 5) surface reconstruction by the (1 x 3) reconstruction typically observed during the growth of GaSb-based compounds at their usual growth temperatures (450 – 500 °C). Finally, once the sample temperature was stabilized at the desired temperature, the Ga, Sb and Bi shutters were simultaneously opened to start the growth of the GaSbBi layer. The substrate rotation speed was set to 10 revolutions per minute to ensure a good composition

and thickness uniformity. A (1 x 3) RHEED pattern was consistently observed during the growth of GaSbBi.

After growth, the samples were characterized by different *ex-situ* methods. The morphology of the surface was studied by optical and atomic force microscopies (AFM). The surface defects were observed by scanning electron microscopy (SEM) and their composition determined by energy dispersive X-ray spectrometry (EDS). The optical properties were measured by photoluminescence (PL) and photoreflectance (PR) spectroscopies. Temperature-dependent PL spectroscopy was performed using a Brucker-Vertex 70 Fourier Transformed Infra-Red Spectrometer equipped with a KBr separator and a cooled InSb detector, the PL being excited by a 780 nm laser diode. The experimental setup is shown in Fig. 2.2. PR measurements were carried out by the team of Pr. Robert Kudrawiec at the University of Wrocław. The samples' microstructure was investigated by transmission electron microscopy (TEM) by the team of Dr. Achim Trampert at the Paul Drude Institute in Berlin. Cross-sectional TEM specimens were prepared in the [110] and [$\bar{1}$10] projections using mechanical thinning, followed by Ar-ion milling. In order to minimize the sputtering damage, the Ar-ion energy was reduced to 2 – 0.5 keV. The samples were investigated on a scanning (S)TEM JEOL 2100F microscope operating at 200 kV.
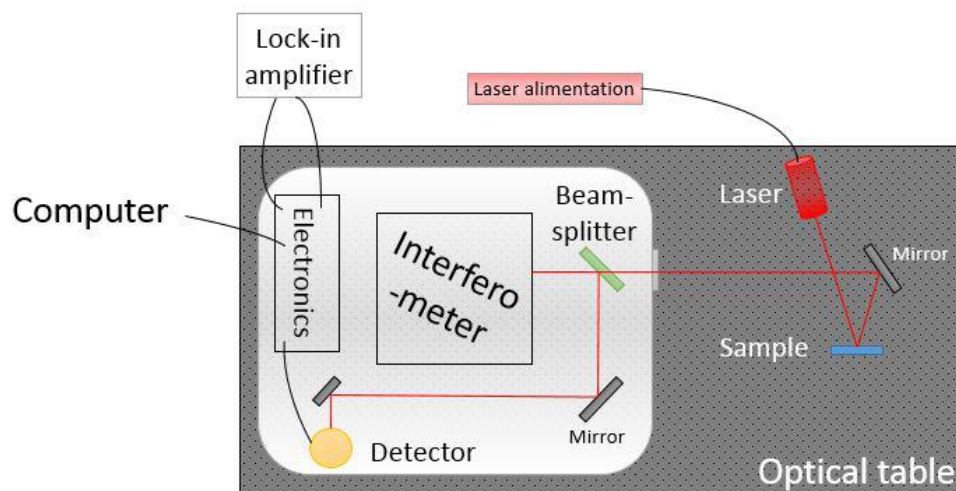
Fig. 2.2: PL experimental setup, picture taken from [Tournet-2019]

Finally, the crystal quality and the Bi concentrations were assessed by high-resolution X-ray diffraction (HR-XRD) measurements using a PANalytical X'Pert3 MRD equipped with a PIXcel1D linear detector, an X-ray tube delivering the $CuK\alpha_1$ radiation and a four-bounce asymmetric Ge(220) monochromator. However, the accurate determination of the Bi content by HR-XRD is difficult for GaSbBi alloys. Indeed, several important parameters such as the lattice parameter of GaBi, required

for the estimation of the composition from HR-XRD, are missing. Instead, Rutherford Backscattering Spectrometry (RBS) was used to measure the Bi concentration. In fact, RBS is the only direct method allowing measuring the absolute concentration of Bi as well as the fraction of atoms in interstitial position in the crystal.

RBS was performed at the Centre d'Etudes Nucléaires of Bordeaux Gradignan on GaSbBi layers of 120 nm with Bi concentrations comprised between 3.8 and 11.4%. Fig. 2.3 shows the strained and relaxed lattice parameters of GaSbBi layers as a function of the Bi content determined by RBS. Assuming that the layer is totally strained, the strained lattice constant was extracted from the position of the GaSbBi peak obtained by HR-XRD ω-2θ measurements around the (004) reflection. The corresponding free-standing lattice parameter was calculated using the following equation [Calmes-2003]:

$$a_{GaSbBi\_relaxed} = \frac{c_{11}}{c_{11}+2c_{12}} * a_{\perp GaSbBi\_strained} + \frac{2 * c_{12} * a_{substrate}}{c_{11}+ 2c_{12}} \quad (2.1)$$

where $a_{substrate}$ and $a_{\perp GaSbBi\_strained}$ are the lattice parameters of GaSb and of the strained GaSbBi layer, respectively. c_{11} and c_{12} are the elastic constants of GaSbBi. However, as these constants are unknown for GaBi, they cannot be calculated for GaSbBi and those of GaSb were used instead, which we consider a reasonable assumption given the relatively low Bi content in our layers. Using a linear fit extrapolated to 100 % Bi, the relaxed lattice parameter of GaBi was estimated to a value of a_{GaBi} = 6.272 Å. Rajpalke *et al.* reported the very same value, using GaSbBi samples as well [Rajpalke-2014a]. Our data is also in good agreement with the relaxed GaBi lattice constant obtained from GaAsBi alloys, which was found in the 6.23 to 6.37 Å range [Tixier-2003b, Takehara-2006, Lewis-2014]. Based on these results, the composition of the samples grown in this work was thereafter determined using HR-XRD only, assuming a GaBi lattice parameter of 6.272 Å.
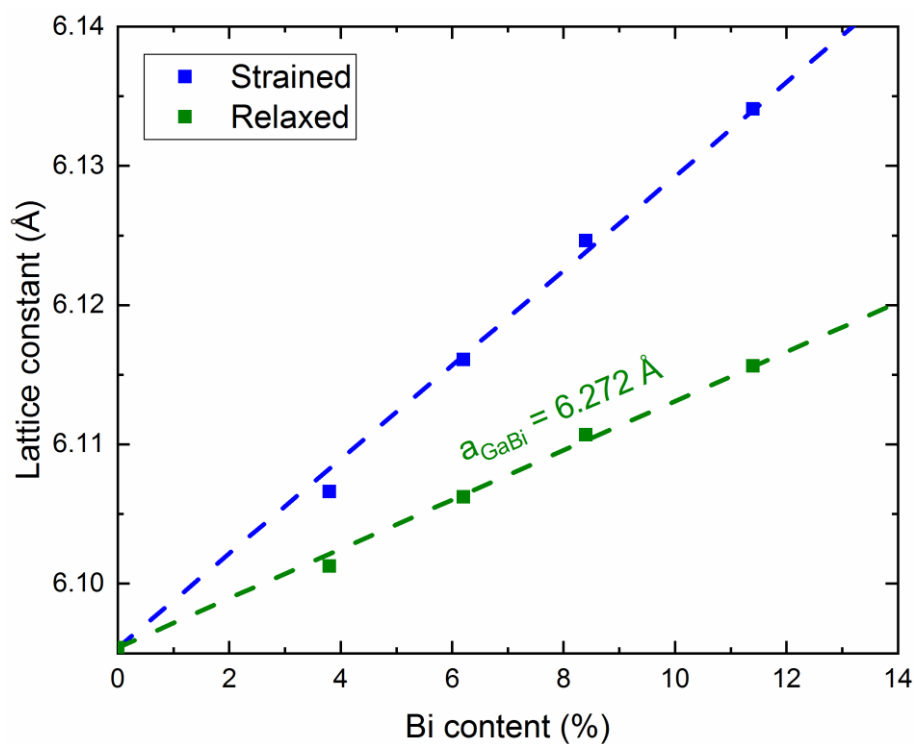
Fig. 2.3: GaSbBi strained lattice parameter (in blue) calculated from HR-XRD and the corresponding relaxed lattice parameter (in green) as a function of the Bi content measured by RBS. The dashed lines are linear fits.

2.2   Incorporation of Bi into GaSb

Since the first growth of GaSbBi in 2012 [Das-2012, Song-2012], it is known that the growth temperature and the V/III flux ratio have a tremendous impact on the Bi incorporation [Rajpalke-2013, Rajpalke-2014a, Rajpalke-2015]. These parameters need to be carefully adjusted to enhance the Bi incorporation while maintaining a high material quality. In the next paragraphs, we investigate the influence of the growth conditions on the incorporation of Bi into GaSb. These results were published in [Delorme-2017a].

2.2.1 Influence of the growth temperature

The common knowledge found in the literature is that Bi requires low temperatures to incorporate into III-V alloys. In the case of GaSbBi, Rajpalke *et al*. reported that the Bi content severely drops above approximately 275°C [Rajpalke-2013]. Such a low temperature is complicated to control in our MBE system because the optical pyrometer is not suited for temperatures below 380°C. Therefore, the thermocouple temperature reading (TTR) was used as a reference for temperatures lower than 380°C, whereas the substrate temperature was measured using the optical pyrometer for higher temperatures. The TTR is the temperature read by the thermocouple located between the substrate heater and the substrate. It is obviously different from the real temperature of the sample, and can vary from one MBE system to another. However, we have verified that in the conditions used in our experiments, the TTR is reproducible in our MBE reactor over a growth campaign. In this context, our first objective was to determine the optimal growth temperature of GaSbBi in our MBE system. To this end, a range of temperatures between 170 and 330°C TTR was explored. In comparison, GaSb is usually grown around 500°C TTR in our MBE system. Due to the low growth temperature and thus to the weak thermal energy, the impinging group-V atoms which are not incorporated do not readily desorb from the surface of the sample as it is the case for the growth of III-V alloys at usual temperatures. Therefore, 120-nm thick GaSbBi layers were grown using a constant near-stoichiometric Sb/Ga flux ratio to avoid the deposition of metallic droplets on the surface. The Bi BEP and the growth rate were arbitrarily set to ~2.3 x 10^{-8} Torr and 0.3 ML/s, respectively, and only the substrate temperature was changed from one sample to the next one.

Fig. 2.4a presents the HR-XRD ω-2θ scans measured around the (004) reflection of the GaSbBi layers. The peaks at 30.36° correspond to the GaSb substrate. At 330°C, the GaSbBi peak is nearly matched to the GaSb peak, showing that the Bi incorporation is close to zero. But as the growth

temperature is decreased, the GaSbBi peak shifts toward smaller angles, indicating an increase of the GaSbBi lattice parameter with respect to the substrate. The resulting compressive strain is obviously caused by the incorporation of Bi and the larger lattice parameter of GaBi (6.272 Å) in comparison with GaSb (6.0954 Å). The incorporation of Bi increases as the growth temperature decreases and a maximum Bi content of 5.65% is obtained for the lowest temperatures (≤ 200°C TTR). All scans exhibit clear *Pendellösung* fringes attesting high crystal quality, but metallic droplets are visible on the surface of the layers grown at 310 and 330 °C TTR: with the increase of the temperature, the thermal desorption of group-V species raises and the resulting excess of Ga atoms forms droplets. The other samples are droplet free. The variation of the Bi content is shown in Fig. 2.4b. A temperature of 200°C TTR seems to be optimal for the growth of GaSbBi alloys in our MBE system: it is indeed the highest temperature allowing the maximum incorporation of Bi. Higher temperatures result in a strong reduction of the Bi incorporation, while lower temperatures give the same maximum Bi content but cause a degradation of the material quality. By comparing with available data from literature [Rajpalke-2013], we can estimate the corresponding real substrate temperature to be about 275°C.

The temperature influence on the Bi incorporation in GaSb has been modeled using the kinetic approach described by Wood *et al.* [Wood-1982] and Pan *et al.* [Pan-2000]. According to this model, the Bi content (%Bi) can be described by:

$$\%Bi = \frac{\alpha * J_{Bi}}{\alpha * J_{Ga} + D_0 * \exp(-\frac{E_d}{k*(TTR+T_{offset})})} \tag{2.2}$$

where J_{Ga} and J_{Bi} are the incident flux of Ga and Bi, respectively, α is a constant, k is the Boltzmann constant, E_d is the activation energy for desorption and $D_0 = 1/\tau_s$, where τ_s is the surface residence lifetime of the Bi atoms. A temperature offset of 75°C (T_{offset}) was added to the TTR in order to obtain the real substrate temperature and to compare our fitting parameters with the ones of the litterature. The formula fits well our data using E_d = 1.75 eV and τ_s = 6.5 µs, which are the same values as the ones reported by Rajpalke *et al.* [Rajpalke-2013]. This E_d value is also in good agreement with the 1.7 eV activation energy reported for the desorption of Bi from a GaSb substrate by Sarney in 2014 [Sarney-2014]. The data reported for the desorption of Bi from GaAs are also similar (1.8 ± 0.4 eV and 1.3 eV) [Young-2005, Lu-2008].
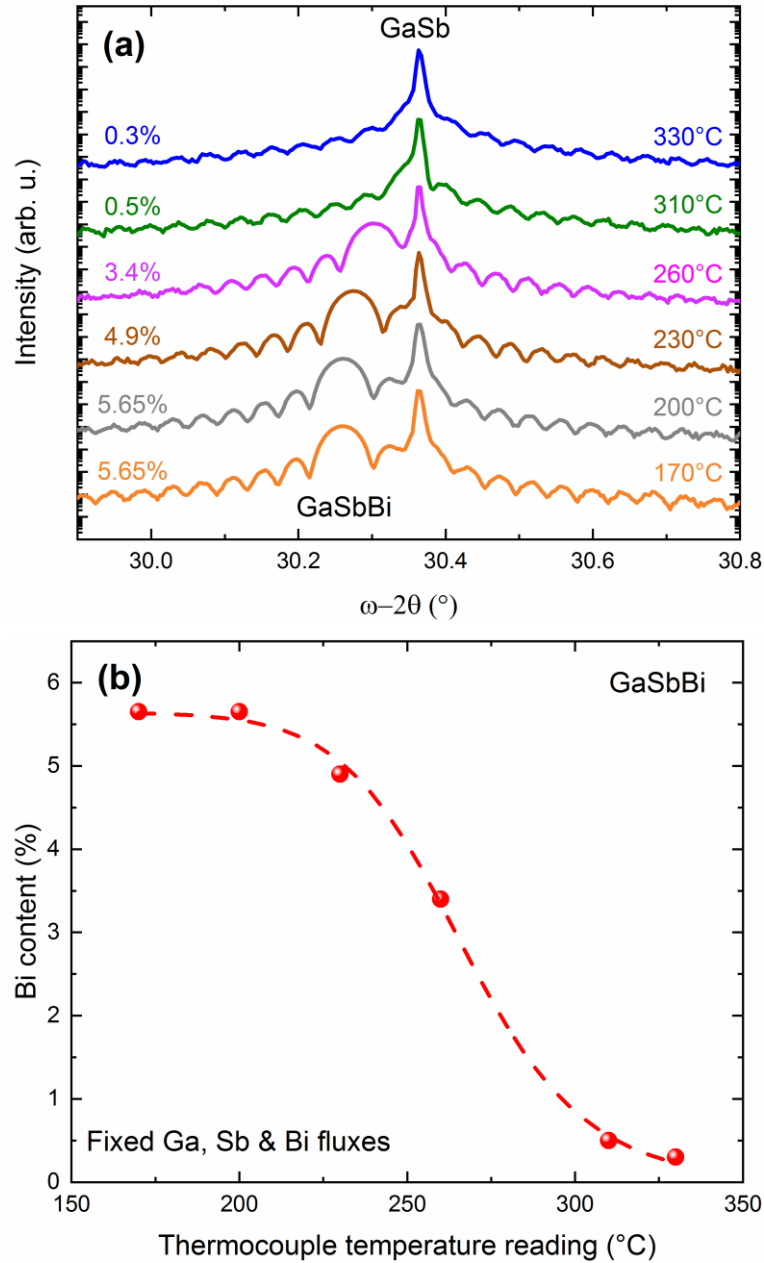
Fig. 2.4: (a) ω-2θ scans of the (004) Bragg reflection of 120-nm thick GaSbBi samples grown at various temperatures using fixed fluxes. The influence of the growth temperature on the Bi incorporation is depicted in (b). The dashed line was calculated using a kinetic model.

2.2.2 Influence of the Sb flux

The other critical parameter for the growth of GaSbBi is the V/III flux ratio, for two main reasons. First, the V/III flux ratio must be set close to stoichiometry to avoid the deposition of excess group-V elements on the surface (see paragraph 2.2.1). Second, it has been reported for GaAsBi alloys that a too high As flux strongly reduces the incorporation of Bi [Yoshimoto-2003, Lewis-2012]. A set of

20

GaSbBi samples was thus grown to study the influence of the Sb flux on the Bi incorporation. The growth temperature and the growth rate were fixed at 200 °C TTR and 0.3 ML/s, respectively. The Bi BEP was kept constant at ~2.3 x 10^{-8} Torr while the Sb BEP was varied between 2.60 x 10^{-7} and 3.65 x 10^{-7} Torr. Fig. 2.5 shows the evolution of the Bi content as a function of the Sb flux. Similarly to the evolution of the Bi content with the As flux in the case of GaAsBi, the Bi incorporation is severely hindered for large Sb fluxes whereas a plateau around 5.7% is obtained for the lowest fluxes. The Sb BEP for which the Bi content starts dropping corresponds to a maximum Sb incorporation rate close to 0.28 ML/s, slightly below the Ga incorporation rate. Accounting for the Bi maximum incorporation rate (5.7% of 0.3 ML/s), the total V/III ratio needed to achieve maximum incorporation rate falls very close to unity, *i.e.*, when the stoichiometric condition is achieved. This result clearly illustrates the fact that the Sb flux must be adjusted precisely, and depends not only upon the growth rate, but also upon the Bi flux used.
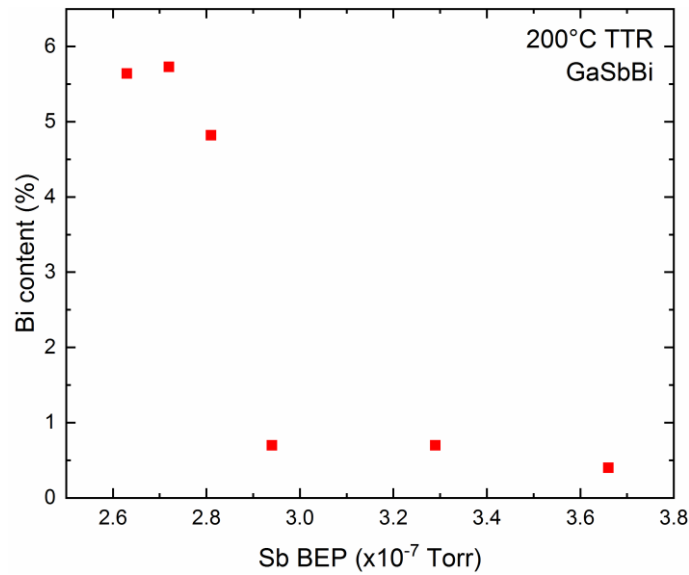
Fig. 2.5: The Bi content in 120-nm thick GaSbBi layers as a function of Sb BEP at a fixed growth rate of 0.3 ML/s and fixed Bi flux.

2.2.3 Influence of the Bi flux

The last growth parameter that strongly influences the Bi incorporation is of course the Bi flux itself. To study the impact of the Bi flux on the growth of GaSbBi, a set of samples was grown using a range of Bi BEPs between 2.3 x 10^{-8} and 6.6 x 10^{-8} Torr while keeping constant the other parameters.

As expected, the Bi concentration increases linearly with the Bi flux (Fig. 2.6a) and a Bi content as high as 11.3% was obtained for a Bi BEP of 4.5 x 10^{-8} Torr. The HR-XRD scans (Fig. 2.6b) of the three samples grown with the lowest Bi fluxes show well defined *Pendellösung* fringes, demonstrating their high crystal quality. However, a slight damping of the first *Pendellösung* fringe next to the GaSb substrate peak (~30.3°) can be observed for the sample with 11.3%, as well as a few metallic droplets on the surface (Fig. 2.6c), indicating a lower crystal quality. Finally, the highest Bi fluxes (5.5 x 10^{-8} and 6.6 x 10^{-8} Torr) resulted in inhomogeneous compositions and no clear peak / *Pendellösung* fringes could be observed on the HR-XRD scans. It is thus impossible to accurately determine the Bi concentration based on these measurements. Additionally, the surface of these two samples are covered by a high density of droplets (Fig. 2.6d). This deterioration can be explained easily as follows: by increasing the Bi flux while keeping the Sb flux constant, the V/III flux ratio becomes higher than unity, raising the density of group-V atoms in excess. Since Sb is easier to incorporate than Bi, we can suppose that the non-incorporated atoms are mainly Bi atoms which do not desorb from the surface due to the low thermal energy. Furthermore, Bi atoms have a strong tendency to segregate toward the surface and form droplets [Wang-2017]. The presence of droplets leads to a local disorganisation of the lattice and the apparition of defects, ultimately leading to a low material quality.
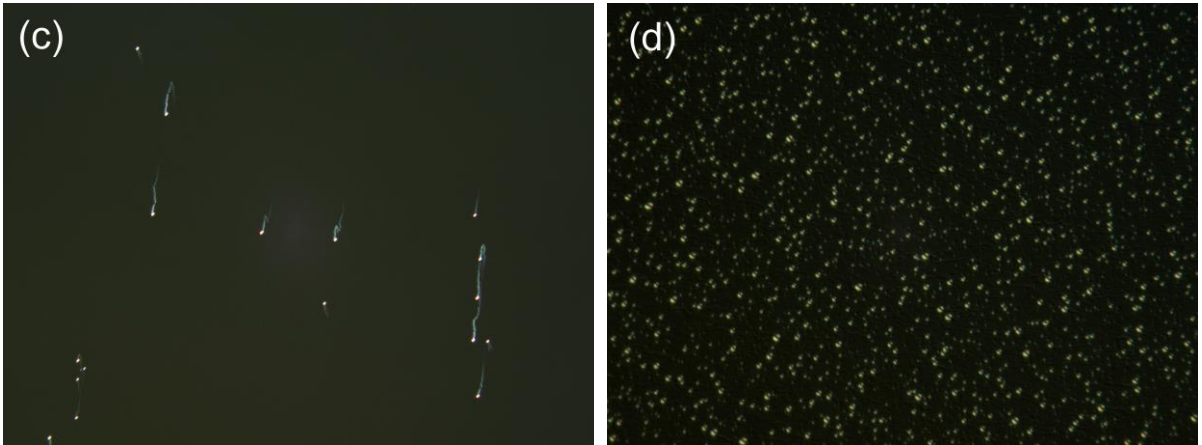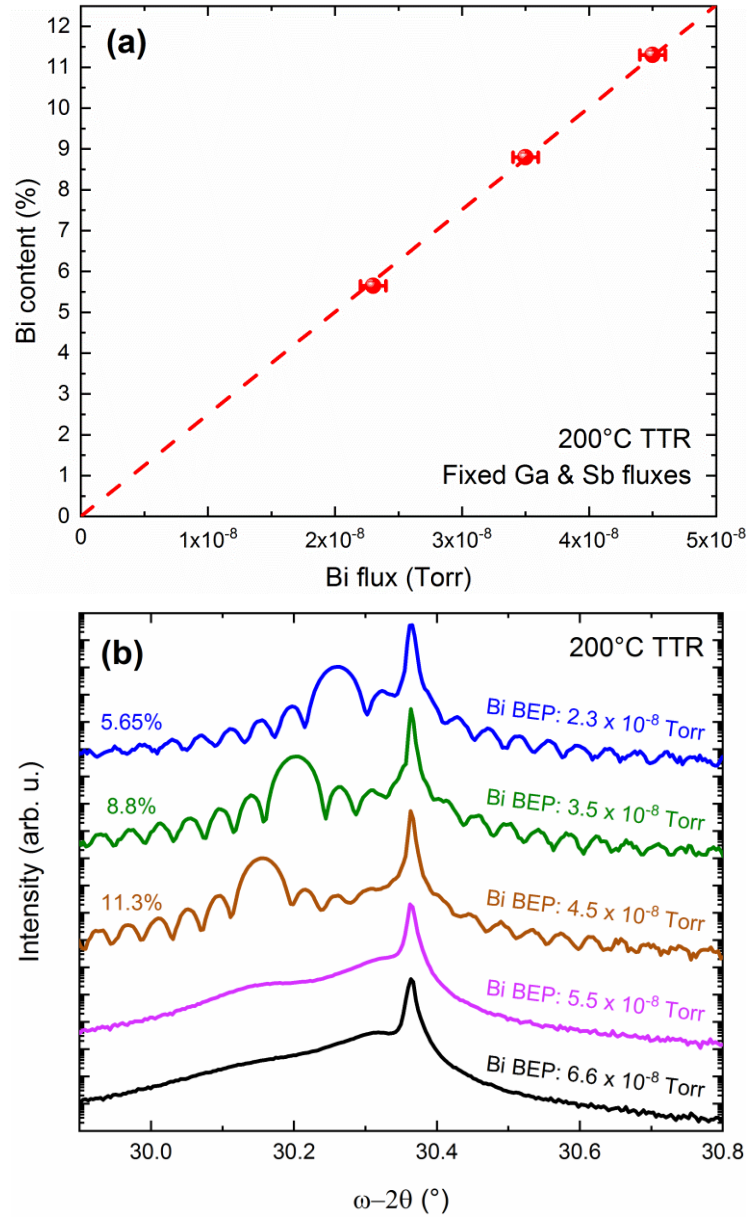
Fig. 2.6: (a) Variation of the Bi content as a function of the Bi flux. (b) HR-XRD ω-2ϑ scans of the (004) Bragg reflection of 120-nm thick GaSbBi layers grown at 200°C TTR and 0.3 ML/s, using different Bi fluxes. The Sb BEP was set at 2.65 x 10⁻⁷ Torr. Surface observation of the samples grown under Bi BEPs of (a) 4.5 x 10⁻⁸ Torr (600 x 450 μm) and (b) 5.5 x 10⁻⁸ Torr (120 x 90 μm).

2.3 *In situ* determination of the optimal growth conditions using RHEED intensity oscillations

As shown in the previous paragraph, the growth of good quality GaSbBi alloys becomes extremely challenging when the Bi content is high. Due to the particular growth conditions and the characteristics of Bi, droplets easily form at the surface if the growth parameters are not carefully adjusted. Thus, the growth of numerous calibration samples is required and this trial-and-error approach is both time- and money- consuming. A new, efficient method was therefore searched for. Our investigations were published in [Delorme-2018].

The experiments presented in this part were not carried out during the same growth campaign as the samples of parts 2.2 and 2.4. Therefore, some differences can be noticed, in particular regarding the BEPs.

2.3.1 Reflection high-energy electron diffraction (RHEED)

RHEED is a useful *in-situ* monitoring tool in MBE giving information on the surface structure and quality, growth rates and temperature.[1] Our RHEED setup is composed of a 12 keV electron gun providing a high energy electron beam at grazing incidence angle (< 3°) to the substrate surface. The incident electrons are diffracted and reflected by the surface of the substrate and then collected on a phosphorus screen (Fig. 2.7). The image is then recorded by a camera connected to a computer and the "KSA" software is used to display and process the data.
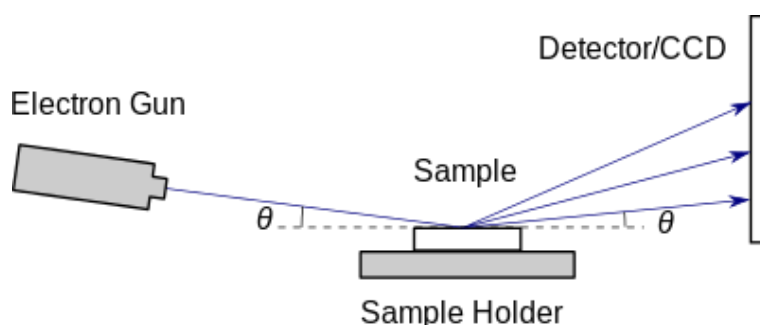
Fig. 2.7: Schematic representation of a typical RHEED setup.

---

[1] The surface reconstructions can be modified by the growth conditions (temperature and fluxes). For instance, The typical (1 x 3) pattern obtained in the case of a high quality GaSb changes to a (2 x 5) pattern for sample temperatures lower than 415°C when exposed to a Sb flux corresponding to a maximum incorporation rate of 1 ML/s [Bracker-2000]. This (1 x 3) – (2 x 5) transition was used to calibrate our optical pyrometer.

In addition, RHEED intensity oscillations allow a fast and accurate determination of the growth rate, *i.e.* of the thickness of material deposited in one second. The growth rate is directly related to the incorporation rate of the elements composing the material, which also depends on the flux of atoms used during the growth. What we call flux corresponds to the total impinging atoms per time and area units. They are not all necessarily incorporated, due to desorption or segregation for example. In fact, depending on their properties, the species react differently on the surface. Regarding III-V alloys, group-V elements have a higher vapor pressure than group-III elements. Group-V species in excess can thus desorb from the surface at a lower temperature. On the contrary, at usual growth temperatures, group-III elements have a sticking coefficient close to 1, and atoms in excess would form clusters on the surface (Fig. 2.8b top panel). III-V alloys are therefore usually grown in excess of group-V species (V/III flux ratio > 1) to ensure a high material quality (Fig. 2.8a top panel). In that case, the growth rate is limited by the flux of group-III elements and the RHEED oscillations are induced by the group-III elements (Fig. 2.8a bottom panel). Our group-III (Al, In, Ga) cells were calibrated using this method, as usual in the growth of III-V compounds. Similarly, the relationship between the group-V species flux and the corresponding incorporation rate can be measured by using a slight excess of group-III elements (V/III flux ratio < 1) (Fig. 2.8b bottom panel). In this case, the growth is limited by the group-V species and the amplitude of the RHEED intensity oscillations is much weaker due to the rapid increase of the surface roughness caused by the formation of Ga droplets. In the following, the wording "maximum incorporation rate" of an element is the growth rate measured by RHEED oscillations when this element is the limiting specie of the growth. For instance, let us consider growing a III-V alloy in standard conditions, *i.e.* in excess of group-V atoms, at 1 ML/s with a V/III ratio of 2. The growth is limited by the group-III elements, both group -III and -V species incorporate at 1 ML/s and the growth rate is the maximum incorporation rate of the group-III elements. In contrast, the maximum incorporation rate of the group-V species is 2 ML/s and it ensures the excess of group-V elements at the surface. In this example, the difference between the actual growth rate (1 ML/s) and the maximum incorporation rate (2 ML/s) of the group-V species is desorbed. Conversely, when growing a III-V compound under an excess of group-III element, the growth rate is the maximum incorporation rate of the group-V species, whereas the maximum incorporation rate of the group-III elements is larger. In that case however, the group-III elements excess, *i.e.* the difference between the maximum incorporation rate and the actual growth rate, does not desorb but accumulates on the surface.
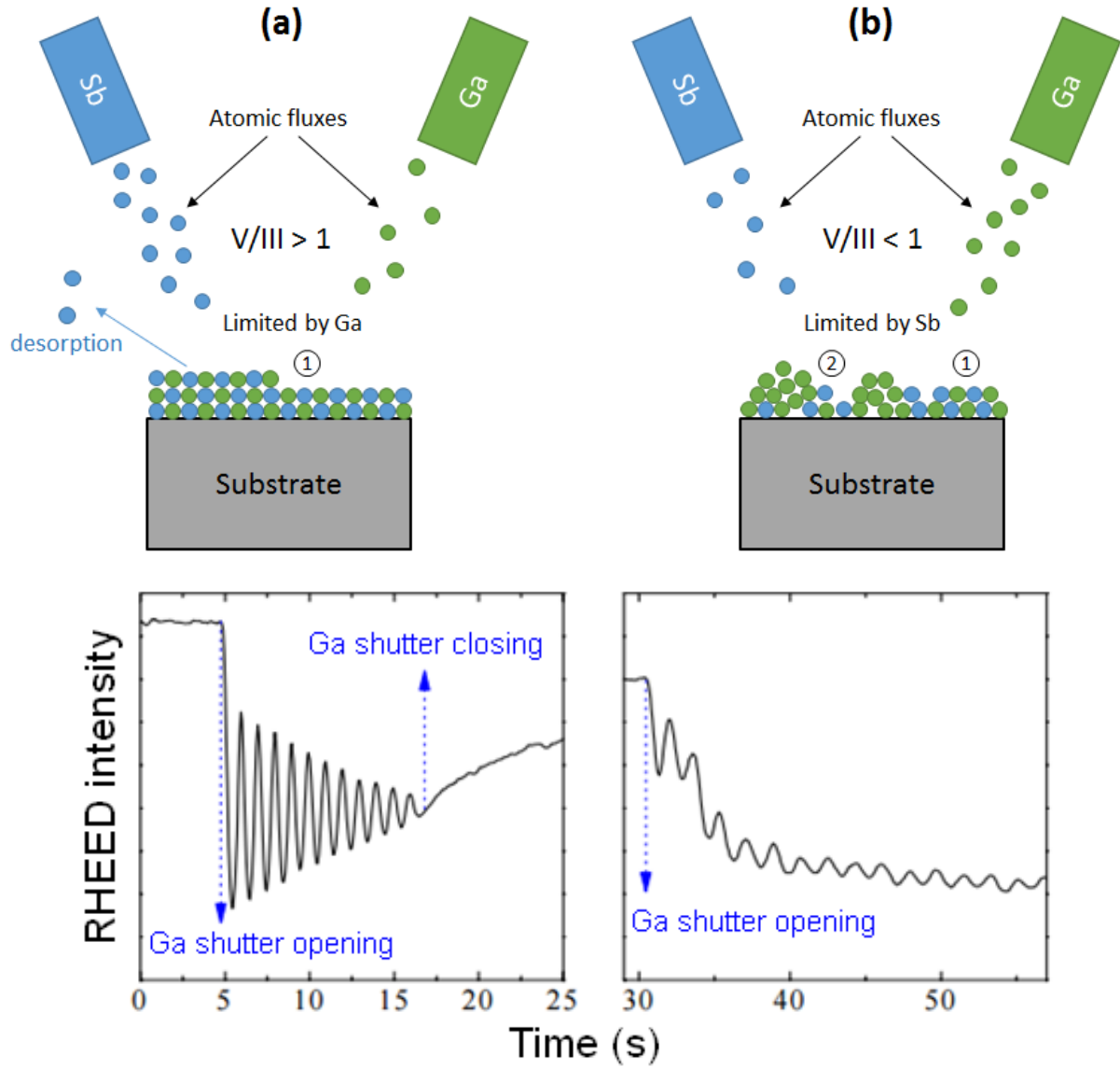
Fig. 2.8: Schematic representation of the epitaxy of GaSb in Sb-rich (V/III flux ratio $\geq$ 1) (a) and Ga-rich (V/III flux ratio < 1) conditions and their associated RHEED intensity oscillations. ① Incorporation of the impinging atoms and formation of Ga-Sb bonds. ② Formation of Ga clusters due to the excess of group-III elements at the surface. The thermal desorption of Sb is depicted by the blue arrow in the upper pannels.

Interestingly, during the growth of GaSbBi, the V/III ratio has to be set very close to stoichiometry. In these conditions, a slight change of any of the fluxes may change the nature of the limiting element (III or V) and cause a variation of the final growth rate. In particular, the growth rate is expected to be different with and without Bi (for given Ga and Sb fluxes) because, in the latter case, the V/III ratio falls below unity, which results in a lower growth rate. Therefore, the comparison between the GaSb and the GaSbBi growth rates could in principle allow for a direct observation of Bi incorporation.

However, one might expect that the very low temperatures required for the growth of III-V-Bi make the observation of clear RHEED intensity oscillations challenging. Nevertheless, RHEED oscillations have been reported during the growth of GaAsBi at 345°C, allowing *in-situ* measurements of the alloy growth rate [Tominaga-2008]. In our case, we have observed strong intensity oscillations for both GaSbBi and GaSb, allowing an accurate and reproducible measurement of the growth rate. Fig. 2.9 shows an example of RHEED intensity oscillations recorded during the growth of both GaSbBi and GaSb at 200°C TTR, using Sb and Bi BEPs of 2.3×10^{-7} and 1.2×10^{-8} Torr, respectively. The Ga flux was also kept constant for the two alloys. Although the total group-V fluxes are different (due to the Bi flux), very similar growth rates (± 0.003 ML/s) are obtained in both cases. It means that the RHEED intensity oscillations are not induced by the group-V species but that the growth rate is instead limited by the Ga flux for both materials. We can therefore conclude that the (Sb+Bi)/Ga and Sb/Ga ratios are both larger than unity in this example.
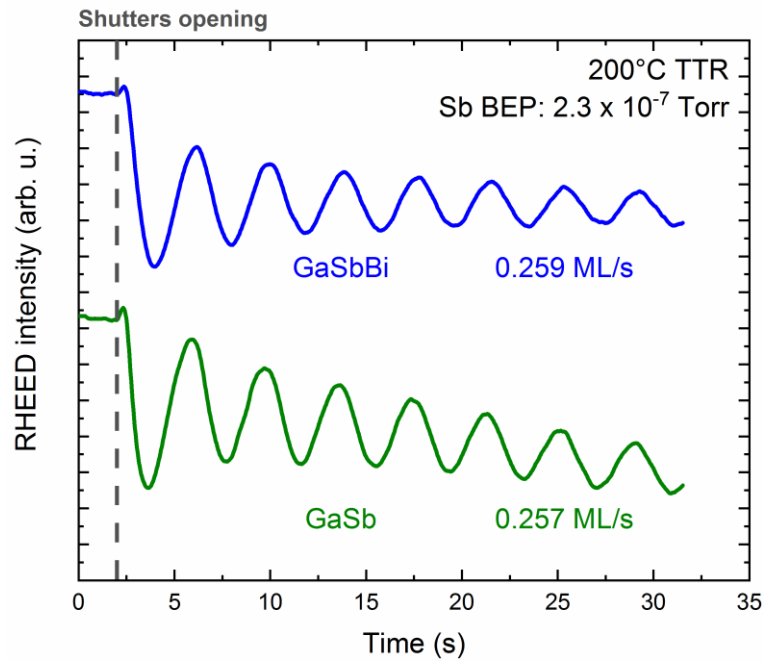
Fig. 2.9: RHEED intensity oscillations measured during the growth of GaSbBi and GaSb alloys using an Sb BEP of 2.3×10^{-7} Torr. The Ga flux was also fixed. In the case of GaSbBi, the Bi BEP was set at 1.2×10^{-8} Torr.

In the next paragraphs, we demonstrate that monitoring RHEED intensity oscillations allows much more than just measuring the growth rate.

2.3.2 Optimization of the V/III flux ratio

As described previously in this chapter, the V/III flux ratio is a critical parameter for the successful growth of GaSbBi alloys. The usual way to set the growth conditions thus consists of first adjusting the Ga and Bi flux to get the desired growth rate and Bi content, and then to grow series of samples with slight variations of the Sb flux in order to determine the optimum V/III ratio.

To demonstrate the possibility of using RHEED oscillations for adjusting the Sb flux, three sets of measurements corresponding to three Bi fluxes, were carried out at a TTR of 200°C and various Sb fluxes. Then, 100-nm thick GaSbBi layers were grown using the parameters determined from RHEED to confirm the reliability of this measurement for the epitaxy of thick layers. The Bi BEP for each set of measurements was fixed to 1.2×10^{-8} (set A), 2.4×10^{-8} (set B) and 3.5×10^{-8} Torr (set C), corresponding respectively to Bi contents of ~ 4, 8 and 12% (using optimized Sb flux and growth temperature for the considered Ga incorporation rate). The Ga incorporation rate was kept constant at 0.257 ML/s for the A and B sets whereas it was 0.246 ML/s for the C series). Table 2.1 summarizes the growth conditions used for the RHEED measurements and for the growth of the subsequent GaSbBi epilayers. The Bi concentrations obtained are also indicated.

Table 2.1: Growth conditions used for the different sets of RHEED oscillations measurements and GaSbBi single layers epitaxy. The Bi concentrations measured by HR-XRD are also listed. For three samples, the Bi content could not be estimated due to the graded composition and the low crystal quality.

	RHEED oscillations		GaSbBi sample	
	Ga growth rate (ML/s)	Bi BEP (Torr)	Sb BEP (Torr)	Bi content (HR-XRD)
Series A	0.257	1.2×10^{-8}	2.00×10^{-7}	-
			2.20×10^{-7}	4.1%
			2.40×10^{-7}	2.6%
Series B	0.257	2.4×10^{-8}	1.95×10^{-7}	-
			2.15×10^{-7}	8.7%
			2.40×10^{-7}	6.3%
Series C	0.246	3.5×10^{-8}	1.75×10^{-7}	-
			1.90×10^{-7}	12.3%
			2.10×10^{-7}	11.4%
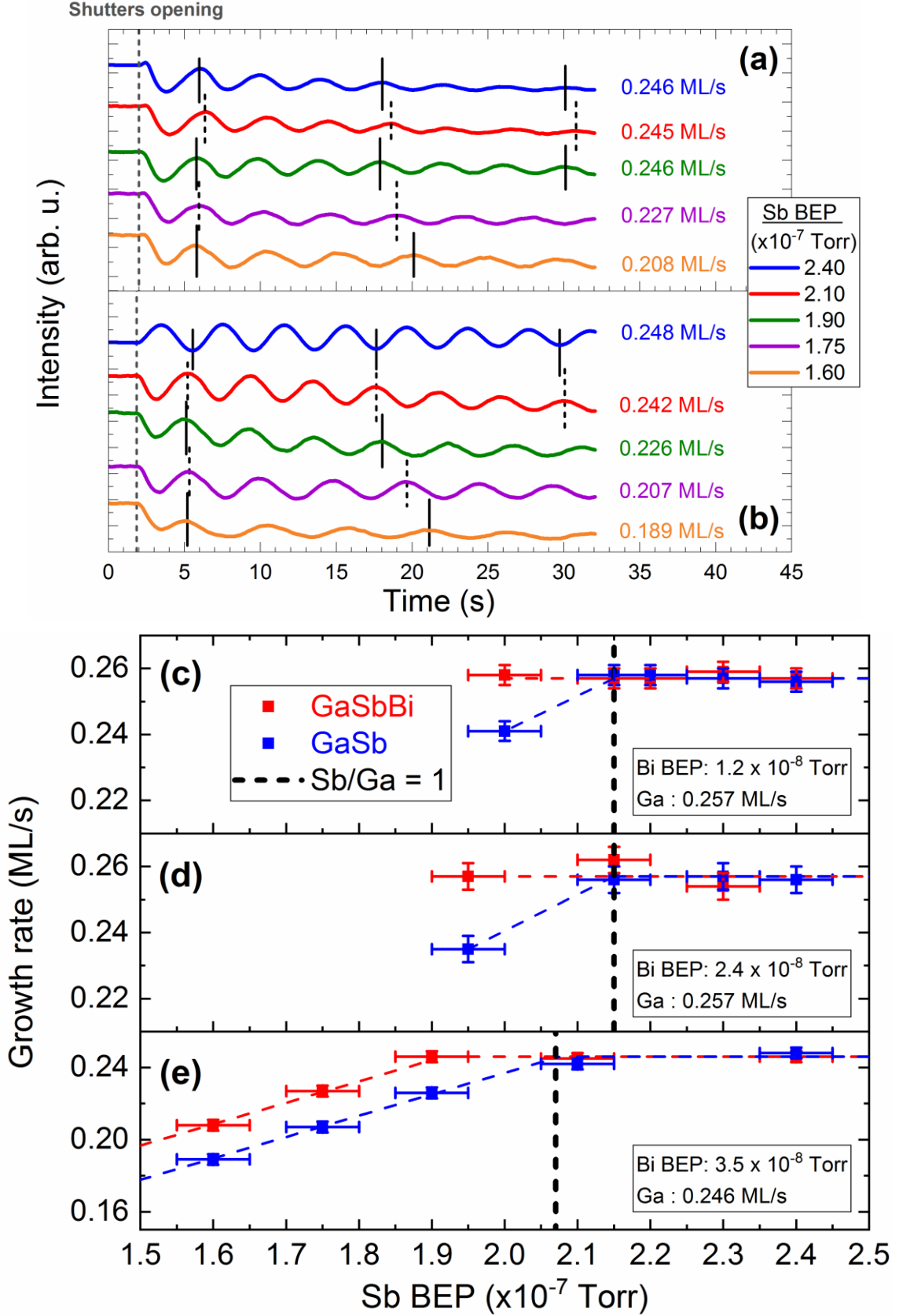
Fig. 2.10: RHEED oscillations recorded for GaSbBi (a) and GaSb (b) grown at 200°C TTR as a function of the Sb flux, for a Bi BEP of 3.5 x 10⁻⁸ Torr, and fixed Ga flux. The curves have been vertically shifted for clarity, and black lines are a guide for the eye. GaSbBi and GaSb calculated growth rates as a function of the Sb flux using fixed Bi BEPs of 1.2 x 10⁻⁸ Torr (c), 2.4 x 10⁻⁸ Torr (d) and 3.5 x 10⁻⁸ Torr (e). Each data point is the average of several measurements.

Fig. 2.10 a and b show the RHEED oscillations recorded during the growth of GaSbBi for the C series (Bi BEP of 3.5×10^{-8} Torr) and for GaSb, respectively. Very similar set of curves were obtained for the two other Bi BEPs but are not presented here for sake of conciseness. The GaSbBi and GaSb growth rates calculated from the RHEED oscillations for each Bi BEP are shown as a function of the Sb flux in Fig. 2.10 c, d and e. Different regimes can be seen on the two first set of curves (Fig. 2.10 c and d):

-   For Sb BEPs larger than $\sim 2.15 \times 10^{-7}$ Torr, the growth rate does not significantly evolve with the Sb flux, and is similar for GaSb and GaSbBi, confirming that the Ga incorporation rate is the limiting mechanism in both cases.

-   When the Sb BEP falls below 2.15×10^{-7} Torr, damped oscillations were recorded during the growth of GaSb and the growth rate decreased with the Sb BEP, clearly indicating an Sb induced growth. However, the oscillations recorded at the same Sb BEP during GaSbBi growth were comparable to the ones obtained at higher Sb flux, revealing a (Sb+Bi)/Ga flux ratio larger or very close to 1. In this regime, the element limiting the growth rate is therefore different for GaSb and GaSbBi.

-   Finally, for Sb fluxes smaller than $\sim 1.95 \times 10^{-7}$ Torr, the RHEED intensity decreased quickly and no oscillation could be measured during either growth, certainly due to excess Ga on the surface.

The same different regimes could also be observed in the case of the highest Bi BEP (3.5×10^{-8} Torr, Fig 2.10e), but interestingly, oscillations could also be recorded for GaSbBi even for the group-V limited case, occurring for Sb BEPs lower than 1.90×10^{-7} Torr.[2] The larger number of data for the growth with excess Ga allows to linearly fit the evolution of the growth rate with the Sb BEP for both GaSbBi and GaSb (Fig. 2.10e). As expected, the slope for the two lines is the same because the growth rate variation is only induced by the variation of the Sb BEP, with the same impact for both alloys. The difference between GaSbBi and GaSb growth rates at a given Sb BEP is thus constant and found to be equal to about 0.019 ML/s. It is important to remember that in this regime, the growth rate is limited by the group-V elements in both cases (Sb or Sb+Bi), therefore for a constant Sb BEP, this difference unambiguously corresponds to the Bi incorporation rate. However, 0.019ML/s represents only 7.7% of the Ga incorporation rate (0.246 ML/s), which is significantly lower than the expected $\sim 12\%$ Bi found from HR-XRD scans from epilayers grown using the same Bi and Sb BEPs (Table 2.1). The discrepancy between the Bi content measured by HR-XRD and the RHEED technique (12.3 and 7.7% respectively) seems to corroborate the fact that a lower Bi incorporation rate occurs during the first nanometers of

---

[2] In this case, the Sb BEP for which Sb/Ga rate ratio is unity is 2.07×10^{-7} Torr, slightly lower than for previous sets due to the slightly lower value of the Ga rate.

the growth, in agreement with some previous reports [Fan-2013, Makhloufi-2014]. However, this point is still subject to discussion since both experimental [Reyes-2014, Tait and Millunchick-2016] and theoretical studies [Rodriguez and Millunchick-2016] have also reported an initial higher Bi incorporation. Further work is therefore needed to clarify the situation.

These observations clearly indicate that RHEED oscillations can be used despite the very low growth temperature to finely adjust the Sb flux to the chosen Ga rate and Bi content. To confirm the possibility to use these data for setting the growth conditions of GaSbBi alloys, layers were grown using different Sb fluxes and the three Bi BEP used before. Fig. 2.11 a and b show the ω-2θ scans measured on the (004) reflection for the samples grown with the two highest Bi BEP (B and C sets). With a Bi BEP of 2.4×10^{-8} Torr, the sample grown with an Sb/Ga flux ratio of one (Sb BEP of 2.15×10^{-7} Torr) is droplet free, and *Pendellösung* fringes are clearly visible on the corresponding HR-XRD scan, attesting the high material quality of the film. The Bi content extracted from this measurement is about 8.7%. A smaller Sb BEP (1.95×10^{-7} Torr, Sb/Ga ratio = 0.91), resulted in a graded Bi composition and the absence of *Pendellösung* fringes indicates a low crystal quality. Moreover, optical microscopy observation shows a surface covered by droplets. The same droplets were observed on the surface of the sample grown with the highest Sb BEP to 2.40×10^{-7} Torr (Sb/Ga ratio of 1.12). *Pendellösung* fringes are still visible, but not as well defined as for the previous sample, and the Bi concentration decreased to 6.3%. This reduction of the Bi content can be ascribed to an excess of Sb preventing Bi incorporation, as described in paragraph 2.2.2. The best sample from this set appears to be the one grown with an Sb BEP of 2.15×10^{-7} Torr, which corresponds, according to Fig. 2.10d to an Sb/Ga ratio of one and therefore an overall V/III ratio slightly larger than unity. The same result arises from the samples grown with the highest Bi BEP (3.5×10^{-8} Torr), with an optimum Sb/Ga rate ratio close to 0.9 (Fig. 2.10e) resulting again in an overall (Sb+Bi)/Ga flux ratio slightly above unity. In this case however, due to the large Bi flux, droplets are visible on the three samples of series C (Bi BEP: 3.5×10^{-8} Torr). But the sample grown with the Sb BEP of 1.90×10^{-7} Torr shows the lowest density (Fig. 2.11 c, d and e), in good agreement with HR-XRD data.
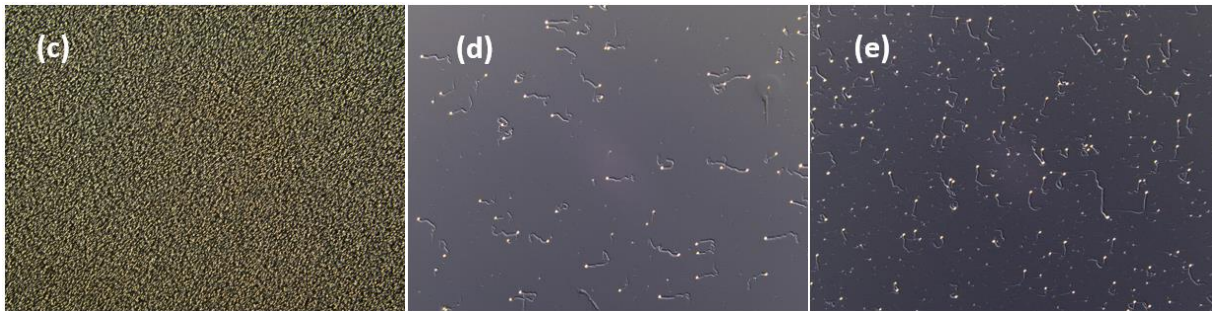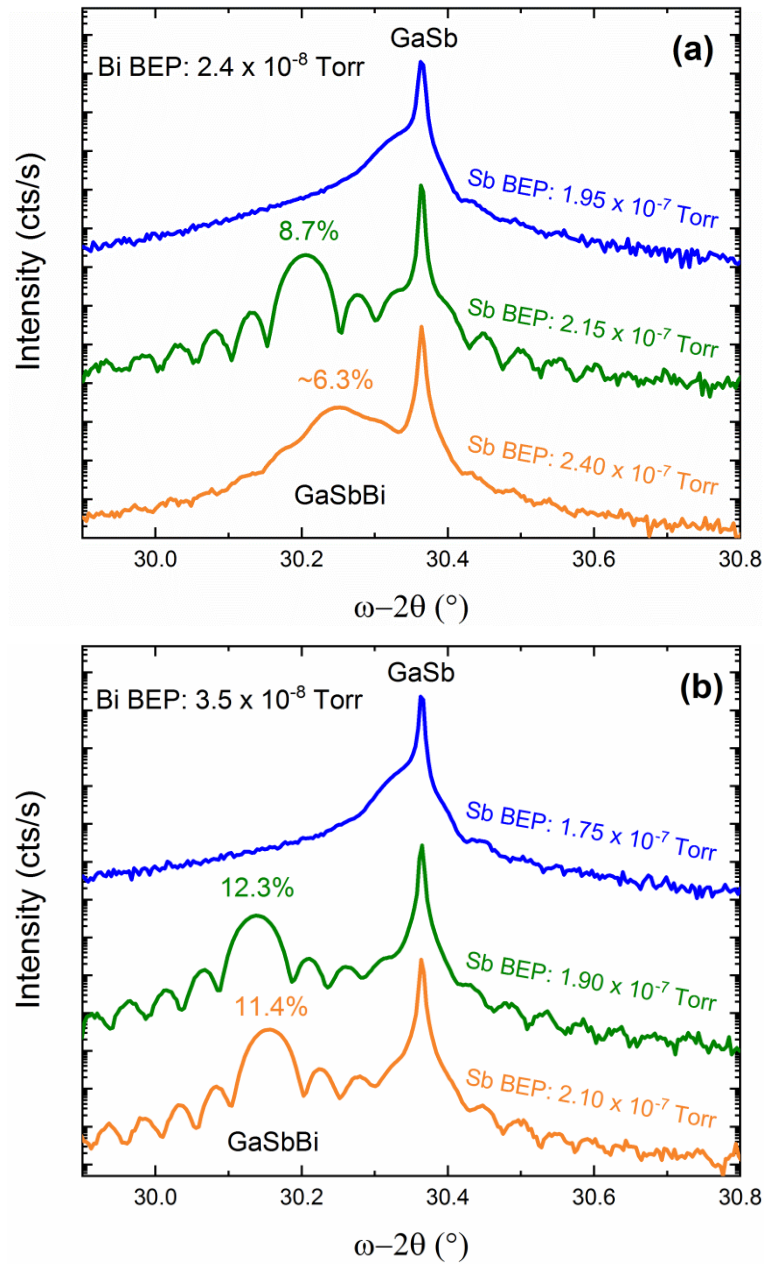
Fig. 2.11: HR-XRD scans of the 004 Bragg reflection of 100-nm thick 120GaSbBi films grown at 200°C TTR using different Sb fluxes and Bi BEPs of 2.4 x 10^{-8} Torr (a) and 3.5 x 10^{-8} Torr (b). Optical microscope images (600 x 400 µm) of the surface of the GaSbBi samples grown with a fixed Bi BEP of 3.5 x 10^{-8} Torr and Sb BEPs of (c) 1.75 x 10^{-7} Torr, (d) 1.90 x 10^{-7} Torr, (e) 2.10 x 10^{-7} Torr.

2.3.3 Determination of the optimal growth temperature for the incorporation of Bi

The other critical parameter for the incorporation of Bi is the substrate temperature. As mentioned above, the substrate temperature for GaSbBi growth is not measurable by standard pyrometer and is therefore particularly challenging to set. Indeed, we have verified that the TTR is reproducible during a whole growth campaign. But we also observed that the TTR could change after a maintenance of the MBE system. Therefore, a set of samples is grown after each maintenance to determine the optimal temperature of GaSbBi. Moreover, the TTR is not a value transferable from one MBE system to the other. In the following, we demonstrate that it is possible to use RHEED intensity oscillations to overcome this difficulty, taking advantage from the observation made earlier that the growth rates of GaSbBi and GaSb are different below or very close to the Ga-Sb stoichiometry, due to the incorporation of Bi.

Starting at low temperature, where Bi is incorporated, the Sb BEP is first set such that the (Sb + Bi) atomic flux is just slightly larger than the Ga flux. In this case, the growth rate measured by RHEED oscillations corresponds of course to the Ga maximum incorporation rate. The temperature is then increased, leading at some point to a decrease of the Bi incorporation rate, following the trend shown in Fig. 2.4b. Increasing the temperature therefore gradually changes the group-V elements maximum incorporation rate from a value corresponding to the (Sb+Bi) flux, to a value corresponding to the Sb flux only because no more Bi atom is incorporated. In this very specific situation, where (Sb+Bi)/Ga > 1 > Sb/Ga, this translates into the fact that the V/III ratio eventually becomes smaller than one, giving rise to a group-V limited growth. As a result, the measured growth rate should decrease as the temperature increases and eventually reach a constant value corresponding to the Sb maximum incorporation rate. Therefore, by setting the Sb BEP at a value where the GaSbBi growth rate is limited by the Ga incorporation while it is limited by the Sb incorporation for GaSb, it should be possible to clearly measure the decrease of the Bi incorporation when the substrate temperature is increased. For a better understanding, we have modeled in Fig. 2.12 the variation of the GaSbBi growth rate as a function of the temperature using the kinetic approach described by Wood *et al.* [Wood-1982] and Pan *et al.* [Pan-2000], the same values as the ones used previously in paragraph 2.2.1 for desorption energy barrier and surface residence lifetime (1.75 eV and 6.5 µs respectively), a Ga growth rate of 0.25 ML/s and a maximum Bi content of 10%. This contour plot illustrates that by choosing a Sb/Ga flux ratio slightly below unity (0.9 in this example), the growth rate evolves with the substrate temperature, reflecting the evolution of the Bi incorporation.
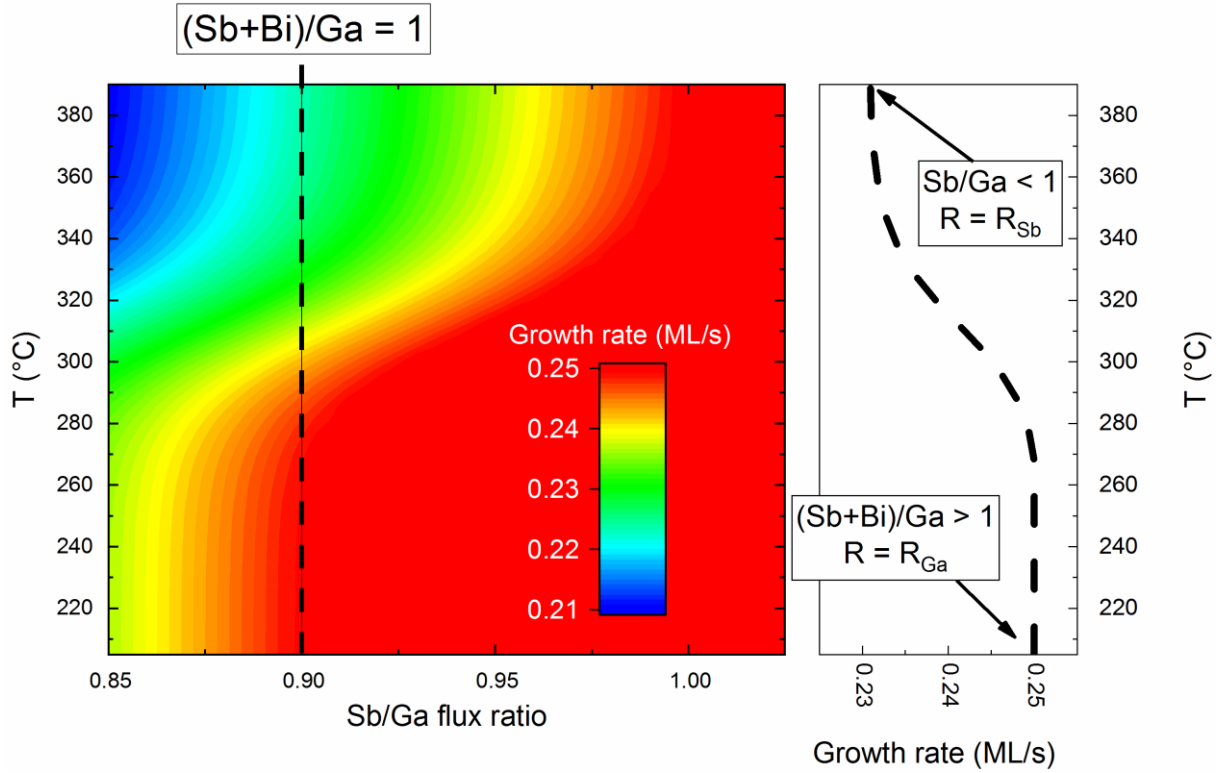
Fig. 2.12: Illustration of the variation of the GaSbBi growth rate as a function of the Sb/Ga flux ratio and temperature and the growth temperature, for a Ga maximum incorporation rate of 0.25 ML/s and a Bi flux corresponding to a maximum incorporation of 10%. The graph on the right panel is the line profile extracted from the contour plot for an Sb/Ga flux ratio of 0.9 (corresponding to a (Sb+Bi)/Ga ratio of one). The decrease of the Bi incorporation caused by the increase of the growth temperature results in a variation of the overall growth rate which can be measured by RHEED.

In order to demonstrate this, we recorded RHEED intensity oscillations during the epitaxy of GaSbBi and GaSb at an initial TTR of 200°C. The Ga incorporation rate was fixed at 0.255 ML/s and the Bi BEP was slightly larger than the one used for the last set of RHEED oscillations measurements (3.7 x 10^{-8} Torr). The Sb flux was reduced until different growth rates for GaSbBi and GaSb could be noticed. For an Sb BEP of 2.0 x 10^{-7} Torr, the GaSb growth rate decreased to 0.240 ML/s while the GaSbBi growth rate remained constant at 0.255 ML/s. Keeping constant this Sb flux, the GaSbBi growth rate was then measured as a function of the growth temperature, from 170 to 320°C TTR (Fig. 2.13a). As expected, the GaSbBi growth rate decreased from 0.256 ML/s at 170°C to 0.239 ML/s at 300°C TTR, clearly showing the reduction of the Bi incorporation rate with the increase of the temperature. At 300°C TTR, the GaSbBi growth rate was almost equal to the GaSb growth rate measured at 200°C TTR and it can thus be considered that there is no more Bi incorporation at 300°C TTR. The influence of the temperature on the Bi incorporation is similar to those observed in paragraph 2.2.1 and was fitted using the same formula (Fig. 2.13b). The very same parameters previously determined from the evolution of the Bi content in GaSbBi calculated by HR-XRD [Rajpalke-2013, Delorme-2017a] could be

used (desorption energy barrier of 1.75 eV and surface residence lifetime of 6.5 µs), which validates the methodology employed, and confirms that RHEED is a powerful technique to determine the optimum growth temperature of GaSbBi, with the added benefit of using only one sample and a limited number of oscillations measurements.

In conclusion, these experiments demonstrate that the critical parameters for the growth of GaSbBi alloys can be determined efficiently and accurately by RHEED intensity oscillation measurements, despite the very low growth temperatures used. This new method could also be useful for other III-V-Bi alloys and help to overcome the growth difficulties caused by the challenging Bi incorporation.
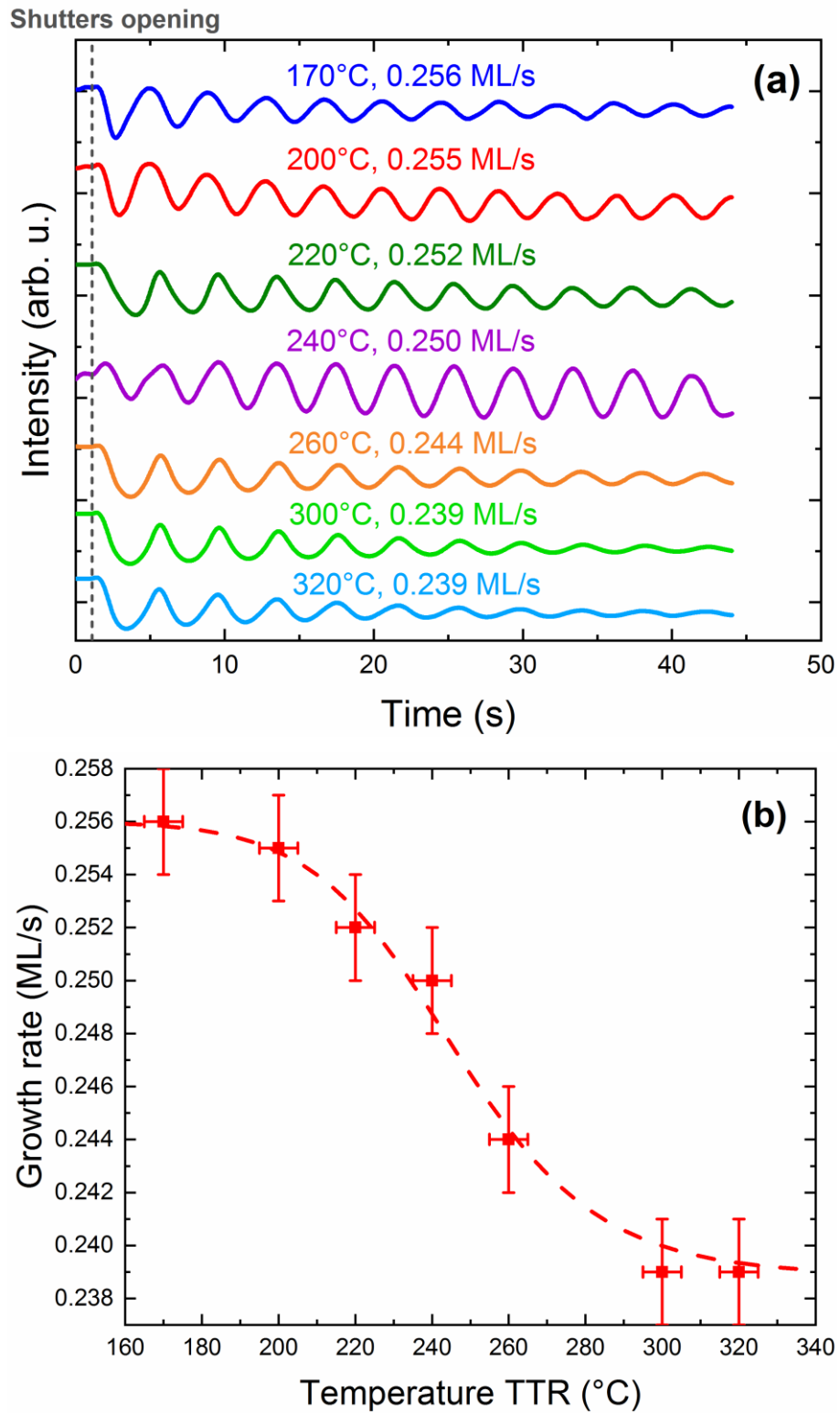
Fig. 2.13: (a) RHEED oscillations from GaSbBi grown at different temperatures using fixed fluxes (Sb BEP: 2.00 x 10^{-7} Torr, Bi BEP: 3.7 x 10^{-8} Torr). The calculated growth rates are indicated for each curve. The curves have been vertically shifted for clarity. (b) GaSbBi growth rate calculated from the RHEED oscillations as a function of the growth temperature. The dashed line was calculated using a kinetic model.

2.4   High Bi content GaSbBi layers

Once the critical parameters for the growth of GaSbBi were identified and determined in our MBE system, the next objective was to reach high Bi concentrations. It was shown in the paragraph 2.2.3 that the Bi content increases linearly with the Bi flux, but droplets form as the V/III ratio is not stoichiometric anymore. The following paragraphs describe our attempts to reach high Bi concentrations while preventing the formation of droplets to maintain a high crystallographic quality. A maximum Bi content of 14 % was obtained in the end. The optical and structural properties of our high Bi-content GaSbBi epilayer are characterized in details. Finally, a preliminary study of the droplets is also presented.

2.4.1 Attempts to increase the Bi content

In paragraph 2.2.3, a Bi content of 11.3% was obtained thanks to an increase of the Bi flux to 4.5×10^{-8} Torr. However, due to a non-stoichiometric V/III flux ratio, a degradation of the crystal quality and the formation of droplets were observed. To avoid this, the Sb flux must be carefully adjusted to maintain a near-stoichiometric V/III flux ratio. By decreasing the Sb BEP to $\sim 2.5 \times 10^{-7}$ Torr while keeping the Bi BEP at $\sim 4.5 \times 10^{-8}$ Torr, we managed to obtain a droplet free GaSbBi layer with 11.4% Bi (measured by RBS). This is the highest Bi concentration ever reported for a droplet free GaSbBi sample [Delorme-2017a]. The simulated HR-XRD curve agrees very well with the experimental one, and no damping of the *Pendellösung* fringe can be noticed for this sample (Fig. 2.14a). The surface RMS roughness measured by AFM is below 0.2 nm, with clearly visible atomic steps (Fig. 2.14b). TEM measurements show a homogeneous layer without any dislocation, extended defect, composition modulation (CMs) or clustering (Fig. 2.14c). Additionnaly, this GaSbBi sample demonstrated PL emission at RT near 2.8 µm, showing the significant bandgap reduction caused by the Bi incorporation (Fig. 2.14d).
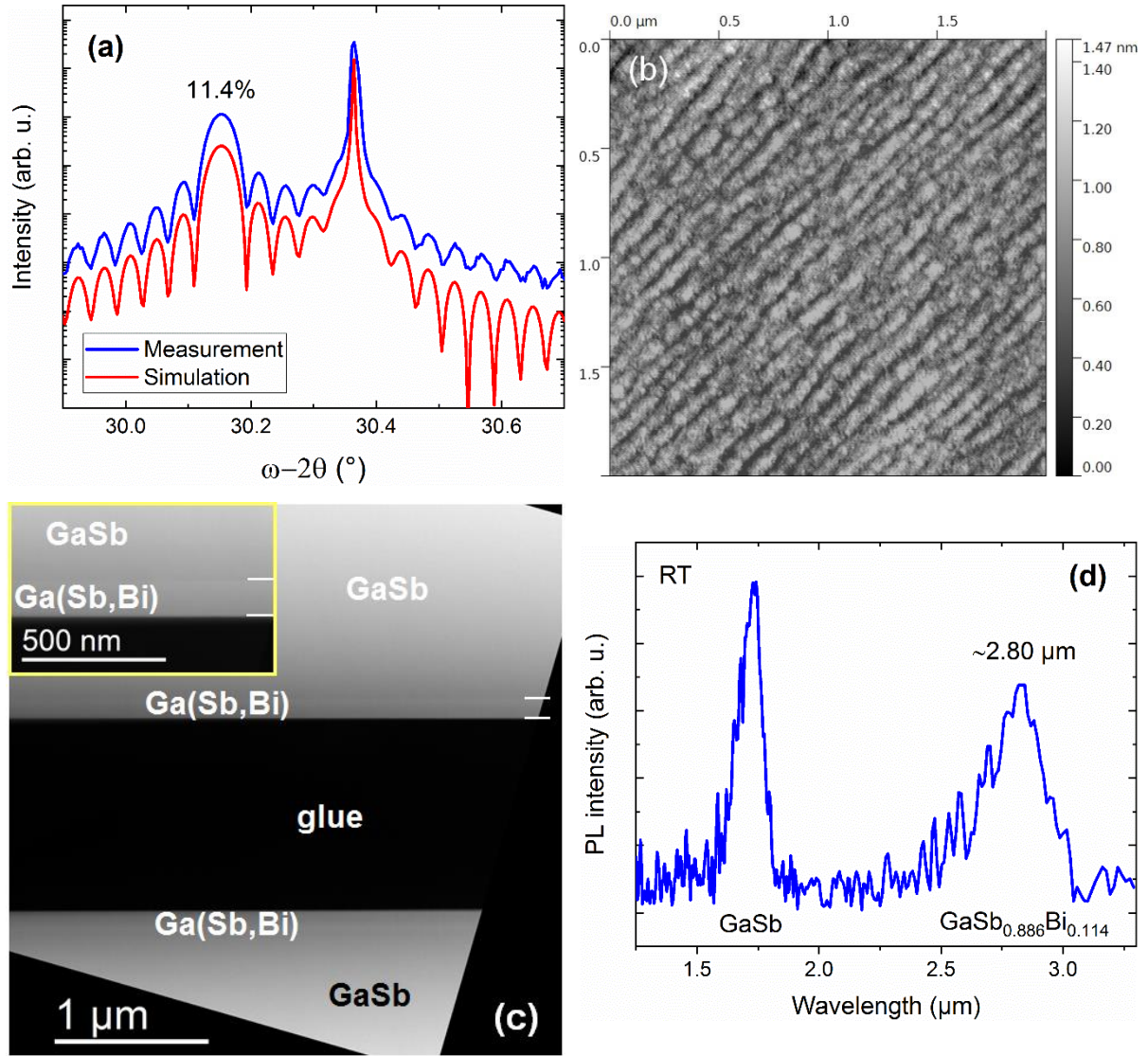
Fig. 2.14: Study of the 120-nm thick GaSbBi epilayer with 11.4% Bi. (a) and (b) represent the HR-XRD scan (measurement in blue, simulation in red) and the surface observed by AFM, respectively. (c) is a HAADF overview image and the inset was taken at higher magnification. (d) shows the photoluminescence emission at RT.

The high crystal quality demonstrated by the sample with 11.4% Bi encouraged us to further increase the Bi flux. Unfortunately, our attempts to reach higher Bi concentrations systematically resulted in the formation of droplets, despite a careful adjustement of the Sb flux. Indeed, the flux range allowing a droplet free growth and a high material quality tends to shrink as the Bi flux and content increase. To illustrate this, a set of samples was grown with a Bi BEP of 6.0×10^{-8} Torr and various Sb fluxes, between 2.10×10^{-7} and 2.60×10^{-7} Torr (Fig. 2.15). The layer grown with an Sb flux of 2.25×10^{-7} Torr is the best of the series. A Bi concentration of 14% was measured by RBS, the highest Bi content reported in GaSbBi alloys to date [Delorme-2017a]. Despite the very high Bi composition, *Pendellösung* fringes are still visible on the HR-XRD scan, attesting a satisfactory crystal quality.

However, changing the Sb BEP by as little as 0.15 x 10^{-7} Torr, leads to a dramatic degradation of the overall quality. Indeed, the other samples of this series exhibit a surface covered by a high density of droplets and an inhomogeneous composition. The extreme sensitivity to the Sb flux found for these layers illustrates well the difficulty to achieve the growth of GaSbBi with high Bi concentration.
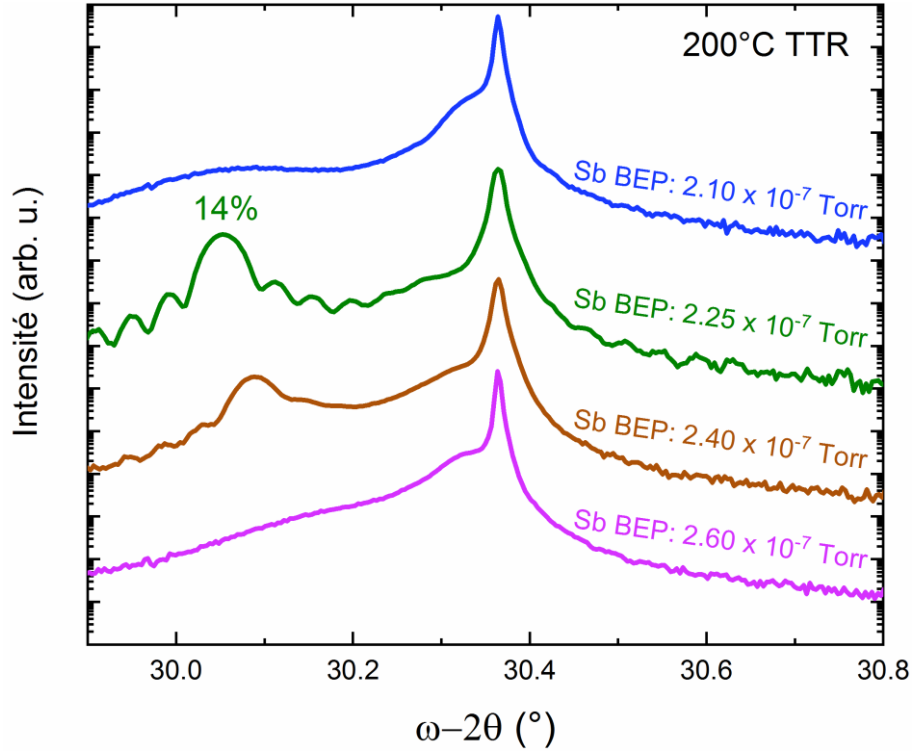
Fig. 2.15: HR-XRD scans of 120-nm thick GaSbBi layers grown at 200°C TTR with a Bi BEP of 6.0 x 10^{-8} Torr and different Sb fluxes.

In fact, a degradation of the material quality compared to samples with lower Bi content can be noticed even for the best sample from this set. Indeed, a closer inspection of the ω-2θ scans reveals that the *Pendellösung* fringes are not as well defined as with the previous sample with 11.4% Bi. Moreover, a stronger-than-expected intensity close to the substrate angle (~30.275°) seems to indicate a non-uniform distribution of Bi across the layer thickness. Additionally, a large density of droplets is observed on the surface (Fig. 2.16a). Droplet-free areas of about 50x50 µm² could however be found, and AFM scans (Fig. 2.16b) carried out in these regions showed smooth surfaces although the atomic steps were less well defined than for layers with smaller Bi content.
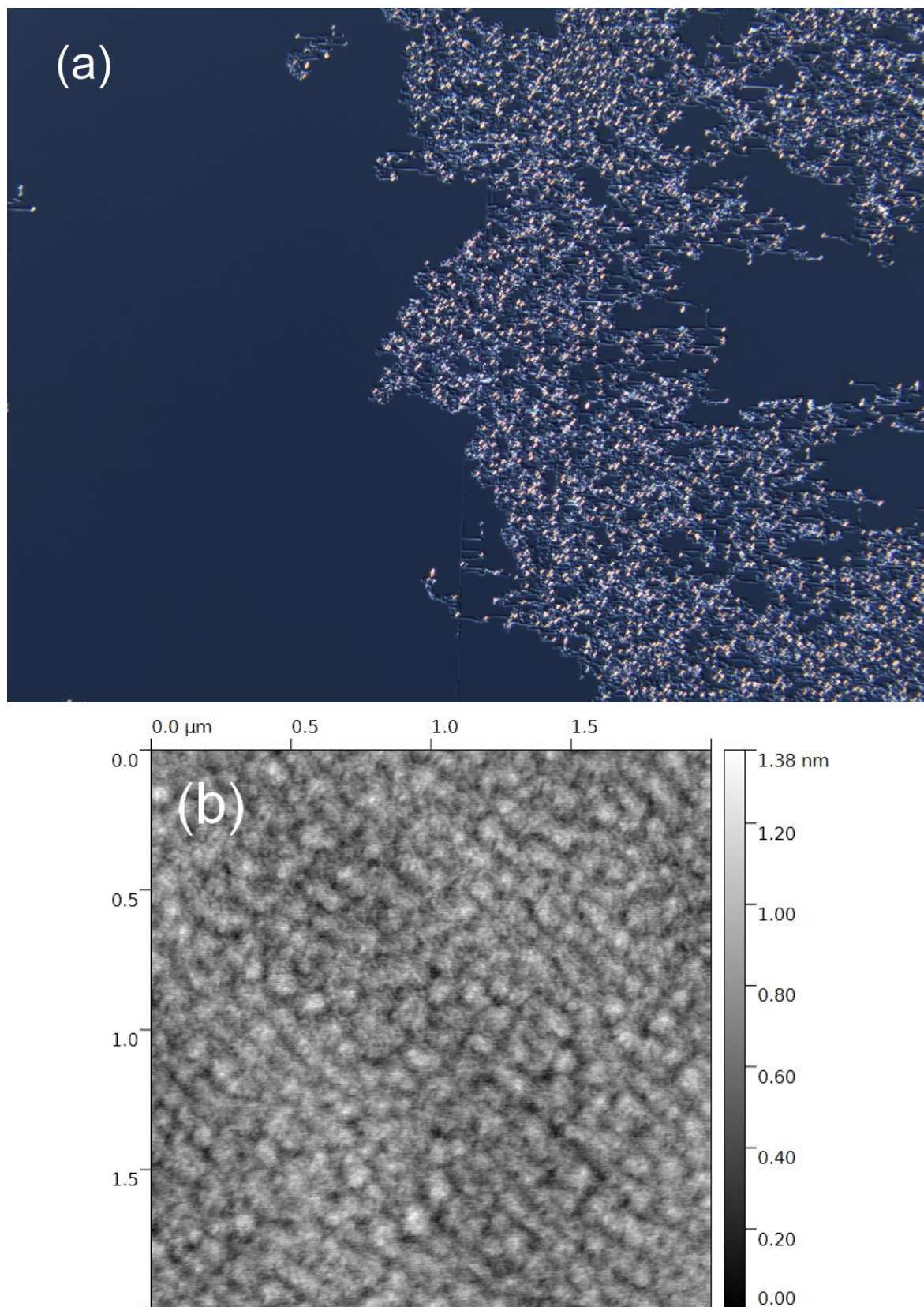
Fig. 2.16: Surface observation of the sample with 14% by (a) optical microscopy (600 x 450 µm) and AFM (b).

The lower crystal quality of the $GaSb_{0.86}Bi_{0.14}$ layer was also confirmed by RBS measurements. Fig. 2.17a shows that the lattice parameter of the layer with 14% Bi is larger than expected from the Vegard's law previously established (see Fig. 2.3, paragraph 2.1.2). This lattice expansion could be caused by point defects and interstitial atoms, as observed in GaAs layers grown at low temperature [Chen-1996]. To check this assumption, the Bi interstitial fraction was estimated by RBS channeling measurements. Fig. 2.17b shows the evolution of the Bi interstitial fraction as a function of the Bi content. An overall increase of the interstitial rate as the Bi content raises can be noticed, but the interstitial rate remains relatively low for the droplet free samples. Indeed, the Bi interstitial fraction of the GaSbBi layer with 11.4% Bi is only 2.6%, meaning that more than 97% Bi atoms are substitutionnal. On the contrary, the sample with 14% Bi has a much larger interstitial rate (10.2%), which supports well our explanation of the observed lattice constant expansion.

The narrowing of the growth conditions allowing high quality GaSbBi layers at high Bi concentrations, as well as the Bi-content threshold of ~12% for the formation of droplets, was also reported recently by Hilska *et al.* [Hilska-2019]. The systematic formation of droplets for Bi content higher than 12% raises questions. The first possibility is that this general degradation of the crystal quality could be caused solely by non-optimum growth conditions, and in that case, Bi concentrations as high as 20 or 30% should be achievable hypothetically by using a perfect setting of the growth conditions. However, our numerous attempts (confirmed by the similar results of Hilska *et al.*) showed that such a precision cannot be achieved experimentally using a conventional growth mode. Eventually, the use of another epitaxial technique (MOVPE, etc...) may help to overcome this issue, but the highest Bi incorporation in III-V alloys ever reported was in fact obtained by MBE [Lewis-2012]. The fact that we observe the same incorporation limit than in [Hilska-2019] probably using slightly different growth methods tends to point out a solubility limit of Bi into GaSb. Indeed, as GaBi was never successfully synthetized, a large miscibility gap between Ga and Bi is expected. In that case however, the solubility limit should allow a lower Bi incorporation in GaAs than in GaSb, as Bi is closer to Sb than to As (see below). But surprisingly, the maximum Bi concentration achieved in GaAsBi (22%) is much higher than our 14% Bi in GaSbBi. This last point could be simply explained by the fact that researches on GaSbBi lag far behind than that of GaAsBi. Futher investigations on GaSbBi are required to have a better understanding of the growth mechanisms and the potential solubility limits.
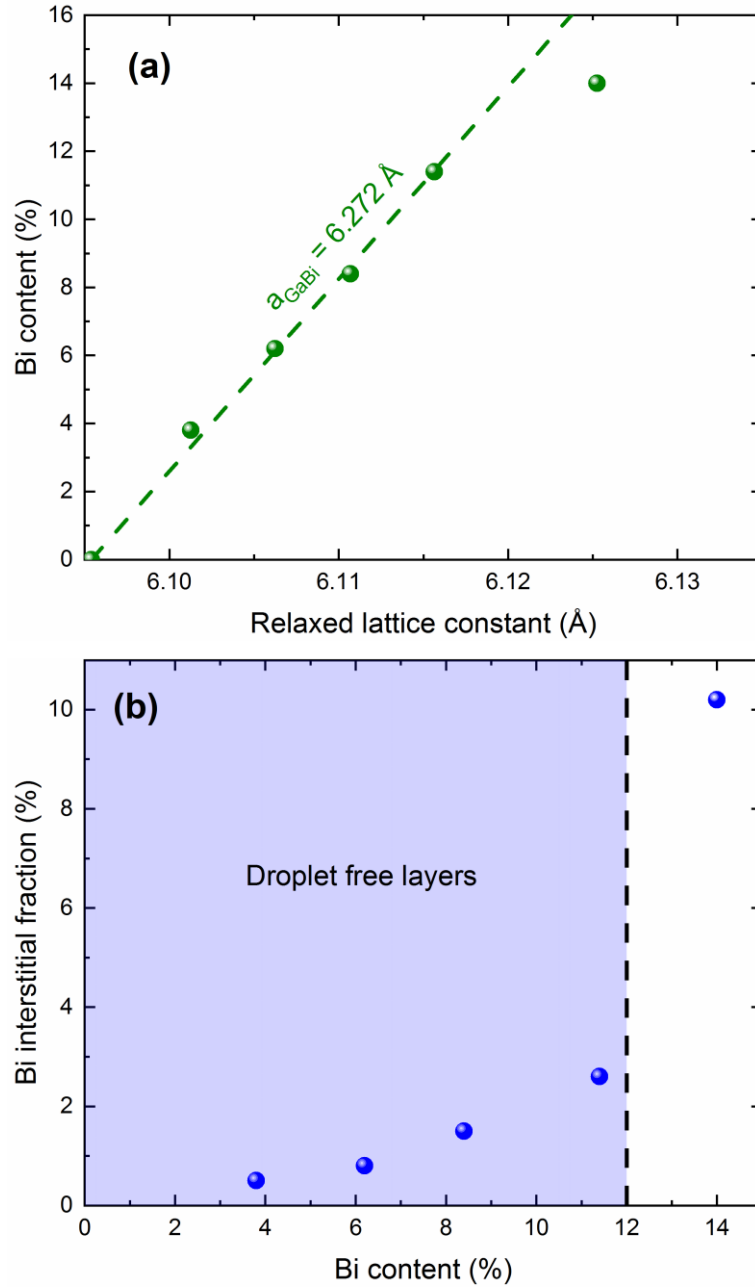
Fig. 2.17: (a) Bi concentrations measured by RBS as a function of the relaxed lattice constant extracted from HR-XRD. (b) Bi interstitial fraction as a function of the Bi content, both determined by RBS.

This sample's microstructure was carrefully studied by TEM. The following analysis was carried out at the PDI and further details are given in [Luna-2018a]. Local quantitative chemical determination from the analysis of the g_{002} diffracted intensity and using GaSb as a reference yields an average Bi content of 14.2 ± 0.8 %, in good agreement with RBS measurements. Fig. 2.18 a and b show cross-sectional g_{002} DFTEM and high-angle annular dark-field (HAADF) micrographs, respectively. The homogeneous intensity contrast in the chemically sensitive g_{002} DFTEM image suggests a homogeneous layer, where no clustering or CM are detected. Neither dislocation nor extended defect

could be observed. Similar information was provided by HAADF micrographs with so-called Z-contrast. Finally, the EDS maps in Fig. 2.18c also evidence the homogeneity of the layer, where the GaSbBi layer is well-delimited from the adjacent GaSb, as indicated by the decrease in the Sb signal and the concomitant increase in the intensity of the Bi signal.
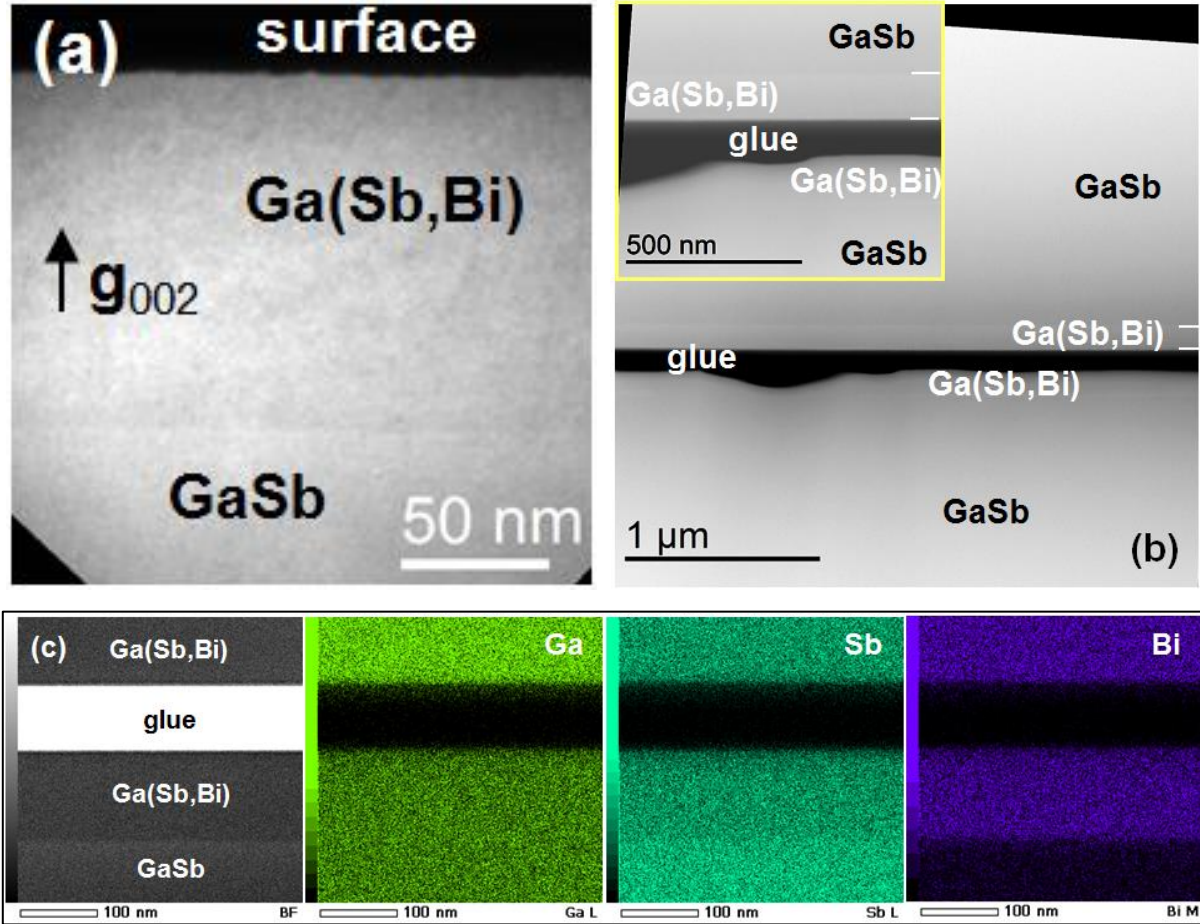
Fig. 2.18: (a) Chemically sensitive g_{002} DFTEM and (b) HAADF micrographs of the 120-nm thick GaSbBi layer with 14% Bi. The HAADF images in the insets are taken at a higher magnification. (c) Bright-field STEM image and EDS compositional map from a droplet-free uniform area.

However, the images shown in Fig. 2.19 a and b, taken in an area with surface droplets, evidence two interesting features: (i) there are local variations in the layer thickness ranging from 80 to 120 nm depending on the area; and (ii) the presence of a "two-composition layer" with a second layer of unknown composition close to the sample surface. The darker contrast of this second layer would suggest that it is Bi-depleted. On the other hand, the systematic dark and well-delimited contrast in this region, even darker than for GaSb, also points to the possibility of a layer with a different point defect density than the underlying GaSbBi. The presence of a "two-composition layer"

(or sequences of layers with different Bi contents and a morphology similar to the one detected here) has already been observed in dilute bismide epilayers in most cases in connection with the existence of Bi droplets on the surface [Steele-2016, Tait and Millunchick-2016, Wood-2016, Tait-2017, Yue-2018a]. Indeed, both features (i) and (ii) seem to correlate with the presence of surface droplets, since none of the features could be detected in the droplet free GaSbBi epilayer with 11.4% Bi (see Fig. 2.14c). However, the role of surface droplets during the growth of dilute bismides and its impact on Bi incorporation inhomogeneities are complex to understand and currently under active investigation [Duzik and Millunchick-2014, Steele-2016, Tait and Millunchick-2016, Wood-2016, Tait-2017, Yue-2018a].
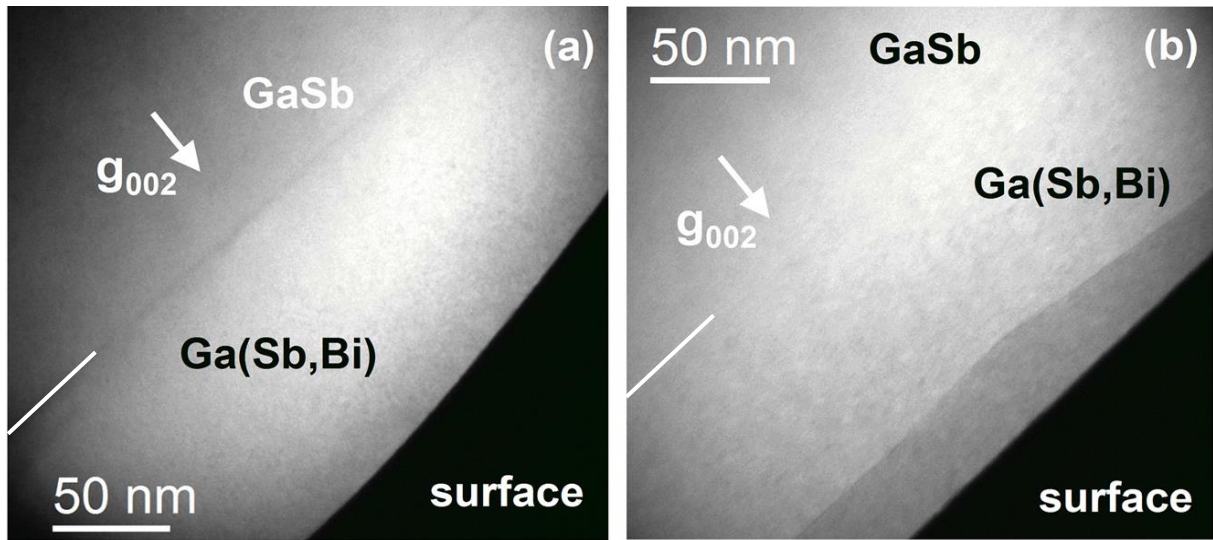
Fig. 2.19: Chemically sensitive g_{002} DFTEM micrographs of the pseudomorphic 120-nm thick GaSbBi epilayer with 14% Bi from an area with surface droplets, leading to thickness irregularities (a) and a "two-composition" layer (b).

Finally, this sample exhibited a surprisingly strong PL intensity at room-temperature (Fig. 2.20a), with a peak position at 3.8 μm ($E_{PL} \sim 325$ meV). The resulting bandgap reduction is close to 28 meV/%Bi, in good agreement with the published experimental data [Kopaczek-2013, Rajpalke-2013, Kopaczek-2014b, Rajpalke-2015, Yue-2018a] and the theoretical calculations [Polak-2014, Samajdar-2014, Polak-2015]. Water absorption is visible near 3 and 4.2 μm. The width of the PL peak is quite large, with a full-width-at-half-maximum (FWHM) close to 80 meV, which can be ascribed to a non-uniform Bi composition, or to radiative recombination on defect-related energy levels.
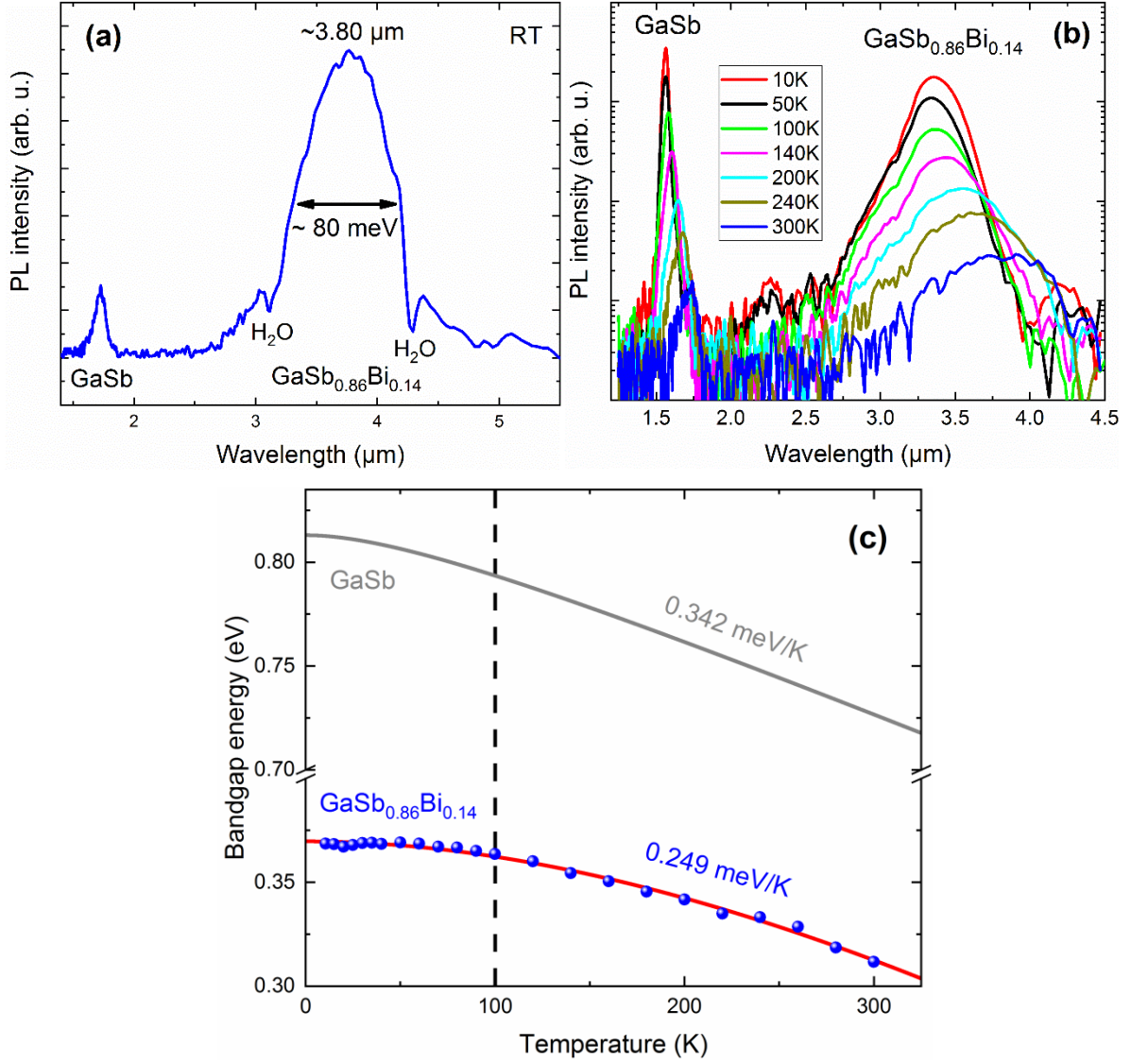
Fig. 2.20: PL emission of the 120-nm thick GaSbBi layer with 14% Bi at RT (a) and between 10 and 300 K (b). (c) Temperature dependence of the bandgap energy of GaSb$_{0.86}$Bi$_{0.14}$ layer and GaSb in the 10 - 300 K range. The bandgap energy was extracted from the PL emission peak energy using Eq. 2.3. The solid lines are the Varshni fits using Eq. 2.4.

The PL emission of this sample was studied down to 10 K (Fig. 2.20b). From the PL emission peak energy, the bandgap energy E$_G$ was extracted using the following equation:

$$E_G(T) = E_{PL}(T) - \frac{k*T}{2} \qquad (2.3)$$

where E$_{PL}$(T) is the PL emission peak energy and k is the Boltzmann's constant. The temperature dependence of E$_G$ is depicted in Fig. 2.20c. The temperature induced shift of E$_G$ of GaSb is also represented, as a comparison. The data for GaSb were taken from [Vurgaftman-2001]. As expected, E$_G$ redshifts with the increase of the temperature. Interestingly, the linear variation of E$_G$ between 100 and 300 K is weaker in the GaSb$_{0.86}$Bi$_{0.14}$ layer (-0.249 meV/K) than in GaSb (-0.342 meV/K). This result

tends to show that the incorporation of Bi makes the bandgap less sensitive to the temperature, as it has been already observed for GaAsBi [Oe and Okamoto-1998, Oe-2002, Yoshida-2003, Pettinari-2008]. Yet, this point is still under debate as contradictory results were also obtained [Francoeur-2003, Kudrawiec-2012b, Kopaczek-2013]. This point will be further discussed in Chapter 3 and 4.

The temperature induced narrowing of E_G was fitted using the Varshni (Fig. 2.20c) [Varshni-1967] and Bose-Einstein (B-E) [Logothetidis-1985, Lautenschlager-1987] equations. The Varshni expression is given by Eq. (2.4):

$$E(T) = E_0(0) - \frac{\alpha * T^2}{\beta + T} \qquad (2.4)$$

where $E_0(0)$ is the bandgap energy at 0 K while α and β are the Varshni coefficients. The B-E expression is given by Eq. (2.5):

$$E_G(T) = E_0(0) - \frac{2 * a_B}{\exp\left(\frac{\theta_B}{T}\right) - 1} \qquad (2.5)$$

where a_B is the strength of the electron-average phonon interaction and θ_B is the average phonon temperature. The Varshni and B-E fitting parameters are listed in Table 2.1. Values of GaSbBi layers with Bi content up to 4.2% taken from [Kopaczek-2013] were also added as a comparison and marked with a K. Regarding our $GaSb_{0.86}Bi_{0.14}$ sample, both α and β values are much higher than those of the other GaSbBi layers with lower Bi concentrations. It could be attributed to the fact that the PL energy is challenging to estimate accurately at high temperatures (> 200 K), due to the broadening of the PL peak. On the contrary, our B-E parameters values are very consistent with the results of Kopaczek *et al*. and show that the Bi incorporation increases the strength of the electron-average interaction (a_B) and the average phonon temperature (θ_B).

Table 2.2: Varshni and Bose-Einstein parameters extracted from the fitting of the bandgap E_G variation between 11 and 300 K (Fig. 2.20c). The parameters of GaSb were taken from [Vurgaftman-2001]. The parameters of the GaSbBi layers with Bi content between 0.7 and 4.2% were taken from [Kopaczek-2013].

Sample	Varshni parameters			Bose-Einstein parameters		
	E_0 (eV)	α (x 10^{-4} eV/K)	β (K)	E_0 (eV)	a_B (meV)	θ_B (K)
GaSb	0.813	3.78	94	0.811	22	127
$GaSb_{0.993}Bi_{0.007}$ (K)	0.785	3.9	120	0.781	35	190
$GaSb_{0.879}Bi_{0.021}$ (K)	0.740	3.7	110	0.738	46	220
$GaSb_{0.958}Bi_{0.042}$ (K)	0.685	3.2	160	0.683	42	230
$GaSb_{0.86}Bi_{0.14}$	0.370	9.3	1155	0.369	45	292

Regarding localization at low temperature, a weak S-shape is visible up to 50 K, but it is negligible in comparison with GaAsBi alloys. Indeed, strong S-shapes of dozens of meV were observed in GaAsBi layers, while it is confined to a few meV in our sample despite a much higher Bi content [Kudrawiec-2009, Mohmad-2011, Yoshimoto-2013, Mazzucato-2014]. Likewise, localization at 10 K is remarkably low (about 1 meV). From this perspective, GaSbBi therefore seems to behave as a conventionnal alloy, in contrast with GaAsBi and other highly mismatched alloys (HMA), which are usually characterized by a strong localization. The explanation for this probably arises from the fact that Bi is closer to Sb than to As in terms of atomic size, mass and, overall, electronegativity: 115, 145 and 160 ppm (atomic radius); 74.9, 121.7 and 209 u (atomic mass); 2.18, 2.05, 2.02 (electronegativity in Pauling scale) for As, Sb and Bi, respectively.

To further study the localized states, the excitation-power dependence of the PL was studied at 10, 80 and 150 K. Fig. 2.21 a and b depict the influence of the incident power on the bandgap and the FWHM, respectively. At 10 K, the bandgap energy blueshifts and the FWHM raises significantly as the excitation power is increased, which can be explained by the saturation of the localized levels. As a consequence, the contribution of the delocalized excitons raises, causing an increase of the bandgap energy and of the FWHM. The variation of both the bandgap energy and the FWHM becomes flat at the highest excitation intensities, meaning that the PL emission is dominated by recombination between delocalized states at this point. The bandgap energy and FWHM show a similar behaviour at 80 K, but their variation is somewhat smaller. Finally, no significant shift can be observed at 150 K, indicating the delocalized character of the PL emission at this temperature.

Additionally, the integrated PL intensity was also measured as a function of the excitation at different temperatures, and fitted with the following expression (Fig. 2.21c):

$$I_{PL-Int} = A * I_{exc}^{\alpha} \tag{2.6}$$

where I_{PL-Int} and I_{exc} are the integrated PL intensity and the excitation power, respectively. A is a fitting parameter and α represents the type of recombination mechanism. α is equal to 1 for a purely excitonic emission (free- and bound exciton), while its value decreases below unity for free-to-bound and donor–acceptor pair recombination [Schmidt-1992]. Finally, an α coefficient equals to 2 indicates a band-to-band recombination. In our case, α is close to one at the three temperatures considered here, and no clear increase can be noticed. Therefore, the PL emission of our GaSbBi layer is mainly dominated by recombination between excitons.

Finally, to finish our study of the GaSbBi layers, we have investigated the droplets observed on the surface of our samples.
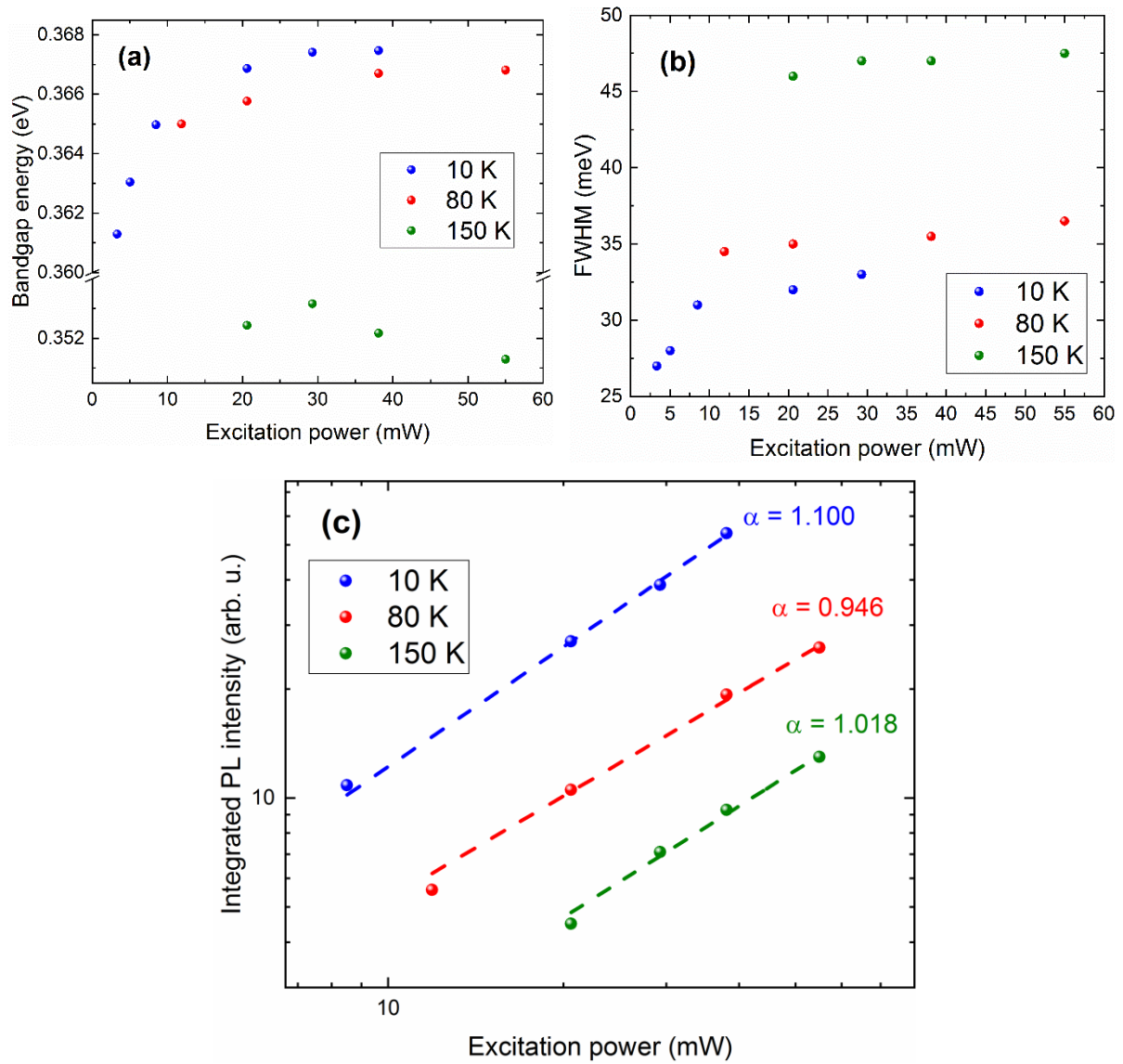
Fig. 2.21: (a) Bandgap energy, (b) FWHM and (c) integrated PL intensity of the 120-nm thick $GaSb_{0.86}Bi_{0.14}$ layer as a function of the excitation intensity at 11, 80 and 150 K. The dashed lines in (c) show the fits using Eq. 2.6.

2.4.2 Study of the droplets

As explained previously, metallic droplets easily form during the growth of GaSbBi. During this thesis, our efforts were naturally focused toward the growth of droplet free layers. Nevertheless, it is important to study their behavior in order to try to avoid their formation. Moreover, these droplets look specific and attracted our attention. Therefore, preliminary investigations (optical, scanning electronic and atomic force microscopies, EDS analysis) were carried out.

First of all, we observed that the density and the behavior of the droplets change a lot with the flux conditions. Fig. 2.22 a, b and c depicts the surface of three samples from the series with 14% Bi described in part 2.4.1. Various Sb BEPs were used, resulting in different V/III flux ratio. A V/III flux ratio below or well above unity results in a large density of droplets, as shown in Fig. 2.22 a and c. Conversely, the density of droplets is strongly reduced by a near-stoichiometric V/III flux ratio (Fig. 2.22b). The droplets also become larger as their density decreases, probably due to an enhanced diffusion length of the atoms on the surface. AFM measurements indicate that the largest droplets have a width of about 3 µm for the samples grown with a V/III flux ratio close to unity (Fig. 2.23 a and c) while they are smaller than 1 µm for a V/III flux ratio far from unity (Fig. 2.23b). The droplets can be also much higher than the GaSbBi layer thickness: the line profile shown in Fig. 2.23c indicates that the height of the droplet is 460 nm while the thickness of the GaSbBi layer underneath is only 120 nm.

Additionally, nanotracks can be seen on both optical microscope (Fig. 2.22b) and AFM images (2.22 a and b), indicating that the droplets move during growth. Such behavior was previously reported for GaAsBi [Moussa-2008a, Sterzer-2014, Steele-2016, Wood-2016]. In GaSbBi, Yue *et al.* reported that only small droplets can move, as no motional traces could be observed for large droplets [Yue-2018a]. In our case, nanotracks were observed for both small and large droplets, demonstrating that the size does not play a role in the droplet behavior. When the droplet density is high, these motional traces are more difficult to distinguish using optical microscopy (Fig. 2.22 a and c), but they are still clearly visible on AFM observation (Fig. 2.23b). The formation of these nanotracks was attributed to the growth of a nanowire [Wood-2016] or to a vapor-liquid-solid deposition mechanism [Steele-2016] in GaAsBi. But in our case, the AFM observations demonstrate that the droplets etch the layer while moving. Line profiles performed across the nanotracks, as depicted in Fig. 2.23d, clearly show that the droplets leave deep trenches while moving. A similar "etching" behavior has been also reported by Duzik and Millunchick in 2014 [Duzik and Millunchick-2014]. Logically, the width and the depth of nanotracks seem to depend on the size of droplets. Finally, material redeposition can also be noticed on both sides of some nanotracks.
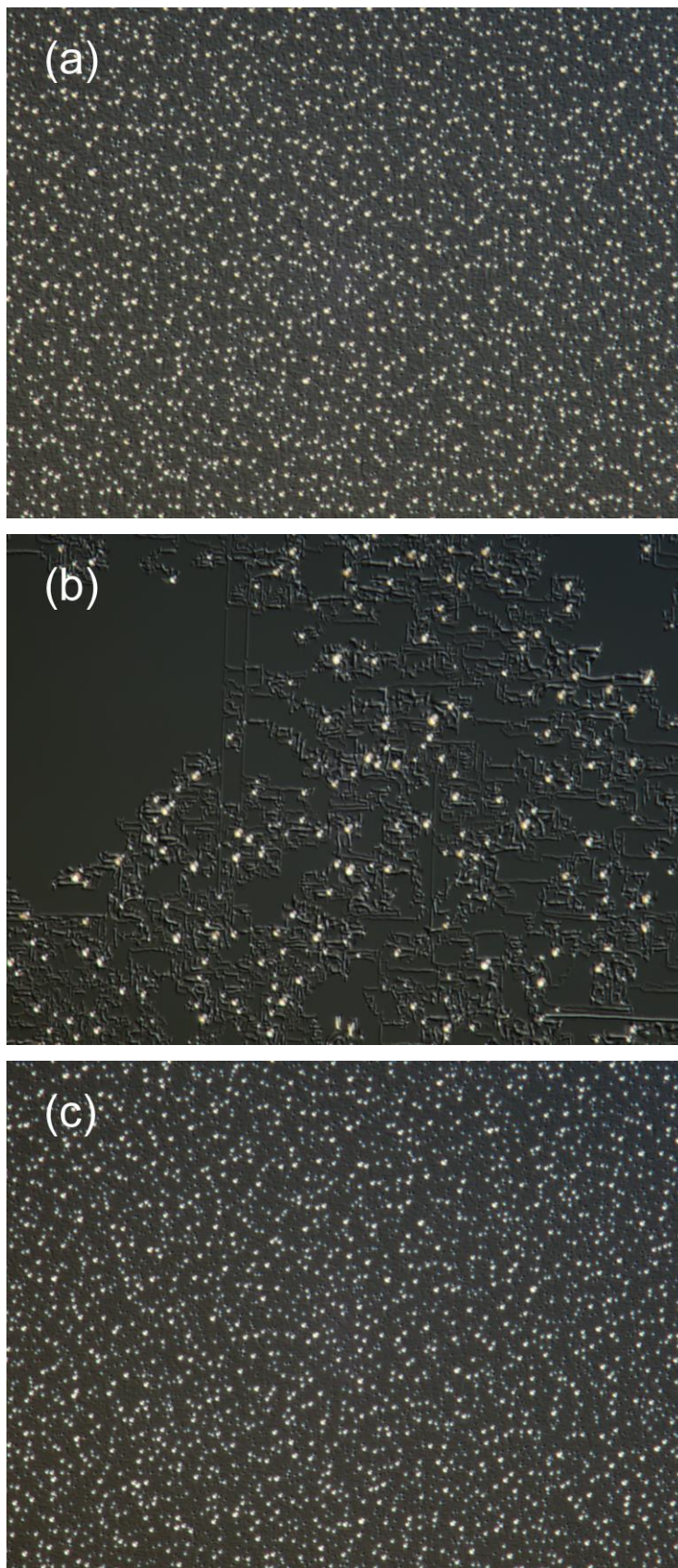
Fig. 2.22: Optical microscope observations (90 x 120 µm) of the surface of 120-nm thick GaSbBi layers grown at 200°C TTR using Sb BEPs of (a) 2.10 x 10^{-7} Torr (V/III flux ratio < 1), (b) 2.25 x 10^{-7} Torr (V/III flux ratio ~ 1), (c) 2.65 x 10^{-7} Torr (V/III flux ratio >> 1). The Bi and Ga fluxes were kept constant.

50
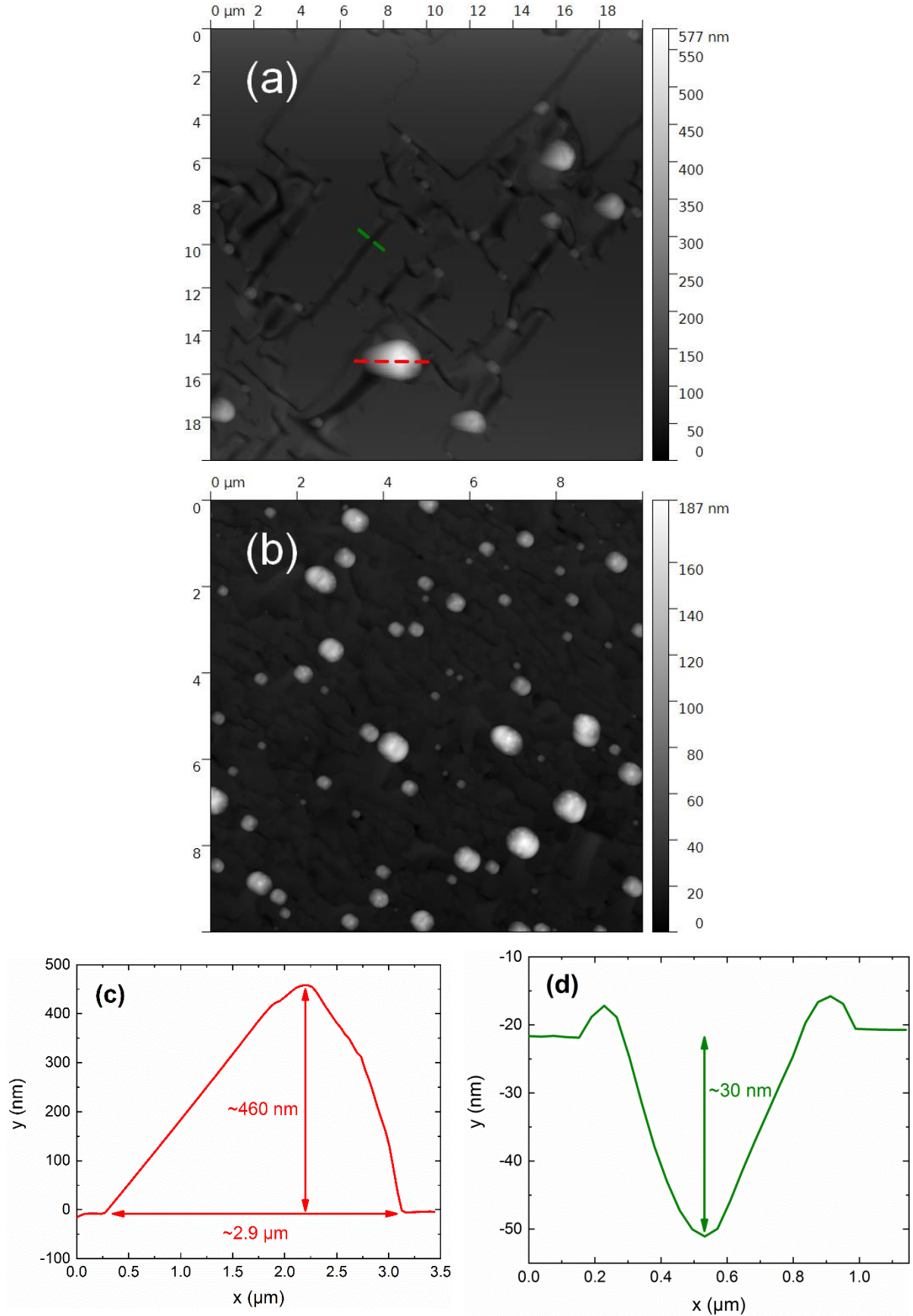
Fig. 2.23: AFM measurements of (a) the 120-nm thick $GaSb_{0.86}Bi_{0.14}$ layer shown in Fig. 2.22b (V/III flux ratio ~ 1), and of (b) a GaSbBi layer grown under a V/III flux ratio larger than one, respectively. The red and green dashed lines in (a) indicate the positions of the line profiles which are depicted in (c) and (d), respectively.

51

Fig. 2.24 shows an AFM observation of the complete migration of a droplet. It is very clear that the nanotrack becomes larger and deeper as the droplet moves. This could demonstrate that the droplet partially absorbs the etched atoms and grows during the movement. It could also explain the unexpected height of the droplets mentioned above. However, this variation of width and depth could also be explained by a regrowth after the passage of the droplet.
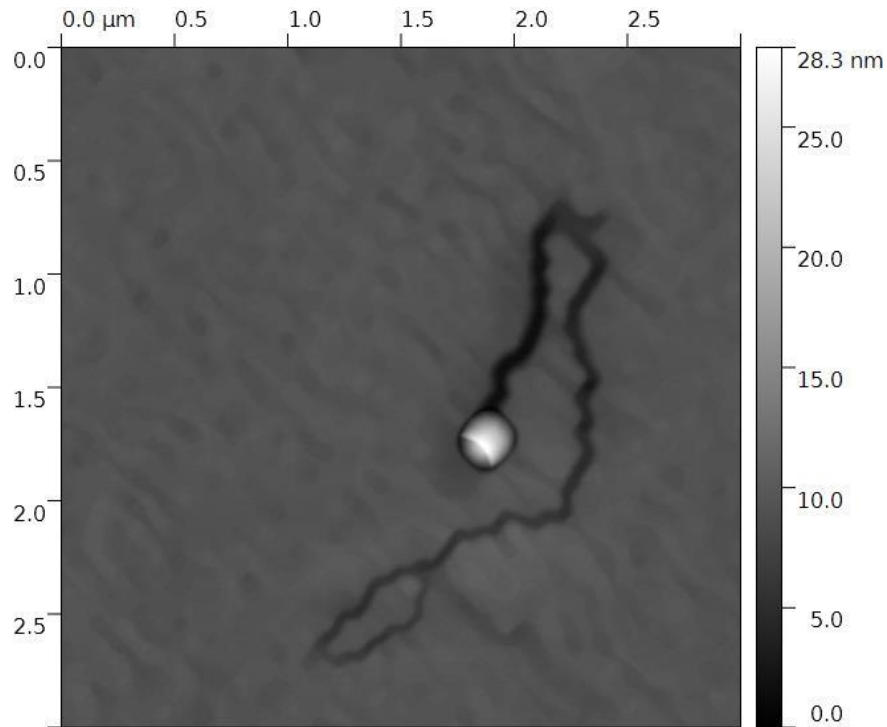
Fig. 2.24: AFM image of the migration of a droplet during the growth of a 100-nm thick GaSbBi layer with 12.3% Bi.

Lastly, the previous AFM images (Fig. 2.23 a and b, Fig. 2.24) show that the droplets are composed of two separate phases. This interesting point was investigated using SEM and EDS analysis. Fig. 2.25a shows the surface of a GaSbBi layer with 12.3% Bi, and more specifically three biphasic droplets of approximately 3 µm width. Again, the nanotracks are perfectly visible. EDS analysis indicates that the bright and dark parts of the droplets are composed exclusively of Bi and Ga (Fig. 2.25 b, c and d), respectively. No Sb atoms could be detected in the droplets (Fig. 2.25e). Such Ga-Bi droplets have already been reported by several groups for the growth of both GaAsBi [Vardar-2013, Forghani-2014, Sterzer-2014, Wood-2016] and GaSbBi [Duzik and Millunchick-2014, Yue-2018a] alloys.

Additionally, a decrease of the Bi signal behind the droplets can be noticed in Fig. 2.25c. These Bi depleted areas correlate well with the nanotracks visible on Fig. 2.25a, indicating that the droplets absorb Bi atoms while moving. On this point, different groups have observed a Bi-depleted nanowire

left by the droplet [Sterzer-2014, Steele-2016, Wood-2016]. Finally, these biphasic Ga-Bi droplets were also observed on GaSbBi layers grown with a V/III flux ratio below unity, showing that Bi atoms are incorporated in the droplets rather than in the lattice even in case of excess of Ga. It demonstrates once again how challenging the Bi incorporation is, even without Sb competition.
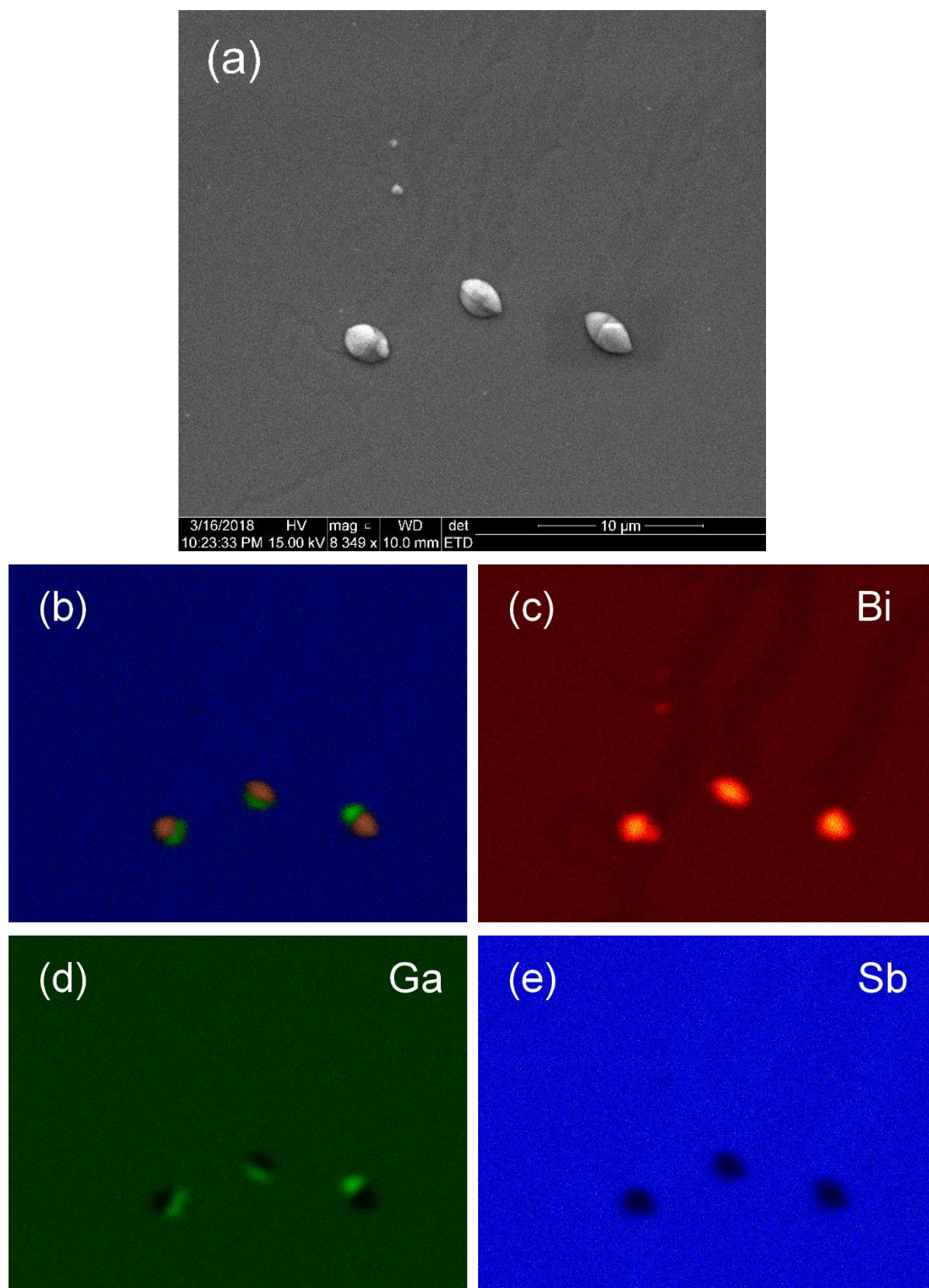
Fig. 2.25: (a,b) SEM observation and EDS mapping of the surface of a 100-nm thick GaSbBi layer with 12.3% Bi. EDS analysis of Bi, Ga and Sb elements are detailed in (c), (d) and (e) respectively.

2.5   Conclusion

In this chapter, we demonstrated that the growth parameters need to be carefully adjusted to promote the incorporation of Bi into GaSb. First, we showed that the temperature has a tremendous impact on the Bi incorporation into GaSb. Indeed, a too high growth temperature causes a significant reduction of the incorporation of Bi. Thanks to the growth of calibration GaSbBi layers, the highest growth temperature allowing the best Bi incorporation was determined for our MBE system (200°C TTR). This optimal temperature was used for the growth of the subsequent GaSbBi layers. Second, a near-stoichiometric V/III ratio is required to enhance the Bi incorporation. In fact, a competition between Sb and Bi was observed: as Sb is easier to incorporate, any excess of Sb atoms during the growth results in a strong reduction of the incorporation of Bi and in the formation of droplets on the surface.

However, the optimization of these growth parameters is challenging and requires the growth of several calibration samples. To avoid this time- and money- consuming trial-and-error approach, we demonstrated a new *in-situ* method using RHEED intensity oscillations. Strong oscillations were measured for both GaSbBi and GaSb for different Bi fluxes at very low temperature. During group-V induced growth, we noticed a variation of the growth rate between GaSb and GaSbBi, obviously caused by the incorporation of Bi. Therefore, the study of the RHEED intensity oscillations allows a direct observation of the Bi incorporation. By comparing the growth rate of GaSbBi and GaSb it is possible to rapidly optimize the growth parameters with the additional benefit to use a limited number of calibration samples. This technique could also be used for the growth of other III-V-Bi alloys.

Finally, we managed to reach high Bi content by increasing the Bi flux. By carefully adjusting the Sb flux to the Bi flux, the growth of droplet free GaSbBi epilayers with Bi content up to 11.4% was achieved. These samples demonstrated a high crystal quality with more than 97% substitutional Bi. However, the Sb flux window allowing a droplet free growth narrows as the Bi flux raises. As a consequence, the formation of mobile biphasic Ga-Bi droplets could not be avoided for higher Bi concentrations, and a concomitant degradation of the material quality was clearly noticed. In this context, we obtained a maximum Bi concentration of 14%, which is the highest Bi content reported in GaSb to date. Despite a higher interstitial rate, the material quality remains satisfying and this sample exhibits a strong PL emission at RT close to 3.8 µm, and a weak localization at low temperature. This last point tends to demonstrate that GaSbBi behaves more as a regular alloy than as a highly-mismatched alloy.

In the next chapter, we show how we used these different findings to achieve the growth of GaSbBi-based heterostructures.

Chapter 3:   GaSbBi/GaSb heterostructures

Once the growth of high Bi content GaSbBi epilayers was mastered, the next step was to use GaSbBi alloys in the active region of MQW structures. To this end, we first investigated the stability of the GaSbBi material upon annealing. Then, several GaSbBi/GaSb MQW samples were grown with Bi contents up to ~15% which demonstrated PL emission up to ~3.5 μm at RT. The structural and optical properties of these samples were characterized by TEM and PL measurements. The bandgap alignment was also studied by PR spectroscopy coupled to theoretical calculations. Finally, we fabricated the first GaSbBi-based laser diode, demonstrating pulsed operation at 300 K and CW emission at 80 K.

3.1   Growth of GaSbBi/GaSb Multi Quantum Well structures

To achieve the growth of a GaSbBi/GaSb MQW structure, some points have first to be clarified. First, we need to ensure that the growth of thick layers at high temperature on top of the GaSbBi-based active region would not cause any material degradation or composition change. Second, the way the substrate temperature is managed during the growth of the GaSbBi/GaSb active zone has to be studied. Our investigations are detailed in the following.

3.1.1 Thermal stability of GaSbBi alloys

When growing a GaSbBi single layer, the substrate temperature is decreased right after the target thickness has been deposited. In contrast, a MQW structure is a more complex layer stacking. The optimal growth temperature can be different for each layer and it is expected to vary significantly between the layers with or without Bi, as discussed in the previous chapter. In particular, confinement or contact layers grown atop the QWs are usually grown at much higher temperature ($\geq$ 450 °C), which may impact the quality of the thin GaSbBi layers. At the beginning of my PhD, no study on the annealing of GaSbBi layers had been reported, and it was therefore necessary to know whether the post-growth annealing would cause a diffusion of the Bi atoms out of the GaSbBi layer and/or degrade the material quality, or on the contrary improve the optical performances as it was observed for GaAsBi [Moussa-2008b, Rodrigo-2010, Mazzucato-2013, Lemine-2014].

To investigate this important aspect, we carried out several annealing cycles on a thick GaSbBi layer with 6.2% Bi. The sample was characterized right after the growth using PL and HR-XRD, and then reloaded in the MBE growth chamber for annealing at 450°C under Sb flux for one hour. The sample was again characterized and the process repeated several times, to track the evolution of the layer quality with the annealing duration. The temperature of 450°C is appropriate because it is a usual growth temperature for the III-V alloys commonly used in quantum well and laser structures (GaSb, AlGaAsSb, GaInAsSb). $\omega-2\theta$ curves and room-temperature PL were measured after each annealing, and compared to those obtained for the as-grown sample. HR-XRD data are shown on Fig. 3.1a, and the perfect superposition of the different curves clearly indicates that no degradation or modification of the composition of the GaSbBi layer occurred during annealing. On the other hand, a strong effect was observed on the PL (Figure 3.1b). The PL intensity raises with increasing annealing duration up to two hours and then decreases for longer annealing. The peak position in contrast remains constant whatever the duration, confirming that the band-gap of the material, and hence its composition, is not affected by annealing. For two-hours annealing, the PL intensity is improved by a factor of 12, which we ascribe to the cure of point defects. The degradation of the PL for longer annealing duration could be the result of clustering or phase separation effects as previously reported in the case of GaAsBi alloys [Moussa-2008b].
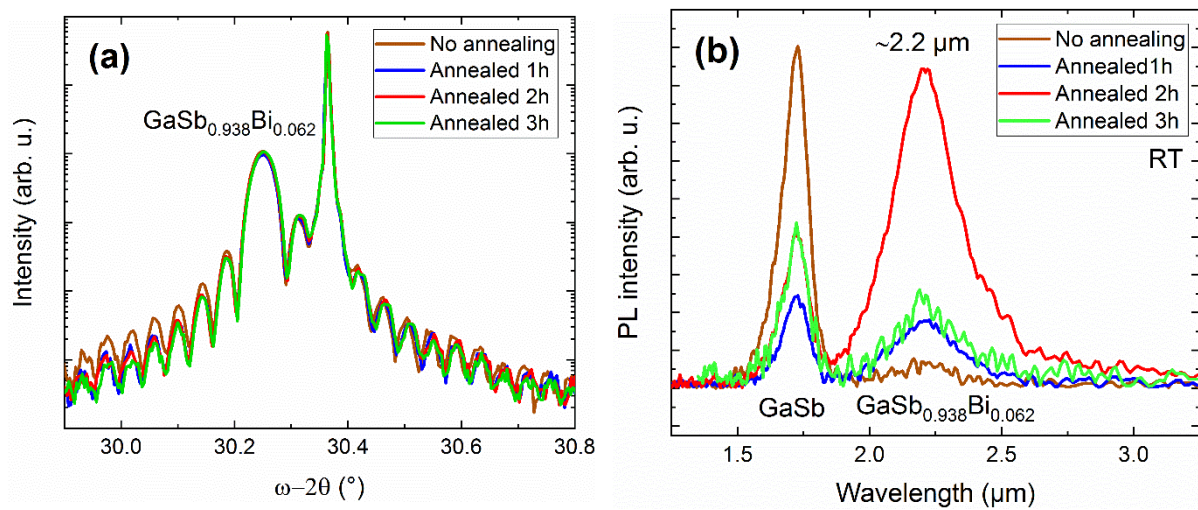
Fig. 3.1: HR-XRD scans (a) and photoluminescence measurements at room-temperature (b) of a 120-nm thick GaSbBi sample with 6.2% before and after successive annealing at 450°C during 60 minutes.

We thus conclude that an annealing as long as 2 hours at 450°C does not affect the composition of the GaSbBi layer, and furthermore, the PL emission is strongly improved. These results indicate that

it is indeed possible to realize a more complex QW structure or even a complete laser without compromising the GaSbBi crystal quality and homogeneity.

3.1.2 Management of the substrate temperature during the growth of the GaSbBi/GaSb active region

Next, we have investigated the growth of MQW samples. We designed an active region composed of three 15 nm thick GaSbBi QWs separated by 20 nm thick GaSb barriers. This MQW is sandwiched between 180-nm thick GaSb layers and 20 nm thick AlSb barrier layers to confine the photogenerated carriers during PL spectroscopy. A 20 nm thick GaSb cap layer is added to avoid oxidation of the topmost AlSb layer. These GaSb and AlSb layers were grown at 450°C. The whole structure is shown in Fig. 3.2a

The main growth challenge here is the substrate temperature management during the epitaxy of the MQW. Indeed, the GaSbBi wells have to be grown at 200°C TTR to promote the Bi incorporation, as discussed before. But if such a low temperature is maintained to grow the GaSb barriers, a high density of point defects is expected to be created by low adatoms mobility, which could strongly degrade the optical performances. On the other hand, a high temperature growth of the GaSb barriers would require several long growth interruptions (~30 minutes repeated twice) to change the substrate temperature. Such growth interruptions are not only impractical but could also allow the deposition of impurities at the well/barrier interfaces and therefore result in the formation of non-radiative recombination channels. As the quality of the active region interfaces is critical for the optical performances of the MQW structure, growth interruptions should in principle be avoided as much as possible.

To find the best strategy, we have grown two MQW structures. The GaSb barriers in the first sample were grown at 450°C (sample 1), while the active zone in the second sample was entirely grown at low temperature (sample 2). The growth conditions of the GaSbBi layers were set to allow a Bi incorporation of 14%, but a slight decrease and increase of the Bi and Sb fluxes, respectively, was noticed during the epitaxy of sample 1 and corrected for sample 2. Finally, the GaSb barriers were grown in both cases under a large Sb excess (Sb/III flux ratio >> 1).

Fig. 3.2b shows the ω-2θ HR-XRD spectra measured on the two samples. The peaks associated to the AlSb layers and to the GaSbBi/GaSb MQW partly overlap, which complicates the analysis because most of the MQW satellites peaks are not visible. In particular, an accurate determination of

the MQW thicknesses and composition is not possible. Nevertheless, the first satellite peaks of the MQW pattern are visible near 30.14° and 30.30°. The satellite peaks of sample 1 are closer to the GaSb substrate than the ones of sample 2, indicating a lower Bi concentration. This change of Bi content could be attributed to the flux fluctuation mentioned above, or to the different growth conditions of the GaSb barriers.

Optical microscopy observation of the samples shows mirror-like and droplet-free surfaces in both cases. However, AFM reveals two totally different surface morphologies: well-defined atomic steps are visible for sample 1 with a very low RMS roughness (~0.15 nm) (Fig. 3.2c), while sample 2 shows large rectangular structures with small holes (Fig. 3.2d) and a RMS roughness larger than 1 nm. We propose that these nano-holes could have been caused by the very high Sb flux used during the growth of the GaSb barriers at 200°C TTR. At such a low temperature, the Sb atoms in excess may have nucleated into small Sb clusters. Then, with the increase of the substrate temperature following the epitaxy of the active region, these clusters might have desorbed from the surface, leaving nano-holes behind them.
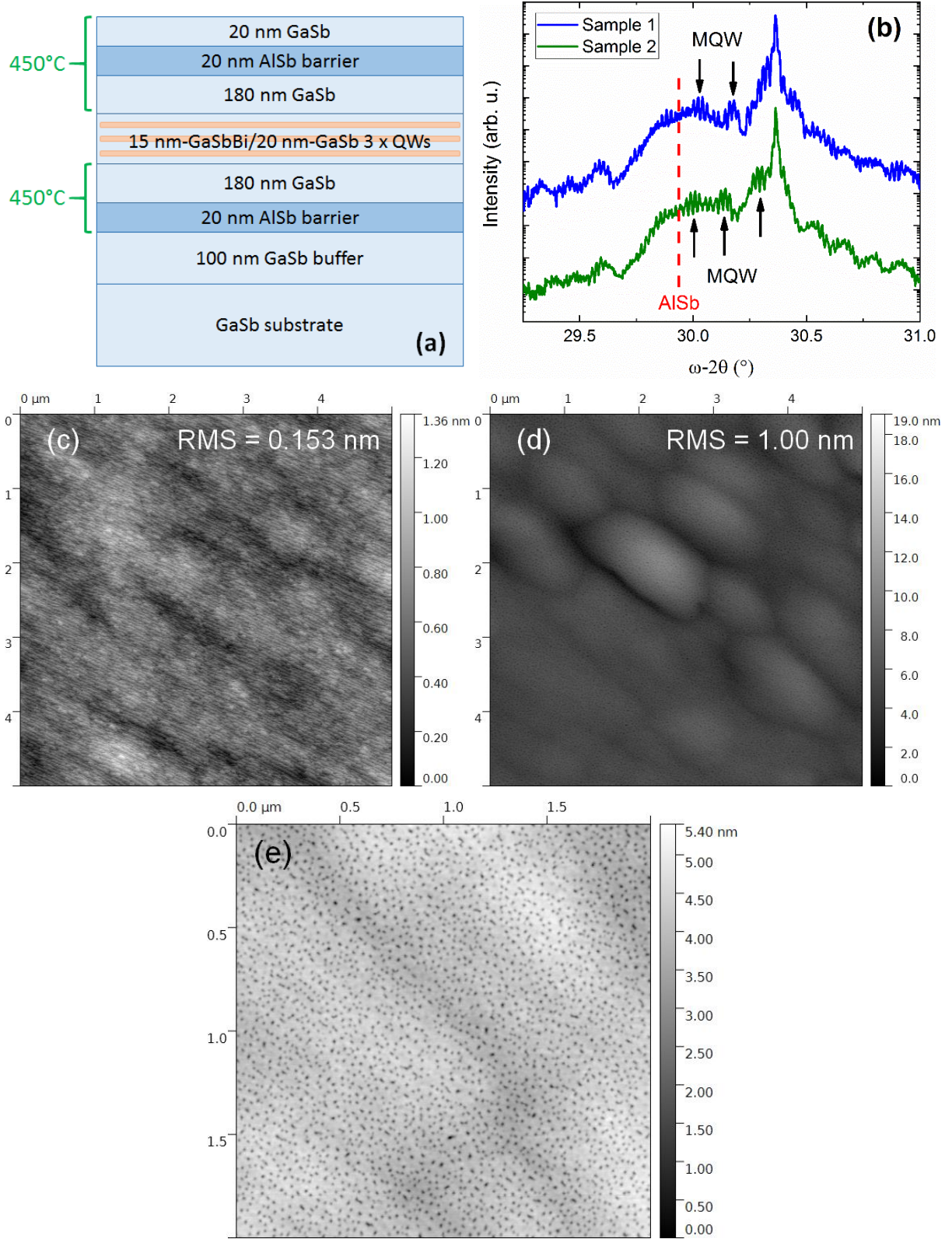
Fig. 3.2: (a) GaSbBi/GaSb MQW structure. (b) ω-2θ scans of the (004) Bragg reflection of the two GaSbBi/GaSb MQW samples. For sample 1, the GaSb barriers were grown at 450°C, while the whole active region of sample 2 was grown at 200°C TTR. The black and red arrows show the satellite peaks of the MQW and the AlSb layers, respectively. (c,d) represents the surface of sample 1 and 2, respectively. (e) depicts the surface of sample 2 at higher magnification.

Finally, both samples 1 and 2 demonstrated PL emission at RT close to 2.7 and 3.3 µm (Fig. 3.3), respectively. This wavelength difference is in good agreement with the difference of Bi content deduced from the HR-XRD scans (Fig. 3.2b). However, emission wavelengths are challenging to estimate accurately, as the emission peaks are strongly distorted by water absorption around 2.6 and 3.1 µm. Nevertheless, sample 2 shows overall better optical performances.
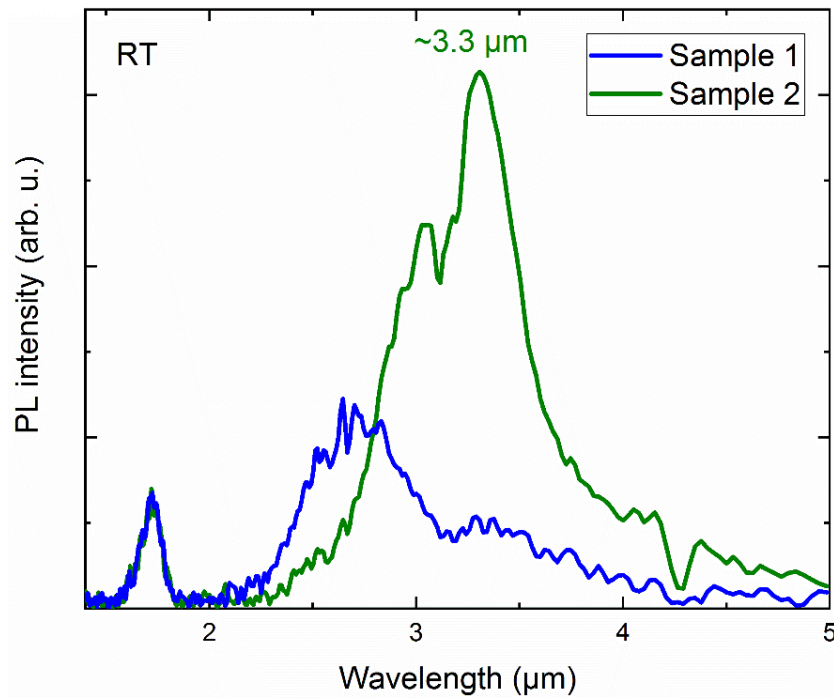
Fig. 3.3: PL measurements at RT of the two GaSbBi/GaSb MQW structures. For sample 1, the GaSb barriers were grown at 450°C, while the whole active region of sample 2 was grown at 200°C TTR.

To summarize, sample 2 has a degraded surface in comparison with sample 1, but shows a stronger PL intensity. The defects visible on the AFM images are surely due to the Sb excess during the growth of the GaSb barriers at 200°C TTR, and can be avoided by the use of a stoichiometric Sb/Ga ratio, as demonstrated in the next paragraph. Growing the whole active region at the same temperature (200°C TTR) thus seems to be the best strategy, resulting in improved optical performance and reduced growth duration.

3.2   Properties of the GaSbBi/GaSb MQW structures

Following these preliminary experiments, we have grown several GaSbBi/GaSb MQW structures. The structural and optical properties were investigated by TEM and PL measurements, respectively. The band alignment of the GaSbBi/GaSb system was also studied using PR spectroscopy coupled with theoretical calculations. A large range of QW compositions and thicknesses were studied to allow the determination of important parameters, such as the valence band offset (VBO) or the electron effective mass in GaSbBi.

3.2.1 Presentation of the samples

Several GaSbBi/GaSb MQW structures were grown with various Bi compositions in the 6 to 15% range and different QW widths (7, 11 and 15 nm). AlSb barriers were replaced by $AlAs_{0.08}Sb_{0.92}$ layers lattice-matched with GaSb to allow a better analysis of the HR-XRD scans, but otherwise, the structures were identical to the one studied in the previous paragraph (Fig. 3.2a). All the layers were grown at 425°C, except for the active region where a temperature of 200°C TTR was used. Care was taken to use a V/III flux ratio close to stoichiometry for both GaSb barriers and GaSbBi wells in order to avoid the formation of the nano-holes discussed previously.

HR-XRD scans from GaSbBi/GaSb MQW with different Bi concentrations are shown in Fig. 3.4a. By using AlAsSb instead of AlSb barriers, the patterns associated to the MQW are now clearly visible and well defined. The data collected for the sample with 15% Bi show however broader and less intense satellite peaks, which could indicate a roughening of the MQW interfaces or a lower material quality. This is in good agreement with the results found on bulk layers, where the onset of the degradation of the crystal quality was clearly noticed for %Bi around 12% (see paragraph 2.4.1). This deterioration is also corroborated by the analysis of the surface morphology. The MQW samples with Bi content below 12% show droplet free surface, a RMS roughness around 0.2-0.3 nm and well defined atomic steps (Fig. 3.4b). In contrast, a few droplets are visible on the samples with ~15% Bi, and very particular morphological features are observed for these samples. Fig. 3.4 c, d and e depict AFM images of GaSbBi/GaSb MQW with ~15% Bi and GaSbBi widths of 7, 11 and 15 nm, respectively. The large rectangular features strongly resemble the ones found in the previous paragraph for sample 2 (Fig. 3.2d), which had a similar %Bi content and was fabricated using the same technique, with both the QW and the barrier grown at low temperature. This is a clear indication that they are caused by the large Bi flux when this growth strategy is used. It is also interesting to note that their shape changes

63

with the thickness of the GaSbBi wells, which together with the increase of the surface roughness illustrates the impact on the overall structure caused by the low QW crystal quality. Note also that the nanoholes previously found on the surface of the sample 2, where the barriers were grown with an excess of Sb are not visible on these last samples. This confirms that the use of a nearly stoichiometric V/III flux ratio during the growth of the GaSb barriers allows avoiding the formation of these defects.

To further investigate the properties of the GaSbBi/GaSb QWs, we then focused on two series of three samples having Bi concentrations of 6 and 11% and various GaSbBi thicknesses (7, 11 and 15 nm, nominally). The structural properties of these samples were investigated first by TEM, and the results are detailed in the next paragraph.
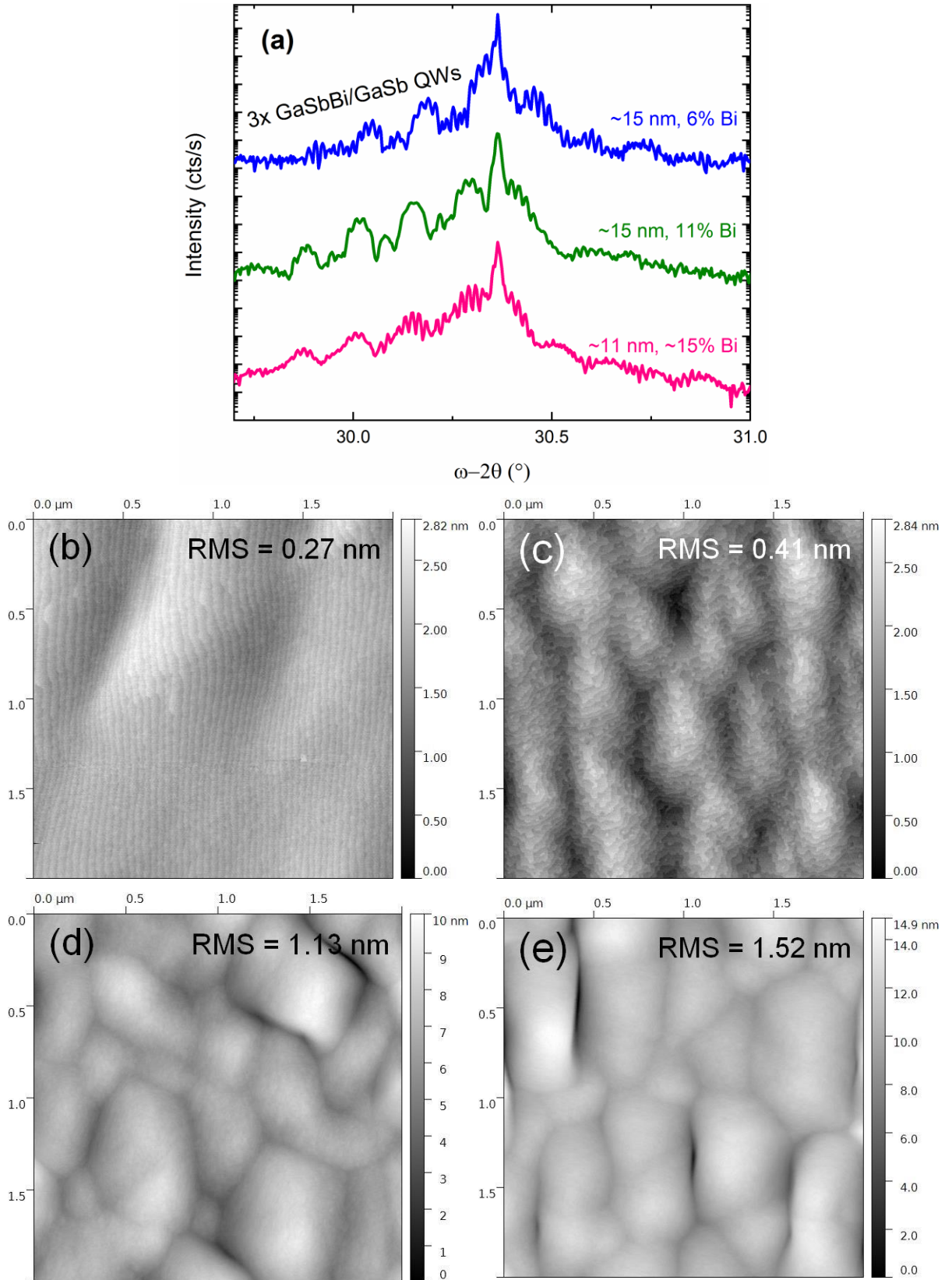
Fig. 3.4: (a) HR-XRD scans and (b, c, d, e) AFM observations of GaSbBi/GaSb MQW structures with various Bi concentrations and GaSbBi widths. (b) is a 2 x 2 µm observation of a 15-nm thick GaSbBi/GaSb structure with ~11% Bi. (c, d, e) depict the surface of samples with ~15% Bi and 7, 11 and 15 nm thick GaSbBi QWs, respectively.

3.2.2 Structural properties: TEM characterization

The structural properties of these MQW samples were closely investigated using TEM at the Paul-Drude-Institute in Berlin by the team of Dr. Achim Trampert, and in particular by Dr. Esperanza Luna. Composition homogeneity, QWs interfaces and morphologies were studied in-depth. We summarize below the most important findings from this study, but more details can be found in [Luna-2018a, Luna-2018b].
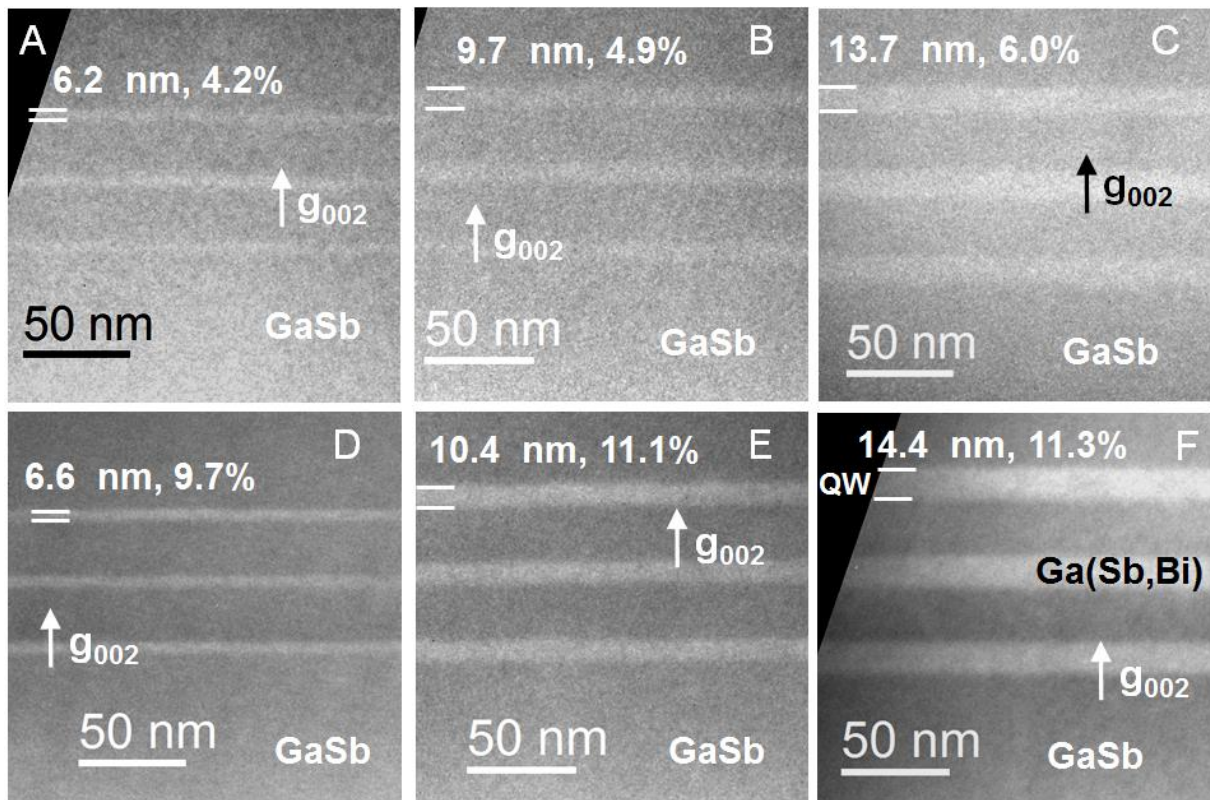
Fig. 3.5: Chemically sensitive g_{002} DFTEM images of the investigated GaSbBi/GaSb MQW. The Bi concentrations and the GaSbBi widths estimated by TEM are indicated for each sample. The QWs in the top panels display a lower contrast in the g_{002} DFTEM micrographs compared to those in the bottom panels due to their smaller Bi content.

Fig. 3.5 displays chemically sensitive g_{002} DFTEM images of the six investigated GaSbBi/GaSb MQW structures. Similarly to the GaSbBi epilayers, no dislocation, clustering or extended defect can be observed. Regardless of their different Bi content, all QW samples seem to be homogeneous in composition and no composition fluctuation are detected.

The QW thicknesses and the Bi contents given in Fig. 3.5 were estimated by TEM [3]. These data are listed in Table 3.1 together with the HR-XRD values for the sake of comparison. Significant deviations from the nominal QW thickness and, in particular, from the nominal barrier thickness (20 nm) can be noticed. Indeed, TEM measurement reveals GaSbBi layers slightly thinner than the nominal values and thicker than expected GaSb barriers. More specifically, HR-XRD and TEM estimations of the GaSbBi thickness and the Bi content are relatively close, but the GaSb thicknesses given by TEM are systematically much larger than the ones measured by HR-XRD. It can also be noticed that the deviation from the nominal barrier thickness also raises with the GaSbBi thickness. This observation is still under discussion. The fact that the GaSbBi wells and the GaSb barriers are, respectively, thinner and thicker than expected could indicate that the growth rate is different for these two layers. A systematic change of the Ga flux between the two layers is unlikely as we used the same Ga cell kept at the same operating temperature for both materials. We could also imagine that the growth rate of the GaSbBi layer is smaller due to a V/III flux ratio lower than unity, in which case the growth rate is controlled by the element V, Sb and Bi. However, to explain such a large deviation of the barrier thickness, a large excess of Ga in the QW would be expected, and as a result Ga droplets should be formed, which were not detected by TEM. The most striking fact is however the larger MQW period thickness measured by TEM compared to the thickness deduced from HR-XRD. Indeed, while some assumptions have to be made and some technique-dependent uncertainties have to be taken into account to determine the Bi content or individual layer thicknesses within the MQW for example, both techniques are expected to give the period thickness with a very good accuracy, and it is unclear for now where this discrepancy comes from.

Interestingly, a lower Bi content was found by TEM in the 7-nm GaSbBi layers in comparison with the thicker QWs. To investigate this point, a Bi composition profile was performed across the first QW of sample E and is shown in Fig. 3.6 a and b. It is very clear that the Bi incorporation increases across the first nanometers of the GaSbBi layer. Therefore, for a layer as thin as 6-7 nm, it could result in an overall lower Bi content than expected. Besides, this result is in line with our RHEED observation of a lower incorporation rate of Bi at the beginning of the layer (see paragraph 2.3.2).

---

[3] The estimated Bi content and QW or barrier widths were obtained from the analysis of numerous $\mathbf{g}_{002}$ DFTEM micrographs, using several TEM specimens per sample. Each individual TEM specimen was investigated on at least four different areas of about 300 nm length. The TEM data are obtained from the analysis of 50-80 micrographs per sample where we have locally measured the composition and layer thicknesses at, at least, 200 different positions (400 positions for some samples). This includes, for each individual micrograph, scans at different positions along the MQW at a distance of about 20–50 nm each.

Table 3.1: Summary of the main parameters (thickness and Bi content) deduced from HR-XRD and TEM measurements. The Bi concentration given by TEM is the average Bi content experimentally determined using g_{002} DFTEM. The displayed values are averaged over both (110) and (1̄ 10) zones axes and over the three QWs. The thickness and Bi content of the thinnest GaSbBi QWs could not be estimated accurately by HR-XRD, due to the insufficient lattice mismatch with the GaSb substrate.

Sample	Bi content (%)			GaSbBi / GaSb thickness (nm)		
	Expected	HR-XRD	TEM	Expected	HR-XRD	TEM
A	6	NA	4.2 ± 0.9	7 / 20	NA	6.2 ± 0.7 / 24.2 ± 0.9
B	6	5.5 ± 0.5	4.9 ± 1.1	11 / 20	10.5 ± 0.5 / 22.0 ± 2.0	9.7 ± 0.8 / 25.2 ± 0.9
C	6	6.0 ± 0.5	6.1 ± 1.4	15 / 20	13.0 ± 0.5 / 22.5 ± 2.0	13.7 ± 0.7 / 25.8 ± 0.9
D	11	NA	9.7 ± 2.3	7 /20	NA	6.6 ± 0.5 / 23.5 ± 0.9
E	11	11.0 ± 0.5	11.1 ± 2.4	11 / 20	9.5 ± 0.5 / 22.5 ± 0.5	10.4 ± 0.6 / 24.8 ± 0.9
F	11	11.0 ± 0.5	11.3 ± 2.2	15 / 20	13.5 ± 0.5 / 23.0 ± 0.5	14.4 ± 0.5 / 25.3 ± 0.7

Additionally, a faint change in contrast between the high-temperature (HT) grown GaSb layers and the low-temperature (LT) grown GaSb layers can be noticed on the chemically sensitive cross-section g_{002} DFTEM images as Fig. 3.6 a and c. A similar change in contrast was previously observed between LT GaAs and the GaAs-substrate in GaAsBi structures. We tentatively attribute this difference to the sensitivity of g_{002} DFTEM to even detect local variations in point defect density, as has already been reported [Glas-2004]. Hence, this would be an indication of the presence of point defects in the LT GaSb barriers, which would likely have an impact on the emission properties of the GaSbBi/GaSb MQW structures. Further investigations are nevertheless required to confirm this point.
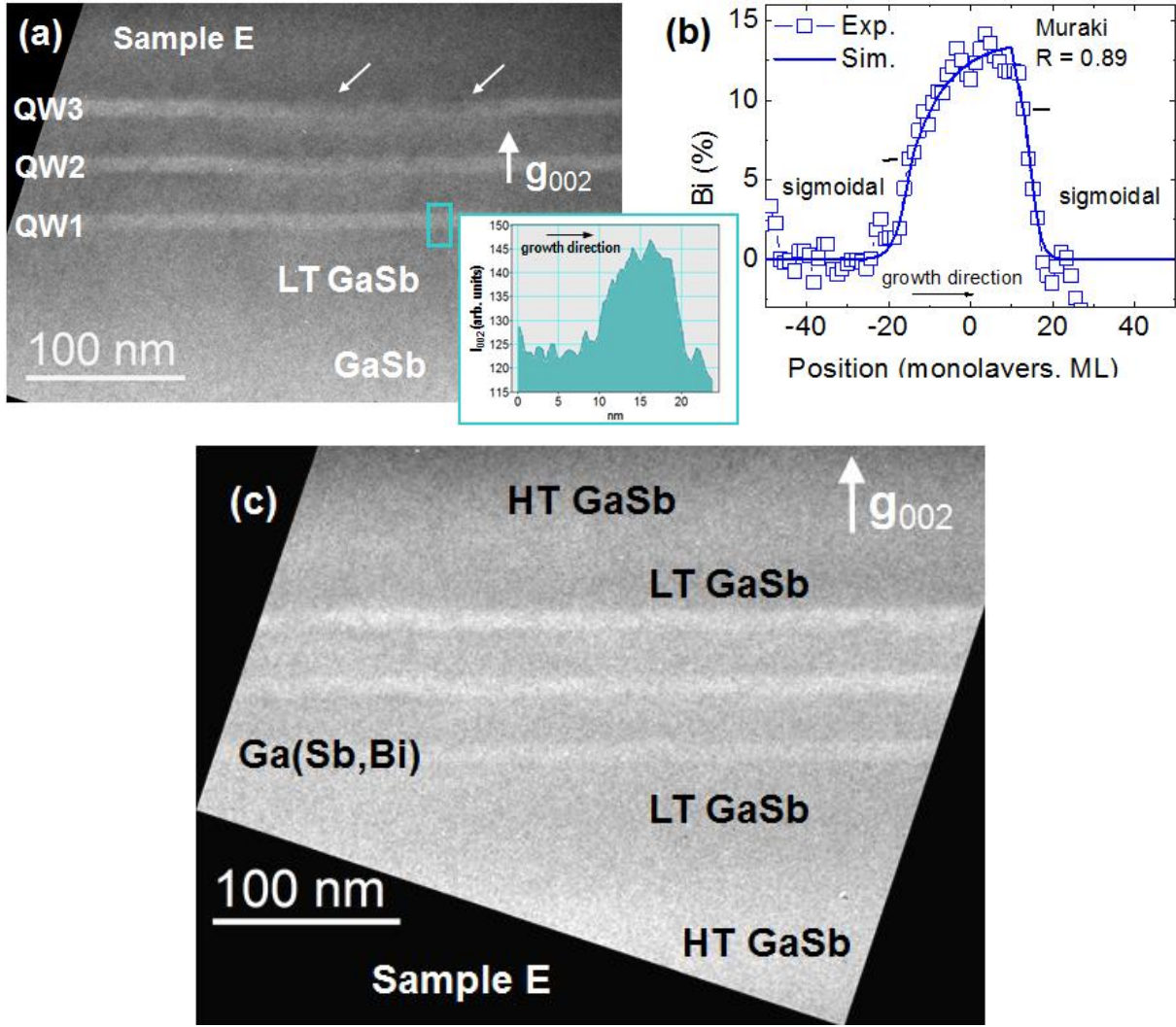
Fig. 3.6: (a,c) Chemically sensitive g_{002} DFTEM micrograph of the GaSbBi/GaSb QWs in sample E together with (b) a representative Bi composition profile across the QW, extracted from the analysis of the g_{002} DFTEM diffracted intensity. The white arrows in (a) point out the local irregularities.

Despite the overall good quality and homogeneity of the samples, the MQW are affected by different features. First, some interface roughness, more pronounced at the GaSbBi-on-GaSb interface, is visible for the three QWs. This feature does not seem to depend on the Bi content since the very same characteristics are found in all the samples considered in this paragraph (see, *e.g.*, representative g_{002} DFTEM micrographs in Fig. 3.6c and Fig. 3.7a). The Bi composition profile shown in Fig. 3.6b shows well that the GaSb-on-GaSbBi interface is smoother than the GaSbBi-on-GaSb interface, which could be ascribed to a surfactant effect of Bi [Tixier-2003a, Young-2005, Tiedje-2008]. In fact, a similar interface smoothing at the GaSb-on-GaSbBi interface of 6 nm thick GaSbBi/GaSb QWs has also been recently reported by Li Yue *et al*. [Yue-2018b]. The presence of Bi is indeed expected to alleviate the roughness introduced due to the LT growth, in particular next to the GaSb barriers. This smoother

GaSb-on-GaSbBi interface does not relate to the Bi composition (for the range of Bi contents considered here) since all samples in this work exhibit it, except for the samples with the thinnest QWs where the lower and upper interfaces appear similar. In that respect, the similar roughness at the GaSb-on-GaSbBi and GaSbBi-on-GaSb interfaces for samples A and D suggests that, at their specific growth conditions, the accumulation of Bi at the surface of the thin 6-7 nm GaSbBi layers may not be sufficient to produce an effective smoothing effect, as it was also observed for the incorporation of Bi (see above and Chapter 2).

Second, all samples exhibit perceptible lateral thickness fluctuations (on the 100-nm-length scale of the TEM images). Variation in QW thickness is visible among the three QWs, as shown in Fig. 3.7a for sample C. The plot in Fig. 3.7b represents the QW and barrier thickness measured at about 300 different (lateral) positions for sample B, together with the average values. The spread of the data is apparent for both the QW and the barrier. The impact of the fluctuations is particularly noticeable in the samples with the smallest QW thickness of 6-7 nm since their amount represents ~11% of the total QW thickness. Finally, some MQWs are affected by local morphological irregularities as those marked by a small white arrow in Fig. 3.6a and 3.7c. The origin of these features, mainly affecting the third QW, is still unclear.
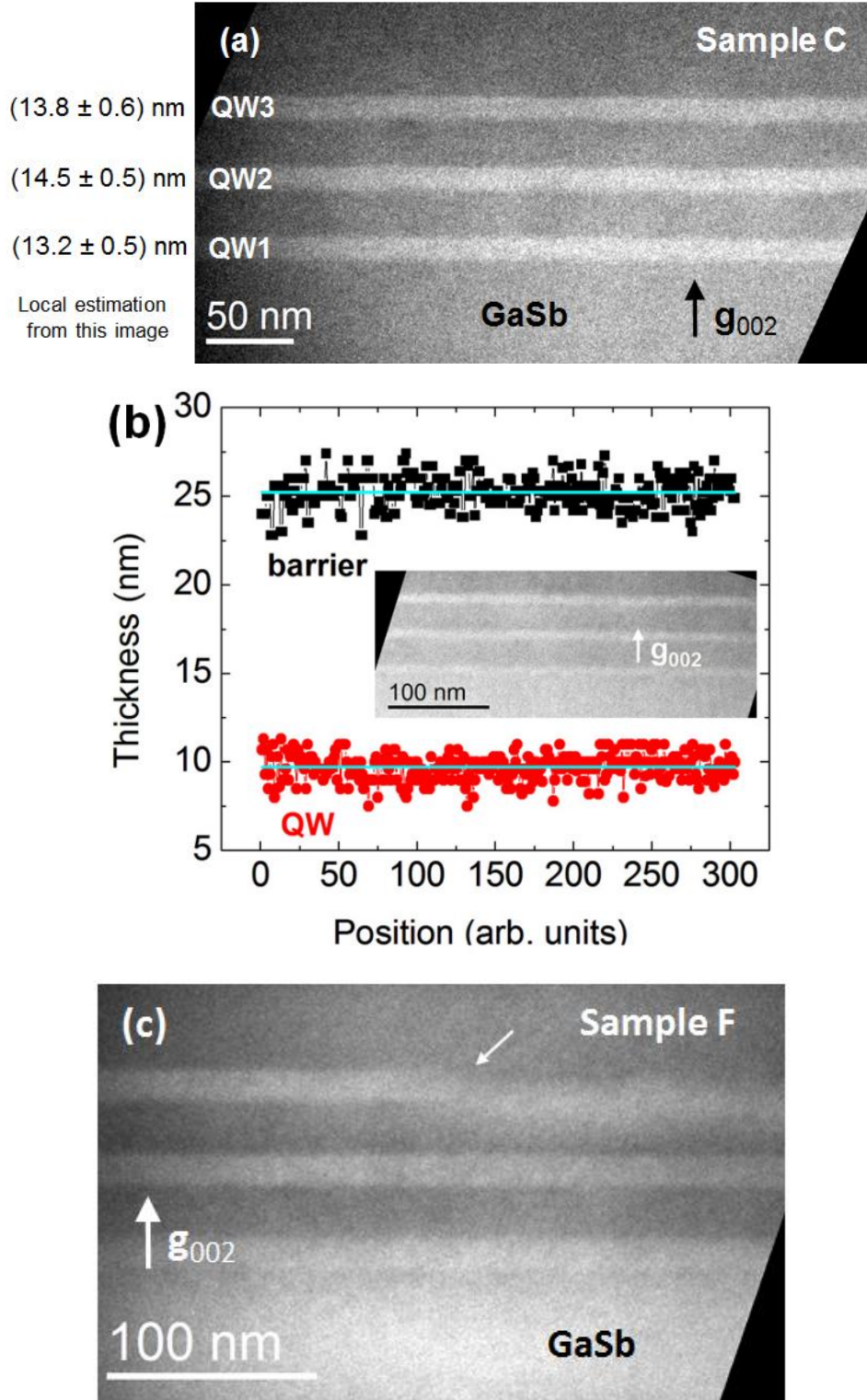
Fig. 3.7: (a) Representative chemically sensitive g_{002} DFTEM micrograph of sample C, displaying the smoothening effect at the GaSb-on-GaSbBi interface and the QW thickness variations. (b) Plot of the QW and barrier thickness of sample B measured at different lateral positions. The thickness fluctuations are evident. The data are obtained from the analysis of numerous TEM micrographs. The averaged values of QW/barrier thickness (solid lines) are represented as a guide for the eye. (c) Chemically sensitive g_{002} DFTEM micrograph of the GaSbBi/GaSb MQW in sample F. Local irregularities in the growth of the third QW are marked by the white arrow.

As mentioned earlier, interface roughness, thickness fluctuation and local morphological irregularities have been found in all the six samples (A to F) presented here. However, other QW samples with similar structures have been grown and characterized during this study. Interestingly enough, some of them did not exhibit any of these features. For the sake of comparison we present here a 15-nm thick GaSbBi /GaSb MQW sample (sample G) with a Bi content of 11.5 ± 1.5 % (Fig. 3.8a). First, the thickness variations from one QW to the other one are much smaller. The thickness of the QWs (in growth sequence) in this sample were indeed measured to be 14.5 ± 0.4 nm, 14.6 ± 0.4 nm and 14.8 ± 0.4 nm, respectively. Second, the interfaces are remarkably abrupt. Fig. 3.8b shows a representative local Bi distribution profile across the QW obtained from the analysis of the g_{002} diffracted intensity [Bithell and Stobbs-1989, Luna-2016]. The interface width ranges between 2.2 and 2.7 nm. This width is extremely small, on the same order as the chemical interface in other III-V heterointerfaces, *e.g.* 2.1 nm for high quality (Al,Ga)As/GaAs [Luna-2012]. Furthermore, the asymmetric profile attributed to the smoothing surfactant effect of Bi in samples A to F is not observed here. Both Ga(Sb,Bi)-on-GaSb and GaSb-on-Ga(Sb,Bi) interfaces are symmetric and exhibit a similar interface width, which also rules out the presence of strong Bi segregation [Luna-2016, Patil-2017].
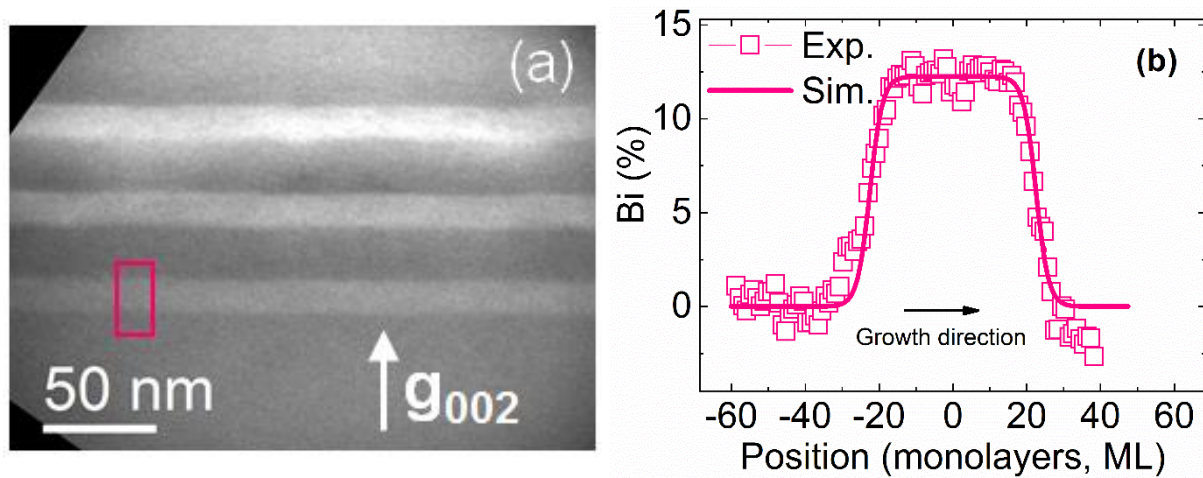
Fig. 3.8: (a) Chemically sensitive g_{002} DFTEM micrographs of the GaSbBi/GaSb MQW in the reference sample, together with (b) the Bi composition profile extracted from the analysis of the g_{002} DFTEM diffracted intensity in the area marked in (a). The experimental data are fitted to a sigmoidal function.

For now, we do not have a clear explanation regarding this differences observed between the two sets of samples. This sample was realized during the same growth campaign using the same growth method as the previous samples. We used the same cells and the same substrate temperature management. Therefore, we can only make one conclusion for now: it is possible to achieve the growth

of high quality GaSbBi/GaSb QWs without important interface roughness, thickness fluctuation or local morphological irregularities. Further investigations are required to understand the origin of these different features affecting some of our QWs, and their impact on their electronic properties. Regarding this last point, we have carried out PR and PL measurements which are detailed in the following.

3.2.3 Photoreflectance measurements

To allow an in depth investigation of the band structure, the two sets of MQW were investigated by PR spectroscopy. Indeed, PR measurement allows the observation of the optical transitions in the QW. The PR data were analyzed using 8 x 8 *k.p* calculations and compared to *ab-initio* DFT calculations to determine different parameters of the GaSbBi/GaSb QWs, such as the valence band offset (VBO) or the electron effective mass. The experiments and the simulations described in the following were performed by the team of Pr. Robert Kudrawiec of the Wrocław University of Science and Technology. The GaSbBi thicknesses and Bi concentrations were determined by TEM (see paragraph 3.2.2, the values are given in Table 3.1), as this technique provides a nanometer scale precision. Further details are given in [Kudrawiec-2019].

Fig. 3.9 shows PR and PL spectra measured at 10 K for GaSbBi/GaSb QW samples with various QW thicknesses and Bi concentrations. The PR signal observed around ~0.80 eV is caused by the photon absorption by the GaSb layers (substrate/buffer, QW barriers, cap) within the structure. The PR features observed at lower energies are associated with the optical transitions in the GaSbBi/GaSb QWs. The fundamental transition is easy to identify since it has the lowest energy and its resonance position correlates very well with the PL peak energy. In our samples, the fundamental transition occurs between the heavy-hole and the conduction subbands due to the compressive strain present in the QW. It is worth noticing that the Stokes shift (*i.e.* the difference between the PR fundamental resonance and the PL emission) is negligible at 10 K at the excitation density ~100 W/cm^2, attesting a low carrier localization. This is quite unusual, as dilute bismides often show strong carrier localization [Kudrawiec-2009, Shakfa-2013, Fitouri-2015, Kopaczek-2015]. Strong carrier localization is typical of highly mismatched alloys and is associated with alloy inhomogeneities and other imperfections like point defects or discrete energy levels close to the energy bands [Kudrawiec-2012a, Kudrawiec-2013]. The weak Stoke shift observed indicates that the studied QWs are overall homogeneous in terms of thickness and composition. The features observed in the previous paragraph by TEM at the nanometer

scale therefore do not seem to affect the PR measurement which analyzes a much larger (micrometric) areas.
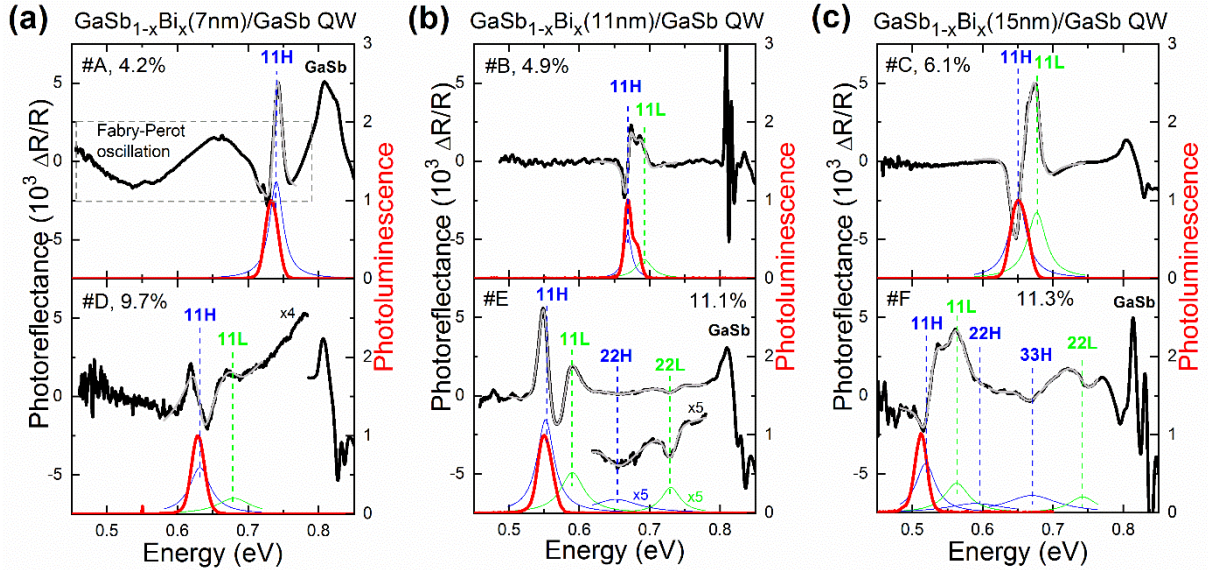
Fig. 3.9: Photoreflectance (black lines) and photoluminescence (red lines) spectra of GaSbBi/GaSb QWs of various widths and Bi concentrations measured at 10K. Thick solid grey lines represent theoretical fits and thin lines correspond to the moduli of individual PR resonances (blue – heavy hole transitions, green – light hole transitions). The notation nmH(L) denotes the transition between n-th heavy-hole (light-hole) valence subband and m-th conduction subband. The thicknesses given correspond to the nominal values.

PR resonances observed in the spectral range between the QW fundamental transition and the GaSb signal are associated with the QW transitions between excited states of higher energy. The identification of PR resonances – and thus of the QW transitions energies – was made possible by a series of calculations. The resonance at the lowest energy is attributed to the 11H transition (between the first heavy-hole and the first electron sub-bands), which is the fundamental transition for all GaSbBi/GaSb MQW samples. The fundamental transition for light-holes (11L -between the first light-hole and the first electron sub-band) is also clearly resolved for samples with large Bi concentrations (bottom panels in Fig. 3.9). For the MQW structures with the lowest Bi content (top panels in Fig. 3.9), the 11L transition overlaps with the 11H transition but can still be resolved for the two samples with the thicker GaSbBi wells (11 and 15 nm). Additionally, 22H and 22L transitions can be observed for samples E and F (bottom panels in Fig. 3.9 b and c). For this last sample, even the 33H transition is visible. The observation of such optical transitions related to excited states is a clear experimental evidence that these QWs are of type I with a deep quantum confinement in both the conduction and the valence band. In order to correlate the experimental data with the theory and determine the value of VBO for this material system, the procedure is the following: the QW transition energies are

calculated as functions of the VBO using 8-band *kp* Hamiltonian which includes strain effects. These energies are then compared with those extracted from PR spectra as shown in Fig. 3.10. Using this method, the optimal match between theory and PR data can be determined by comparing the data with calculated energies.

For the QWs analyzed in Fig. 3.10a the best correlation between PR data and theoretical calculations is observed for the VBO $\sim$ 45-50%. The same procedure for correlating PR data with theoretical predictions has been applied to the remaining GaSb$_{1-x}$Bi$_x$/GaSb QWs. For all samples a good agreement between PR data and calculations has been observed for very similar VBO.

In the *kp* calculations the electron effective mass was properly corrected in order to obtain matching between experimental data and calculations for the fundamental transition and excited state transitions. This can be done by the comparison of the energy difference between 22H and 11H transition as shown in Fig. 3.10b. In order to match experimental data with 8-band *kp* calculations with two free parameters (the VBO and the electron effective mass), a few iteration is needed. However it is quite easy to recognize the reasonable range of VBO and the electron effective mass for a given QW.
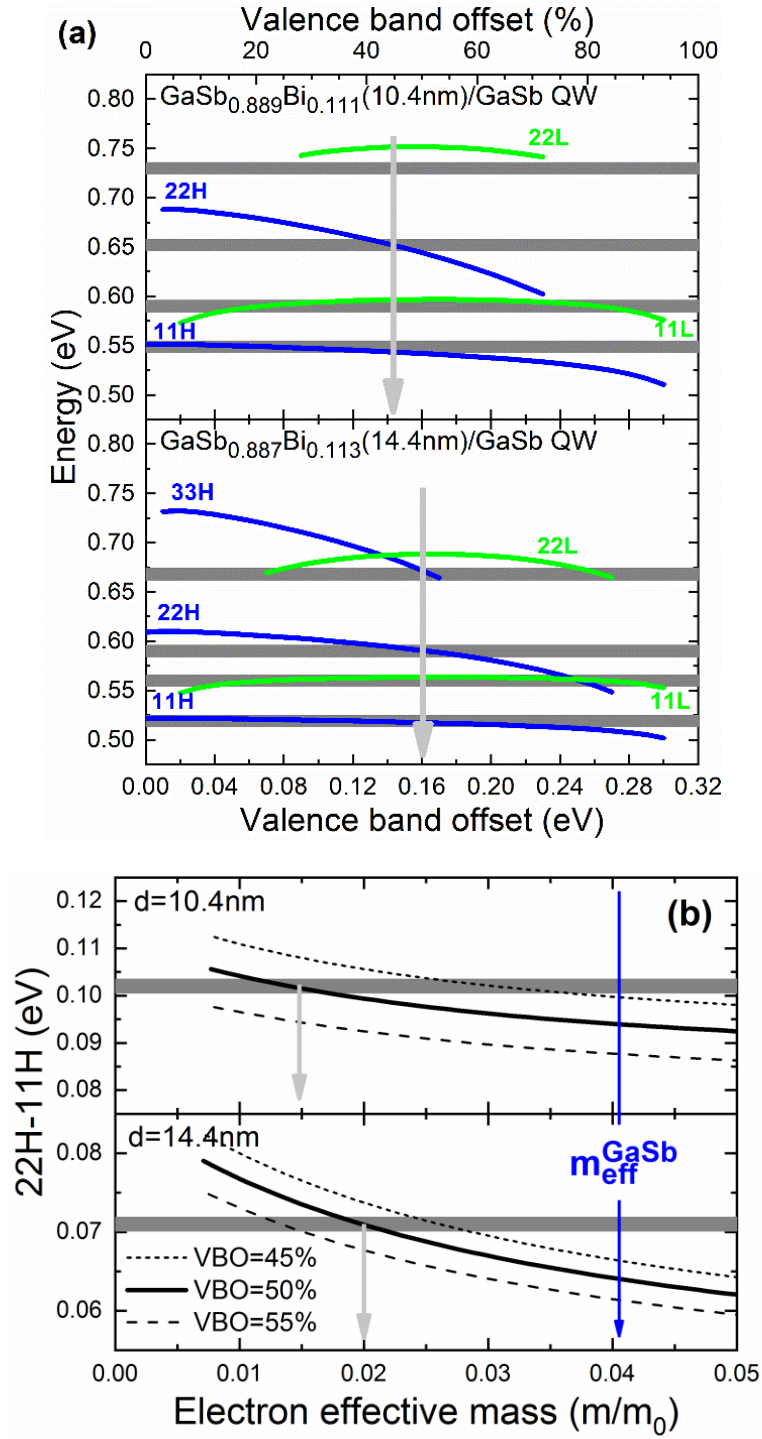
Fig. 3.10: (a) Method used to analyze the VBO in GaSbBi/GaSb QWs: examples for samples E (top panel) and F (bottom panel). The horizontal thick grey lines correspond to energies of 11H, 22H, 33H, 11L, and 22L transitions obtained from PR measurements and the solid lines represent theoretical calculations of energies of QW transitions for various values of VBO. (b) The energy difference between the 22H and 11H transition of sample E and F (top and bottom panels, respectively) extracted from PR measurements (grey thick horizontal line) and 8-band **kp** calculations for different VBO and various electron effective mass.

In addition, the evolution with the Bi concentration of the electron effective mass in $GaSb_{1-x}Bi_x$ can also be compared to the values obtained from *ab-initio* DFT calculations. The electron effective mass determined from PR studies combined with *kp* calculations is plotted in Fig. 3.11 (open square points) together with the electron effective mass at Γ-points extracted from the DFT calculations (solid line). The low value of the electron effective mass at the Γ point calculated for pure GaSb is consistent with the literature [Vurgaftman-2001]. The effective mass decreases monotonously and almost linearly with the increase of Bi concentration, as expected from the band gap narrowing. This dependence can be fitted by the following linear dependence:

$$m_{eff}^{GaSbBi} = m_{eff}^{GaSb} - 0.2x \tag{3.1}$$

where x is the Bi concentration and m_{eff}^{GaSb} is the electron effective mass in GaSb. A change of the hole effective mass with the Bi concentration was also observed but this effect is much weaker than the Bi-related change in the electron effective mass and therefore is neglected in our analysis.
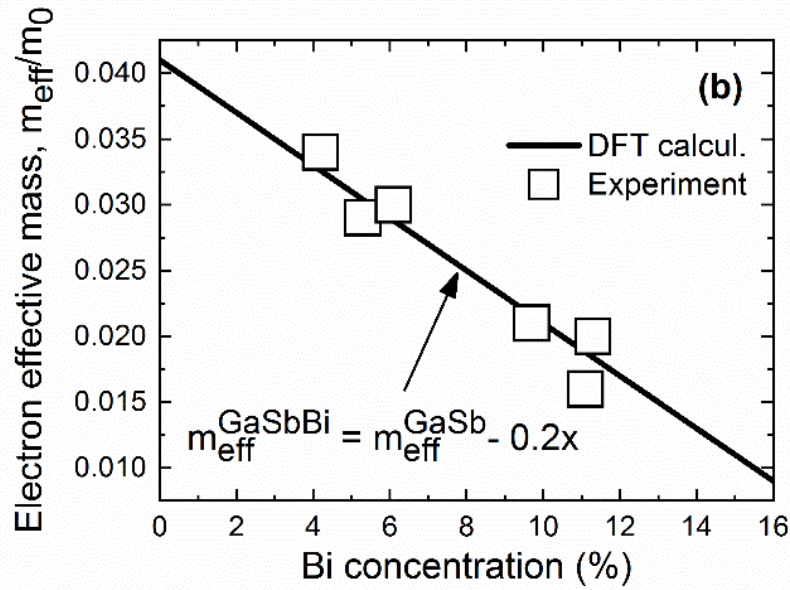
Fig. 3.11: Electron effective mass at the Γ point of the Brillouin zone in GaSbBi with various Bi concentrations obtained from ab-initio calculations (solid line – linear fit) and from PR measurements combined with kp calculations (open points).

Finally, the results are summarized in Fig. 3.12a, where the conduction and valence band positions in GaSbBi calculated by DFT are represented by black thick lines. Open squares represent the conduction and valence band energies in GaSbBi (relative to the GaSb VB) obtained from PR measurements and *kp* analysis. In addition, positions of the conduction band, and heavy- and light-hole valence bands in compressively strained GaSbBi on GaSb are plotted as thin lines. It is worth emphasizing the good confinement for both holes and electrons offered by the incorporation of Bi,

allowing to design type-I QWs in the mid-infrared wavelength range using simple GaSb barriers. To illustrate this point, the band energy alignment as well as electron and hole levels for two of the QWs studied have been plotted in Fig. 3.12b. Next, the PL emission of these samples was investigated.
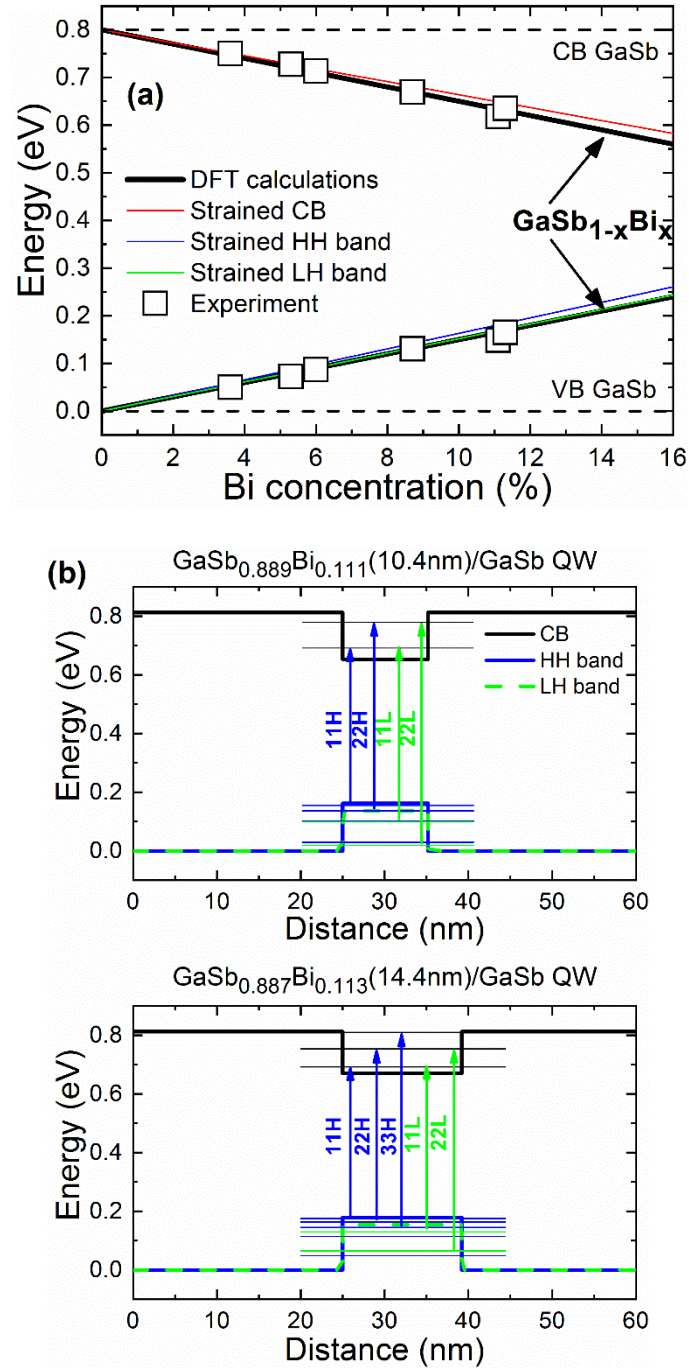
Fig. 3.12: Conduction and valence band positions in unstrained GaSbBi obtained from PR measurements (open squares) and DFT calculations (thick black lines). Thin lines show position of conduction (red line), heavy hole (blue line), and light-hole (green line) bands in GaSbBi compressively strained on GaSb. In this energy scale zero corresponds to the valence band position in GaSb. (b) represents the quantum confinement potential for the two samples analyzed in (a), together with energy levels.

3.2.4 Photoluminescence study

We have studied the PL emission of samples A to G. Additionally, a series of 7-, 11- and 15-nm GaSbBi/GaSb MQWs with ∼15% Bi was also characterized. This last set of samples was not investigated by TEM.

All the MQW structures show PL emission at RT, between 2 and ∼3.5 µm (Fig. 3.13a). However, an overall degradation of the optical performances as the Bi content raises can be observed. Indeed, the PL emission peak broadens and the PL intensity decreases strongly as longer wavelengths are reached, as shown in Fig. 3.13b. This deterioration of the PL emission is certainly to be related to the deterioration of the crystal quality that was observed when the Bi content increases, in particular above 12%. The spectrum measured from sample G is also shown for comparison. Interestingly, despite much better microstructure characteristics (very low QW thickness fluctuations, interface roughness and local morphological irregularities, *cf* paragraph 3.2.2), this sample exhibits a similar PL intensity than the other MQW. Its emission peak is not thinner either, despite the superior structural properties assessed by TEM. Therefore, it seems that the features affecting samples A to F in the previous paragraph do not substantially affect the optical performances.
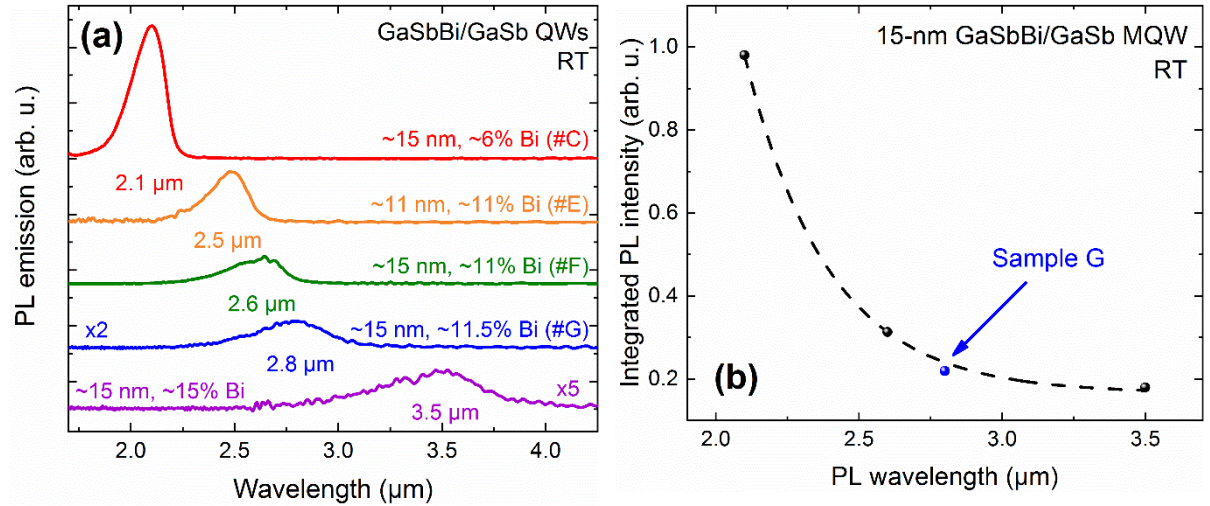
Fig. 3.13: (a) PL emission at RT of GaSbBi/GaSb MQW structures with various Bi content and GaSbBi widths. The intensity of the two last samples was multiplied by a factor 2 and 5, respectively, for a sake of clarity. (b) RT integrated PL intensity of 15-nm GaSbBi/GaSb MQW with various Bi concentrations. The dashed line is a guide for the eye.

The PL emission of three GaSbBi/GaSb MQW samples was studied between 11 and 300 K (Fig. 3.14a). The QWs in the three samples are 15 nm wide, and the structure is the same, apart from the

Bi content: 6% (sample C), 11% (sample F) and 15%, respectively. A GaInAsSb/GaSb MQW structure with a comparable PL emission (0.572 eV at 300 K) was also characterized for comparison's sake.
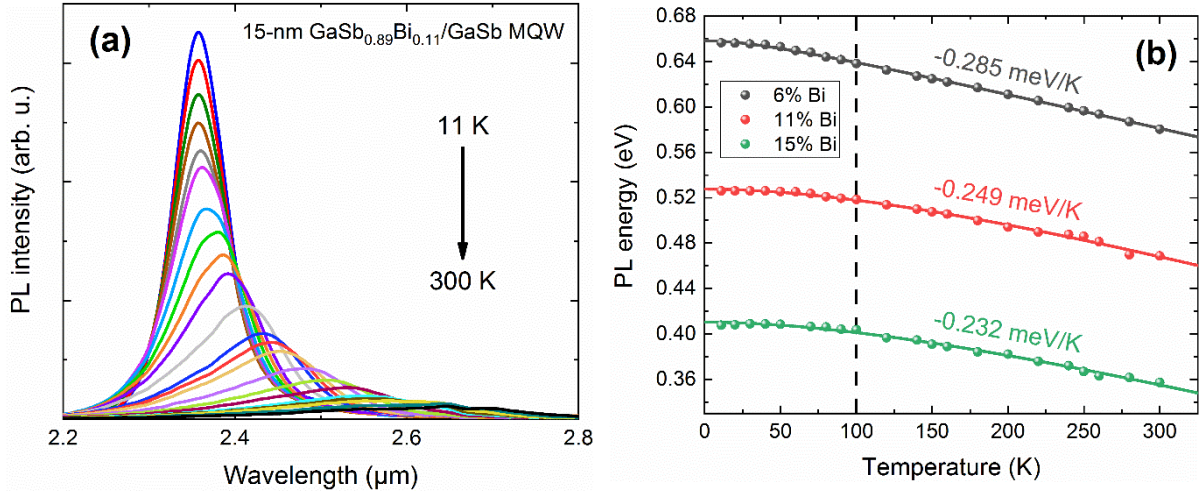
Fig. 3.14: (a) PL emission of the 15-nm GaSbBi/GaSb MQW structure with 11% Bi between 10 and 300 K. (b) Temperature dependence of the PL energy of 15-nm GaSbBi/GaSb MQW with 6, 11 and 15% Bi in the 10 - 300 K range. The solid lines are the Varshni fits using Eq. 2.4. The dashed black line delimits the temperatures used for the linear fit.

The PL energy temperature dependence is depicted in Fig. 3.14b. The PL energy of Sample C (6% Bi) decays at a linear rate of 0.285 meV/K in the 100 to 300 K range, a value somewhat smaller than for the GaInAsSb-based MQW structure (-0.301 meV/K). Interestingly, the variation of the PL energy with temperature seems to decrease as the Bi content raises: -0.249 and -0.232 meV/K for the samples with 11 and 15% Bi, respectively. Of course, it must be kept in mind that in such a MQW structure, the temperature sensitivity of the PL energy not only depends on the GaSbBi wells, but also on the GaSb barriers. However, as the structure and layers thicknesses are identical in those three samples, the variations observed can confidently be related to the Bi concentration. Therefore, this result tends to confirm our initial observation about the influence of the Bi on the bandgap temperature dependence (see paragraph 2.4.1): the incorporation of Bi seems to make the bandgap less sensitive to temperature, as also reported by Yue *et al.* on GaSbBi/GaSb single-QW [Yue-2018b].

The data in Fig 3.14.b were fitted using Varshni (Eq. 2.4) and Bose-Einstein (Eq. 2.5) models and the corresponding parameters are listed in Table 3.2 and Table 3.3, respectively. In addition, data of the 6-nm GaSbBi/GaSb single-QW structures of Yue *et al.* are also included in Table 3.2 and marked by a Y [Yue-2018b]. Although no clear trend emerges from these data, our Varshni parameters are consistent with the ones of Yue *et al.* and the values of the GaInAsSb-based structure. Regarding the

B-E parameters, a_B and in particular θ_B increase with the rise of the Bi content, confirming our preliminary result obtained on the GaSb$_{0.86}$Bi$_{0.14}$ layer and those reported by Kopaczek *et al.* [Kopaczek-2013].

Table 3.2: E_G linear variation in the range 100 – 300 K and Varshni parameters extracted from the fitting of the PL energy variation between 11 and 300 K (Fig. 3.14b).

Sample	PL energy linear variation 100 – 300 K (meV/K)	Varshni parameters		
		E_0 (eV)	α (x 10^{-4} eV/K)	β (K)
GaInAsSb / GaSb	-0.301	0.657	4.1	208
GaSb$_{0.934}$Bi$_{0.066}$ / GaSb (Y)	-	0.699	5.1	298
GaSb$_{0.917}$Bi$_{0.083}$ / GaSb (Y)	-	0.632	3.4	217
GaSb$_{0.899}$Bi$_{0.101}$ / GaSb (Y)	-	0.567	6.3	731
GaSb$_{0.94}$Bi$_{0.06}$ / GaSb	-0.285	0.658	3.1	59
GaSb$_{0.89}$Bi$_{0.11}$ / GaSb	-0.249	0.528	4.1	318
GaSb$_{0.85}$Bi$_{0.15}$ / GaSb	-0.232	0.41	3.7	310

Table 3.3: B-E parameters extracted from the fitting of the PL energy variation between 11 and 300 K.

Bi content (%)	Bose-Einstein parameters		
	E_0 (eV)	a_B (meV)	θ_B (K)
GaInAsSb / GaSb	0.655	30	187
GaSb$_{0.94}$Bi$_{0.06}$ / GaSb	0.657	14	94
GaSb$_{0.89}$Bi$_{0.11}$ / GaSb	0.526	30	218
GaSb$_{0.85}$Bi$_{0.15}$ / GaSb	0.409	30	228

Our three MQW structures show very low carrier localization at low temperature, which is consistent with the weak Stoke shift observed previously (see paragraph 3.2.3), and confirms the good crystal quality of our samples. However, a slight "S-shape" variation of the PL energy at low temperature (below 30 K) can be noticed for the sample with the highest Bi content. It is very small in comparison with what was reported in the literature by Yue *et al.* [Yue-2018b], but it nevertheless reveals the existence of localized states in the QWs of this sample. Besides, the localization at 11 K is slightly larger in this sample (2.5 meV) than in the two others (1.5 meV). This rise of the localization effect correlates well with the degradation of the material quality caused by the very high Bi content.

It is the obvious consequence of the lattice disorder and the point defects introduced by the incorporation of Bi.
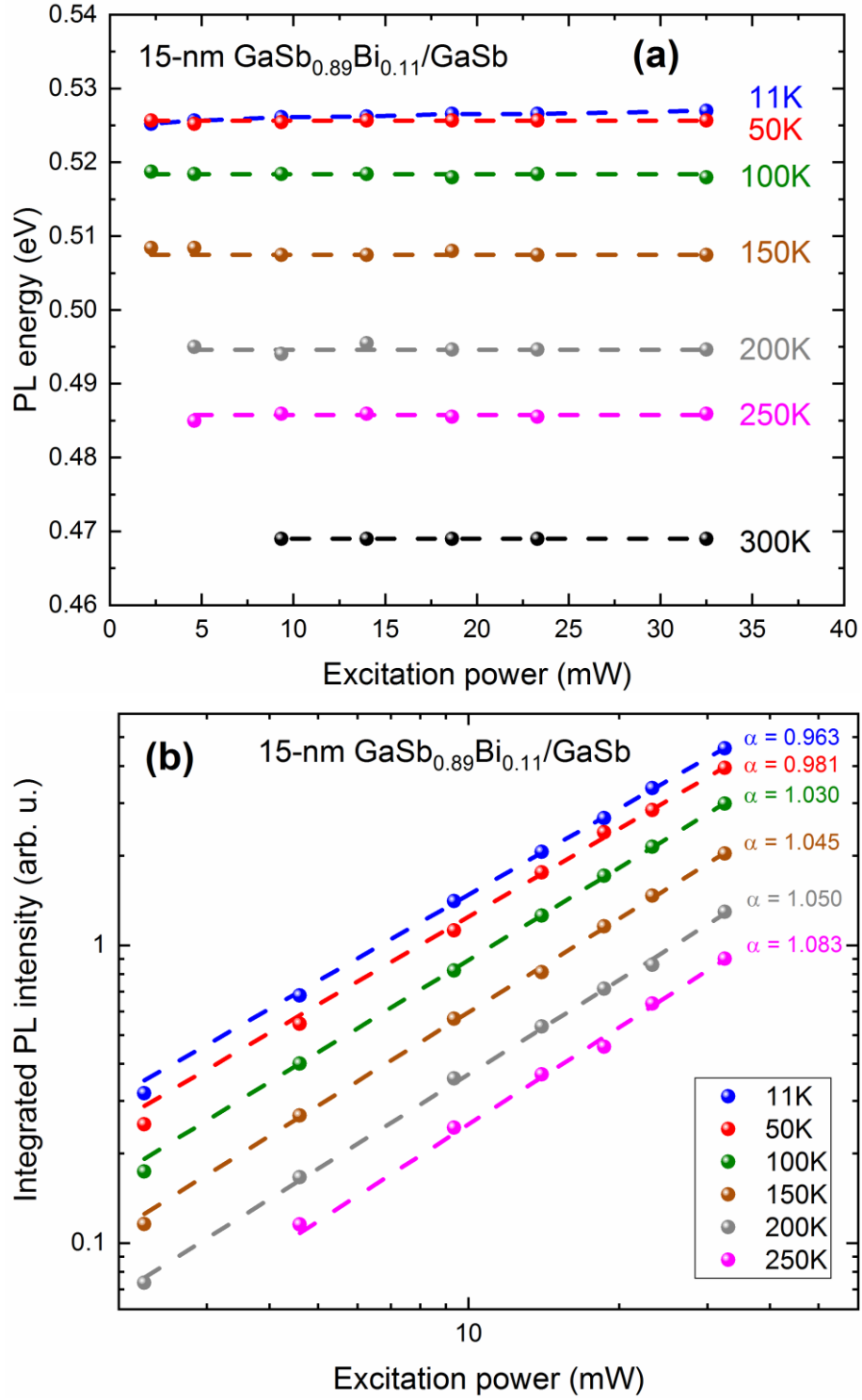
Fig. 3.15: (a) PL energy and (b) integrated PL intensity of the 15-nm GaSb$_{0.89}$Bi$_{0.11}$ / GaSb MQW structure as a function of the excitation intensity in the range 11 – 300 K. The dashed lines in (b) show the fits using Eq. 2.6.

Localization was also studied as a function of the excitation power (Fig. 3.15a). At 11 K, the PL peak energy of the three samples was found to increase with the excitation intensity, but the variation remains weak (about 2 meV). However, above 50 K, the PL peak energy does not change anymore with the excitation power for the samples with 6 and 11% of Bi in the QWs, which points to the delocalized character of the emission. Regarding the sample with 15% of Bi, the measurement becomes very challenging due to the low PL intensity and the broad emission peak. Therefore, it is unclear if localization effect still exists at 50 K and above. The integrated PL intensity was also measured as a function of the excitation power, and fitted using Eq. 2.6. As previously found for the GaSbBi layers, α is close to one at all temperatures (between 0.911 and 1.194) for the three samples, indicating a PL emission dominated by excitonic recombination. Nevertheless, it is very clear that the value of α increases with the temperature, as shown for the sample with 11% in Fig. 3.15b. It illustrates the delocalization mechanism of the excitons caused by the thermalization.

To summarize, we have obtained PL emission at room temperature up to ~3.5 μm although the PL emission is degraded as longer wavelengths and larger Bi concentrations are reached, in good agreement with the deterioration of the crystal quality observed in chapter 2 (see paragraph 2.4.1). PL measurements at low temperature confirm a negligible localization, which tends to slightly increase with the Bi content. We also observed that the Bi incorporation in GaSb seems to make the bandgap less sensitive to the temperature. The PL emission was dominated by exciton recombination at all temperatures. Finally, we observed similar PL properties for all samples which indicates that the features (thickness modulations, asymmetric composition profile across the QWs) observed on some samples by TEM do not affect significantly their optical properties.

3.3   GaSbBi/GaSb laser diode

Next we have fabricated the first ever GaSbBi-based laser structure. Indeed, no lasing device using GaSbBi had ever been reported at this point, contrarily to GaAsBi [Tominaga-2010, Fuyuki-2013, Ludewig-2013, Butkute-2014, Fuyuki-2014, Marko-2015, Liu-2017, Wu-2017, Kim-2018]. This paragraph describes the structure design, the growth conditions and the laser characteristics. These results have been published in [Delorme-2017b].

3.3.1 Growth of the GaSbBi-based laser

Fig. 3.16a displays the MQW laser structure. The three 15-nm GaSbBi / 20-nm GaSb type-I QWs composing the active region are sandwiched between 263 nm-thick GaSb waveguide layers and 1.65 µm thick $Al_{0.8}Ga_{0.2}AsSb$ cladding layers. Te and Be were used as *n*- and *p*-type dopants, respectively. A 300-nm-thick highly *p*-type doped GaSb layer was grown to form the top contact layer. The layers on top of the active region were grown at 450°C, and the different thicknesses were determined to maximize the optical gain in the active region (Fig. 3.16b). The laser's active region was realized using the growth conditions previously used for sample G (same substrate temperature for the QWs and the barriers, V/III flux ratio close to one for both layers). The layers grown on top of the active region are much thicker (almost 2 µm) for the laser structure than in previous MQW samples. We therefore used sample G as a reference in order to be able to detect if any difference or degradation occurs due to the growth of these thicker upper layers.
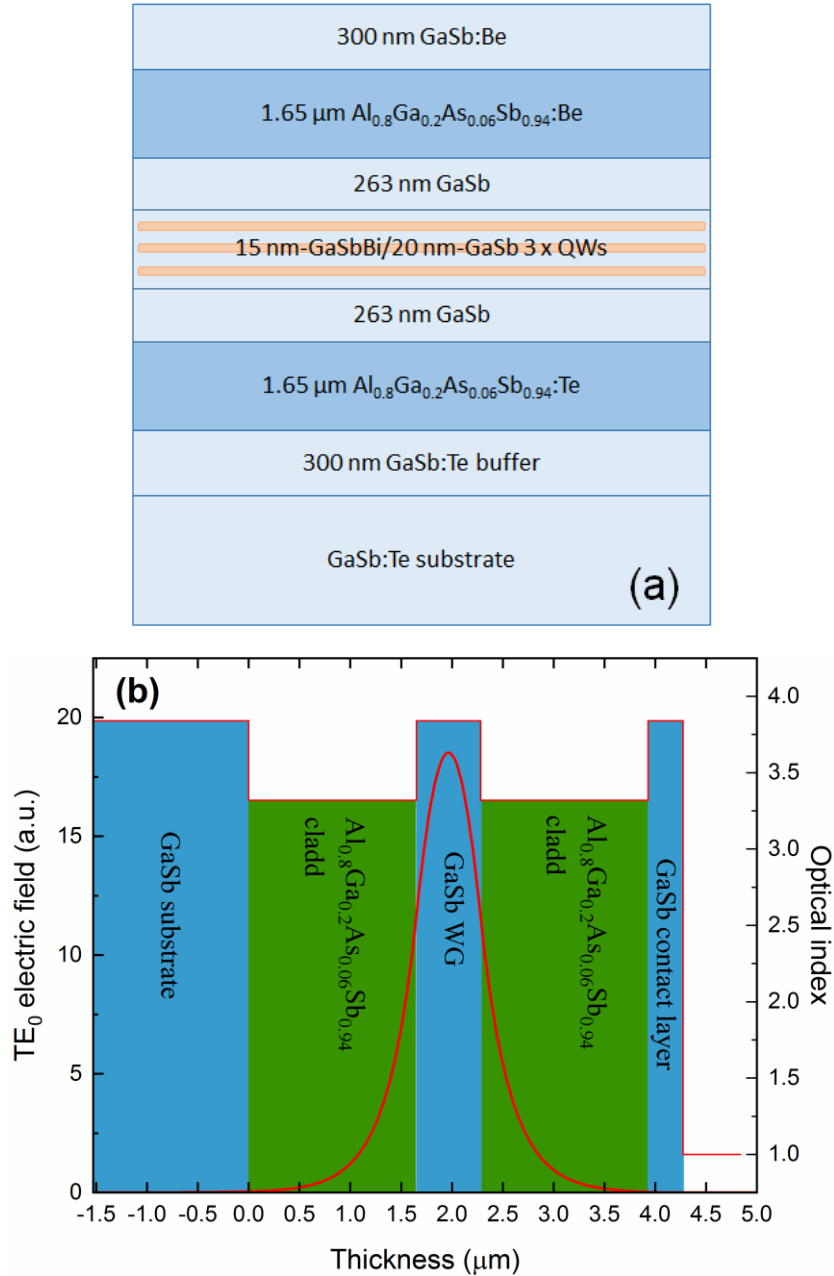
Fig. 3.16: (a) Schematic view of the GaSbBi/GaSb MQW laser structure. (b) Representation of the calculated optic mode

The two samples show a droplet free surface. For both samples, AFM cartography reveals RMS roughness below 0.2 nm and the presence of monolayer steps, indicating a step-flow growth mode (Fig. 3.17 a and b). The HR-XRD $\omega-2\theta$ scans of the two samples are displayed in Fig. 3.17c. The high crystal quality of the MQW sample is demonstrated by the well-defined QWs satellite peaks and the excellent agreement between simulated and experimental curves. The laser structure exhibits slightly broader features near the substrate peak, probably due to a slight mismatch of the cladding layers. Nonetheless, the overall experimental curve is also in excellent agreement with the simulation. Notably, the GaSbBi/GaSb QW-related features are clearly visible which shows that the whole

85

periodicity has been preserved. For both sample, an average Bi content of 11.5 ± 1.5 % was estimated from the HR-XRD simulations.
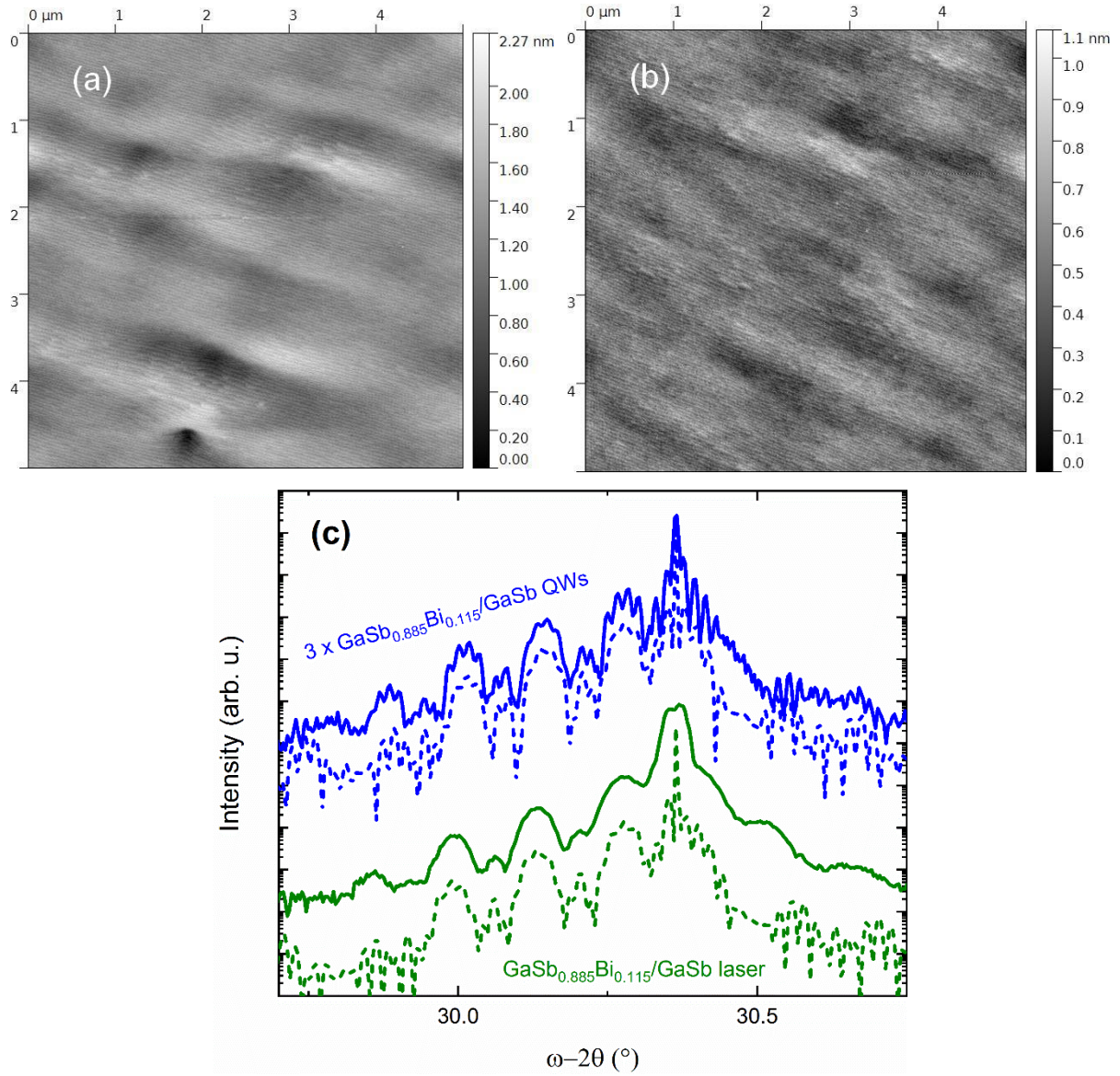
Fig. 3.17: 5 x 5 µm AFM observation of the GaSbBi/GaSb MQW reference sample (a) and the laser structure (b). (c) HR-XRD (004) ω−2θ scans of the MQW reference sample (solid blue line) and of the laser structure (solid green line). The simulated curves are given as dashed lines. The curves have been vertically shifted for clarity.

The high structural quality of the laser sample was confirmed by TEM investigations. No extended defect or clustering were detected in the pseudomorphic layers, as shown in the TEM micrographs of Fig. 3.18a. The QWs in the active zone are regular and homogeneous, with smooth and abrupt interfaces, and very low thickness fluctuation. In fact, as far as TEM analysis is concerned, the

active region of the laser is very similar to the one of sample G. Fig. 3.18b shows a representative local Bi distribution profile across the QW obtained from the analysis of the $\mathbf{g}_{002}$ diffracted intensity [Bithell and Stobbs-1989, Luna-2016] for the laser structure. The interface width ranges between 2 – 2.8 nm for the laser structure, very close to the value found for sample G (2.2 – 2.7 nm). Moreover, the GaSbBi-on-GaSb and GaSb-on-GaSbBi interfaces appear symmetric. Finally, quantitative determination of the Bi content from the analysis of chemically sensitive g_{002} DFTEM micrographs yields a Bi content for the laser sample (11.6 ± 1.4 %), again very similar to sample G (11.8 ± 1.4 %), and in excellent agreement with the average composition deduced from HR-XRD. Therefore, the absence of degradation observed in the laser structure demonstrates that *in situ* annealing during MBE growth of the top cladding and contact layers at the higher T_s = 450 °C does not have a detrimental effect on the layers.
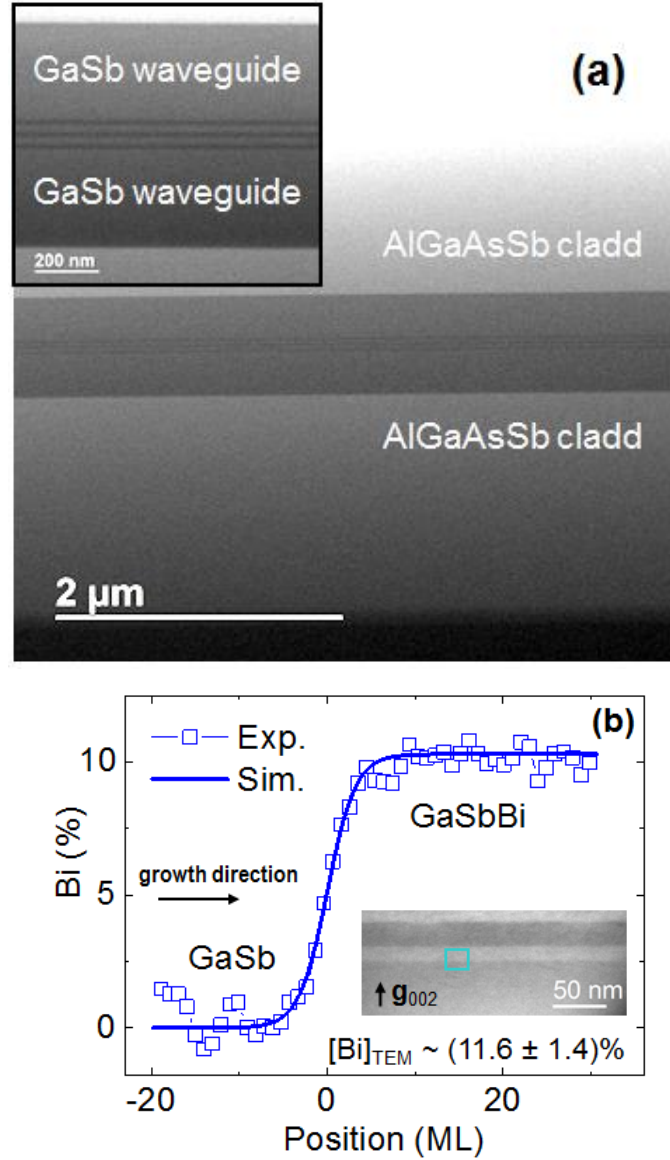
Fig. 3.18: (a) Bright-field STEM overview of the laser structure. A closer look at the active zone is shown in the inset. (b) Bi distribution profile at the GaSbBi-on-GaSb interface in the laser structure, extracted from the analysis of the g_{002} DFTEM diffracted intensity. The experimental data are fitted to a sigmoidal function.

87

3.3.2 Characterization of the GaSbBi-based laser diode

The sample was processed into ridge laser diodes of 10x1160 µm² in the clean room of the University of Montpellier using standard photolithography and wet etching. Ti-Au and AuGeNi were used as contact metals for the *p*- and *n*-type contacts, respectively. Electrical insulation and protection of the etched sidewalls was obtained using the AZ1518 photoresist. Laser cavities were formed by simple cleaving of the facets, without any antireflection coating. Finally, the devices were soldered epi-side down with indium on Cu heat-sinks.

Electroluminescence (EL) from the laser structure was measured at RT under 350 mA pulsed current injection and compared to the PL emission of sample G (Fig. 3.19). Both spectra are distorted by the water absorption bands between 2.5 and 2.9 µm. It is however clear that the laser EL spectrum overlaps well with the MQW PL emission, which confirms the reproducibility of the MQW growth.
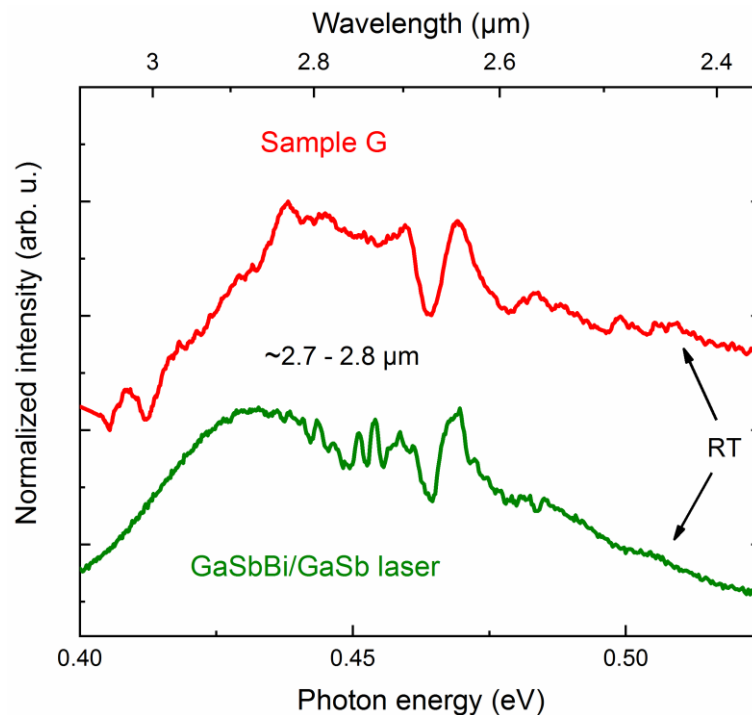
Fig. 3.19: PL emission of sample G (in red) and facet emission spectra of the GaSbBi laser (in green) measured at RT. The intensities are normalized to 1.

The GaSbBi/GaSb laser diodes were characterized at different temperatures under pulsed injection (200 ns pulse width, 21 kHz repetition rate). Fig. 3.20a shows the light-current (L-I) and voltage-current (V-I) characteristics and Fig. 3.20b the laser emission spectrum at different temperatures measured for an injected current slightly above threshold. The V-I characteristic

measured at RT clearly shows a diode behavior with a turn-on voltage close to 0.7 V and a threshold voltage of 1.25 V. At RT, the threshold current density J_{th} for the 10 x 1160 µm² area diode is 4.22 kA/cm² with a lasing wavelength of 2.71 µm (0.457 eV) under pulsed operation. At 80 K, the threshold current density is 431 A/cm² and the emitted wavelength is 2.50 µm. The T_0 characteristic temperature of this laser diode is 111 K between 80 and 250 K, decreasing to 60 K in the 250 to 300 K temperature range (Fig. 3.20c). The peak emission wavelength redshifts linearly at a rate of 1.3 nm/K (-0.235 meV/K) when increasing the temperature from 130 to 300 K (Fig. 3.20d). This variation rate is similar to the characteristics of the GaInAsSb/AlGaAsSb lasers operating between 2 and 3 µm [Choi-1994, Choi and Turner-1997, Kim-2003, Lin-2004].
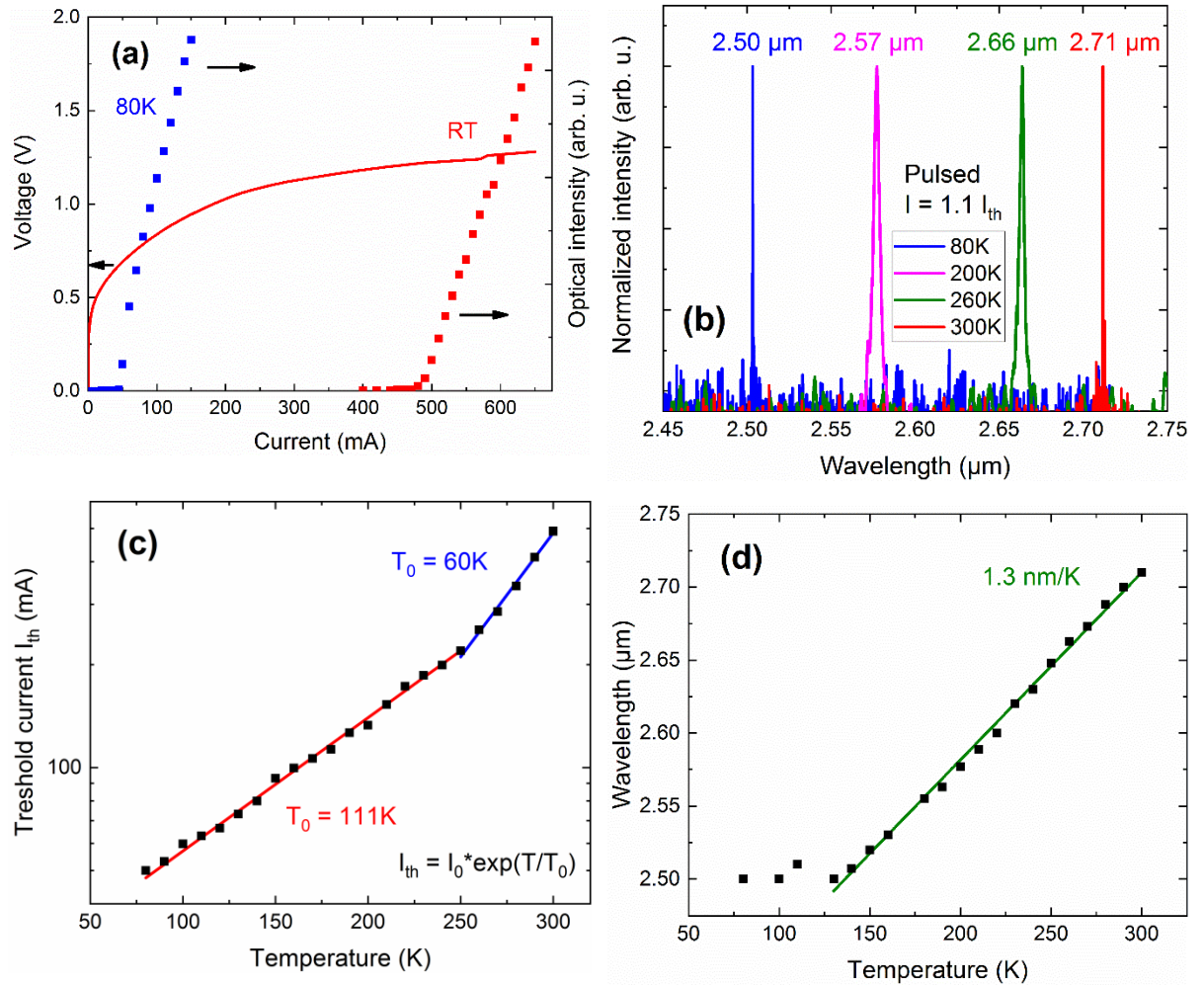
Fig. 3.20: (a) I-V and L-I (under pulsed operation) characteristics at RT (in red) and 80K (in blue). (b) Laser emission spectrum at different temperatures under pulsed operation. The intensities are normalized to 1. Temperature dependence of threshold current density (c) and laser emission peak wavelength (d) for pulsed operation.

Finally, CW operation was achieved at 80 K from this laser structure with a lasing wavelength of 2.52 µm (Fig. 3.21) and a threshold current density J_{th} of 586 A/cm². The J_{th} of our device is still high compared to the standard GaInAsSb/AlGaAsSb laser diodes developed for many years in this spectral range but is comparable to those of early laser diodes [Choi-1994, Garbuzov-1995, Lee-1995]. Our J_{th} is also in the same range of those of GaAsBi-based lasers [Ludewig-2013, Butkute-2014, Fuyuki-2014, Marko-2015, Liu-2017, Wu-2017, Kim-2018], although the Bi content is higher in our case (7.6% Bi maximum in GaAsBi lasers). This high threshold current density is consistent with the degradation of the optical and structural properties observed when increasing the Bi content. It may be also related to a still too-low crystal quality arising in particular from the very low growth temperature of the GaSb barrier layers in the MQW structure. However, this first lasing device confirms the potential of GaSbBi for optoelectronics in the mid-IR.
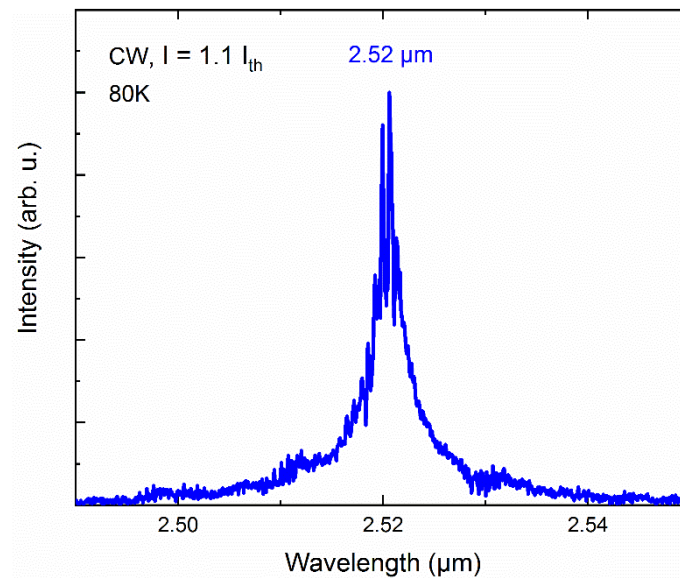
Fig. 3.21: CW laser emission at 80K

3.4   Conclusion

In this chapter, we have investigated the growth and the properties of GaSbBi/GaSb MQW structures. First, we studied the stability of GaSbBi upon annealing. To this end, a GaSbBi epilayer was annealed several times in the MBE system and no change in composition nor degradation of the crystal quality was observed. On the contrary, the PL intensity was increased by a factor of 12 after two hours of annealing at 450°C, showing an improvement of the material quality. Once the good thermal stability of GaSbBi was demonstrated, the influence of the temperature management during the growth of the GaSbBi/GaSb QWs was investigated. Two MQW samples were grown using different temperatures for the GaSb barriers. As the MQW sample with the GaSb barriers grown at low temperature showed better PL performances, the active region of the subsequent MQW structures were grown at 200°C TTR.

Then, we have grown several GaSbBi-based MQW structures with Bi contents up to ~15% and different GaSbBi widths (7, 11 and 15 nm, nominally). Their properties were investigated by different methods. First, the structural properties were characterized by TEM investigations which demonstrated that most samples were homogeneous in composition and of high crystallographic quality as no dislocation, clustering or extended defect could be observed. However, some GaSbBi/GaSb QWs were affected by thickness fluctuations, local morphological irregularities and non-abrupt interfaces. The origin of these features remains unclear, but no clear impact on the optical properties was noticed.

Second, the band alignment of the GaSbBi/GaSb system was investigated by PR measurements coupled with theoretical calculations. The numerous optical transitions related to excited states observed confirmed the type I band alignment of the GaSbBi/GaSb QWs and the deep confinement of both holes and electrons. It was also determined that Bi incorporation modifies the conduction and valence bands at the same rate (GaSbBi/GaSb VBO ~50%), resulting in a bandgap reduction of ~30-32 meV/%Bi. Finally, the variation of the electron effective mass in GaSbBi alloy as a function of the Bi content was estimated.

Third, the PL emission was investigated. All samples demonstrated PL emission up to 300 K between 2 and 3.5 μm. However, an overall degradation of the optical performances was observed as the Bi content raised. Indeed, the PL intensity decreases strongly and the emission peak broadens clearly as the Bi content increases. The PL emission was also studied as a function of the temperature. A very weak localization was observed at low temperature, confirming the high crystal quality. We also observed that the incorporation of Bi makes the bandgap somewhat less sensitive to the temperature.

Finally, the PL emission was found to be dominated by excitonic recombination, as previously observed for the GaSbBi layers.

Finally, the first-ever GaSb$_{0.885}$Bi$_{0.115}$/GaSb laser diode was fabricated and characterized. No degradation caused by the growth of the upper cladding was observed by TEM. CW lasing near 2.5 µm at 80 K and pulsed laser emission close to 2.7 µm at RT was achieved. Despite the relatively high threshold current density (~4.2 kA/cm²), this first GaSbBi-based device opens the way to future developments in infrared optoelectronics.

In the next chapter, we investigate the addition of Indium to GaSbBi to form another new alloy, GaInSbBi.

Chapter 4: Addition of In into GaSbBi alloys

In this fourth chapter, we have grown GaInSbBi layers to study the addition of another element III to GaSbBi and investigate the epitaxy of more complex dilute bismide alloys. A strong influence of In on the Bi incorporation was observed. GaInSbBi/GaSb MQW were also fabricated and their PL emission was studied over a large range of temperature. Finally, a new growth strategy was attempted.

4.1 Ga(In)SbBi alloys

In this part, we investigate the growth of GaInSbBi alloys. In particular, the influence of In on the Bi incorporation was investigated. GaInSbBi/GaSb MQW structures were also grown for the first time. The structural quality was assessed using HR-XRD and TEM, while the optical properties were studied by PL spectroscopy.

4.1.1 Impact of the addition of In

The incorporation of In into GaSbBi should offer a supplementary reduction of the bandgap, due to the low bandgap of InSb (0.235 eV [Vurgaftman-2001]) and the negative bandgap of InBi (-1.63 eV [Janotti-2002]) (Fig. 4.1). The incorporation of In in GaSbBi should also further increase the lattice mismatch with respect to GaSb because both InSb (6.479 Å [Vurgaftman-2001]) and InBi (6.626 Å [Rajpalke-2014b]) have a larger lattice parameter than GaSb (6.0954 Å), as shown in Fig. 4.1. In can thus be useful for the optimization of the strain in the QW layer in order to maximize the optical gain of laser diodes. Additionally, GaInSbBi could be promising for mid-IR applications. Indeed, using an 8-band ***k.p*** Hamiltonian, Gladysiewicz *et al.* theoretically estimated that emission above 3 μm could be achieved from 8 nm GaInSbBi/GaSb QWs with 32% In and 8% Bi [Gladysiewicz-2016].

However, only few reports on GaInSbBi quaternary alloys can be found in the literature. The growth of $Ga_{1-x}In_xSb_{1-y}Bi_y$ layers with $x \leq 5.5\%$ and $y \leq 2.5\%$ by molecular beam epitaxy (MBE) was reported in 2014 [Kopaczek-2014a]. A photoluminescence (PL) study of these samples demonstrated that the incorporation of In results in a significant reduction of the carrier localization, indicating an improvement of the material quality over GaSbBi alloys grown by this group [Linhart-2017]. However,

both Bi and In contents in these GaInSbBi layers remain rather low. A study of the growth of GaInSbBi with higher Bi and In contents is still missing.
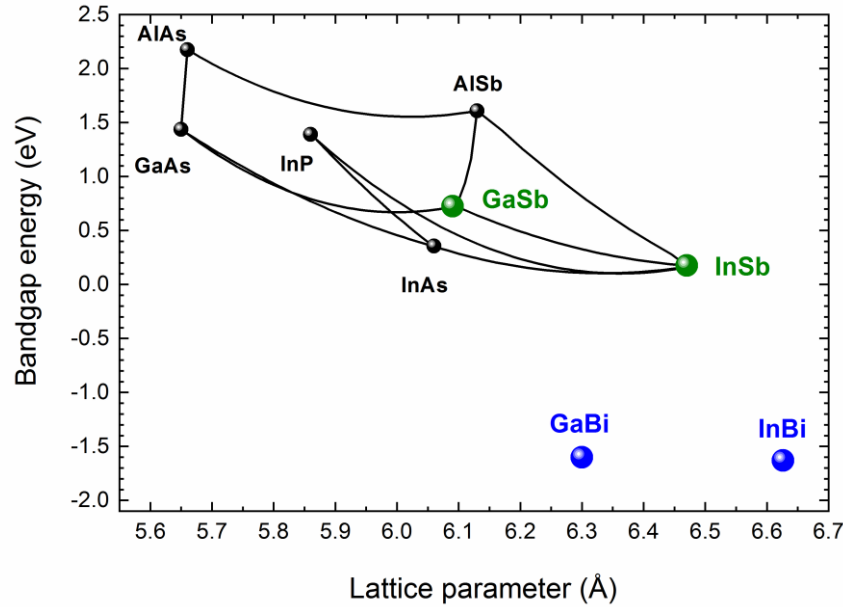
Fig. 4.1: III-V alloys bandgap energy as a function of their lattice parameter

4.1.2 Growth of Ga(In)SbBi layers

To investigate the influence of the addition of In on the incorporation of Bi, we have grown two series of GaInSbBi samples with In concentrations of 3.7 and 10.3%, respectively. The growth temperature was set at 200°C TTR, the optimal growth temperature for Bi incorporation into GaSb. During the growth of GaInSbBi compounds, a (1 x 3) RHEED pattern was consistently observed. The reproducibility of the Ga/In ratio was verified by growing several GaInSb layers using the same growth conditions than for the GaInSbBi layers. The composition of the GaInSbBi layers was then estimated using HR-XRD, assuming Zinc-Blende GaBi and InBi lattice constants of 6.272 and 6.626 Å [Rajpalke-2014b], respectively, and that Bi incorporation does not significantly change the In content.

The samples of the first set are composed of a GaInSbBi single layer with 3.7% In capped with a 20-nm thick GaSb layer. The Bi content in this series was raised up to 10.5% by increasing the Bi flux while adjusting the Sb flux to maintain a near stoichiometric V/III ratio. The thickness of the GaInSbBi layers was reduced from 120 to 40 nm as the %Bi was increased in order to avoid any lattice relaxation.

Fig. 4.2: (a,b) HR-XRD scans of the 004 Bragg reflection of GaInSbBi films grown at 200°C TTR, with In content close to ~3.7% and Bi concentrations up to 5.2% and 10.5%, respectively. The samples are droplet free up to 4.7% Bi. (c) HR-XRD spectra (in blue) and the corresponding simulation (in red) of the 40-nm thick GaInSbBi layer with 10.5% Bi and 3.8% In.

Fig. 4.2 a and b show the ω-2θ scans measured around the (004) reflection of these GaInSbBi layers with Bi contents up to 10.5%. The GaInSbBi peak appears broad due to the overlapping of interference fringes arising from the presence of the thin GaSb cap layer. Besides, the experimental HR-XRD measurements fit well with the simulated curves, see Fig. 4.2c. Up to 5% Bi, no droplet was observed on the surface while a few droplets could be observed for 5.2% Bi. As the Bi concentration further increased, the density of droplets rapidly raised. In the end, the surface of the sample with 10.5% Bi was completely covered by droplets. Still, *Pendellösung* fringes were clearly visible for all samples, demonstrating that the crystallographic quality and the composition homogeneity of the

GaInSbBi layers remained satisfying despite the formation of droplets. In addition, all these samples demonstrated PL emission at RT, and the results are detailed in paragraph 4.1.4. Attempts to reach higher Bi contents resulted in poor crystal quality, inhomogeneous compositions and extinction of the *Pendellösung* fringes on the HR-XRD scans.
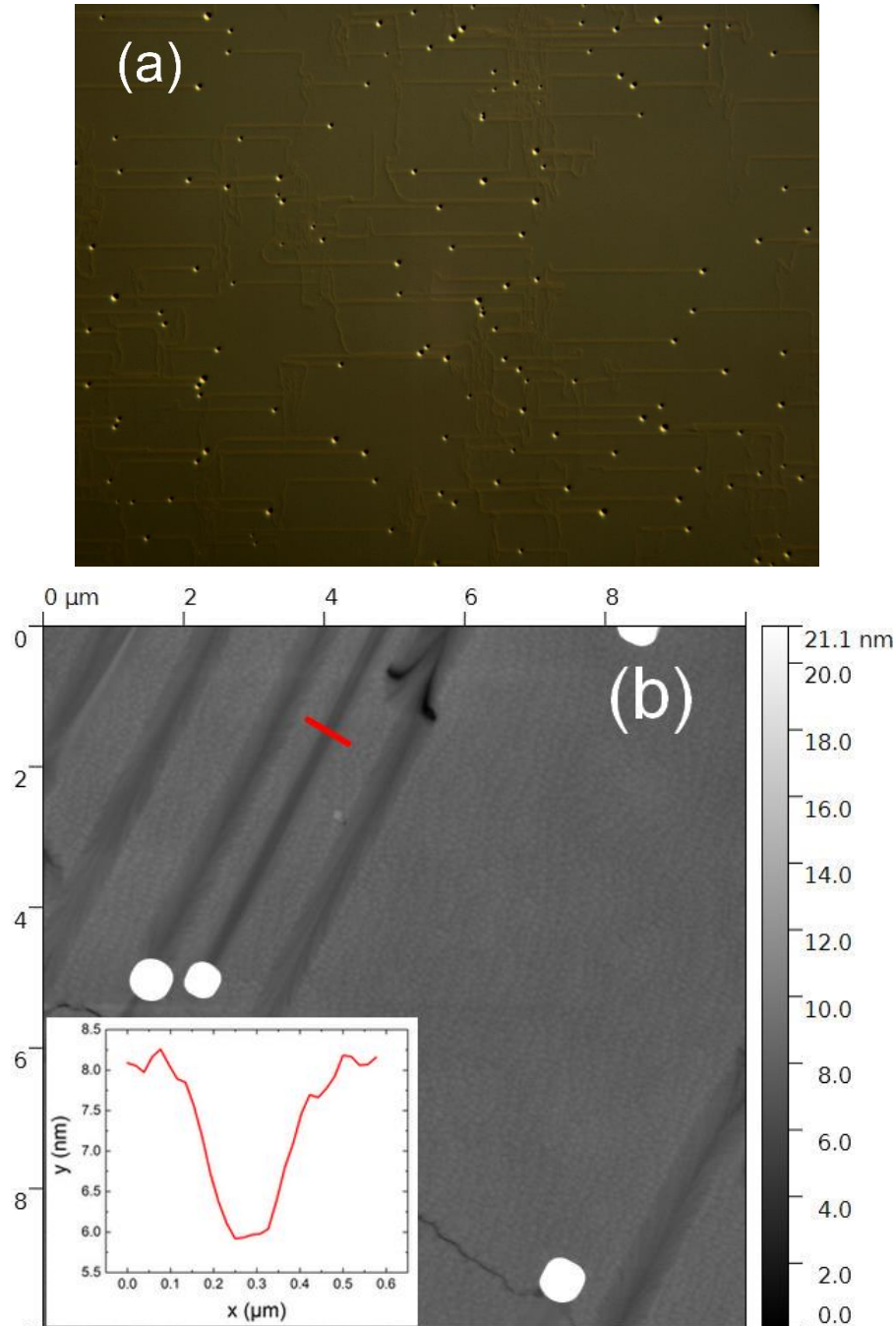
Fig. 4.3: Surface observation of 40-nm thick GaInSbBi layers with 10.5 (a) and 6.7% Bi (b) by optical microscopy (120 x 90 µm) and AFM, respectively. The red line in (b) indicate the position of the line profile which is depicted in the inset. The In concentration is close to 3.8%. In the last image, the contrast was adapted to make the motional traces more visible.

The droplets observed on the GaInSbBi layers are very similar to the Ga-Bi droplets visible on the GaSbBi alloys. It is very clear that the droplets moved during growth and etched the layer, forming nanotracks (Fig. 4.3 a and b). Phase separation in the droplet is also visible on SEM images (Fig. 4.4a). Bi, Ga and In signals are detected by the EDS mapping analysis (Fig. 4.4 b,d,e,f), but no Sb signal was observed in the droplet (Fig. 4.4c). The Bi and Ga phases are clearly separated, while it is not clear in the case of In. Indeed, due to a low SEM resolution, it is difficult to confirm if In is mixed with Bi or forms a third separated phase.
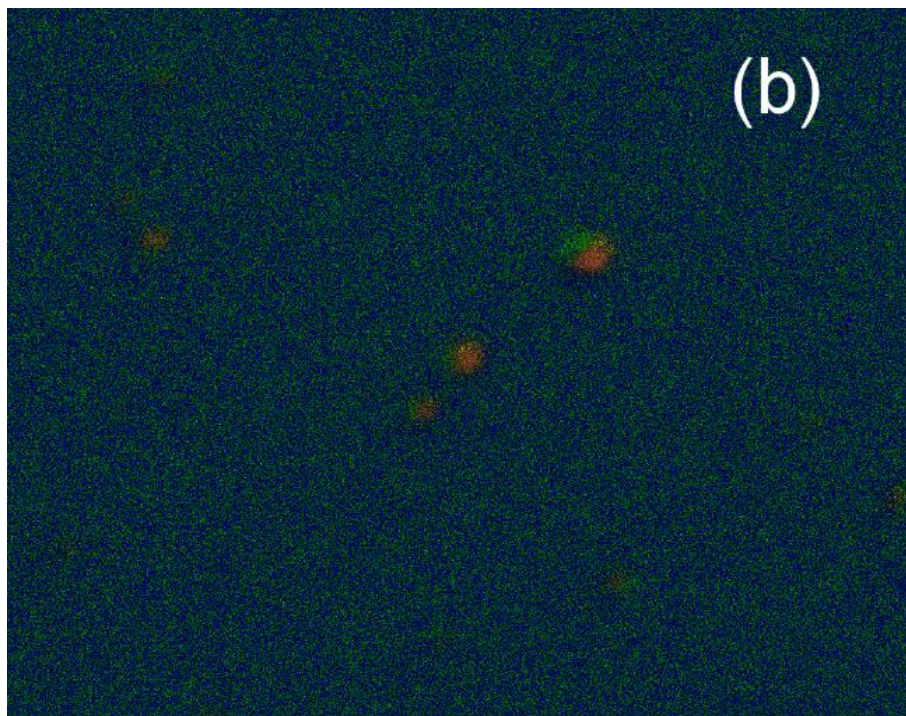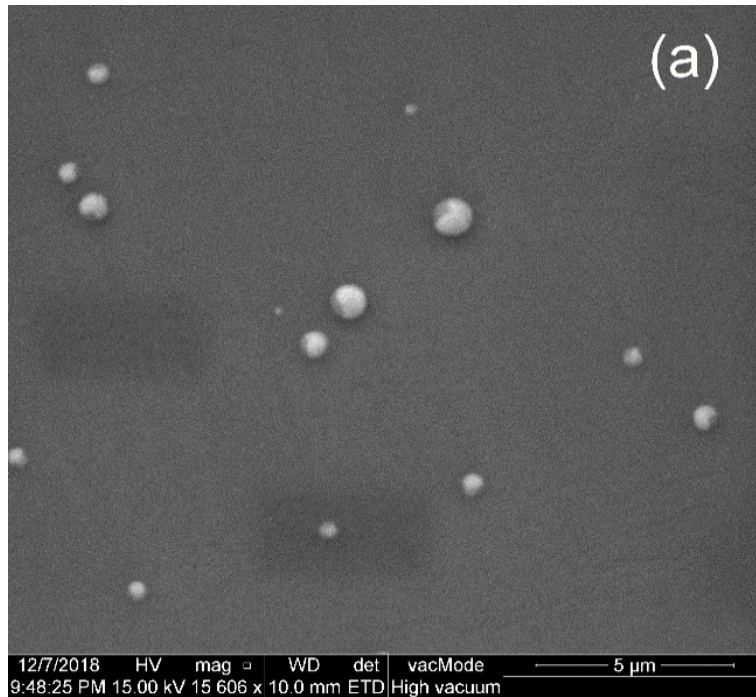
Fig. 4.4: (a) SEM image and EDS mapping (b) of GaInBi droplets on the surface of a 40-nm thick GaInSbBi film with 10.5% Bi and 3.8% In. EDS analysis of Sb, Ga, Bi and In elements are detailed in (c), (d), (e), (f), respectively.

A second set of GaInSbBi single layers was grown with a higher In content of 10.3% using the same temperature as for the previous samples, and a thickness of 40 nm. No GaSb cap layer was added. Fig. 4.5a shows ω-2θ scans measured around the (004) reflection of these GaInSbBi layers with Bi contents between 0 and 3%. Up to 2% Bi, the *Pendellösung* fringes are well defined and no droplet was observed on the surface. The high structural quality of the epilayer with 10.3% In and 2% Bi is confirmed by the STEM investigations performed at the PDI, as shown in Fig. 4.5b. No extended defect, clustering or composition modulation are detected in the 40 nm thick pseudomorphic layer. At these In and Bi concentrations, the incorporation of In into GaSbBi does not seem to alter the material quality and the microstructure of the GaInSbBi epilayer resembles that of high quality GaSbBi material. Furthermore, high-angle annular dark-field (HAADF) with so-called Z-contrast and EDS in the STEM evidences a homogeneous layer, at least at this level of detection, and confirm the statement arising from the large scale bright field (BF)-STEM shown in Fig. 4.5b. The EDS compositional mapping shown in Fig. 4.5c also demonstrates the presence of both In and Bi atoms in the epilayer. Due to their small

concentrations, - the Bi content is only about 2% -, the associated Bi and In EDS signals are very low and close to the measurement noise.
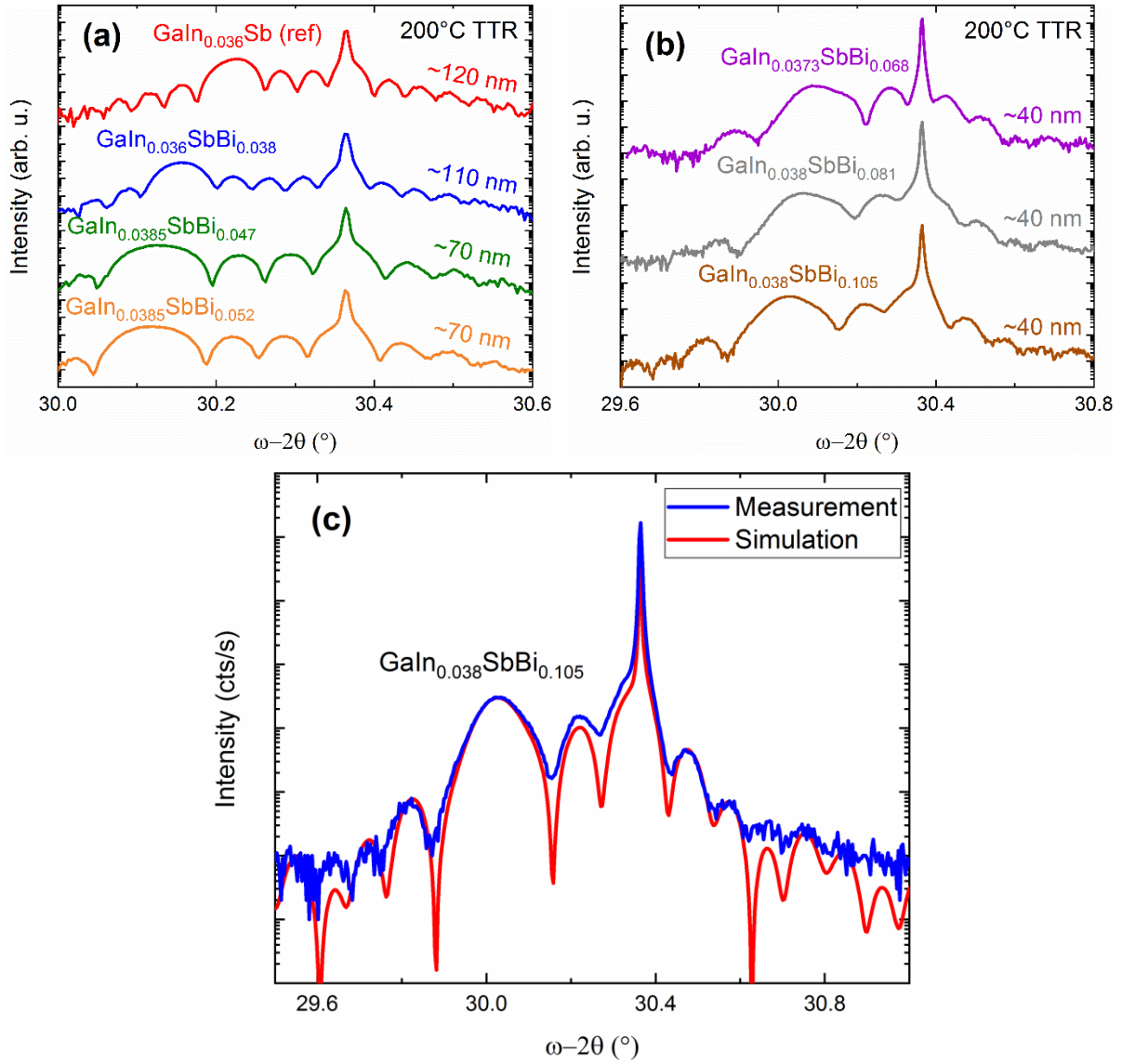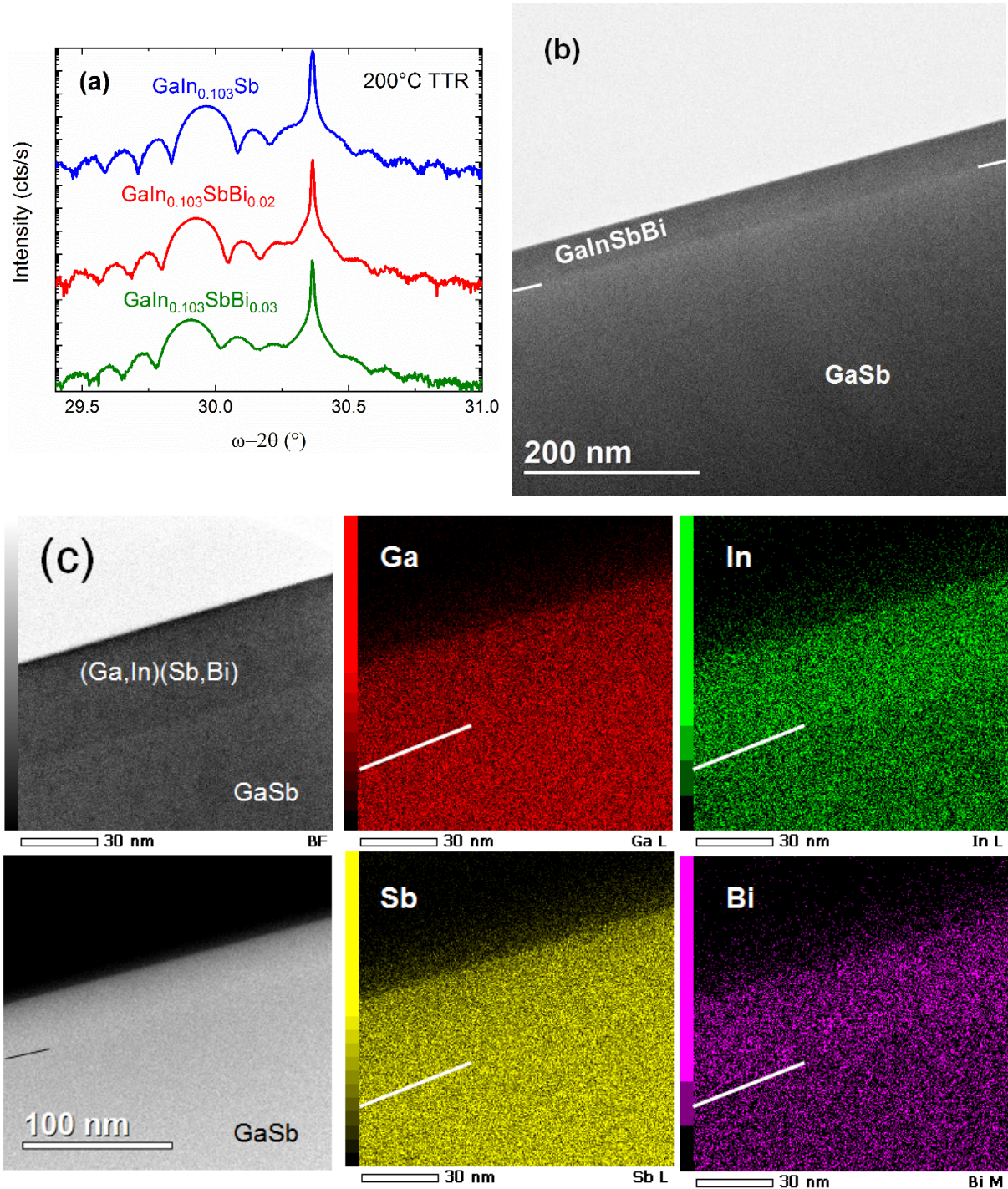

Fig. 4.5: (a) HR-XRD scans of the 004 Bragg reflection of 40-nm thick GaInSbBi films grown at 200°C TTR, with In content close to ~10.3% and Bi concentrations up to 3%. (b) Overview STEM and (c) bright-field images coupled with EDS compositional map from the GaInSbBi epilayer with 10.3% In and 2% Bi content. The Bi and In signals measured in the GaSb substrate are due to experimental TEM issue.

99

For a Bi concentration of 3%, droplets start to form and the *Pendellösung* fringes are damped in comparison with the previous samples, showing a degradation of the material quality and a possible composition inhomogeneity. For higher Bi fluxes, the density of droplets raised quickly and poor material quality was observed on HR-XRD scans, as for the previous set of samples. The droplets exhibit the same motional and etching behavior as seen previously. However, the morphology and the In composition of the droplets are different. In this case, the droplets are monophasic (Fig. 4.6a) and they are exclusively composed of In and Bi (Fig. 4.6b,c,d,e). Neither Ga (Fig. 4.6d) nor Sb atoms (Fig. 4.6c) could be detected in the droplets. This change of droplet morphology and composition, as well as the etching and motion mechanisms, are still unclear for now and further investigations are required to clarify this point.

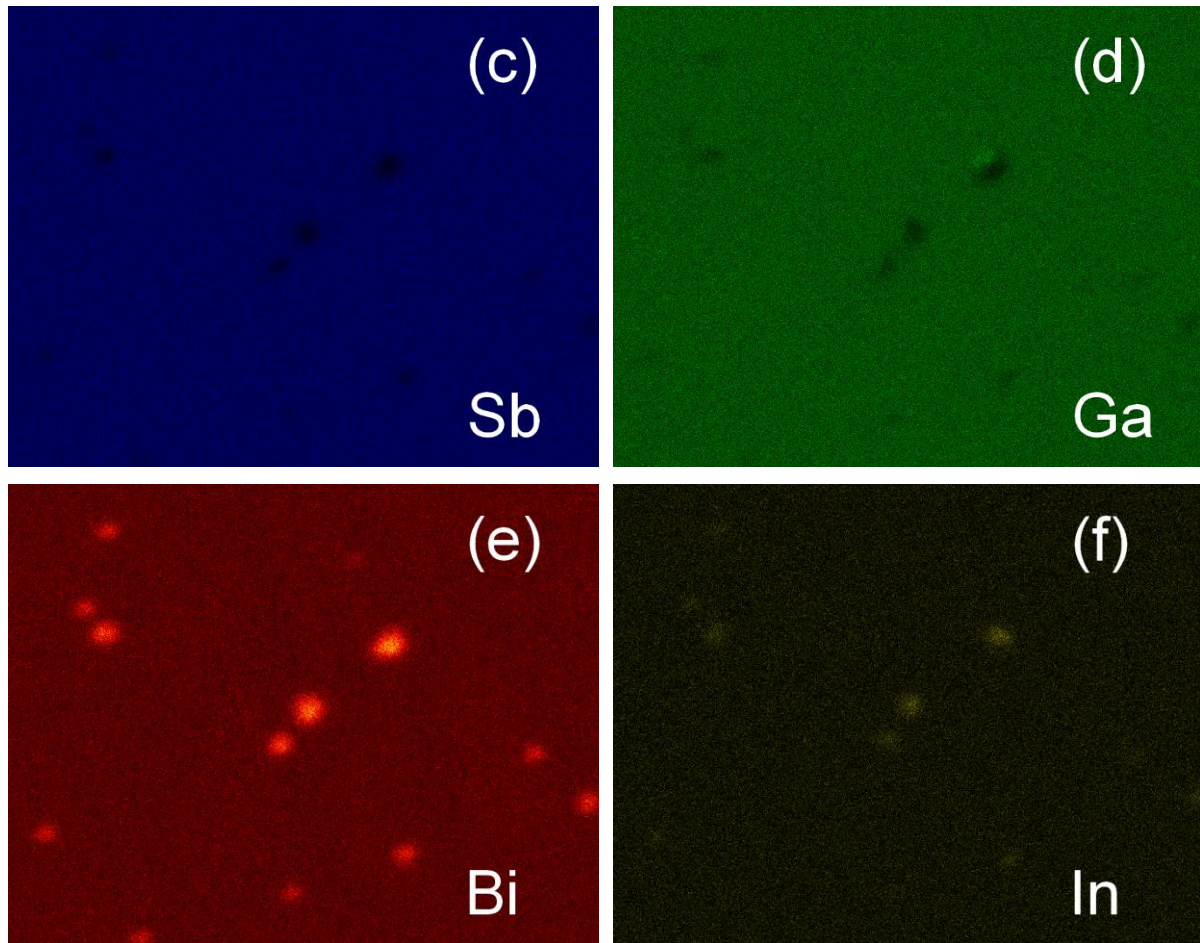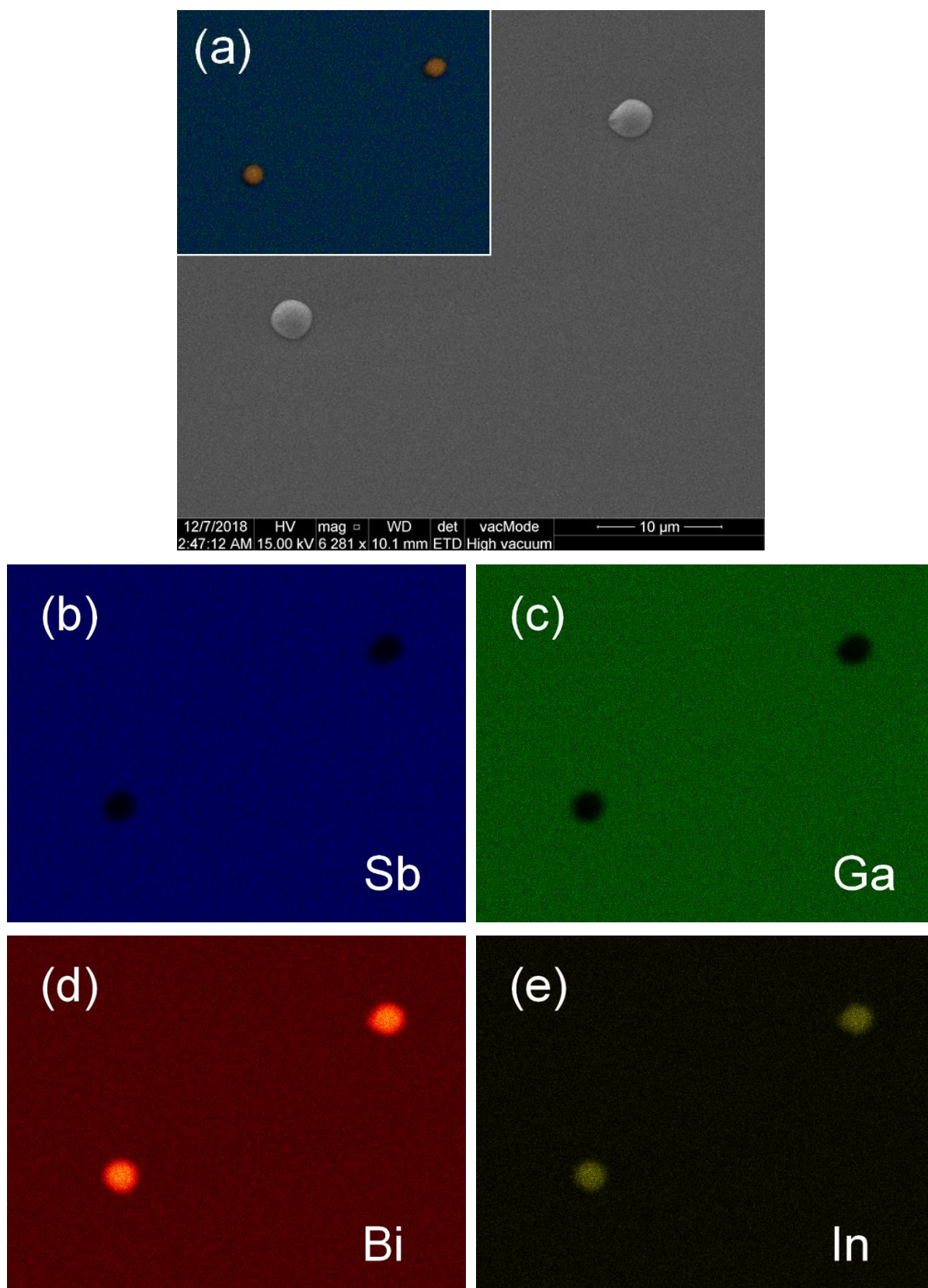*Fig. 4.6: (a) SEM image and EDS mapping of InBi droplets on the surface of a 40-nm thick GaInSbBi film with 3% Bi and 10.3% In. EDS analysis of Sb, Ga, Bi and In elements are detailed in (b), (c), (d), (e), respectively.*

As previously observed for GaSbBi, the GaInSbBi alloy remains of high quality up to a certain %Bi above which degradation of the microstructure and formation of droplets are systematically found. The most striking feature arising from these series of samples is that the Bi-content threshold for the formation of droplets decreases when the In content increases. Fig. 4.7, where the %Bi threshold is plotted as a function of the In content, illustrates this trend. The value for 0% In corresponds to the study made on GaSbBi layers described in Chapter 2. From this graph, it is clear that the addition of In reduces the Bi incorporation. Several reasons can explain this point. First, theoretical calculations and experiments on III-Bi binaries demonstrated that GaBi and InBi crystals have different structures, Zinc-Blende (ZB) [Ferhat and Zaoui-2006] and PbO tetragonal structures [Binnie-1956, Zilko and Greene-1980, Degtyareva-1998, Mohan-2000, Ferhat and Zaoui-2006], respectively. For instance, InBi tetragonal clusters were observed during the growth of InAsBi (ZB) layers [Dominguez-2013]. These structural differences between two binaries part of GaInSbBi are likely to significantly expand the miscibility gap of the alloy and therefore make the growth even more challenging. In addition, the optimal growth temperature of InSbBi is significantly lower than the one of GaSbBi. Indeed, Rajpalke *et al.* showed that the highest Bi content in InSbBi alloys was obtained for a growth temperature of 200°C [Rajpalke-2014b], about 75°C lower than the optimum growth temperature for GaSbBi [Rajpalke-2013]. The possible impact of the optimum temperature difference between InSbBi and GaSbBi is schematically illustrated in the inset of Fig. 4.7, assuming that the influence of the growth temperature on the Bi content is similar in these two alloys: when GaInSbBi is grown at the optimum temperature for the growth of GaSbBi (275°C), little incorporation of Bi is likely to occur by the formation of In-Bi bonds, while if the temperature is lowered in order to favor this kind of bonding, the material quality degrades rapidly because of a too low temperature for Ga-Sb-Bi to form a perfect crystal structure.
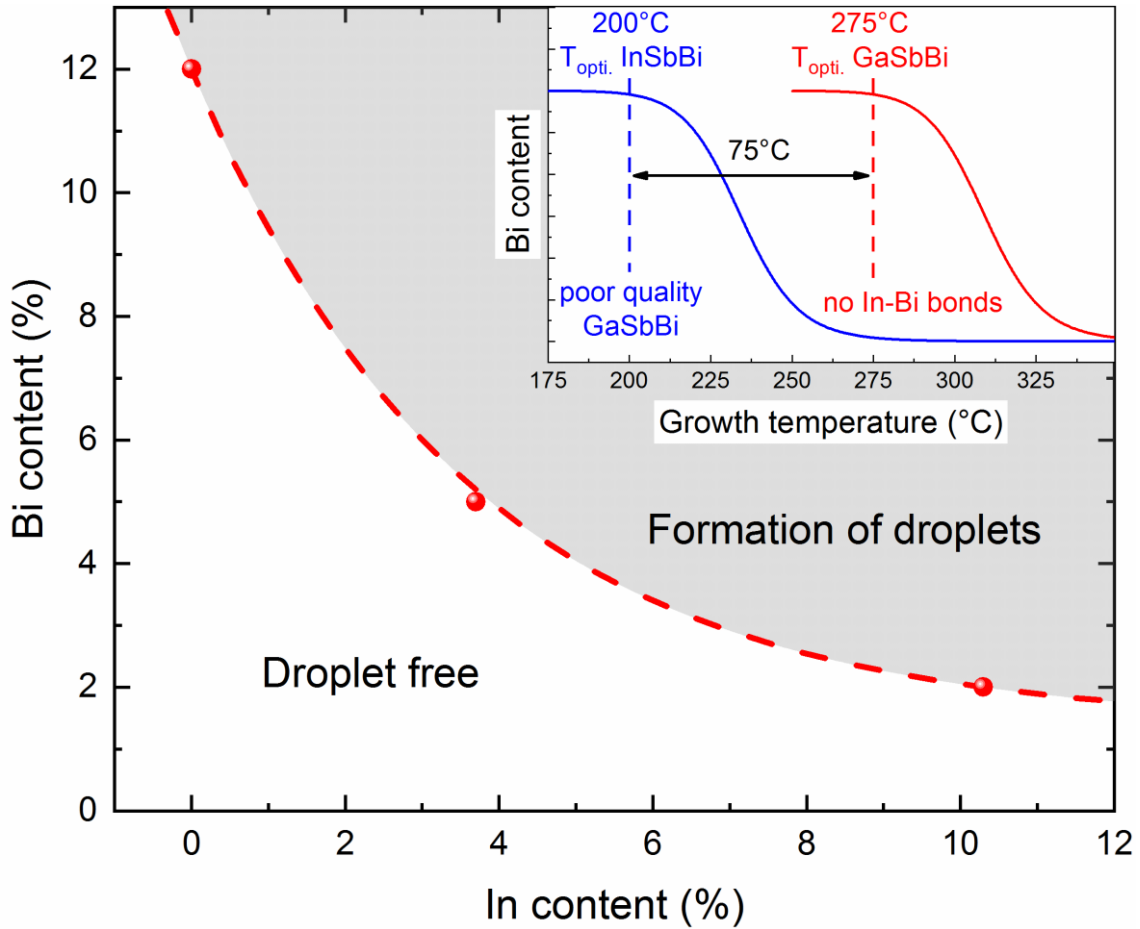
Fig. 4.7: Influence of the In composition on the threshold Bi content required for the formation of droplets at TTR = 200 °C. The inset represents schematically the effect of the temperature gap between InSbBi and GaSbBi alloys, making the assumption that the influence of the temperature is similar on these two materials.

To investigate this last point, and verify if an intermediate temperature could improve the %Bi while keeping a good material quality, we have grown GaInSbBi layers at various temperatures under the same flux conditions. The In concentration was fixed at 10.3%. The ω-2θ scans measured on the (004) reflection are shown in Fig. 4.8a. As expected, the Bi content dropped for higher growth temperatures (from 2 to 0.3% when the temperature was increased from 200 to 230°C TTR). The composition however remained unchanged when the temperature was decreased down to 170°C TTR. For this latter sample, one can however notice a slight damping of the *Pendellösung* fringes, demonstrating a lower crystal quality. AFM measurements revealed that the surface was also degraded. At 230°C TTR, atomic steps are well defined and the RMS roughness is lower than 0.15 nm (Fig. 4.8d). At 200°C TTR (Fig. 4.8c), a few round holes appear, causing a small increase of the roughness (~0.2 nm). Finally, at 170°C TTR, the atomic steps are still visible but a large density of defects can be observed, raising the roughness above 0.5 nm (Fig. 4.8b). To summarize, decreasing the growth

temperature from 200 °C TTR to 170 °C TTR does not increase the Bi incorporation but instead degrades the material and surface qualities. It would probably be necessary to further reduce the growth temperature to significantly promote the formation of In-Bi bonds and thus increase Bi incorporation. But such a low temperature would also result in an even more severe deterioration of the overall material quality, and is thus not a viable option.
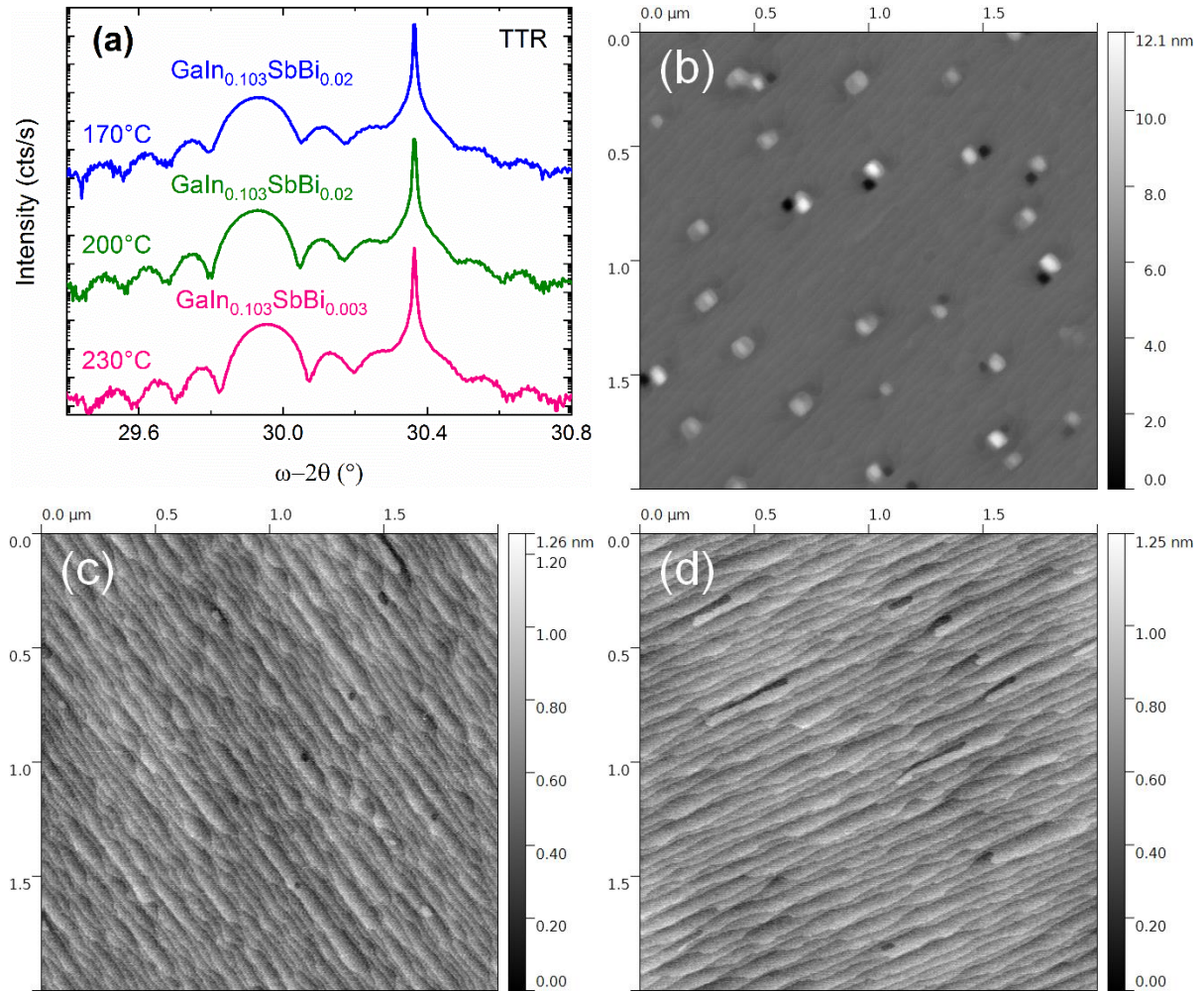
Fig. 4.8: (a) HR-XRD scans of the 004 Bragg reflection of 40-nm thick GaInSbBi films grown at different temperatures, using the same flux conditions. The temperatures indicated on the graph were measured by the thermocouple temperature reading (TTR). AFM surface observations of the samples grown at 170°C TTR (b), 200°C TTR (c) and 230°C TTR (d).

In summary, we have grown GaInSbBi layers with different compositions. We observed that the addition of In into GaSbBi alloys makes the incorporation of Bi more challenging. Droplet form at lower Bi concentrations, and the maximum Bi content achieved is 10.5% for 3.7% In, significantly lower than the 14% reached in GaSbBi.

4.1.3 GaInSbBi/GaSb MQW structures

Three GaInSbBi/GaSb MQW structures were grown, with ~3.7% In and 6, 6.8 and 10.5 % Bi, respectively. We assume that the actual composition is the same as that in the GaInSbBi single layers grown under the same conditions. The structure is similar to the GaSbBi-based MQW samples detailed in the previous chapter (see part 3.2). The MQWs are composed of three type-I 15-nm GaInSbBi/20 nm GaSb QWs and were grown at 200°C TTR. The samples with 6 and 6.8% Bi have droplet-free and mirror-like surfaces. On the contrary, numerous defects are observed on the MQW structure with 10.5% Bi.
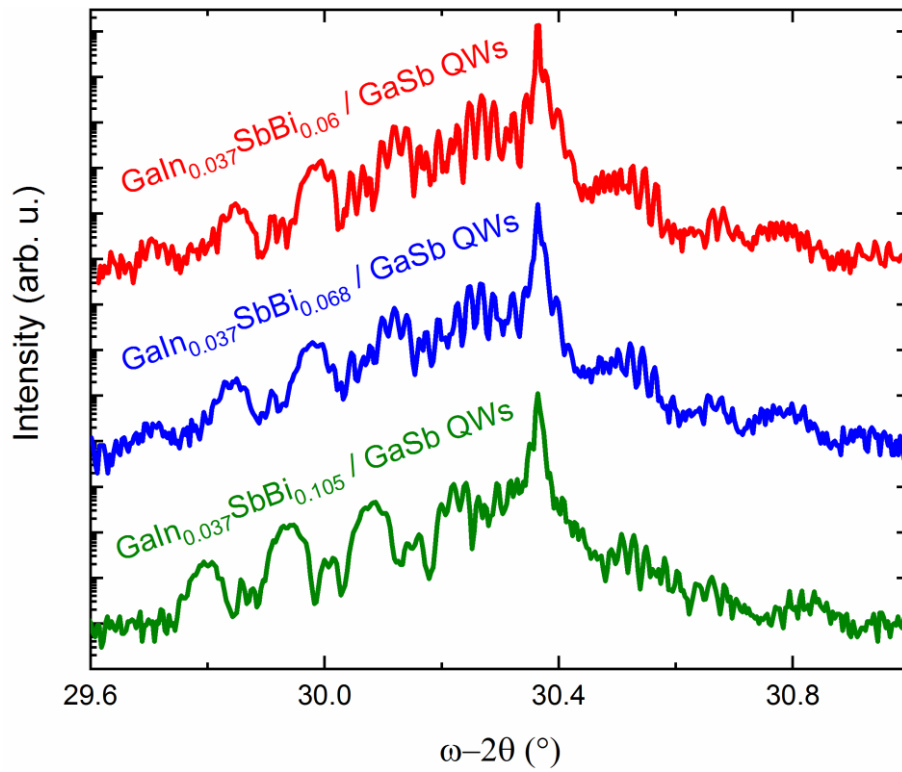
Fig. 4.9: HR-XRD spectra of 15-nm GaInSbBi/GaSb MQW with ~3.7 % In and various Bi concentrations.

Regarding structural properties, the QWs features are well defined for the three samples on the HR-XRD scans, indicating a good material quality (Fig. 4.9). The MQW with 6% Bi has also been studied by TEM (Fig 4.10). The GaInSbBi/GaSb MQW grows pseudomorphically on GaSb and no extended defect or cluster is detected. At first glance there is no apparent difference in the morphology of the three QWs, which are regular and homogeneous in composition. Similarly to GaSbBi-based MQW, the GaSb-on-GaInSbBi interface is more abrupt than the GaInSbBi-on-GaSb one, which is

relatively broad. The different abruptness of the two interfaces is clearly detected in BF-STEM (Fig. 4.10a) and, in particular, in BF conventional TEM images, cf. Fig. 4.10b. As for GaSbBi/GaSb MQW, we assume that the smoothing effect at the upper GaSb-on-GaInSbBi interface is caused by a surfactant effect of Bi.
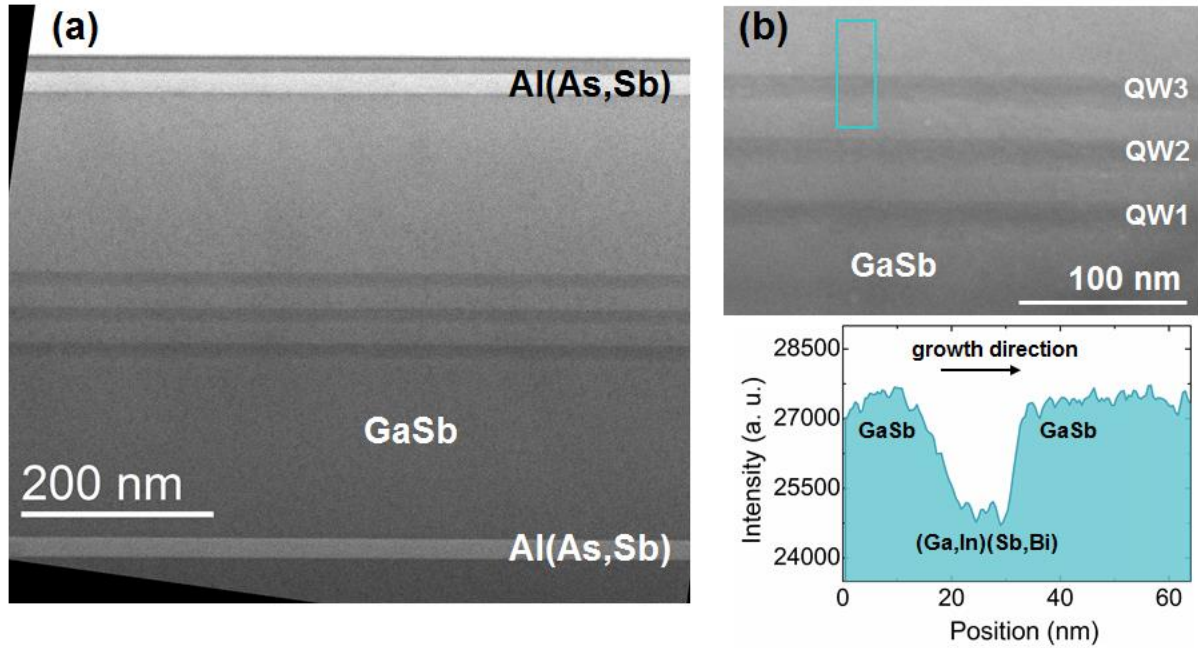
Fig. 4.10: GaInSbBi MQW with 3.7% In and 6% Bi content. (a) Overview bright-field STEM image and (b) bright-field conventional TEM image close to two-beam g_{002} imaging conditions. Linescan on the marked area showing the smoothing effect at the GaSb-on-GaInSbBi interface.

4.1.4 Photoluminescence analysis

Next we have investigated the optical properties of these samples and of the GaInSbBi layers by PL spectroscopy. The GaInSbBi layers with 3.7% In and the GaInSbBi/GaSb MQW structures demonstrated PL emission at RT (Fig. 4.11 a and b, respectively). The longest PL emission observed from the GaInSbBi layers is close to 2.85 µm, while it is about 2.6 µm for the MQW samples. It is interesting to note that the PL intensity obtained from the GaInSbBi layers increases with the Bi concentration. Since this is not the case for the GaInSbBi- and GaSbBi-based MQW samples, such behavior cannot be attributed to the variation of Bi content. In fact, the density of droplets on the surface seems to be the only factor that correlates well with this increase of the PL intensity, as shown in Fig. 4.11c. It could also explain the strong PL emission observed for the $GaSb_{0.86}Bi_{0.14}$ layer (see

paragraph 2.4.1 and Fig. 2.19a). For the MQW structures, the droplets which form during the growth of the bismide layers are probably buried within the upper layers (about 200 nm thick) and are not visible on the surface, preventing their influence on the PL emission eventually. Regarding the PL emission of the MQW samples, the increase of the Bi content correlates with a degradation of the PL signal: the intensity decreased and the emission peak broadened, which is consistent with the degradation of the surface morphology and confirms the worsening of the material quality. Finally, the GaInSbBi samples with 10.3% In did not exhibit any PL emission, even at 10 K. This does not necessarily mean that their crystal quality is worse than that of the samples with 3.7% In. Indeed, the GaInSbBi layers with 3.7% In are capped by a GaSb layer which improves the confinement of the photo-generated electron-hole pairs. In addition, the low thickness of the layers with 10.3% In (only 40 nm) limits the absorption of the exciting photons.
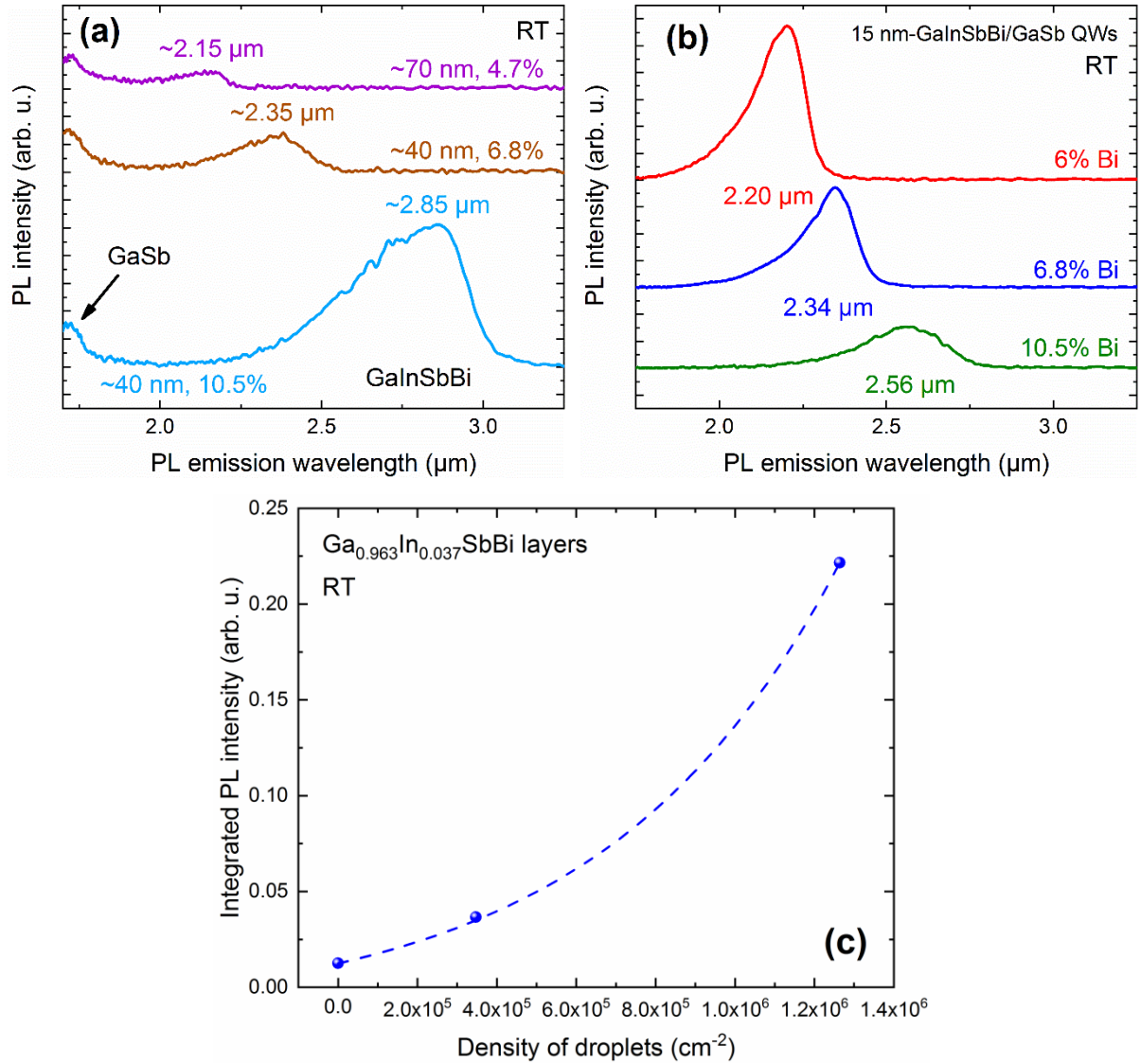
Fig. 4.11: PL emission of the GaInSbBi layers with 3.7% In (a) and of the 15-nm GaInSbBi/GaSb MQW structures at RT (b). The curves have been shifted vertically for clarity. (c) Integrated PL intensity of the GaInSbBi layers depicted in (a) as a function of the density of droplets observed on the surface. The dashed blue line is a guide for the eye.

The PL emission of the samples depicted in Fig. 4.11 was studied between 11 and 300 K. The temperature dependence of the PL emission is shown in Fig. 4.12 a and b for the GaInSbBi bulk layers and the MQW structures, respectively. The PL energy decrease was linearly fitted between 100 and 300 K. The PL energy variation slightly increases from 0.273 to 0.299 meV/K when the %Bi raises from 6 to 10.5% in the case of the MQW samples, while no clear trend emerges for the GaInSbBi layers. These data contrast with our previous observations on the less temperature-sensitive character of the bandgap of GaSbBi alloys (cf. paragraph 2.4.1 and 3.2.4). It tends to confirm the statements of Linhart and Kudrawiec on the incapacity to assess the bandgap temperature dependence using PL measurements [Linhart and Kudrawiec-2018]. Therefore, based on our measurements, the question of the enhanced insensitivity of the bandgap to temperature of dilute bismides remains an open topic.
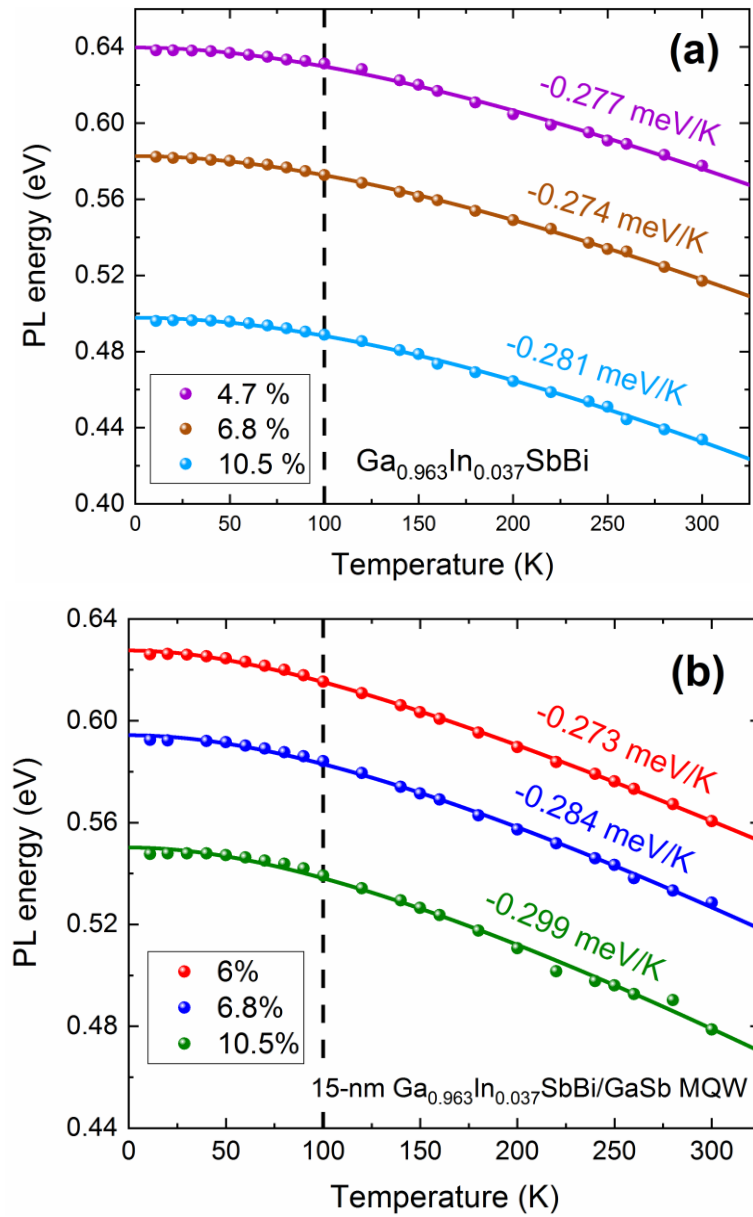
Fig. 4.12: Temperature dependence of the PL energy (a) Ga$_{0.963}$In$_{0.037}$SbBi layers and (b) of 15-nm Ga$_{0.963}$In$_{0.037}$SbBi/GaSb MQW with various Bi concentrations in the 10 - 300 K range. The solid lines are the Varshni fits using Eq. 2.4.

The data were also fitted using the Varshni (Eq. 2.4) and B-E expressions (Eq. 2.5), and the different parameters obtained are listed in Table 4.1 and Table 4.2. For all samples, α clearly raises with the Bi content, in good agreement with the evolution arising from the linear temperature dependence of E_G, but it is more unclear for the β parameter. Regarding the B-E fit, a_B and θ_B increase with the Bi content, as it was previously observed for GaSbBi alloys.

Table 4.1: PL energy linear variation in the range 100 – 300 K and Varshni parameters extracted from the fitting of the PL energy variation between 11 and 300 K (Fig. 4.12b).

Sample	E_G linear variation 100 – 300 K (meV/K)	Varshni parameters		
		E_0 (eV)	α (x 10^{-4} eV/K)	β (K)
GaInSb$_{0.953}$Bi$_{0.047}$	-0.277	0.640	4.9	392
GaInSb$_{0.932}$Bi$_{0.068}$	-0.274	0.583	5.1	407
GaInSb$_{0.895}$Bi$_{0.105}$	-0.281	0.498	6	529
GaInSb$_{0.953}$Bi$_{0.06}$ / GaSb	-0.273	0.628	3.7	198
GaInSb$_{0.932}$Bi$_{0.068}$ / GaSb	-0.284	0.594	4.4	292
GaInSb$_{0.895}$Bi$_{0.105}$ / GaSb	-0.299	0.550	4.6	282

Table 4.2: B-E parameters extracted from the fitting of the PL energy variation between 11 and 300 K.

Bi content (%)	Bose-Einstein parameters		
	E_0 (eV)	a_B (meV)	θ_B (K)
GaInSb$_{0.953}$Bi$_{0.047}$	0.638	40	250
GaInSb$_{0.932}$Bi$_{0.068}$	0.581	37	236
GaInSb$_{0.895}$Bi$_{0.105}$	0.496	43	262
GaInSb$_{0.953}$Bi$_{0.06}$ / GaSb	0.626	27	188
GaInSb$_{0.932}$Bi$_{0.068}$ / GaSb	0.592	36	223
GaInSb$_{0.895}$Bi$_{0.105}$ / GaSb	0.548	37	222

Similarly to GaSbBi alloys, we observed a weak carrier localization at low temperature. However, the PL energy was found to increase up to 30 K for the MQW sample with 10.5% Bi. A slight "S-shape" of the PL energy variation up to 30 K was also observed for the GaInSbBi layer with 10.5 % Bi. These results point to an increase of the localized states density with the Bi content, as previously noticed for GaSbBi. Localization was also investigated by studying the PL peak energy as a function of the excitation power. For the GaInSbBi MQW with the lowest Bi concentrations, the PL energy

blueshifts by 3.5 meV and 2 meV at 11 and 50 K, respectively, as the incident intensity raises (Fig. 4.13a). At higher temperatures, the PL energy remains constant, indicating the delocalized character of the emission. However, a blueshift is still measured at 100 K for the MQW structure with 10.5 % Bi, showing a higher density of localized states in comparison with the two other samples (Fig. 4.13b). A similar trend was observed for the GaInSbBi layers. Finally, the integrated PL intensity was also measured as a function of the excitation power, and the data were fitted using Eq. 2.6. As for the GaSbBi samples, α was found to increase from 0.84 to 1.12 with temperature but remains close to 1 in the case of the GaInSbBi MQW structures. Nevertheless, the GaInSbBi layers show a much stronger variation of α, as shown in Fig. 4.13c. At 11 K, α is about 1 for the three samples. At 250 K, α reaches 1.48, 1.38 and 1.22 for the GaInSbBi layers with 4.7, 6.8 and 10.5 % Bi, respectively. It illustrates the transition of the PL emission's character, from the recombination between localized excitons at low temperature to the dominance of band-to-band recombination at RT. We can also notice that the value of α decreases as the Bi composition raises, confirming the higher density of localized states in the high Bi content layers. Nevertheless, the localization remains weak for all samples (< 5 meV) and similar in magnitude to the conventional III-V alloys.
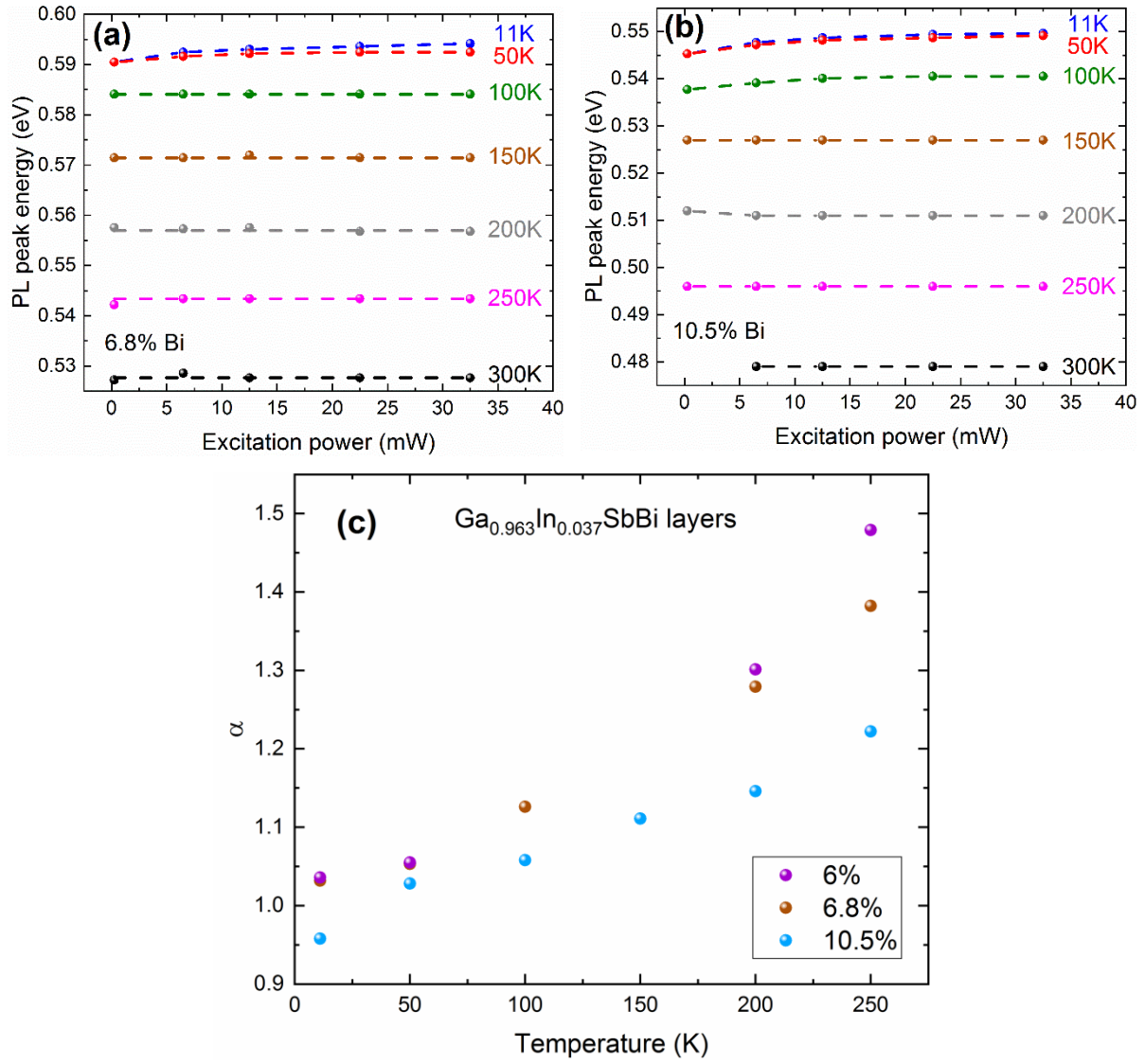
Fig. 4.13: Influence of the excitation power on the PL peak energy for GaInSbBi MQW with (a) 6.8 and (b) 10.5 % Bi. The In content is close to 3.7% for both samples. (c) Variation of the alpha coefficient obtained from Eq. 2.6 with the increase of the temperature for GaInSbBi layers with various Bi concentrations.

4.2   GaSbBi/InSb digital alloy

From the studies described in the previous paragraphs, it appears that the presence of In into GaInSbBi drastically decreases the possibility to incorporate Bi while maintaining a good material quality. We have decided to try a strategy where In and Bi would be spatially separated within very thin layers, to form a so-called digital alloy (DA). A DA is a short-period superlattice, *i.e.* a periodic stacking of very thin layers of different materials. Due to the extremely thin period (typically less than 8 MLs), the coupling between the different QWs is very strong and the DA is seen from the carrier perspective as an effective medium having a composition corresponding to the average composition of its different layers. For example, a GaSb(x MLs)/InAs(y MLs) DA can be used to create a layer having the same properties as a $Ga_xIn_yAs_ySb_x$ alloy, and it is often used to have a better composition control or an improved flexibility when growing a large number of layers having different compositions [Kaspi and Donati-2003]. In our case, the idea is to grow a GaSbBi/InSb DA in order to emulate the bulk GaInSbBi layers.

4.2.1 InSb/GaSb and GaSbBi/GaSb DA structures

Before studying the GaSbBi/InSb DA, we first started by fabricating GaSb/InSb and GaSbBi/GaSb DAs in order to set the different parameters and to characterize the Bi incorporation in such a configuration. Fig. 4.14 a and b present the design of the GaSb/InSb and GaSbBi/GaSb DA structures. The DAs are composed of six periods of 2.3-nm GaSb / 0.2 nm InSb and 2.3-nm GaSbBi / 1.4-nm GaSb, respectively. The thickness of the InSb layer is limited to 0.5 ML to avoid any strain relaxation that could occur due to the 6.3% lattice mismatch between InSb and GaSb. During the growth of the GaSbBi layers, the fluxes are set to obtain a Bi content of 11.8% in bulk GaSbBi layers. To mimic active regions, the DAs are repeated 3 times and embedded between 20-nm GaSb barriers to form a MQW. The whole active zone was grown at 200 °C TTR while the GaSb capping layer was grown at 450 °C (real).
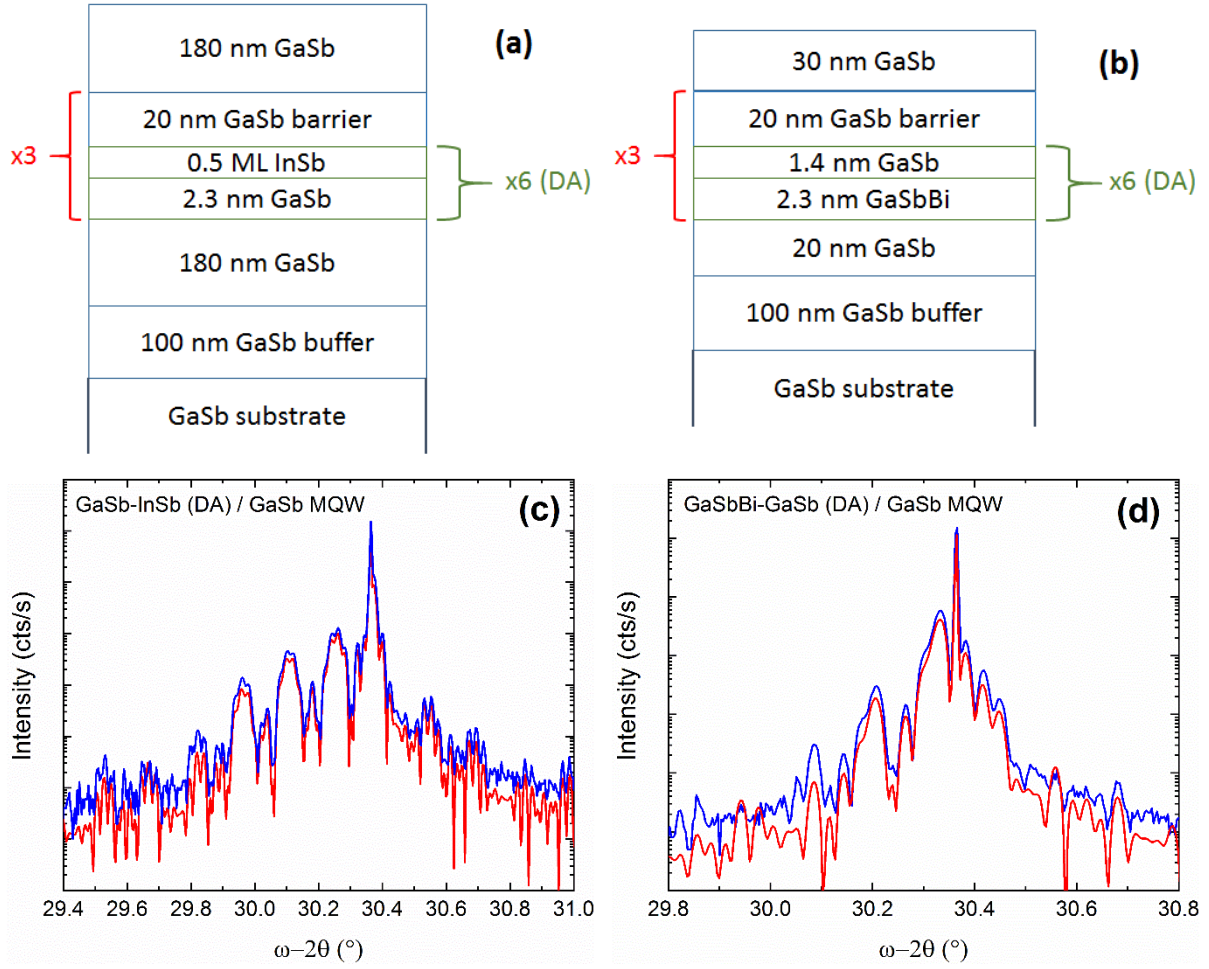
Fig. 4.14: (a,b) Structure of the InSb-based and GaSbBi-based sample, respectively. The SLs are depicted in green, while the active zones are delimited in red. ω-2θ HR-XRD spectra of the GaSbBi/GaSb SL (c) and the GaSb/InSb SL samples (d). The experimental curve is in blue, while the simulation is represented in red.

The two samples show droplet free and homogeneous surfaces. Fig. 4.14 c and d depict the HR-XRD scans of the GaSbBi/GaSb and GaSb/InSb structures, respectively. The patterns associated to the MQW are well defined for both samples and are in excellent correlation with simulation assuming fully strained layers, demonstrating a high crystal quality. No apparent relaxation can be observed either, confirming that the thickness of the InSb layers is lower than the critical value. The experimental curve of the InSb-based sample was fitted using a 15-nm $Ga_{0.935}In_{0.065}Sb$/ 20-nm GaSb MQW structure, in agreement with the structure design. As for the GaSbBi-based sample however, the simulation indicates a Bi content of only 7.5% which represents a decrease of approximately 40% with respect to the target value of 11%. A possible explanation could be that during the growth of these very thin (~8 ML) layers the surface does not reach the Bi-saturated state which allows the maximum Bi incorporation rate. The Bi atoms remaining at the surface after the growth of the GaSbBi layer are

surely removed by the incident Sb flux during the growth of the subsequent GaSb barrier layers. Therefore, the incorporation of Bi is lower than in the case of a thicker GaSbBi layer.
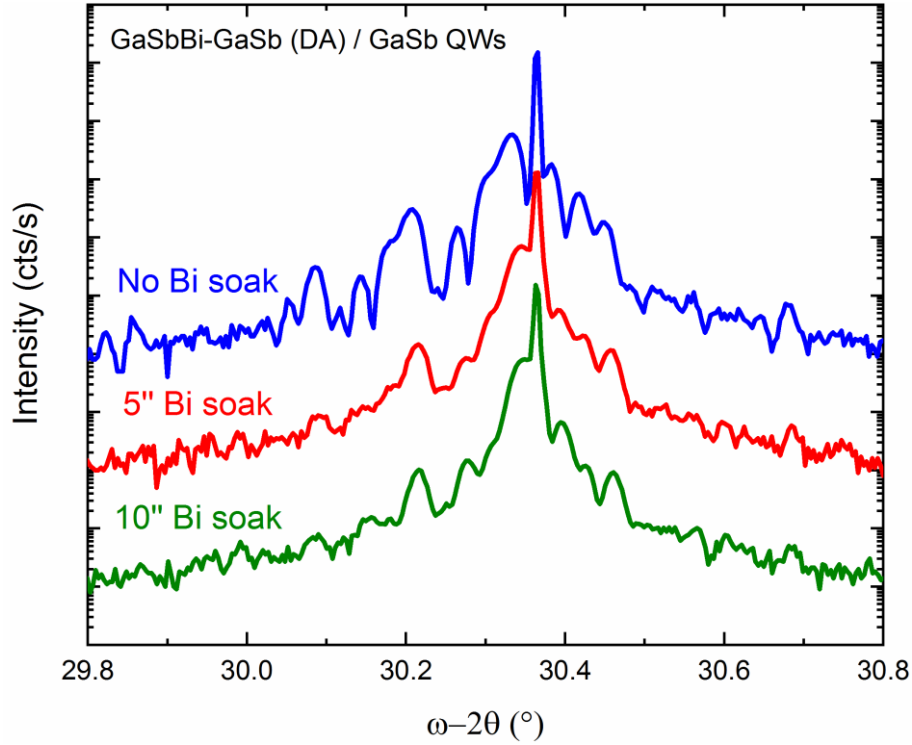
Fig. 4.15: HR-XRD scans of GaSbBi-GaSb/GaSb SL MQW samples grown using different Bi soak durations.

Pre-deposition of Bi prior to the growth of the GaSbBi layers (Bi soak) could help recovering the saturation of the surface by Bi atoms, and result in a higher Bi incorporation. To test this hypothesis, two samples were grown using a Bi soak before each GaSbBi layer. Two different soak durations were tested, 5 and 10 seconds. The rest of the structure was kept similar to the previous GaSbBi-based DA sample. The ω-2θ HR-XRD spectra are shown in Fig. 4.15. The satellite peaks related to the QWs move to higher angles as the Bi soak duration increases, indicating a lower Bi concentration. We can also notice that the MQW features are less visible. Moreover, droplets can be observed on the surface of the sample grown using the longer Bi soak. Therefore, a Bi soak does not allow increasing the Bi incorporation but rather results in a degradation of the material quality and eventually droplet formation.

4.2.2 GaSbBi/InSb DA

We have nevertheless grown a GaSbBi/InSb DA structure, to see whether it solves the issue between Bi and In. The DA is composed of a six periods 2.3-nm GaSbBi / 0.2 nm InSb (Fig. 4.16a), resulting in a total period thickness of 2.5 nm. As with other samples, the three GaSbBi/InSb DAs are separated by 20-nm GaSb barriers to form the active region, entirely grown at 200°C TTR. The active zone is sandwiched between 180-nm GaSb layers grown at 450°C. The Sb flux was adjusted to maintain a near-stoichiometric V/III flux ratio and to obtain a Bi content of 11.8% in bulk GaSbBi layers. A GaSbBi/GaSb MQW structure using standard GaSbBi growth instead of GaSbBi/InSb DA was also grown using the same fluxes for reference. The HR-XRD spectra of these two samples are shown in Fig. 4.16b. Whereas the scan of the reference structure exhibits well defined MQW features, those of the DA-based structure are almost not visible, indicating a strong degradation of the material quality. This deterioration was not caused by an inappropriate V/III flux ratio or a hypothetic relaxation during the growth of the InSb layer, as demonstrated previously with the GaSbBi-GaSb and GaSb-InSb DAs samples. It seems finally that the issue between Bi and In persists. Even if they are not used simultaneously, these two elements are obviously still in contact on the surface. To separate Bi and In, thin GaSb spacer layers were added between the InSb and the GaSbBi layers, to bury or remove the atoms on the surface. Firstly, a 0.04 nm GaSb layer was grown atop the GaSbBi layer. Then, a second 0.04 nm GaSb layer was added after the InSb layer, but no significant improvement was observed on HR-XRD scans (Fig. 4.16c). The thickness of the GaSb spacer layers was finally increased to 0.66 nm, leading to a slightly better crystal quality. However, the use of thicker spacer layers is not a viable solution, as it further decreases the average Bi and In content in the overall structure. Moreover, we can also expect the remaining Bi on the surface to desorb during the growth of the GaSb spacers, as it was observed for the GaSbBi/GaSb DA. A much higher Bi content would be necessary to compensate this loss, and it is not achievable with the reduced Bi incorporation. Therefore, the fact that non-negligible GaSb thicknesses are required to obtain efficient spacing between Bi and In make this technique not helpful to grow GaSbBi/InSb DAs with significant Bi contents. Anyway, the potential of a GaSbBi/InSb DA structure can be questioned in the end. Indeed, in a similar fashion to what was already observed in the case of GaSbBi/GaSb DA, we can assume that the inclusion of a very thin layer of InSb leads to a depletion of the Bi reservoir sitting at the surface of the GaSbBi and prevents its incorporation into the subsequent GaSbBi layer. It would be reasonable to further assume that in the case of InSb, the depletion is even more effective than with GaSb: as described previously the incorporation of Bi into InSb requires a much lower substrate temperature, and therefore, at the temperature used here, the Bi atoms in contact with the InSb will tend to desorb from the surface at a faster rate than with GaSb.
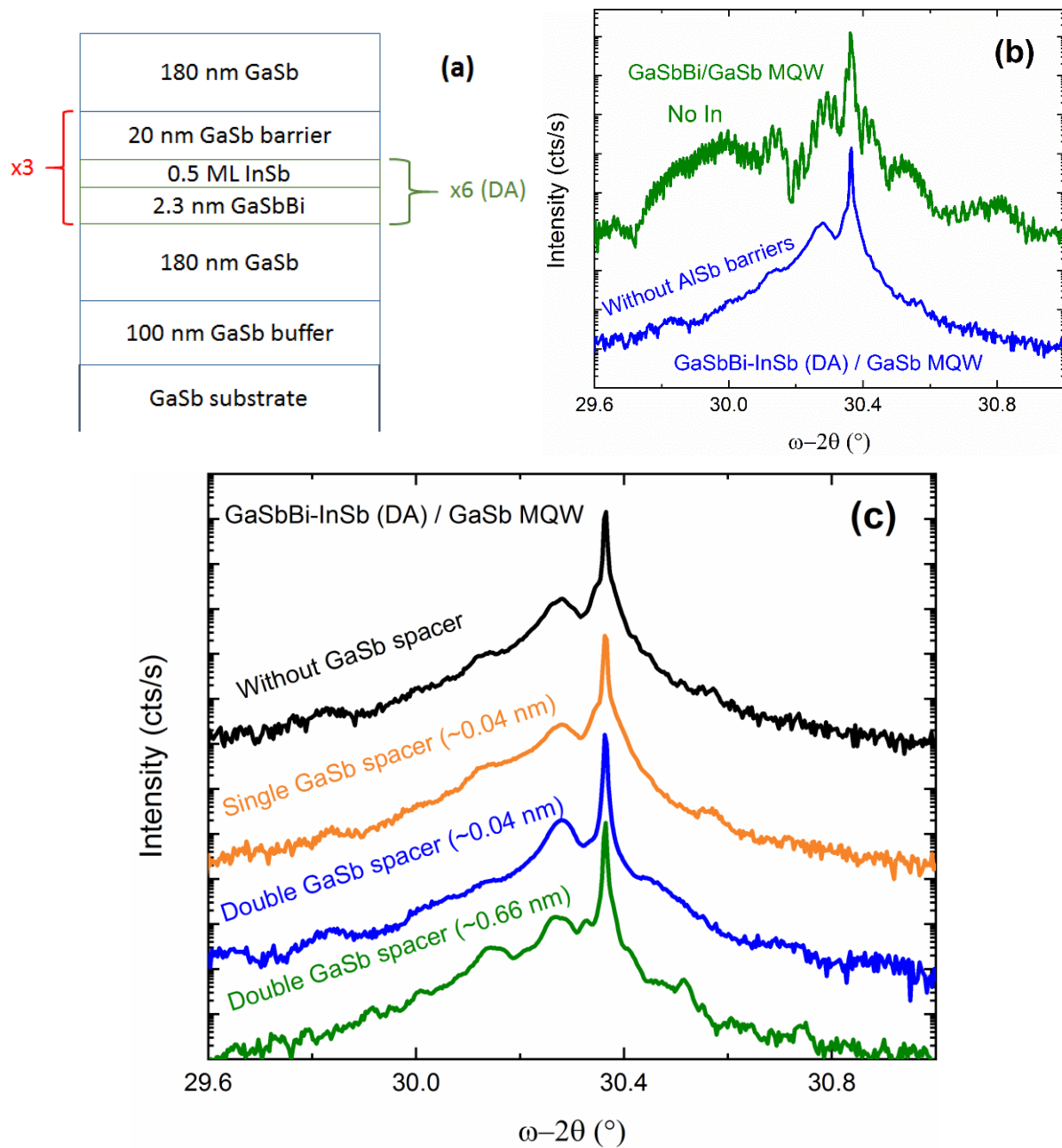
Fig. 4.16: (a) Structure and (b) ω-2θ HR-XRD spectra of the GaSbBi-InSb (SL) / GaSb MQW structure. The HR-XRD scan of the GaSbBi/GaSb MQW reference was added in (b). (c) HR-XRD spectra of GaSbBi-InSb (SL) / GaSb MQW samples using GaSb spacers of various thickness.

4.3   Conclusion

In this chapter, we have investigated the growth of GaInSbBi alloys and MQW. We observed that the addition of In strongly modifies and reduces the Bi incorporation into GaSb. For an In concentration of ~3.7%, we reached a maximum Bi content of 10.5% while the highest Bi concentration falls down to 3% with 10% of In. Additionally, droplets appear at lower Bi composition than in GaSbBi alloys. Biphasic GaInBi droplets were observed on the samples with ~3.7% In, while monophasic InBi droplets are visible on the ones with 10.3% In. Additionally, GaInSbBi MQW structures were also realized with ~3.7% In and Bi concentrations between 6 and 10.5%. The GaInSbBi layers with ~3.7% In and the MQW structures demonstrated PL emission at RT up to ~2.85 µm and 2.6 µm, respectively. A weak carrier localization was observed at low temperature but a slight increase was noticed as the Bi content raised, similarly to the GaSbBi alloys.

Finally, a new GaSbBi/InSb DA structure was grown to prevent the issues between Bi and In. Unfortunately, the Bi incorporation was found to be lowered by the extremely low thickness of the GaSbBi layers. A strong degradation of the material quality was also observed, showing that the In/Bi problem persists. None of our attempts (Bi soaks, GaSb spacers) improved significantly these two points.

Conclusion and perspectives

Despite their unique properties, dilute bismides semiconductors stands far behind the other III-V semiconductors. Indeed, the growth of III-V-Bi alloys represents a great challenge as Bi incorporation requires very unconventional conditions. Among the bismide compounds, GaSbBi has been little studied for now, in spite of its potential for mid-IR optoelectronics. In this thesis, we proposed an in-depth investigation of the molecular beam epitaxy and properties of this relatively new alloy.

In chapter 1, we studied the influence of the different growth parameters on the incorporation of Bi into GaSb. We found out that an extremely low growth temperature was necessary to allow the formation of the Ga-Bi bonds. The V/III flux ratio is the other critical parameter. Indeed, we observed that a near stoichiometric V/III flux ratio was essential to reduce the density of Sb competing with Bi for the incorporation and therefore promote the Bi incorporation. Any slight fluctuation of the growth conditions resulted in a strong reduction of the Bi concentration and, when the Bi flux is high, a degradation of the crystal quality with the formation of droplets on the surface. Setting the growth parameters is thus very challenging and usually requires the growth of numerous calibration samples. To avoid this time- and cost-consuming step, we established an *in-situ* method using RHEED intensity oscillations. Indeed, this allows a direct observation of the Bi incorporation and therefore a rapid optimization of the growth parameters. Interestingly, this technique is not limited to the growth of GaSbBi, but could also be used for any III-V-Bi alloys.

Thanks to the careful study of the growth parameters, we succeeded to reach high Bi contents by gradually increasing the Bi flux. By properly adjusting both the Sb and Bi flux, the growth of droplet free GaSbBi epilayers with Bi content up to 11.4% was achieved. A maximum Bi concentration of 14% was obtained, but the formation of droplets could not be avoided and a degradation of the material quality was noticed. Nevertheless, this sample demonstrated PL emission at 3.8 μm at RT, showing a significant bandgap reduction of ~28 meV/%Bi.

We also found that GaSbBi exhibits a good stability upon thermal annealing, which allows fabricating heterostructures. In particular, we have grown GaSbBi/GaSb MQW structures with Bi content up to 15%. These samples demonstrated PL emission up to 3.5 μm at RT. However, a deterioration of the optical performances was observed as longer wavelengths were reached that correlates well with the aforementioned lower structural quality at high Bi content. The MQW samples

were characterized by photoreflectance (PR) and transmission electron microscopy (TEM) measurements at the Wroclaw University and Paul-Drude-Institute of Berlin, respectively. PR spectroscopy confirmed the type I alignment of the GaSbBi/GaSb system and showed a VBO of ~50% of the total bandgap variation. The evolution of the electron effective mass with the Bi content was also established. TEM analysis demonstrated that the samples were homogeneous in composition and of high crystallographic quality as no dislocations, clustering or extended defects could be observed. However, some thickness fluctuations, a few local morphological irregularities and non-negligible abrupt interfaces roughness were occasionally observed on some MQWs. For now, the origin of these features remains unclear. Lastly, we fabricated the first ever GaSbBi-based laser diode, which exhibited continuous lasing at 80 K and emission at RT close to 2.7 µm under pulsed operation. The threshold current density is relatively high in comparison with the current standard devices, but this result confirms the potential of GaSbBi for applications in the mid-IR.

In the last chapter, we studied another dilute bismide alloy: GaInSbBi. We found that the addition of In strongly modifies and reduces the Bi incorporation into GaSb. For an In content as low as 3.7%, the maximum Bi concentration dropped down to 10.5%. Additionally, droplets started to form at lower Bi content. The negative impact of In on Bi incorporation may arise from the difference of structure between the crystal of InBi and GaBi, and/or a difference of optimal growth temperature between InSbBi and GaSbBi. Still, we have fabricated GaInSbBi/GaSb MQW structures with 3.7% In and Bi compositions in the 6 to 10.5% range, which demonstrated PL emission up to 2.6 µm at RT. Finally, the growth of a GaSbBi/InSb digital alloy (DA) was studied in an attempt to increase the Bi content in this alloy by spatially separating In and Bi atoms. Unfortunately, the DA structure did not solve the In:Bi issue due to a rapid decrease of the Bi incorporation when extremely thin layers are used, which is obviously the case in a DA configuration.

The optical properties of all samples were assessed by PL measurements between 11 and 300 K. A weak localization was observed at low temperature for both GaSbBi and GaInSbBi layers. From this result, we found that GaSbBi and GaInSbBi rather behave has regular III-V compounds and can hardly be considered as highly mismatched alloys. Still, the density of localized states was found to increase with the Bi content, agreeing with the aforementioned degradation of the material quality at high Bi compositions.

In this thesis, we have extensively investigated the growth of GaSbBi, as well as structural and optical aspects. However, further work is still undoubtedly necessary. For instance, the electrical properties of this alloy have not been addressed yet. Likewise, we have not attempted to improve the performances of the GaSbBi-based laser. For this, the post-growth annealing of the active region

caused by the epitaxy of the upper claddings needs to be studied. Indeed, we have observed that post-growth annealing could increase or decrease the PL intensity (and the crystal quality) of GaSbBi layers. Therefore, the temperature and the duration of the growth of the upper layers have to be optimized in order to obtain the best output performances. Additionally, migration enhanced epitaxy (MEE) could also be useful to improve the material quality of the GaSb MQW barriers grown at low temperature. Indeed, MEE was found to improve the crystal quality of GaAs and AlGaAs layers grown at low temperature [Horikoshi-1988].

To extend the maximum Bi content in GaSb, a new growth technique has definitely to be found. Alternate growth methods as sequenced pulsed fluxes or MEE have been proposed for this purpose, but their capability to overcome the possible solubility limit of Bi into GaSb has to be demonstrated and a comprehensive comparison with the outcomes obtained using conventional growth is still missing [Butkutė-2014, Butkutė-2015].

Another interesting aspect of Bi is its surfactant effect. Promising results have been obtained since the early 2000s: increase of the doping level, smoothing of the surface, improvement of incorporation of N into GaAs [Tixier-2003a, Young-2005, Liu-2007, Maddox-2012]... We carried out preliminary investigations, but we did not have time to fully investigate this aspect. The surfactant effect of Bi and its impact on the growth of III-V alloys is definitely worth an in-depth study.

Last but not least, mixed III-As-Sb alloys lattice matched to GaSb such as InAsSb are interesting for mid-IR optoelectronic applications. Incorporating Bi to these alloys opens news perspectives in terms of accessible bandgap ranges. Preliminary results have been reported, but detailed studies are still missing.

List of publications

Journal papers

1. **O. Delorme**, L. Cerutti, E. Luna, G. Narcy, A. Trampert, E. Tournié and J.-B. Rodriguez (2017). "GaSbBi/GaSb quantum well laser diodes." <u>Applied Physics Letters</u> **110**(22): 222106.

2. **O. Delorme**, L. Cerutti, E. Tournié and J. B. Rodriguez (2018). "In situ determination of the growth conditions of GaSbBi alloys." <u>Journal of Crystal Growth</u> **495**: 9-13.

3. E. Luna, **O. Delorme**, L. Cerutti, E. Tournie, J. B. Rodriguez and A. Trampert (2018). "Transmission electron microscopy of Ga(Sb, Bi)/GaSb quantum wells with varying Bi content and quantum well thickness." <u>Semiconductor Science and Technology</u> **33**(9): 8.

4. E. Luna, **O. Delorme**, L. Cerutti, E. Tournie, J. B. Rodriguez and A. Trampert (2018). "Microstructure and interface analysis of emerging Ga(Sb,Bi) epilayers and Ga(Sb,Bi)/GaSb quantum wells for optoelectronic applications." <u>Applied Physics Letters</u> **112**(15): 5.

5. R. Kudrawiec, J. Kopaczek, **O. Delorme**, M. Polak, M. Gladysiewicz-Kudrawiec, E. Luna, L. Cerutti, E. Tournié and J. B. Rodriguez (2019). "Type I GaSb$_{1-x}$Bi$_x$/GaSb quantum wells dedicated for mid infrared laser applications: Photoreflectance studies of band gap alignment." <u>Journal of applied physics</u> **125**, 205706.

6. **O. Delorme**, L. Cerutti, E. Luna, G. Narcy, A. Trampert, E. Tournié and J.-B. Rodriguez. "Molecular-beam epitaxy of GaInSbBi alloys" Submitted to <u>Journal of applied Physics</u>

7. E. Rogowicz, W. M. Linhart, M. Syperek, J. Kopaczek, **O. Delorme**, L. Cerutti, E. Luna, E. Tournié, J.-B. Rodriguez and R. Kudrawiec "Optical properties and dynamics of excitons in Ga(Sb,Bi)/GaSb quantum wells: evidence for a regular alloy behavior". Submitted to <u>Semiconductor Science and Technology</u>

Conference proceeding paper

O. Delorme, L. Cerutti, E. Tournié and J.-B. Rodriguez (2017). "Molecular beam epitaxy and characterization of high Bi content GaSbBi alloys." <u>Journal of Crystal Growth</u> **477**: 144-148.

Book chapter

O. Delorme, L. Cerutti, R. Kudrawiec, E. Luna, J. Kopaczek, M. Gladysiewicz, A. Trampert, E. Tournié, and J.-B. Rodriguez (2019). "GaSbBi alloys and heterostructures: fabrication and properties" <u>Springer Series Materials</u>, Vol. 285: *Bismuth-Containing Alloys and Nanostructures* (125-161).

Communications at international conferences

Oral presentations

1. <u>**O. Delorme**</u>, L. Cerutti, E. Tournié and J.-B. Rodriguez, "Molecular Beam Epitaxy and characterization of high Bi content GaSbBi alloys", 19th International Conference on Molecular-Beam Epitaxy (MBE2016), 4 – 9 September 2016, Montpellier (France)

2. **O. Delorme**, <u>L. Cerutti</u>, E. Tournié and J.B. Rodriguez "Molecular Beam Epitaxy and characterization of high Bi content GaSbBi alloys " Oral: 13th Infrared Optoelectronics: Materials and devices (MIOMD-XI), Beijing, China, 18-22 September 2016

3. <u>**O. Delorme**</u>, L. Cerutti, E. Luna, A. Trampert, E. Tournié and J.-B. Rodriguez, "GaSbBi/GaSb quantum well laser diodes", 8th International Workshop on Bismuth-Containing Semiconductors, July 23rd - 26th, 2017, Marburg, Germany

4. <u>**O. Delorme**</u>, L. Cerutti, E. Tournié, J.B. Rodriguez, High Bi-content GaSbBi alloys for mid-IR applications, CSWeek 2017, 14 – 18 May 2017, Berlin (Germany)

5. **O. Delorme**, L. Cerutti, E. Tournié and <u>J.-B. Rodriguez</u>, GaSbBi alloys for mid-infrared optoelectronics Freiburg Infrared Colloqium, 14 – 15 March 2017, Freiburg, Germany

6. <u>Esperanza Luna</u>, **O. Delorme**, L. Cerutti, E. Tournié, J.-B. Rodriguez and A. Trampert, "Transmission Electron Microscopy of Ga(Sb,Bi) Epilayers and Quantum Wells for Optoelectronic Applications", 8th International Workshop on Bismuth-Containing Semiconductors, July 23rd - 26th, 2017, Marburg, Germany

7. <u>I. Marko</u>, **O. Delorme**, L. Cerutti, E. Tournié, J.B. Rodriguez, and S. Sweeney, "Mid-Infrared 2.7 µm GaSbBi/GaSb quantum well lasers studied under high hydrostatic pressure" Conference on Mid-infrared Optoelectronics: Materials and Devices (MIOMD), Paper MIOMD-TuM11, Flagstaff, USA, 7-10 October 2018

8. **O. Delorme**, L. Cerutti, E. Luna, A. Trampert, E. Tournié and J.-B. Rodriguez, "Study of In incorporation into GaSbBi alloys", 20th European Workshop on Molecular Beam Epitaxy (EuroMBE 2019), 17-20 February 2019, Lenggries, Germany

9. **O. Delorme**, L. Cerutti, E. Luna, A. Trampert, E. Tournié and J.-B. Rodriguez, "Molecular-beam epitaxy of GaInSbBi alloys and QWs", 10th International Workshop on Bismuth-Containing Semiconductors, July 21 – 24, 2019, Toulouse, France

10. Esperanza Luna, **O. Delorme**, L. Cerutti, E. Tournié, J.-B. Rodriguez and A. Trampert, "Transmission Electron Microscopy of (In,Ga)(Sb,Bi) epilayers and quantum wells", 10th International Workshop on Bismuth-Containing Semiconductors, July 21 – 24, 2019, Toulouse, France

Invited communications

1. **O. Delorme**, L. Cerutti, E. Luna, R. Kudrawiec, J. Kopaczek, M.P. Polak, M. Gladysiewicz, A. Trampert, E. Tournié and J.-B. Rodriguez, "Development of GaSbBi for the Fabrication of Mid-IR Laser Diodes", (oral invité) 14th International Conference on Mid-IR Optoelectronics: Materials and Devices MIOMD-XIV (MIOMD 2018), October 2018, Flagstaff, AZ (USA)

2. **O. Delorme**, L. Cerutti, R. Kudrawiec, E. Luna, J. Kopaczek, M. P. Polak, M. Gladysiewicz, A. Trampert, E. Tournié, and J.-B. Rodriguez, Recent advances in the molecular beam epitaxy of GaSbBi alloys and quantum wells, 20th International Conference on Molecular-Beam Epitaxy (MBE 2018), 2 – 8 September 2018, Shanghai (China).

Poster presentations

1. **O. Delorme,** L. Cerutti, E. Tournié and J.-B. Rodriguez, "Growth and characterization of high Bi content GaSbBi alloys" 19th Euro-MBE conference, St Petersburg, Russia, March 2017

2. **O. Delorme**, L. Cerutti, E. Tournié and J.-B. Rodriguez, *"Ga(In)SbBi alloys for mid-IR applications: growth and characterization"*, 16ème Journées Nano, Micro et Optoélectronique (JNMO 2018), 13-15 June, Cap Esterel (France)

3. **O. Delorme**, L. Cerutti, R. Kudrawiec, E. Luna, J. Kopaczek, M. P. Polak, M. Gladysiewicz, A. Trampert, E. Tournié, and J.-B. Rodriguez, *"GaSbBi/GaSb quantum wells for Mid-Infrared: growth and*

characterization", 34th International Conference on the Physics of Semiconductors (ICPS 2018), 29th July – 3rd August, Montpellier (France)

4. **O. Delorme**, L. Cerutti, E. Tournié and J. B. Rodriguez (2018), "In situ determination of the optimized growth conditions of GaSbBi alloys", 10th International Workshop on Bismuth-Containing Semiconductors, July 21 – 24, 2019, Toulouse, France

Award

Best poster award at the 16ème Journées Nano, Micro et Optoélectronique (JNMO 2018), 13-15 June, Cap Esterel (France)

Bibliography

[Abedin-2004] M. N. Abedin, T. F. Refaat, I. Bhat, Y. G. Xiao, S. Bandra and S. D. Gunapala (2004). Progress of multicolor single detector to detector array development for remote sensing. Infrared Spaceborne Remote Sensing Xii. M. Strojnik. Bellingham, Spie-Int Soc Optical Engineering. **5543:** 239-247.

[Bahriz-2015] M. Bahriz, G. Lollia, A. N. Baranov and R. Teissier (2015). "High temperature operation of far infrared (λ ~ 20 μm) InAs/AlSb quantum cascade lasers with dielectric waveguide." Optics Express **23**(2): 1523-1528.

[Beaton-2010] D. A. Beaton, R. B. Lewis, M. Masnadi-Shirazi and T. Tiedje (2010). "Temperature dependence of hole mobility in GaAs1–xBix alloys." Journal of Applied Physics **108**(8): 083708.

[Binnie-1956] W. Binnie (1956). "The structural crystallography of indium bismuthide." Acta Crystallographica **9**(8): 686-687.

[Bithell and Stobbs-1989] E. Bithell and W. Stobbs (1989). "Composition determination in the GaAs/(Al, Ga) As system using contrast in dark-field transmission electron microscope images." Philosophical Magazine A **60**(1): 39-62.

[Bolshov-2015] M. A. Bolshov, Y. A. Kuritsyn and Y. V. Romanovskii (2015). "Tunable diode laser spectroscopy as a technique for combustion diagnostics." Spectrochimica Acta Part B-Atomic Spectroscopy **106**: 45-66.

[Bracker-2000] A. Bracker, M. Yang, B. Bennett, J. Culbertson and W. Moore (2000). "Surface reconstruction phase diagrams for InAs, AlSb, and GaSb." Journal of crystal growth **220**(4): 384-392.

[Butkute-2014] R. Butkute, A. Geizutis, V. Pacebutas, B. Cechavicius, V. Bukauskas, R. Kundrotas, P. Ludewig, K. Volz and A. Krotkus (2014). "Multi-quantum well Ga(AsBi)/GaAs laser diodes with more than 6% of bismuth." Electronics Letters **50**(16): 1155-1156.

[Butkutė-2014] R. Butkutė, V. Pačebutas, A. Krotkus, N. Knaub and K. Volz (2014). "Migration-enhanced epitaxy of thin GaAsBi layers." Lithuanian Journal of Physics **54**(2).

[Butkutė-2015] R. Butkutė, K. Stašys, V. Pačebutas, B. Čechavičius, R. Kondrotas, A. Geižutis and A. Krotkus (2015). "Bismuth quantum dots and strong infrared photoluminescence in migration-enhanced epitaxy grown GaAsBi-based structures." Optical and Quantum Electronics **47**(4): 873-882.

[Calmes-2003] C. Calmes (2003). "Apport des techniques d'épitaxie à la technologie du MOSFET ultime : Réalisation et étude d'hétérostructures IV-IV contraintes en tension sur Si(001)" PhD thesis, Université Paris Sud.

[Carrier and Wei-2004] P. Carrier and S.-H. Wei (2004). "Calculated spin-orbit splitting of all diamondlike and zinc-blende semiconductors: Effects of p 1/ 2 local orbitals and chemical trends." Physical Review B **70**(3): 035212.

[Castellano-2017] A. Castellano, L. Cerutti, J. B. Rodriguez, G. Narcy, A. Garreau, F. Lelarge and E. Tournie (2017). "Room-temperature continuous-wave operation in the telecom wavelength range of GaSb-based lasers monolithically grown on Si." Apl Photonics **2**(6): 5.

[Cerutti-2015] L. Cerutti, A. Castellano, J.-B. Rodriguez, M. Bahri, L. Largeau, A. Balocchi, K. Madiomanana, F. Lelarge, G. Patriarche and X. Marie (2015). "GaSb-based composite quantum wells for laser diodes operating in the telecom wavelength range near 1.55-μm." Applied Physics Letters **106**(10): 101102.

[Chen-1996] N. Chen, Y. Wang, H. He and L. Lin (1996). "Effects of point defects on lattice parameters of semiconductors." Physical Review B **54**(12): 8516.

[Choi-1994] H. Choi, S. Eglash and G. Turner (1994). "Double-heterostructure diode lasers emitting at 3 μm with a metastable GaInAsSb active layer and AlGaAsSb cladding layers." Applied physics letters **64**(19): 2474-2476.

[Choi and Turner-1997] H. Choi and G. Turner (1997). "Antimonide-based strained quantum-well diode lasers." Physica Scripta **1997**(T69): 17.

[Coffey-2011] V. C. Coffey (2011). "Seeing in the dark: Defense applications of IR imaging." Optics and Photonics News **22**(4): 26-31.

[Das-2012] S. Das, T. Das, S. Dhar, M. De La Mare and A. Krier (2012). "Near infrared photoluminescence observed in dilute GaSbBi alloys grown by liquid phase epitaxy." Infrared physics & technology **55**(1): 156-160.

[Degtyareva-1998] V. Degtyareva, M. Winzenick and W. Holzapfel (1998). "Crystal structure of InBi under pressure up to 75 GPa." Physical Review B **57**(9): 4975.

[Delorme-2017a] O. Delorme, L. Cerutti, E. Tournié and J.-B. Rodriguez (2017a). "Molecular beam epitaxy and characterization of high Bi content GaSbBi alloys." Journal of Crystal Growth **477**: 144-148.

[Delorme-2017b] O. Delorme, L. Cerutti, E. Luna, G. Narcy, A. Trampert, E. Tournié and J.-B. Rodriguez (2017b). "GaSbBi/GaSb quantum well laser diodes." Applied Physics Letters **110**(22): 222106.

[Delorme-2018] O. Delorme, L. Cerutti, E. Tournié and J. B. Rodriguez (2018). "In situ determination of the growth conditions of GaSbBi alloys." Journal of Crystal Growth **495**: 9-13.

[Dominguez-2013] L. Dominguez, D. F. Reyes, F. Bastiman, D. L. Sales, R. Richards, D. Mendes, J. P. David and D. Gonzalez (2013). "Formation of tetragonal InBi clusters in InAsBi/InAs (100) heterostructures grown by molecular beam epitaxy." Applied Physics Express **6**(11): 112601.

[Duzik and Millunchick-2014] A. Duzik and J. M. Millunchick (2014). "Surface morphology and Bi incorporation in GaSbBi (As)/GaSb films." Journal of Crystal Growth **390**: 5-11.

[Fan-2013] D. Fan, P. C. Grant, S.-Q. Yu, V. G. Dorogan, X. Hu, Z. Zeng, C. Li, M. E. Hawkridge, M. Benamara and Y. I. Mazur (2013). "MBE grown GaAsBi/GaAs double quantum well separate confinement heterostructures." Journal of Vacuum Science & Technology B, Nanotechnology and Microelectronics: Materials, Processing, Measurement, and Phenomena **31**(3): 03C105.

[Ferhat and Zaoui-2006] M. Ferhat and A. Zaoui (2006). "Structural and electronic properties of III-V bismuth compounds." Physical Review B **73**(11): 115107.

[Fitouri-2015] H. Fitouri, Y. Essouda, I. Zaied, A. Rebey and B. El Jani (2015). "Photoreflectance and photoluminescence study of localization effects in GaAsBi alloys." Optical Materials **42**: 67-71.

[Fluegel-2006] B. Fluegel, S. Francoeur, A. Mascarenhas, S. Tixier, E. C. Young and T. Tiedje (2006). "Giant Spin-Orbit Bowing in GaAsBi." Physical Review Letters **97**(6): 067205.

[Forghani-2014] K. Forghani, Y. Guan, A. W. Wood, A. Anand, S. E. Babcock, L. J. Mawst and T. F. Kuech (2014). "Self-limiting growth when using trimethyl bismuth (TMBi) in the metal-organic vapor phase epitaxy (MOVPE) of GaAs1– yBiy." Journal of Crystal Growth **395**: 38-45.

[Francoeur-2003] S. Francoeur, M. J. Seong, A. Mascarenhas, S. Tixier, M. Adamcyk and T. Tiedje (2003). "Band gap of GaAs1-x Bix, 0<x<3.6%." Appl Phys Lett **82**.

[Fuyuki-2013] T. Fuyuki, R. Yoshioka, K. Yoshida and M. Yoshimoto (2013). "Long-wavelength emission in photo-pumped GaAs1-xBix laser with low temperature dependence of lasing wavelength." Applied Physics Letters **103**(20): 4.

[Fuyuki-2014] T. Fuyuki, K. Yoshida, R. Yoshioka and M. Yoshimoto (2014). "Electrically pumped room-temperature operation of GaAs1-xBix laser diodes with low-temperature dependence of oscillation wavelength." Applied Physics Express **7**(8): 4.

[Garbuzov-1995] D. Garbuzov, R. Martinelli, H. Lee, P. York, R. Menna, J. Connolly, S. Narayan and D. Capewell (1995). 2.7-μm InGaAsSb/AlGaAsSb laser diodes with continuous wave operation up to-39° c. IEEE Princeton Section Sarnoff Symposium, IEEE.

[Gardes-2014] C. Gardes, S. Bagumako, L. Desplanque, N. Wichmann, S. Bollaert, F. Danneville, X. Wallart and Y. Roelens (2014). "100 nm AlSb/InAs HEMT for Ultra-Low-Power Consumption, Low-Noise Applications." Scientific World Journal: 6.

[Gladysiewicz-2016] M. Gladysiewicz, R. Kudrawiec and M. Wartak (2016). "Electronic band structure and material gain of III-V-Bi quantum wells grown on GaSb substrate and dedicated for mid-infrared spectral range." Journal of Applied Physics **119**(7): 075701.

[Glas-2004] F. Glas, G. Patriarche, L. Largeau and A. Lemaître (2004). "Determination of the Local Concentrations of Mn Interstitials and Antisite Defects in GaMnAs." Physical review letters **93**(8): 086107.

[Godoy-2015] S. E. Godoy, D. A. Ramirez, S. A. Myers, G. von Winckel, S. Krishna, M. Berwick, R. S. Padilla, P. Sen and S. Krishna (2015). "Dynamic infrared imaging for skin cancer screening." Infrared Physics & Technology **70**: 147-152.

[Gu-2014] Y. Gu, K. Wang, H. Zhou, Y. Li, C. Cao, L. Zhang, Y. Zhang, Q. Gong and S. Wang (2014). "Structural and optical characterizations of InPBi thin films grown by molecular beam epitaxy." Nanoscale research letters **9**(1): 24.

[Gurjarpadhye-2015] A. A. Gurjarpadhye, M. B. Parekh, A. Dubnika, J. Rajadas and M. Inayathullah (2015). "Infrared Imaging Tools for Diagnostic Applications in Dermatology." SM journal of clinical and medical imaging **1**(1): 1-5.

[Hilska-2019] J. Hilska, E. Koivusalo, J. Puustinen, S. Suomalainen and M. Guina (2019). "Epitaxial phases of high Bi content GaSbBi alloys." Journal of Crystal Growth **516**: 67-71.

[Horikoshi-1988] Y. Horikoshi, M. Kawashima and H. Yamaguchi (1988). "Migration-enhanced epitaxy of GaAs and AlGaAs." Japanese journal of applied physics **27**(2R): 169.

[Hosoda-2010] T. Hosoda, G. Kipshidze, G. Tsvid, L. Shterengas and G. Belenky (2010). "Type-I GaSb-Based Laser Diodes Operating in 3.1- to 3.3 µm Wavelength Range." IEEE Photonics Technology Letters **22**(10): 718-720.

[Humphreys-1988] T. P. Humphreys, P. K. Chiang, S. M. Bedair and N. R. Parikh (1988). "Metalorganic chemical vapor deposition and characterization of the In-As-Sb-Bi material system for infrared detection." Applied Physics Letters **53**(2): 142-144.

[Janotti-2002] A. Janotti, S.-H. Wei and S. Zhang (2002). "Theoretical study of the effects of isovalent coalloying of Bi and N in GaAs." Physical Review B **65**(11): 115203.

[Jean-Louis-1969] A. M. Jean-Louis, B. Ayrault and J. Vargas (1969). "Propriétés des alliages InSb1−xBix II. Absorption Optique." physica status solidi (b) **34**(1): 341-350.

[Jean-Louis and Hamon-1969] A. M. Jean-Louis and C. Hamon (1969). "Propriétés des alliages InSb1–xBix I. Mesures électriques." physica status solidi (b) **34**(1): 329-340.

[Joukoff and Jean-Louis-1972] B. Joukoff and A. M. Jean-Louis (1972). "Growth of InSb1-xBix single crystals by Czochralski method." Journal of Crystal Growth **12**(2): 169-172.

[Kaspi and Donati-2003] R. Kaspi and G. P. Donati (2003). "Digital alloy growth in mixed As/Sb heterostructures." Journal of crystal growth **251**(1-4): 515-520.

[Keen-2014] B. Keen, R. Makin, P. Stampe, R. Kennedy, S. Sallis, L. Piper, B. McCombe and S. Durbin (2014). "Growth parameters for thin film InBi grown by molecular beam epitaxy." Journal of electronic materials **43**(4): 914-920.

[Kim-2018] H. Kim, Y. X. Guan, S. E. Babcock, T. F. Kuech and L. J. Mawst (2018). "Characteristics of OMVPE grown GaAsBi QW lasers and impact of post-growth thermal annealing." Journal of Applied Physics **123**(11): 7.

[Kim-2003] J. Kim, L. Shterengas, R. Martinelli and G. Belenky (2003). "High-power room-temperature continuous wave operation of 2.7 and 2.8 μm In (Al) GaAsSb/GaSb diode lasers." Applied physics letters **83**(10): 1926-1928.

[Kini-2009] R. N. Kini, L. Bhusal, A. J. Ptak, R. France and A. Mascarenhas (2009). "Electron Hall mobility in GaAsBi." Journal of Applied Physics **106**(4): 043705.

[Kopaczek-2013] J. Kopaczek, R. Kudrawiec, W. Linhart, M. Rajpalke, K. Yu, T. Jones, M. Ashwin, J. Misiewicz and T. Veal (2013). "Temperature dependence of the band gap of GaSb1– xBix alloys with 0< x≤ 0.042 determined by photoreflectance." Applied Physics Letters **103**(26): 261907.

[Kopaczek-2014a] J. Kopaczek, M. Rajpalke, W. Linhart, T. Jones, M. Ashwin, R. Kudrawiec and T. Veal (2014a). "Photoreflectance spectroscopy of GaInSbBi and AlGaSbBi quaternary alloys." Applied Physics Letters **105**(11): 112102.

[Kopaczek-2014b] J. Kopaczek, R. Kudrawiec, W. Linhart, M. Rajpalke, T. Jones, M. Ashwin and T. Veal (2014b). "Low-and high-energy photoluminescence from GaSb1– xBix with 0< x≤ 0.042." Applied Physics Express **7**(11): 111202.

[Kopaczek-2015] J. Kopaczek, W. Linhart, M. Baranowski, R. Richards, F. Bastiman, J. David and R. Kudrawiec (2015). "Optical properties of GaAsBi/GaAs quantum wells: Photoreflectance, photoluminescence and time-resolved photoluminescence study." Semiconductor Science and Technology **30**(9): 094005.

[Kudrawiec-2009] R. Kudrawiec, M. Syperek, P. Poloczek, J. Misiewicz, R. Mari, M. Shafi, M. Henini, Y. G. Gobato, S. Novikov and J. Ibanez (2009). "Carrier localization in GaBiAs probed by photomodulated transmittance and photoluminescence." Journal of Applied Physics **106**(2): 023518.

[Kudrawiec-2012a] R. Kudrawiec, M. Latkowska, M. Welna, J. Misiewicz, M. Shafi, R. Mari, M. Henini and W. Walukiewicz (2012a). "Correlations between the band structure, activation energies of electron traps, and photoluminescence in n-type GaNAs layers." Applied Physics Letters **101**(8): 082109.

[Kudrawiec-2012b] R. Kudrawiec, J. Kopaczek, J. Misiewicz, W. Walukiewicz, J. Petropoulos, Y. Zhong, P. Dongmo and J. Zide (2012b). "Temperature dependence of E0 and E0+ ΔSO transitions in In0. 53Ga0. 47BixAs1− x alloys studied by photoreflectance." Journal of Applied Physics **112**(11): 113508.

[Kudrawiec-2013] R. Kudrawiec, M. Latkowska, M. Baranowski, J. Misiewicz, L. Li and J. Harmand (2013). "Photoreflectance, photoluminescence, and microphotoluminescence study of optical transitions between delocalized and localized states in GaN 0.02 As 0.98, Ga 0.95 In 0.05 N 0.02 As 0.98, and GaN 0.02 As 0.90 Sb 0.08 layers." Physical Review B **88**(12): 125201.

[Kudrawiec-2019] R. Kudrawiec, J. Kopaczek, O. Delorme, M. Polak, M. Gladysiewicz, E. Luna, L. Cerutti, E. Tournié and J. Rodriguez (2019). "Type I GaSb1-xBix/GaSb quantum wells dedicated for mid infrared laser applications: Photoreflectance studies of bandgap alignment." Journal of Applied Physics **125**(20): 205706.

[Laffaille-2012] P. Laffaille, J. C. Moreno, R. Teissier, M. Bahriz and A. N. Baranov (2012). "High temperature operation of short wavelength InAs-based quantum cascade lasers." Aip Advances **2**(2): 6.

[Lautenschlager-1987] P. Lautenschlager, M. Garriga, S. Logothetidis and M. Cardona (1987). "INTERBAND CRITICAL-POINTS OF GAAS AND THEIR TEMPERATURE-DEPENDENCE." Physical Review B **35**(17): 9174-9189.

[Lee-1995] H. Lee, P. York, R. Menna, R. Martinelli, D. Garbuzov, S. Narayan and J. Connolly (1995). "Room-temperature 2.78 μm AlGaAsSb/InGaAsSb quantum-well lasers." Applied physics letters **66**(15): 1942-1944.

[Lee-1997] J. Lee, J. Kim and M. Razeghi (1997). "Long-wavelength infrared photodetectors based on InSbBi grown on GaAs substrates." Applied physics letters **71**(16): 2298-2300.

[Lee-1998] J. Lee, J. Kim and M. Razeghi (1998). "Room temperature operation of 8–12 μm InSbBi infrared photodetectors on GaAs substrates." Applied physics letters **73**(5): 602-604.

[Lemine-2014] O. Lemine, A. Alkaoud, H. A. Galeti, V. O. Gordo, Y. G. Gobato, H. Bouzid, A. Hajry and M. Henini (2014). "Thermal annealing effects on the optical and structural properties of (1 0 0) GaAs1−xBix layers grown by molecular beam epitaxy." Superlattices and Microstructures **65**: 48-55.

[Lewis-2012] R. Lewis, M. Masnadi-Shirazi and T. Tiedje (2012). "Growth of high Bi concentration GaAs1− xBix by molecular beam epitaxy." Applied Physics Letters **101**(8): 082112.

[Lewis-2014] R. B. Lewis (2014). "Molecular Beam Epitaxy Growth Technology and Properties of GaAsBi Alloys" PhD thesis, University of British Columbia.

[Lin-2004] C. Lin, M. Grau, O. Dier and M.-C. Amann (2004). "Low threshold room-temperature continuous-wave operation of 2.24–3.04 μm GaInAsSb/AlGaAsSb quantum-well lasers." Applied physics letters **84**(25): 5088-5090.

[Linhart-2017] W. Linhart, M. Gladysiewicz, J. Kopaczek, M. Rajpalke, M. Ashwin, T. Veal and R. Kudrawiec (2017). "Indium-incorporation enhancement of photoluminescence properties of Ga (In) SbBi alloys." Journal of Physics D: Applied Physics **50**(37): 375102.

[Linhart and Kudrawiec-2018] W. Linhart and R. Kudrawiec (2018). "Temperature dependence of band gaps in dilute bismides." Semiconductor Science and Technology **33**(7): 073001.

[Liu-2008] C. Liu, T. L. Hughes, X.-L. Qi, K. Wang and S.-C. Zhang (2008). "Quantum spin Hall effect in inverted type-II semiconductors." Physical review letters **100**(23): 236601.

[Liu-2017] J. J. Liu, W. W. Pan, X. Y. Wu, C. F. Cao, Y. Y. Li, X. R. Chen, Y. C. Zhang, L. J. Wang, J. Y. Yan, D. L. Zhang, Y. X. Song, J. Shao and S. M. Wang (2017). "Electrically injected GaAsBi/GaAs single quantum well laser diodes." Aip Advances **7**(11): 8.

[Liu-2007] T. Liu, S. Chandril, A. Ptak, D. Korakakis and T. Myers (2007). "Bismuth surfactant effects for GaAsN and beryllium doping of GaAsN and GaInAsN grown by molecular beam epitaxy." Journal of crystal growth **304**(2): 402-406.

[Logothetidis-1985] S. Logothetidis, L. Via and M. Cardona (1985). "Temperature dependence of the dielectric function and the interband critical points of InSb." Physical Review B **31**(2): 947.

[Lu-2008] X. Lu, D. Beaton, R. Lewis, T. Tiedje and M. Whitwick (2008). "Effect of molecular beam epitaxy growth conditions on the Bi content of GaAs 1– x Bi x." Applied Physics Letters **92**(19): 192110.

[Ludewig-2013] P. Ludewig, N. Knaub, N. Hossain, S. Reinhard, L. Nattermann, I. P. Marko, S. R. Jin, K. Hild, S. Chatterjee, W. Stolz, S. J. Sweeney and K. Volz (2013). "Electrical injection Ga(AsBi)/(AlGa)As single quantum well laser." Applied Physics Letters **102**(24): 3.

[Luna-2012] E. Luna, Á. Guzmán, A. Trampert and G. Álvarez (2012). "Critical role of two-dimensional island-mediated growth on the formation of semiconductor heterointerfaces." Physical review letters **109**(12): 126101.

[Luna-2016] E. Luna, M. Wu, M. Hanke, J. Puustinen, M. Guina and A. Trampert (2016). "Spontaneous formation of three-dimensionally ordered Bi-rich nanostructures within GaAs1– x Bi x/GaAs quantum wells." Nanotechnology **27**(32): 325603.

[Luna-2018a] E. Luna, O. Delorme, L. Cerutti, E. Tournie, J. B. Rodriguez and A. Trampert (2018a). "Microstructure and interface analysis of emerging Ga(Sb,Bi) epilayers and Ga(Sb,Bi)/GaSb quantum wells for optoelectronic applications." Applied Physics Letters **112**(15): 5.

[Luna-2018b] E. Luna, O. Delorme, L. Cerutti, E. Tournie, J. B. Rodriguez and A. Trampert (2018b). "Transmission electron microscopy of Ga(Sb, Bi)/GaSb quantum wells with varying Bi content and quantum well thickness." Semiconductor Science and Technology **33**(9): 8.

[Ma-1989] K. Y. Ma, Z. M. Fang, D. H. Jaw, R. M. Cohen, G. B. Stringfellow, W. P. Kosar and D. W. Brown (1989). "Organometallic vapor phase epitaxial growth and characterization of InAsBi and InAsSbBi." Applied Physics Letters **55**(23): 2420-2422.

[Maddox-2012] S. Maddox, A. Vasudev, V. Dasika, M. Brongersma and S. Bank (2012). Bismuth Surfactant-Mediated Epitaxy of Highly Doped InAs for Mid-Infrared Plasmonics. North American Molecular Beam Epitaxy Conf.(NAMBE).

[Makhloufi-2014] H. Makhloufi, P. Boonpeng, S. Mazzucato, J. Nicolai, A. Arnoult, T. Hungria, G. Lacoste, C. Gatel, A. Ponchet and H. Carrère (2014). "Molecular beam epitaxy and properties of GaAsBi/GaAs quantum wells grown by molecular beam epitaxy: effect of thermal annealing." Nanoscale research letters **9**(1): 123.

[Marko-2015] I. P. Marko, S. R. Jin, K. Hild, Z. Batool, Z. L. Bushell, P. Ludewig, W. Stolz, K. Volz, R. Butkute, V. Pacebutas, A. Geizutis, A. Krotkus and S. J. Sweeney (2015). "Properties of hybrid MOVPE/MBE grown GaAsBi/GaAs based near-infrared emitting quantum well lasers." Semiconductor Science and Technology **30**(9): 10.

[Mazzucato-2013] S. Mazzucato, P. Boonpeng, H. Carrère, D. Lagarde, A. Arnoult, G. Lacoste, T. Zhang, A. Balocchi, T. Amand and X. Marie (2013). "Reduction of defect density by rapid thermal annealing in GaAsBi studied by time-resolved photoluminescence." Semiconductor Science and Technology **28**(2): 022001.

[Mazzucato-2014] S. Mazzucato, H. Lehec, H. Carrère, H. Makhloufi, A. Arnoult, C. Fontaine, T. Amand and X. Marie (2014). "Low-temperature photoluminescence study of exciton recombination in bulk GaAsBi." Nanoscale research letters **9**(1): 19.

[Mohan-2000] P. Mohan, S. M. Babu, P. Santhanaraghavan and P. Ramasamy (2000). "Growth, phase analysis and mechanical properties of InSb1– xBix crystals." Materials chemistry and physics **66**(1): 17-21.

[Mohmad-2011] A. R. Mohmad, F. Bastiman, C. Hunter, J. Ng, S. Sweeney and J. David (2011). "The effect of Bi composition to the optical quality of GaAs1– xBix." Applied Physics Letters **99**(4): 042107.

[Moussa-2008a] I. Moussa, H. Fitouri, A. Rebey and B. El Jani (2008a). "Atmospheric-pressure metalorganic vapour phase epitaxy optimization of GaAsBi alloy." Thin Solid Films **516**(23): 8372-8376.

[Moussa-2008b] I. Moussa, H. Fitouri, Z. Chine, A. Rebey and B. El Jani (2008b). "Effect of thermal annealing on structural and optical properties of the GaAs0. 963Bi0. 037 alloy." Semiconductor Science and Technology **23**(12): 125034.

[Nguyen-Van-2018] H. Nguyen-Van, A. N. Baranov, Z. Loghmari, L. Cerutti, J. B. Rodriguez, J. Tournet, G. Narcy, G. Boissier, G. Patriarche, M. Bahriz, E. Tournie and R. Teissier (2018). "Quantum cascade lasers grown on silicon." Scientific Reports **8**: 8.

[Noreika-1982] A. J. Noreika, W. J. Takei, M. H. Francombe and C. E. C. Wood (1982). "Indium antimonide-bismuth compositions grown by molecular beam epitaxy." Journal of Applied Physics **53**(7): 4932-4937.

[O'Malley-2010] R. O'Malley, E. Jones and M. Glavin (2010). "Detection of pedestrians in far-infrared automotive night vision using region-growing and clothing distortion compensation." Infrared Physics & Technology **53**(6): 439-449.

[Oe-1981] K. Oe, S. Ando and K. Sugiyama (1981). "InSb1-xBix Films Grown by Molecular Beam Epitaxy." Japanese Journal of Applied Physics **20**(4): L303-L306.

[Oe and Okamoto-1998] K. Oe and H. Okamoto (1998). "New semiconductor alloy GaAs1-xBix grown by metal organic vapor phase epitaxy." Japanese journal of applied physics **37**(11A): L1283.

[Oe-2002] K. Oe (2002). "Characteristics of semiconductor alloy GaAs1-xBix." Japanese Journal of Applied Physics **41**(5R): 2801.

[Pan-2000] Z. Pan, L. Li, W. Zhang, Y. Lin and R. Wu (2000). "Kinetic modeling of N incorporation in GaInNAs growth by plasma-assisted molecular-beam epitaxy." Applied Physics Letters **77**(2): 214-216.

[Patil-2017] P. K. Patil, E. Luna, T. Matsuda, K. Yamada, K. Kamiya, F. Ishikawa and S. Shimomura (2017). "GaAsBi/GaAs multi-quantum well LED grown by molecular beam epitaxy using a two-substrate-temperature technique." Nanotechnology **28**(10): 105702.

[Pettinari-2008] G. Pettinari, A. Polimeni, M. Capizzi, J. Blokland, P. Christianen, J. Maan, E. Young and T. Tiedje (2008). "Influence of bismuth incorporation on the valence and conduction band edges of Ga As 1– x Bi x." Applied Physics Letters **92**(26): 262105.

[Phillips-1999] A. F. Phillips, S. J. Sweeney, A. R. Adams and P. J. Thijs (1999). "The temperature dependence of 1.3-and 1.5-/spl mu/m compressively strained InGaAs (P) MQW semiconductor lasers." IEEE Journal of selected topics in quantum electronics **5**(3): 401-412.

[Polak-2014] M. Polak, P. Scharoch, R. Kudrawiec, J. Kopaczek, M. Winiarski, W. Linhart, M. K. Rajpalke, K. Yu, T. Jones and M. Ashwin (2014). "Theoretical and experimental studies of electronic band structure for GaSb1– xBix in the dilute Bi regime." Journal of Physics D: Applied Physics **47**(35): 355107.

[Polak-2015] M. Polak, P. Scharoch and R. Kudrawiec (2015). "First-principles calculations of bismuth induced changes in the band structure of dilute Ga–V–Bi and In–V–Bi alloys: chemical trends versus experimental data." Semiconductor Science and Technology **30**(9): 094001.

[Rajpalke-2013] M. Rajpalke, W. Linhart, M. Birkett, K. Yu, D. Scanlon, J. Buckeridge, T. S. Jones, M. Ashwin and T. D. Veal (2013). "Growth and properties of GaSbBi alloys." Applied Physics Letters **103**(14): 142106.

[Rajpalke-2014a] M. Rajpalke, W. Linhart, M. Birkett, K. Yu, J. Alaria, J. Kopaczek, R. Kudrawiec, T. Jones, M. Ashwin and T. Veal (2014a). "High Bi content GaSbBi alloys." Journal of applied physics **116**(4): 043511.

[Rajpalke-2014b] M. Rajpalke, W. Linhart, K. Yu, M. Birkett, J. Alaria, J. Bomphrey, S. Sallis, L. Piper, T. Jones and M. Ashwin (2014b). "Bi-induced band gap reduction in epitaxial InSbBi alloys." Applied Physics Letters **105**(21): 212101.

[Rajpalke-2015] M. Rajpalke, W. Linhart, K. Yu, T. S. Jones, M. Ashwin and T. D. Veal (2015). "Bi flux-dependent MBE growth of GaSbBi alloys." Journal of Crystal Growth **425**: 241-244.

[Rao-2002] M. L. N. Rao, S. Shimada, O. Yamazaki and M. Tanaka (2002). "Cross-coupling reaction of organobismuth dialkoxides with aryl bromides and iodides catalyzed by Pd(PPh3)4." Journal of Organometallic Chemistry **659**(1): 117-120.

[Razeghi and Nguyen-2014] M. Razeghi and B.-M. Nguyen (2014). "Advances in mid-infrared detection and imaging: a key issues review." Reports on Progress in Physics **77**(8): 082401.

[Reboul-2011] J. R. Reboul, L. Cerutti, J. B. Rodriguez, P. Grech and E. Tournie (2011). "Continuous-wave operation above room temperature of GaSb-based laser diodes grown on Si." Applied Physics Letters **99**(12): 3.

[Reyes-Reyes-2014] A. Reyes-Reyes, Z. Hou, E. van Mastrigt, R. C. Horsten, J. C. de Jongste, M. W. Pijnenburg, H. P. Urbach and N. Bhattacharya (2014). "Multicomponent gas analysis using broadband quantum cascade laser spectroscopy." Optics Express **22**(15): 18299-18309.

[Reyes-2014] D. F. Reyes, F. Bastiman, C. J. Hunter, D. L. Sales, A. M. Sanchez, J. P. David and D. González (2014). "Bismuth incorporation and the role of ordering in GaAsBi/GaAs structures." Nanoscale research letters **9**(1): 23.

[Rhiger-2011] D. R. Rhiger (2011). "Performance comparison of long-wavelength infrared type II superlattice devices with HgCdTe." Journal of electronic materials **40**(8): 1815-1822.

[Rodrigo-2010] J. Rodrigo, D. Sales, M. Shafi, M. Henini, L. Turyanska, S. Novikov and S. Molina (2010). "Effect of annealing on the structural and optical properties of (3 1 1) B GaAsBi layers." Applied Surface Science **256**(18): 5688-5690.

[Rodriguez and Millunchick-2016] G. V. Rodriguez and J. M. Millunchick (2016). "Predictive modeling of low solubility semiconductor alloys." Journal of Applied Physics **120**(12): 125310.

[Samajdar-2014] D. Samajdar, T. Das and S. Dhar (2014). Calculation of Direct E 0 Energy Gaps for III–V–Bi Alloys Using Quantum Dielectric Theory. Physics of Semiconductor Devices, Springer**:** 779-781.

[Sandall-2014] I. Sandall, F. Bastiman, B. White, R. Richards, D. Mendes, J. David and C. Tan (2014). "Demonstration of InAsBi photoresponse beyond 3.5 µ m." Applied Physics Letters **104**(17): 171109.

[Sarney-2014] W. Sarney, S. Svensson, E. Anderson, A. Lundquist, C. Pearson and J. Millunchick (2014). "The influence of growth temperature on Sb incorporation in InAsSb, and the temperature-dependent impact of Bi surfactants." Journal of Crystal Growth **406**: 8-11.

[Schmidt-1992] T. Schmidt, K. Lischka and W. Zulehner (1992). "EXCITATION-POWER DEPENDENCE OF THE NEAR-BAND-EDGE PHOTOLUMINESCENCE OF SEMICONDUCTORS." Physical Review B **45**(16): 8989-8994.

[Scholle-2010] K. Scholle, S. Lamrini, P. Koopmann and P. Fuhrberg (2010). 2 µm laser sources and their possible applications. Frontiers in Guided Wave Optics and Optoelectronics, IntechOpen.

[Schwaighofer-2017] A. Schwaighofer, M. Brandstetter and B. Lendl (2017). "Quantum cascade lasers (QCLs) in biomedical spectroscopy." Chemical Society Reviews **46**(19): 5903-5924.

[Shakfa-2013] M. Shakfa, D. Kalincev, X. Lu, S. Johnson, D. Beaton, T. Tiedje, A. Chernikov, S. Chatterjee and M. Koch (2013). "Quantitative study of localization effects and recombination dynamics in GaAsBi/GaAs single quantum wells." Journal of Applied Physics **114**(16): 164306.

[Song-2012] Y. Song, S. Wang, I. Saha Roy, P. Shi and A. Hallen (2012). "Growth of GaSb1– xBix by molecular beam epitaxy." Journal of Vacuum Science & Technology B, Nanotechnology and Microelectronics: Materials, Processing, Measurement, and Phenomena **30**(2): 02B114.

[Steele-2016] J. Steele, R. A. Lewis, J. Horvat, M. J. B. Nancarrow, M. Henini, D. Fan, Y. Mazur, M. Schmidbauer, M. Ware and S.-Q. Yu (2016). "Surface effects of vapour-liquid-solid driven Bi surface droplets formed during molecular-beam-epitaxy of GaAsBi." Scientific reports **6**: 28860.

[Sterzer-2014] E. Sterzer, N. Knaub, P. Ludewig, R. Straubinger, A. Beyer and K. Volz (2014). "Investigation of the microstructure of metallic droplets on Ga (AsBi)/GaAs." Journal of Crystal Growth **408**: 71-77.

[Sweeney and Jin-2013] S. J. Sweeney and S. R. Jin (2013). "Bismide-nitride alloys: Promising for efficient light emitting devices in the near- and mid-infrared." Journal of Applied Physics **113**(4): 043110.

[Tait and Millunchick-2016] C. R. Tait and J. M. Millunchick (2016). "Kinetics of droplet formation and Bi incorporation in GaSbBi alloys." Journal of Applied Physics **119**(21): 215302.

[Tait-2017] C. R. Tait, L. Yan and J. M. Millunchick (2017). "Droplet induced compositional inhomogeneities in GaAsBi." Applied Physics Letters **111**(4): 042105.

[Takehara-2006] Y. Takehara, M. Yoshimoto, W. Huang, J. Saraie, K. Oe, A. Chayahara and Y. Horino (2006). "Lattice distortion of GaAsBi alloy grown on GaAs by molecular beam epitaxy." Japanese journal of applied physics **45**(1R): 67.

[Tan-2018] B.-S. Tan, C.-J. Zhang, W.-H. Zhou, X.-J. Yang, G.-W. Wang, Y.-T. Li, Y.-Y. Ding, Z. Zhang, H.-W. Lei and W.-H. Liu (2018). "The 640× 512 LWIR type-II superlattice detectors operating at 110 K." Infrared Physics & Technology **89**: 168-173.

[Tidrow and Dyer-2001] M. Z. Tidrow and W. R. Dyer (2001). "Infrared sensors for ballistic missile defense." Infrared Physics & Technology **42**(3-5): 333-336.

[Tiedje-2008] T. Tiedje, E. Young and A. Mascarenhas (2008). "Growth and properties of the dilute bismide semiconductor GaAs1-xBix a complementary alloy to the dilute nitrides." International Journal of Nanotechnology **5**(9): 963.

[Tittel and Lewicki-2013] F. K. Tittel and R. Lewicki (2013). Tunable mid-infrared laser absorption spectroscopy. Semiconductor Lasers. A. Baranov and E. Tournié, Woodhead Publishing**:** 579-629.

[Tixier-2003a] S. Tixier, M. Adamcyk, E. Young, J. Schmid and T. Tiedje (2003a). "Surfactant enhanced growth of GaNAs and InGaNAs using bismuth." Journal of crystal growth **251**(1-4): 449-454.

[Tixier-2003b] S. Tixier, M. Adamcyk, T. Tiedje, S. Francoeur, A. Mascarenhas, P. Wei and F. Schiettekatte (2003b). "Molecular beam epitaxy growth of GaAs1-xBix." Appl Phys Lett **82**.

[Tominaga-2008] Y. Tominaga, Y. Kinoshita, K. Oe and M. Yoshimoto (2008). "Structural investigation of GaAs 1– x Bi x/GaAs multiquantum wells." Applied Physics Letters **93**(13): 131915.

[Tominaga-2010] Y. Tominaga, K. Oe and M. Yoshimoto (2010). "Low Temperature Dependence of Oscillation Wavelength in GaAs1-xBix Laser by Photo-Pumping." Applied Physics Express **3**(6): 3.

[Tournet-2019] J. Tournet (2019). "III-Sb-based solar cells and their integration on Si" PhD.

[Tournie-2018] E. Tournie, J.-B. Rodriguez, L. Cerutti, R. Teissier and A. N. Baranov (2018). "Epitaxial Integration of Antimonide-Based Semiconductor Lasers on Si." Silicon Photonics **99**: 1.

[Vardar-2013] G. Vardar, S. Paleg, M. Warren, M. Kang, S. Jeon and R. Goldman (2013). "Mechanisms of droplet formation and Bi incorporation during molecular beam epitaxy of GaAsBi." Applied Physics Letters **102**(4): 042106.

[Varshni-1967] Y. P. Varshni (1967). "Temperature dependence of the energy gap in semiconductors." Physica **34**(1): 149-154.

[Vizbaras-2014] A. Vizbaras, E. Dvinelis, A. Trinkūnas, I. Šimonyte, M. Greibus, M. Kaušylas, T. Žukauskas, R. Songaila and K. Vizbaras (2014). High-performance mid-infrared GaSb laser diodes for defence and sensing applications. Laser Technology for Defense and Security X, International Society for Optics and Photonics.

[Vurgaftman-2001] I. Vurgaftman, J. á. Meyer and L. á. Ram-Mohan (2001). "Band parameters for III–V compound semiconductors and their alloys." Journal of applied physics **89**(11): 5815-5875.

[Vurgaftman-2015] I. Vurgaftman, R. Weih, M. Kamp, J. Meyer, C. Canedy, C. Kim, M. Kim, W. Bewley, C. Merritt and J. Abell (2015). "Interband cascade lasers." Journal of Physics D: Applied Physics **48**(12): 123001.

[Waclawek-2014] J. P. Waclawek, R. Lewicki, H. Moser, M. Brandstetter, F. K. Tittel and B. Lendl (2014). "Quartz-enhanced photoacoustic spectroscopy-based sensor system for sulfur dioxide detection using a CW DFB-QCL." Applied Physics B-Lasers and Optics **117**(1): 113-120.

[Wagener-2000] M. Wagener, J. Botha and A. Leitch (2000). "Characterization of secondary phases formed during MOVPE growth of InSbBi mixed crystals." Journal of crystal growth **213**(1-2): 51-56.

[Wang-2017] L. Wang, L. Zhang, L. Yue, D. Liang, X. Chen, Y. Li, P. Lu, J. Shao and S. Wang (2017). "Novel dilute bismide, epitaxy, physical properties and device application." Crystals **7**(3): 63.

[Wei-2002] Y. Wei, A. Gin, M. Razeghi and G. J. Brown (2002). "Type II InAs/GaSb superlattice photovoltaic detectors with cutoff wavelength approaching 32 μm." Applied Physics Letters **81**(19): 3675-3677.

[Willer-2006] U. Willer, M. Saraji, A. Khorsandi, P. Geiser and W. Schade (2006). "Near- and mid-infrared laser monitoring of industrial processes, environment and security applications." Optics and Lasers in Engineering **44**(7): 699-710.

[Winnewisser-1994] G. Winnewisser (1994). "Submillimeter and infrared astronomy: Recent scientific and technical developments." Infrared Physics & Technology **35**(2-3): 551-567.

[Wood-2016] A. W. Wood, K. Collar, J. Li, A. S. Brown and S. E. Babcock (2016). "Droplet-mediated formation of embedded GaAs nanowires in MBE GaAs1– x Bi x films." Nanotechnology **27**(11): 115704.

[Wood-1982] C. Wood, D. Desimone, K. Singer and G. Wicks (1982). "Magnesium-and calcium-doping behavior in molecular-beam epitaxial III-V compounds." Journal of Applied Physics **53**(6): 4230-4235.

[Wu-2017] X. Y. Wu, W. W. Pan, Z. P. Zhang, Y. Y. Li, C. F. Cao, J. J. Liu, L. Y. Zhang, Y. X. Song, H. Y. Ou and S. M. Wang (2017). "1.142 mu m GaAsBi/GaAs Quantum Well Lasers Grown by Molecular Beam Epitaxy." Acs Photonics **4**(6): 1322-1326.

[Yoshida-2003] J. Yoshida, T. Kita, O. Wada and K. Oe (2003). "Temperature dependence of GaAs1-xBix band gap studied by photoreflectance spectroscopy." Japanese journal of applied physics **42**(2R): 371.

[Yoshimoto-2003] M. Yoshimoto, S. Murata, A. Chayahara, Y. Horino, J. Saraie and K. Oe (2003). "Metastable GaAsBi alloy grown by molecular beam epitaxy." Japanese journal of applied physics **42**(10B): L1235.

[Yoshimoto-2013] M. Yoshimoto, M. Itoh, Y. Tominaga and K. Oe (2013). "Quantitative estimation of density of Bi-induced localized states in GaAs1–xBix grown by molecular beam epitaxy." Journal of Crystal Growth **378**: 73-76.

[Young-2003] D. L. Young, J. F. Geisz and T. J. Coutts (2003). "Nitrogen-induced decrease of the electron effective mass in GaAs 1– x N x thin films measured by thermomagnetic transport phenomena." Applied physics letters **82**(8): 1236-1238.

[Young-2005] E. Young, S. Tixier and T. Tiedje (2005). "Bismuth surfactant growth of the dilute nitride GaNxAs1– x." Journal of crystal growth **279**(3-4): 316-320.

[Yue-2018a] L. Yue, X. Chen, Y. Zhang, F. Zhang, L. Wang, J. Shao and S. Wang (2018a). "Molecular beam epitaxy growth and optical properties of high bismuth content GaSb1-xBix thin films." Journal of Alloys and Compounds **742**: 780-789.

[Yue-2018b] L. Yue, X. Chen, Y. Zhang, J. Kopaczek, J. Shao, M. Gladysiewicz, R. Kudrawiec, X. Ou and S. Wang (2018b). "Structural and optical properties of GaSbBi/GaSb quantum wells." Optical Materials Express **8**(4): 893-900.

[Zilko and Greene-1980] J. Zilko and J. Greene (1980). "Growth and phase stability of epitaxial metastable InSb1– x Bi x films on GaAs. I. Crystal growth." Journal of Applied Physics **51**(3): 1549-1559.

Abstract

Bismuth, a group-V element, has long been neglected in the III-V semiconductor family. However, dilute bismides started to attract great attention since the early 2000s, due to the giant bandgap reduction and the strong increase of the spin-orbit splitting energy introduced by the incorporation of Bismuth. Among the III-V-Bi alloys, GaSbBi is particularly interesting but has only been sporadically studied, mainly due to the very challenging incorporation of Bismuth. Bismuth requires indeed very unusual growth conditions to be incorporated into III-V materials. The main objective of this thesis was to investigate the molecular beam epitaxy and the properties of GaSbBi alloys and heterostructures.

A careful study of the influence of the different growth parameters on the Bismuth incorporation was first carried out. These investigations lead to the fabrication of high quality GaSbBi layers and to the incorporation of 14% Bismuth, the highest content reached in GaSb so far. A bandgap reduction of ~28 meV/%Bismuth was observed. GaSbBi/GaSb multi quantum-wells structures with various thicknesses and compositions were then fabricated and exhibited photoluminescence emission up to 3.5 μm at room-temperature. The first GaSbBi-based laser diode was also fabricated, demonstrating continuous wave operation at 80 K and a room-temperature emission close to 2.7 μm under pulsed excitation. Finally, the growth of another dilute bismide alloy, GaInSbBi, was investigated. The influence of the Indium atoms on the incorporation of Bismuth was particularly studied together with the properties of GaInSbBi/GaSb multi quantum-wells structures.

Résumé

Le Bismuth, un élément V, a longtemps été négligé dans la famille des semiconducteurs III-V. Toutefois, les matériaux bismures connaissent un intérêt croissant depuis le début des années 2000, principalement en raison de l'exceptionnelle réduction de l'énergie de bande interdite couplée à la forte augmentation de l'énergie entre la bande de valence et la bande de spin-orbite introduites par l'atome de Bismuth. Parmi les alliages III-V-Bi, le GaSbBi est particulièrement intéressant pour l'émission dans la gamme de longueurs d'onde entre 2 et 5 μm. Jusqu'à présent, ce matériau n'a été que très peu étudié, principalement à cause des difficultés d'incorporation du Bismuth. En effet, l'incorporation du Bismuth dans les matériaux III-V nécessite des conditions de croissance très spécifiques et inhabituelles. Dans ce contexte, l'objectif premier de cette thèse est d'étudier l'épitaxie par jet moléculaire et les propriétés du GaSbBi.

Ainsi, l'influence des différents paramètres de croissance sur l'incorporation du Bismuth a été étudiée minutieusement. Ces expériences ont permis la réalisation de couches de GaSbBi à forte teneur en Bismuth démontrant une excellente qualité cristalline. La plus importante concentration de Bismuth atteinte est de 14%, ce qui constitue encore aujourd'hui le record mondial dans GaSb. Par ailleurs, une réduction de l'énergie de bande interdite de ~28 meV/%Bismuth a été observée. Des puits quantiques GaSbBi/GaSb, émettant jusqu'à 3.5 μm à température ambiante ont ensuite été épitaxiés et caractérisés. Le premier laser à base de GaSbBi a également été réalisé. Ce composant fonctionne en continu à 80 K et une émission laser pulsée a été observée proche de 2.7 μm à température ambiante. Enfin, un autre alliage bismure méconnu, le GaInSbBi, a été épitaxié. L'influence de l'Indium sur l'incorporation du Bismuth et les propriétés de puits quantiques GaInSbBi/GaSb ont été étudiées.